UNIVERSITÀ DEGLI STUDI DI NAPOLI "FEDERICO II"

Department of Agricultural Sciences

PhD

in

AGROBIOLOGY AND AGROCHEMISTRY

XXVIII Cycle

Ph.D. THESIS

PRESENTED BY

MARCO EVIDENTE

Phytotoxins produced by pathogenic fungi for the integrated management of noxious weeds

Relator: Doctor Alessio Cimmino

2013-2016

CONTENTS

1. INTRODUCTION

1.1. Weeds

The simplest definition of a weed is an "unwanted plant" referring to plants growing in habitats modified or managed by humans, and plants that cause damages to some segments of the human population (Norris, 1992). A further definition of a weed would be that "it is a plant growing at levels that interferes with management objectives in a given area and at a given point in time" (Ross & Lembi, 1985; Charudattan & DeLoach, 1988; Norris, 1992). However, a better definition of weed was given by Kent (1994), which states: "a weed is a green plant that is growing in a location where its presence has become undesirable because of its adverse effects on the ecosystem or human activities". The concept of a weed is site and time specific (Norris, 1992). A plant can be a weed in one situation but may not be classified as a weed in another (Kent, 1994), as weediness is not a fixed attribute of a plant (Norris, 1992).

Weeds have always been and will be an integral part of agricultural systems (Lovett & Knight, 1996). Smith (1983) reported that the most important plant families with the greatest number of species as weeds were Alismataceae, Poaceae, Asteraceae, Fabaceae, Lytheraceae and Scriphulariceae. Nearly 44 percent of the world's worst weeds belong to family Poaceae, which happens to provide eight major crops, namely, wheat, maize, rice, sorghum, barley, millet, oat, and sugarcane (Kohli *et al*., 2006).

Perennial weeds represent a common problem in different crops. Weeds can compete with productive crops or pasture, or convert productive land into unusable scrub. They are often poisonous and distasteful, and able to produce burrs, thorns or other damaging body parts. They can otherwise interfere with the use and management of desirable plants by contaminating harvests or excluding livestock.

Weeds tend to thrive at the expense of the more refined edible or ornamental crops. They compete for light, nutrients, water and space (Glauninger & Holzner, 1982; Kropff, 1993). Without

weed control, yield losses have been estimated in a range from 16% to 86% or even 100% (Zoschke, 1990; Baltazar & De Datta, 1992; Kropff, 1993). Losses are influenced by several factors which can be summarised as: (i) competitive efficiency of weeds, (ii) weed density, (iii) duration of competition, (iv) planting method, (v) crop species and variety, (vi) fertility level, (vii) water management, (viii) and interaction among the preceding factors (Chisaka, 1977; Smith, 1983).

Weeds assume large proportions of the area of their invasion. They possess certain features that make them ideal for proliferation. In fact, the ability to reproduce at a faster rate, rapid growth from seedling to sexual phase, phenotypic plasticity, and high tolerance to environmental heterogeneity are associated with weedy plant species (Baker, 1974). Weed populations are highly adaptable to production system through herbicidal resistance and shifts in their populations. Weeds possess adaptive strategies that determine their survival, productions and success in a particular environment (Holt, 1988). On the basis of intensity of stress and disturbance for successful establishment of a given area, plants can be stress tolerators, competitors or ruderals (Grime, 1979). Weeds, however, fall into two combined categories: they can be competitive ruderals or stress-tolerant competitors (Grime, 1979). They take advantage of human-made habitats and are highly responsive to change in environmental conditions in such a beneficial manner, enabling them to survive and grow in nature (Grime, 1979). Many annual, biennial and even perennial weed species found on arable fertile land are known as competitive ruderals that grow rapidly and the competition inside them occurs before flowering. Stress-tolerant competitors, primarily trees or shrubs and even some perennial herbs, are characterized by rapid dry matter production, large stem extension, and high leaf area production. In addition to grown strategies, weeds possess several other characteristics that make them successful colonizers of a given area (Kohli *et al.*, 2006).

1.2. Weed Management

The weed pest is one of the most serious problems for agriculture and environment. Infesting plants can be a great obstacle to the normal flow of superficial waters and destroy the natural

habitat. They can also be the cause of serious damage for archaeological and monumental areas and generate heavy losses to crop production and to pasture industry. Many plants of agrarian interest may dieback when the weed grows in the same field absorbing water, food substances, and sunlight. Furthermore, they represent a serious impediment to the normal agrarian activity. The diffusion of weed reduces the pasture areas with consequent deterioration of animal food.

In agricultural fields, weeds seem to have coevolved with crop plants since prehistoric time as evidenced by pollen analysis techniques indicating that both share common evolutionary lines. Distribution of weeds is determined by various environmental and biological features. Human activities are the main responsible for their regional patterns and have certainly played an important role in their spread. Plant species are also affected when their habitat are disturbed (Harlan & de Welt, 1965). Weeds have evolved due to continuous selection pressure imposed by humans, technological advancement, and/or through agricultural practices.

The effort to control weeds is as old as agriculture itself. Humans, however, were familiar with weeds even before the dawn of agriculture, as several aboriginal nomadic tribes suffered from allergies, hay fever, and other health problems caused by poisonous plants. The control of weed diffusion has been achieved with agrochemicals belonging to different class of organic compounds. They are usually used in very large amounts in agriculture, causing serious issues to human and animal health and producing grave environmental pollution. This is mainly due to the fact that these substances have frequently low specificity; they are weakly or not biodegradable and can easily accumulate in food plants and drinkable water. Furthermore, the chemical control has short-life and must usually be repeated on an annual or semi-annual basis. Nevertheless, it would not be wise to kill or eradicate weeds because that could creates genetic erosion in the modern era of rapid biodiversity loss causing imbalance in the natural ecosystems. Thus, an urgent need exists to get a suitable ways to fight the adverse effects of weeds without affecting the natural balance.

1.3. Weed Management Strategies

1.3.1. Traditional methods

A number of weed management strategies have been developed throughout the years, but none of them probably provides a satisfactory solution to the weed problems. Broadly, four methods are employed for the management of weeds: mechanical, cultural, chemical and biological, each of them that has certain advantages and disadvantages. Among these, mechanical methods are the oldest, involving physical removals of weeds by soil disturbance before the planting procedure or by hand weeding and/or hoeing during crop growth. On the other hand, cultural methods are largely applied during the active growth period of the crop. This includes crop rotation, the use of cover, smother and green manure crops, crops residues, crop genotypes with better competitive and allelopathic ability and manipulation of sowing or planting date, crop density and crop pattern (Kohli *et al*., 2006). These are effective when they are able to enhance the differential development between crop and weeds to the advantage of the former (Mohler, 1996). However, these methods were used in traditional agroecosystems but they were declined with the modernization of agriculture and herbicide applications.

1.3.2. Chemical methods

The use of chemical methods is probably a twentieth-century technology when the herbicides, especially the hormonal ones discovered in 1940s, revolutionized the agriculture. Their improved efficacy and the production of herbicide-resistant crop have further expanded this revolution becoming an important tool of modern weed management. They are widely used not only in the developed nations but also in developing nations such as India. A 350 percent increase in the use of herbicides occurred from 1971 to 1987 for control of weeds in rice and wheat fields in India (Alstrom, 1990). Several herbicide families widely differ between them in respect to spectrum, unit activity, crop safety, toxicology and environmental effects. However, increasing herbicidal

resistance, environmental and toxicological concerns have put a question mark on their large scale use (Burnside, 1993; Heap, 2005).

The combination of mechanical, cultural and chemical methods is more effective than any single method used alone (Trumble & Kok, 1982). Herbicides recommended for chemical control of the perennials in non-organic cropping systems are restricted to few active substances (clopyralid, dicamba, chlorsulfuron, bentazon, phenoxy-acids) (Lemna & Messersmith, 1990; Grekul *et al.*, 2005). These chemicals are frequently low specific and weakly biodegradable, accumulating in plants and in drinkable water, producing serious environmental pollution and creating problems to human and animal health (Cimmino *et al*., 2015). During the last twenty years there has been mounting public concern about the effect of herbicides on both environment and public health. These include the effects of herbicides on surface and ground water, spray drift and long term impact of herbicide residues in agricultural products. These problems led many governments to set specific targets to reduce the use of herbicides and the adoption of more sustainable crop production and protection methods by encouraging integrated pest management techniques (Evans *et al*., 1996; Lovett & Knights, 1996).

1.3.3. Biological methods

Management of weeds, should, therefore, be achieved through strategies that do not affect the sustainability of agroecosystems and the life support system.

Biological control was defined by Waterhouse (1978), as "the use of a pest's natural enemies to keep its numbers below levels at which the damage caused becomes economically significant". Biological control of weeds is a science evolved in the twentieth century, with the first attempt at controlling weeds with insects in 1902 in Hawaii and a few years later in Australia (Bruzzese, 1990). This method of control has advantages over mechanical and chemical control methods, especially chemical control which is a temporary and expensive method, that is not always applicable (Hassan, 1980).

Unlike chemical compounds, biological control agents can be specific to a particular weed and cause no environmental pollution problems (Hassan, 1980; Templeton, 1985), often with high specificity and represent a long term solution also in the control of weed particularly resistant to chemical herbicides. The application of biological weed control offers significant opportunities not only for farmers, nature conservationists and other vegetation managers but also for institutions and companies that wish to sell plant protection services and products, and for the public that demands safe food and a visually attractive and different environment.

1.3.4. Integrated Weed Management System

Integrated Weed Management Systems (IWMS) is usually considered as part of Integrated Pest Management Systems (IPMS) that is an approach in which principles, practices, methods, materials and strategies are chosen to control pests minimising undesirable results (Shaw, 1982; Smith 1991). IWMS is a systems approach (Swanton & Murphy, 1996) encompassing different methods of weed management together with effective education and extension of the management components that takes into account the whole range of issues from agricultural production to economic losses, risks to human health and the environment and energy requirement (Shaw, 1982; Blair & Parochetti, 1982; Lovett & Knights, 1996). The objectives of IWMS are the reduction of losses caused by weeds, costs of control, energy and labor requirements, ensure adequate supply of food, improve environmental quality and maximise producer profits (Penner, 1982; Shaw, 1982; Fischer *et al*., 1993).

IWMS combines the use of several methods (Chisaka, 1977; Smith, 1991; Lovett & Knights, 1996) which can be summarised as:

- Ecological methods that include multiple-pest-resistant, high yielding, well-adapted crop cultivars that resist to weed competition, fertiliser management to give the crop competitive advantage, careful crop rotation, optimum crop plant population and the use of crop cultivars that form a canopy for shading early season weed growth, are viable parts of the

system as well as the use of allelopathy in crop plants to interfere with weeds. Such methods also include the use of judicious irrigation practices.

- Physical methods include appropriate cultivation, field sanitation and harvesting methods that do not spread weed seeds, appropriate seedbed tillage and seeding methods that enhance crop growth minimising weed growth. Minimum tillage, direct drilling and zero tillage to reduce disturbance of the soil systems which can be enhanced by chemical methods will also fall into this category of control method.
- Chemical methods of weed management include the use of herbicides and genetically engineered herbicide-resistant crops. However, it is important that herbicide-resistant crops are not promoted as a panacea, but as a component of IWMS.
- Biological methods usually include the use of organisms such as pathogens, insects, plants, fungi and herbivores. The use of bioherbicides may present the best choice of biological methods in cultivated crops.

1.3.5. Phytopathogenic fungi

New herbicides have become of great interest due to either the few natural product derived commercial herbicides already in use or the rapidly evolving resistance to current herbicides. This supports the need to expend for more efforts on a natural product derived herbicides and makes attractive the prospect of evaluating a vast number of undiscovered or understudied natural compounds that are likely to have biological activity (Cimmino *et al*., 2015). The identification and the biological and molecular characterization of microorganisms, useful as biocontrol agents or as producers of bioactive compounds, is of great interest for the modern and environmentally friendly agriculture. Among the microorganisms, fungi are the most common pathogens of plants and for weeds as well. Some insects and fungi, which satisfy the criteria of efficacy, specificity and long-time persistence, have been already commercialized mainly outside from Europe (Bottiglieri *et al*., 2000). The use of phytopathogenic fungi in biological control of weeds may represent a promising

alternative to the use of chemicals or in IWMS. Several researches have been carried out in this field according to the two fundamental strategies: the inundative and the classical method. The first one consists in the application of the pathogenic agent in the environment, as for the herbicides, reason for what these pathogens are usually called "mycoherbicides". With the classical approach the biocontrol agent is introduced in a restricted infested area and, subsequently, allowed to spread. An alternative approach for weed biocontrol is the use of toxic metabolites produced by weed pathogens, in addition or in alternative to the pathogen, or in integrated weed control programmes. The replacement or the integration of traditional chemical control methods for plant disease through the use of microorganisms and/or their bioactive metabolites reduces the environmental impact of agricultural productions and increases the agricultural biological production, whose demand is augmenting in the national and international markets. In this view, the bioactive secondary metabolites could play an interesting role in the induction of disease symptoms (phytotoxins, and phytohormones) or defence response (elicitors).

The first approach is the isolation of microorganisms from tissues of infected infesting plants, followed by the selection of the strains with higher specificity and virulence. The second step is to find the best conditions for the *in vitro* growth of the fungi to obtain culture filtrates with high phytotoxicity against the host plants. The following step expects the isolation, characterization and in some cases the derivatization of the phytotoxins which can then be tested as potential herbicides.

Finally, the knowledge of the chemical structure of these substances may allow the partial or total synthesis of the most appropriate natural herbicide. Furthermore, (if they are a virulent factor), the toxins could be used in indirect mode as biomarkers, to select the best fungal strain or to optimize the conditions for their large scale production (Evidente, 2006; Cimmino *et al*., 2015). Moreover, they could be used in combination with low dose of herbicides and the phytopathogenic fungus in order to develop an Integrated Weed Management Strategy.

1.4. Fungal phytotoxins

Plant pathogens are good sources of potent phytotoxins (Abbas & Duke, 1995), as they usually kill tissues before they consume them. In spite of this, the fungi that kill weed species have received relatively little attention in natural product herbicide discovery efforts, with a notable exception. Maculosin, produced by *Alternaria alternata*, a pathogen responsible for diseased spotted knapweed (*Centaurea maculosa* Lam.), is the first phytotoxins with a high degree of host specificity. Moreover, other studies on the biological activity of this phytotoxin and its practical application as a knapweed control agent were described in previous work by Strobel (1991).

Almost all fungal species produce phytotoxic metabolites (Cimmino *et al*., 2015). Phytotoxins are defined as microbial metabolites that are harmful to plants at very low concentrations. A lot of plant pathogenic fungi produce toxins in cultures *in vitro* and on hosts *in vivo*. Frequently, these compounds play an important role in the pathogenesis being able to reproduce some or even all the symptoms of the disease. In many cases the toxins are low molecular weight compounds belonging to a variety of class of natural compounds. They are able to spread from the site of the infection to surround tissues or to move within the plant. The virulence of the plant pathogen may depend on its capability to synthesize one or more toxins.

Fungal phytotoxins have facilitated advances in understanding of various phenomena in plant and fungal physiology, biochemistry, genetics, and molecular biology. During the past few decades, phytotoxins have been employed as tools contributing to fundamental discoveries in plant pathogenesis, host specificity, mechanisms of resistance and susceptibility, secondary metabolism, fungal genome organization, plant cell and organelle functions, and fungal ecology.

Fungal phytotoxins can be classified as host-selective or non-selective. Although it is difficult to find a clear line of demarcation, host selective toxins are usually highly toxic only to host-species or cultivars susceptible to the producing pathogen. Non-host or resistant cultivars are less sensitive to these toxins (Graniti *et al*., 1989).

It is possible to isolate phytotoxins from infected plant tissues and germinating conidia of fungi, but this approach in not productive because of the low content of the target compounds. Therefore, in order to isolate phytotoxins in sufficient amounts for studies of chemical and biological properties, the fungi are cultured in liquid nutrient media (the average yield ranges from 1 to 50 mg per 1 L of liquid culture). In a number of cases, it is possible to isolate phytotoxins in settings that involve solid phase fermentation on natural substrates (Berestetskiy, 2008).

Phytotoxins production is sensitive to a number of different factors (e.g., the composition of the medium, its acidity, the duration and conditions of culturing), most of which are not identified in advance as being able to affect the process. Distinct strains of the same species may be very considerably in their ability for phytotoxins production (Berestetskiy, 2008). Microorganism strains are genetically unstable, and their storage or reinoculation may adversely affect the ability to produce toxins (Kale & Bennet, 1992).

Phytotoxins produced by fungal pathogens cause necrotic symptoms in many cases. It has been long assumed that such pathogens kill host tissue by producing the toxin before the colonization and live as saprophytes from the dead substrate. Actually, leakage of cell constituents frequently occurs after the application of host-specific phytotoxins and non-host-specific phytotoxins.

Some examples of phytotoxic metabolites extracted and purified from different fungal species in the last years with potential practical application for weed control are illustrated in the next paragraph of this section.

1.5 Phytotoxins in the management of weeds.

The perthotrophic fungal species *Ascochyta caulina* was proposed as mycoherbicides against *Chenopodium album* L. (common lambsquarters or fat-hen), one of the most successful colonizing species (Allard, 1965; Evidente *et al*., 1998), which has been reported to be a trouble in plantations of sugar beets, potatoes, maize, cereals, and vegetables all over the world (Holm *et al*., 1977). In most crops it is currently controlled by herbicides, but in maize and some vegetable crops the weed

is relatively insensitive or has become resistant to them (Myers & Harvey, 1993). Thus, biological control using pathogens was considered a suitable option.

From the culture filtrates of *A. caulina*, a new *N*-glucoside of a very unusual *bis*-amino acid, named Ascaulitoxin (**1**, Fig. 1.5.1) and characterized as the N^2-*β*-D-glucopyranoside of the 2,4,7-triamino-5-hydroxy octandioic acid (Evidente *et al*., 1998), was isolated together with its aglycone and another non proteic toxic amino acid characterized as *trans*-4-aminoproline (**2**, Fig. 1.5.1) (Evidente *et al*., 2000). The relative configuration of **1** was assigned by NMR analysis, applying for the first time the Murata's method (Matsumori *et al*., 1999) to a compound containing an amino group (Bassarello *et al*., 2001)**,** while the absolute configuration of **2** was determined by a chemical method adopting a well known synthetic procedure (Portoghese & Mikhail, 1966; Andreatta *et al*., 1967) and the toxin finally identified as (+)-*trans*-4-D-aminoproline. Although the *trans*-4-aminoprolines are well known as synthetic compounds, this represents the first isolation of the (+)-*trans*-4-D-aminoproline as a naturally occurring compound and as a phytotoxin produced by *A. caulina*.

Assayed at 30 µg droplet^{-1} on punctured leaves of host and non-host weeds and cultivated plants, ascaulitoxin (**1**) showed a different degree of phytotoxicity on the tested species. Clear necrosis appeared on some tested weeds (common sowthistle, annual fleabane, noogoora burr and tree of heaven) and on cultivated plants (pea and cucumber) and still clear, but in reduced size, on tomato and redroot pigweed. Compound **1** showed no antimicrobial activity when assayed up to 100 µg per disc on fungi (*Geothricum candidum*) and on bacteria (*Pseudomonas syringae* and *Escherichia coli*) (Evidente *et al*., 1998). Assayed at 1 mg mL^{-1} on punctured leaves **2** had a severe effect on the host plant, causing the rapid appearance of large necrosis surrounding the puncture point. An interesting aspect is the lack of toxicity when it was assayed on several monocots, both cultivated (*Triticum durum*, *Avena sativa* and *Hordeum vulgare* L.) and wild (*Phalaris canariensis* L., *Alopecurus myosuroides* and *Avena fatua* L.). The toxin lacked antifungal and antibiotic activities when assayed up to 50 µg disk^{-1} on *G. candidum* and on *P. syringae* and *E. coli*, as

already described above for ascaulitoxin (**1**) and had no zootoxicity when tested up to 40 µg mL^{-1} of sea solution on brine shrimp larvae (*Artemia salina*) (Evidente *et al*., 2000). Finally, the aglycone of **1**, the 2,4,7-triamino-5-hydroxyoctandioic acid (**3**, Fig. 1.5.1), was isolated from the mixture of toxins obtained by basic eluate of cation exchange chromatography carried out on the fungal culture filtrates (Evidente *et al*., 2001a). The three toxins produced by *A. caulina* were used in mixture to enhance the efficacy of this mycoherbicide agent for the biological control of the noxious weed *C. album* L.. Greenhouse experiments showed that the use of toxin solutions (at 1 mg mL^{-1}) in conjunction with spores of *A. caulina* (at 10^{-6} mL^{-1}) strongly improved the biocontrol efficacy of this fungus by more than 30%. Furthermore, the simultaneous application of toxins or fungal spores, together with low doses of synthetic herbicides (metribuzin and rimsulfuron at 1/5 of the labeled rate), gave better results than single-agent treatments (Vurro *et al*., 2001). To optimize and maximize the toxins production by fermentation, a new, simple and inexpensive HPLC method was developed (Avolio *et al*., 2011). Such new HPLC method allows rapid evaluation of the toxin content in the fungal culture filtrates and thus easy selection of the best fungal strain to use for toxin large scale production. The simplification and scaling up of the entire process was optimized allowing the fast and easy purification of large volumes of fungal filtrates produced also by a bioreactor and the harvest of large amounts of toxins mixture. The method was proposed as potential for scale up to a pre-industrial level (Avolio *et al*., 2011).

The ecotoxicological profile of the toxins produced by *A. caulina* was investigated both on aquatic (algae, *Daphnia*, fish) and terrestrial organisms (earthworms). With the exception of *Daphia magna*, the aquatic organisms were not particularly sensitive. In fact, for algae (*Pseudokirchneriella subcapita*) and fish (*Brachydanio rerio*), according to the GHS (Globally Harmonised System of Classification and Labelling of Chemicals), the mixture of toxins exceeded both class III and class II, respectively, for the acute and chronic aquatic toxicity categories (not harmful). On the other hand, for *D. magna*, the mixture of toxins can be categorized in acute class III and chronic class II, respectively (hazardous to the aquatic environment). Finally, the results obtained in both acute and

chronic toxicity tests with *Eisenia foetida* indicated a very low toxicity for terrestrial organisms. In general, the comparison of the ecotoxicological profile of the toxins with other herbicides has shown a lower ecotoxicity for the tested mixture revealing their potential as ecofriendly herbicide (Fumagalli *et al*., 2013).

A new phytotoxic enol tautomer of 4-pyridylpyruvic acid, named ascosonchine (**4**, Fig. 1.5.1), was isolated from the culture filtrate of *Ascochyta sonchi*, proposed as a potential biocontrol agent of *Sonchus arvensis* L., a very dangerous perennial weed of important agrarian crops. Ascosonchine (**4**), characterized as (*Z*)-2-hydroxy-3-(4-pyridyl)-2-propenoic acid, showed selective herbicidal properties, not associated with antibacterial, antifungal or zootoxic activities (Evidente *et al*., 2004).

Assayed on several weedy and cultivated plants, both monocots and dicots, at 15 mg/droplet, **4** showed interesting selective herbicidal properties, that are not associated with antibacterial, antifungal or zootoxic activities. In fact, **4** was completely ineffective on all the solanaceous species assayed (*Lycopersicon esculentum* L., *Solanum melongena* L., *Caspicum annum* L., *Solanum tuberosum* L.), was slightly active or almost inactive on leguminous (*Phaseolus vulgaris* L. and *Cicer arietinum* L.) and cucurbitaceous (*Cucumis melo* L. and *Cucurbita pepo* L.) plants, but caused severe necrosis on many other species, such as *Euphorbia helioscopia* L., *Salvia officinalis* L., *Valerianella locusta* L., or *T. durum* L.. This semi-selective toxin could have practical applications as a herbicidal compound. It is interesting to note that the toxin is still very active when used at a quite low concentration.

Different strains of *A. sonchi*, collected in Russia and Norway, were investigated for their ability to produce **4** by applying an optimized HPLC method. The majority of them produced ascosonchine, whereas two strains, C-177 and S-9, though virulent to weeds, did not produce such toxin. The fungus was re-classified on the basis of epidemiological, morphological and biochemical studies as *Phoma exigua* var. *exigua* (Cimmino *et al*., 2008). When grown in liquid and solid cultures, they were able to produce *p*-hydroxybenzaldehyde, cytochalasins B, F, Z2 and Z3, and deoxaphomin (**6**, **7**, **8**, **9** and **10**, Fig. 1.5.2). Cytochalasins are a large group of fungal metabolites

produced by several genera of fungi. The first two fungal cytochalasins isolated were cytochalasins A and B (**5** and **6**, Fig. 1.5.2), but then sixty different cytochalasins have been purified, identified and grouped in different sub-groups based on the size of the macrocyclic ring and the substituent at C-3 of the perhydroisoindolyl-1-one residue. The structure of cytochalasins, their biosynthesis, and relationships between structure and activity were recently reviewed (Scherlach *et al*., 2010).

Four new cytochalasins, named phomachalasins A-D (**11**-**14**, Fig. 1.5.2) were successively isolated from the two above cited strains C-177 and S-9 of *P. exigua* var. *exigua*. They were characterized as three new closely related 26-oxa[16] and one new [15]cytochalasan belonging to a new subgroup of cytochalasans bearing a 1,2,3,4,6,7-hexasubstituted bicycle[3.2.0]heptene joined to the macrocyclic ring between the C-20 and C-23. None of the four new metabolites showed either phytotoxic or antimicrobial activity probably due to the heavy modification of both functionalities and the lower conformational freedom of the macrocyclic ring due to its junction with the bulky and quite rigid new bicycle, namely bicycle[3.2.0]heptene moiety (Evidente *et al*., 2011a).

From a wheat solid culture of *Pyrenophora semeniperda*, a pathogen proposed for the biological control of *Bromus tectorum* (cheatgrass, downy brome), an exotic winter annual grass weed that causes serious losses in intensive agriculture, particularly in winter cereal crops (Stahlman & Miller, 1990; Ostlie & Howatt, 2013) and is also a major problem on rangelands in the western U.S, cytochalasins Z2 and Z3 (**15** and **16,** Fig. 1.5.3) were isolated for the first time, together with other well known cytochalasins B, F (**6** and **7**, Fig. 1.5.2), T, Z1, and deoxaphomin (**17** and **18** Fig. 1.5.3; **10**, Fig. 1.5.2) (Vurro *et al*., 1997; Evidente *et al*., 2002). The two cytochalasins Z2 (**15)** and Z3 (**16)**, which showed together with cytochalasin Z1 (**18**) an original structure between the 24-oxa[14]cytochalasans subgroup, were biologically characterized by testing their capacity to inhibit the germination of wheat and tomato seedlings in comparison with the other above cited cytochalasins and the 21,22-dihydroderivative of cytochalasin B (Evidente *et al*., 2002). Assayed on the leaves of both *C. arvense* L. and *S. arvensis* L., deoxaphomin demonstrated the highest level of

toxicity on leaves of *S. arvensis* L.. Cytochalasin **15** appeared to be the less toxic cytochalasan on both plants due to the lack of the secondary hydroxy group on C-7, (Scherlach *et al*., 2010; Cimmino *et al*., 2008) which in the previous SAR study appeared to be one of the most important feature to impart activity (Vurro *et al*., 1997; Evidente *et al*., 2002).

Further investigation of the same culture filtrate led to isolate a new phytotoxic sesquiterpenoid penta-2,4-dienoic acid, named pyrenophoric acid (**19**, Fig. 1.5.3) and characterized as new substituted 3-methylpenta-2,4-dienoic acid (Masi *et al*., 2014a). The relative stereochemistry of **19** was assigned using $^{3}J_{H,H}$ couplings NOESY experiments, while its absolute configuration was determined by applying an adavanced Mosher's method (Ohtani *et al*., 1989). Assayed in a cheatgrass coleoptile elongation test at 10^{-3} M, **19** showed strong phytotoxicity, reducing coleoptile elongation by 51% relative to the control. In a 10^{-4} M mixture, its negative effect on coleoptile elongation was additive with that of cytochalasin B (**6**) demonstrating that the extract toxicity observed in earlier studies was due to the combined action of multiple phytotoxic compounds (Masi *et al*., 2014a).

When the fungus was grown on host cheatgrass (*B. tectorum*) seeds, cytochalasins A, B, F and Z3 (**5**-**7**,**9**), as well as deoxaphomin (**10**) and pyrenophoric acid (**19**) were reisolated together with two new phytotoxic sesquiterpenoid acids, named pyrenophoric acids B and C, and the well known abscisic acid (**20**-**22**, Fig. 1.5.3). Pyrenophoric acids B (**20**) and C (**21**) differed from **19** and themselves for the functionalities and stereochemistry of the heptasubstituted cyclohexane ring (Masi *et al*., 2014b).

Seedling bioassays with **19** and absisic acid (**22**) demonstrated a hierarchical order of toxicity. All four compounds caused significant 5-day coleoptile and radicle length reductions relative to the control even at the lower concentration, demonstrating their potential role as phytotoxins. Not surprisingly, **22** was by far the most active compound and was able to suppress most germination, to delay the germination of seeds which did germinate, to completely suppress coleoptile elongation, and to greatly reduce radicle length relative to the control. Whereas, among the others

only **20** was able to reduce 7-day germination and caused significant germination delay relative to the control. Pyrenophoric acid (**19**) caused more coleoptile growth suppression than pyrenophoric acid C (**21**), but only at the higher concentration. The relative toxicity ranking of the four compounds was therefore abscisic acid >> pyrenophoric acid B > pyrenophoric acid > pyrenophoric acid C. When cytochalasin A (**5**), deoxaphomin (**10**)**,** and cytochalasin F (**7**) were assayed in comparison with cytochalasin B (**6**) on 5-day coleoptile and radicle length at both concentrations (10^{-3} and 10^{-4}M) relative to the control, clearly demonstrated that their toxicity was no additive. When **19** was combined in pairwise tests with each cytochalasin, a synergistic interaction increased toxicity to seedling coleoptiles, especially with **6**, but this synergistic growth suppression effect was not observed for radicles (Evidente *et al*., 2002; Masi *et al*., 2014b).

When grown in liquid culture *P. semeniperda*, showed the ability to produce new spirotoxins, another class of natural compound widely produced from phytopatogenic fungi (Cimmino *et al*., 2015). They were identified as a novel spirocyclic γ-lactam, named spirostaphylotrichin W (**23**, Fig. 1.5.4), and the well known and closely related spirostaphylotrichins A, C, D, R and V, as well as triticone E (**24**-**26**, **27**, **28** and **29**, Fig. 1.5.4). **23** was characterized using essentially spectroscopic methods and comparing its data with those reported for the other above cited spirostaphylothrichin. Its relative configuration was assigned using NOESY experiments and by comparison with data of spirostaphylotrichin V (**28**) and triticone E (**29**). The spirostaphylotrichins isolated from *P. semeniperda* differed between them for the functionalities and stereochemistry of both the cyclohexenone and γ-lactam rings. In a *B. tectorum* coleoptile bioassay at concentration of 10^{-3} M, spirostaphylotrichin A (**24**) proved to be the most active compound, followed by spirostaphylotrichins C (**25**) and D (**26**). Spirostaphylotrichin W (**23**) and V (**28**) showed mild toxicity while spirostaphylotrichin R (**27**) and **26** were not active. When tested on host and non host plants by leaf puncture bioassay, spirostaphylotrichins **24-26** caused the appearance of necrotic spots while the other compounds were inactive (Masi *et al*., 2014c).

A new nonenolide named stagonolide (**30**, Fig. 1.5.5) was isolated as the main phytotoxin from pycnidial fungus *Stagonospora cirsii*, a foliar pathogen proposed as mycoherbicide for the biocontrol of *C. arvense* L. (Evidente *et al*., 2011b). Assayed on the host plant, **30** caused first symptoms (necrotic) about 10 h post-application. At 5 x 10^{-3} M, **30** showed no selectivity among host and non-host Asteraceae members. Besides *C. arvense* L., *Alcea rugosa* , *Heliantus annuus* L., *Lactuca sativa* L., *S. arvensis* L., and *Mentha piperita* were also highly sensitive to the toxin. However, two Solanaceae species were insensitive. Compound **30** was low toxic to *Colpoda steinii* (Protozoa) while weakly suppressive against the fungus *Candida tropicalis* and bacteria (Yuzikhin *et al*., 2007). The same fungus, grown in solid culture, exhibited an increased capacity to produce nonenolides. Eight new nonenolides, named stagonolides B-I (**31**-**38**, Fig. 1.5.5), were isolated together with the well known modiolide A (**39**, Fig. 1.5.5), a nonenolide previously isolated from *Paraphaeosphaeria* sp., a fungus separated from the horse mussel (Evidente *et al*., 2008a; Evidente *et al*., 2008b). They differed from **30** and between them for both the functionalities and the conformational freedom of nonenolide ring. Leaf disk-puncture assays at 1 mg mL^{-1} showed that only stagonolides H and I (**37** and **38**) and modiolide A (**39**) were phytotoxic to *C. arvense* L.. Only **37** inhibited chicory seedling root growth. The most potent toxin, stagonolide H, showed selectivity when tested on leaves of eight different plants. *C. arvense* L. being the most sensitive to the compound (Evidente *et al*., 2008b).

From the culture filtrates of *Phyllosticta cirsii*, another fungal pathogen poposed for the control of *C. arvense* L. four new oxazatricycloalkenones, named phyllostictines A-D (**40**-**43**, Fig. 1.5.6, Table 1 ESI), were isolated and characterized. The absolute configuration of the secondary hydroxylated carbon C-15 of phyllostictine A (**40**) was determined by applying the above cited adavanced Mosher's method (Ohtani *et al*., 1989). **40** was characterized by a pentasubstituted γ-lactam and an hexasubstituted trihydrofurane ring included into a ten membered macrocyclic ring. Phyllostictines B (**41**) and C (**42**) differed from **40** for both the functionalities and ring size, while phyllostictine D (**43**) also differed for the presence of a tetrasubstituted γ-lactam ring instead of the

γ-lactam ring (Evidente *et al*., 2008c). Tested by leaf-puncture assay on the host plant **35** proved to be highly toxic. At first, the phytotoxicity appears to decrease when both the dimension and the conformational freedom of the macrocyclic ring change, as in phyllostictines **41** and **43**, and it is totally lost when also the functionalization of the same ring was heavily modified, as in **42**. Beside its phytotoxic properties, phyllostictine A has no antifungal activity, an interesting antibiotic activity only against Gram+ bacteria, and a noticeable zootoxic activity when tested at high concentrations. The integrity of the oxazatricycloalkenone system appears to be an important feature to preserve these activities (Evidente *et al*., 2008c). Phyllostictines A-D are the first fungal metabolites belonging to the oxazatricycloalkenone group described as natural compounds with interesting biological activities (Evidente *et al*., 2008c). **40** was further studied to develop a rapid analytical method to estimate its content in culture preparations and to assess the phytotoxic effect for potential weed control on tobacco protoplasts by flow cytometric analysis, and on *C. arvense* L. protoplasts, by fluorescence microscopy (Zonno *et al*., 2008).

Further purification of the organic extract of culture filtrates of the same fungus provided two other metabolites, named phyllostoxin and phyllostin (**44** and **45**, Fig. 1.5.6), characterized as a new pentasubstituted bicyclo-octatrienylacetic acid ester and a new pentasubstituted hexahydrobenzodioxine carboxylic acid methyl ester, respectively (Evidente *et al*., 2008d). Tested on punctured *C. arvense* L. leaves, **44** proved to be highly phytotoxic, causing rapid and large necrosis, whereas **45** had no phytotoxicity in this bioassay. These results further support the focused approach of finding novel metabolites with herbicidal properties by looking at the culture extracts of weed fungal pathogens (Evidente *et al*., 2008d).Afterwards, from the same fungus was isolated scytolide (**46**, Fig. 1.5.6), a natural analogue of **45** differing for the presence of an exomethylene group instead of the secondary methyl group of the dioxine ring. The same compound was also previously obtained from *Scytalidium uredinicola* (Ayer *et al*., 1993). The X-ray crystal structure of **45** was successively determined together with the relative configuration of the four chiral centers C3/C4a/C8/C8a, which resulted to be *R*/*S*/*R*/*S* (Tuzi *et al*., 2010). The 3*S*,4a*R*,8*S*,8a*R* absolute

configuration was assigned to naturally occurring (-)-**45** by computational analysis of its optical rotatory dispersion (ORD), electronic circular dichroism (ECD), and vibrational circular dichroism (VCD) spectra, while 4a*R*,8*S*,8a*R* absolute configuration was assigned to (-)-scytolide only by ECD and VCD, because in this case ORD analysis turned out to be unsuitable for absolute configuration assignment (Mazzeo *et al*., 2013). This study shows that in the case of flexible and complex natural products only a concerted application of more than a single chiroptical technique permits unambiguous assignment of absolute configuration (Mazzeo *et al*., 2013).

1.6. Biological control of *Carthamus lanatus*

Saffron thistle (*Carthamus lanatus* L. ssp. *lanatus*) is a widespread winter-growing annual weed of both pastures and crop throughout Australia introduced from the Mediterranean region (Parsons & Cuthbertson, 1992). It is considered the most economically important thistle species in New South Wales (Briese, 1988; Sindel, 1996) and is one of the weeds targeted by the Australian Cooperative Research Centre for Weed Management Systems (Dellow *et al*., 2002). It is declared noxious in all Australian States (Shorten, 2007). Poor results of mechanical (Shorten, 2007) and chemical control have made this weed a suitable target for biological control (Briese, 1988). In order to develop a mycoherbicide against this weed, a number of pathogenic strains of *Phomopsis* sp. have been identified from naturally infected saffron thistle plants in Australia (Crump *et al*., 1996a), and their potential as mycoherbicides against the host has been evaluated (Crump *et al*., 1996b). Ash *et al*. (2010) showed that this pathogen was distinct from other species of *Phomopsis* sp. commonly found on grain legume crops. More recently the teleomorph of this pathogen was identified as *Diaporthe gulyae* on the basis of morphology, DNA sequence analysis, and pathology studies (Thompson, 2011), and it has proved to be pathogenic to sunflower (*Helianthus annuus* L.), causing severe stem cankers. Fungal metabolites have long been studied for their potential direct use as novel agrochemicals or as leads for new natural pesticides and to discover novel mechanisms of action (Dayan *et al*., 2009; Huter, 2010). The ability of *D. gulyae* to produce phytotoxic

metabolites in culture was investigated, and a new phytotoxic geranylhydroquinone, named phomentrioloxin (**47**, Fig. 1.6.1), was isolated as the main phytotoxic metabolite. It was characterized as (1*R*,2*R*,3*R*,4*R*)-3-methoxy-6-(7-methyl-3-methyleneoct-en-1-ynyl)-cyclohex-5-ene-1,2,4-triol using spectroscopic and chemical methods combined with X-ray analysis (Cimmino *et al*., 2012). The absolute configuration of the chiral centers was determined by applying the above cited advanced Mosher's method (Ohtani *et al*., 1991). Subsequently , a structure-relationship study (SAR) was carried out using seven derivatives (**48-55,** Fig. 1.6.1) of the toxin that were tested for phytotoxic, antimicrobial, and zootoxic effects. Results from this study showed that the hydroxy groups at C-2 and C-4, the cyclohexentriol, and to a lesser extent the unsaturations in the geranyl side chain are important for phytotoxicity (Cimmino *et al*., 2013a).

Taking into account that the culture filtrate showed a phytotoxicity higher than expected from the phomentrioloxin content, it seems to be interesting to further investigate the organic extract of the fungus. This is one of the main aim of the present thesis.

Moreover, two novel plant pathogenic fungal species, namely *Diaporte kongii* and *Diaporthe kochmanii*, associated with stem canker in Australia, were recently described (Thompson, 2011). Although less damaging pathogens in respect to *D. gulyae*, both *D. kongii* and *D. kochmanii* in preliminary experiments proved to produce phytotoxic culture filtrates; a study has been then undertaken in order to isolate the toxins and to evaluate their potential as natural herbicides.

1.7. Biological control of *Sonchus arvensis*

Sonchus arvensis L., is commonly called perennial sowthistle (Donald, 1990; Lemna & Messersmith, 1990). This weed grows vigorously and forms dense patches. It spreads with underground shoots growing horizontally that give rise to new aerial shoots. Prolific seed production by *S. arvensis* serves for the occupation of new area. This plant species is considered to be an important weed in Europe and North America as it infests many habitats such as cultivated fields, roadsides, pastures and rangelands, railway embankments, and lawns. It is not easy to

eradicate *S. arvensis*, and all control methods require follow-up: combinations of mechanical, cultural, and chemical methods are more effective than any single method used alone (Kloppenburg & Hall, 1990). Herbicides recommended for chemical control of *S. arvensis* in nonorganic cropping systems are restricted to a few active substances as above reported at paragraph

Recently, the fungus *Alternaria sonchi* has been evaluated as a possible biocontrol agent of sowthistle (Gannibal *et al*., 2006). Species belonging to the genus *Alternaria* are known to produce bioactive metabolites, including non-host phytotoxins: solanapyrones, isolated from cultures of *A. solani*, the causal agent of early blight of tomato and potato (Ichara *et al*., 1983); dextrusins and cyclodepsipeptides, isolated from *A. brassicae*, which causes diseases on numerous oil-yielding, vegetable, condiment, ornamental, and wild and some cultivated and wild noncruciferous plants (Tewari & Bains, 1997); brefeldin and α,β-dehydrocurvularin isolated from *A. zinniae* (Vurro *et al*., 1998) ;several phytotoxins belonging to different groups of natural compounds including toxic tetramic acids, dibenzo[α]pyrone moiety containing compounds, and alternatoxins I and II (Cole & Cox, 1981, Turner & Altridge, 1983).

Phytotoxins produced by *A. sonchi* have not been studied so far.

Two new phytotoxic polycyclic ethanones, alternethanoxin A, **56** and B, **57** (Fig. 1.7.1), were isolated from the solid culture of *Alternaria sonchi* (Evidente *et al*., 2009). They appeared to be toxic on the fungal host plant and a number of non-host plants but did not possess antimicrobial activity. The absolute stereochemistry of the secondary hydroxylated carbon C-6 of alternethanoxin A (**56**) was determined by applying the above cited Mosher's method (Ohtani *et al*., 1991). The triacetyl and 4,6-*O*,*O*′-dimethyl ether derivatives of **56** (**58** and **59,** Fig. 1.7.1) were hemisynthesized and assayed in comparison to **56** and **57** on *S. arvensis*. The results obtained demonstrated that the hydroxy group at C-4 of the C ring is a structural feature important for the phytotoxicity while the other one at C-1 and the hemiacetal hydroxy group at C-6 are not essential (Evidente et al., 2009).

A further investigation of organic extracts of *A. sonchi* solid culture allowed the isolation of three other bioactive metabolites, whose isolation and chemical and biological characterization is another objective of the present thesis.

1.8. Biological control of *Chenopodium album*

More recently, another pathogenic Sphaeropsidales, *Phoma chenopodiicola*, was proposed as a potential mycoherbicide for the control of *Chenopodium album* for previously as above reported had been proposed *A. caulina*. Considering that leaf and stem pathogenic Sphaeropsidales are well known as toxin producers, it was considered to be worthwhile studying the production of toxic metabolites by *P. chenopodiicola*. A new phytotoxic unrearranged *ent*-pimaradiene diterpene, named chenopodolin (**62,** Fig. 1.8.1), was isolated from the liquid culture of this pathogen and characterized as (1*S*,2*S*,3*S*,4*S*,5*S*,9*R*,10*S*,12*S*,13*S*)-1,12-acetoxy- 2,3-hydroxy-6-oxopimara-7(8),15-dien-18-oic acid 2,18-lactone (Cimmino *et al*., 2013b). At a concentration of 2 mg/mL, the toxin showed phytotoxic activity, causing necrotic lesions to leaves of *Mercurialis annua*, *Cirsium arvense* and *Setaria viridis*. Five key derivatives (**63-67**, Fig. 1.8.1) were prepared in order to figure out the structural features responsible of the activity of the toxin. The bioassays indicated that the hydroxy group at C-3 and the α,β-unsaturated ketone at C-6 are important features for the phytotoxicity (Cimmino *et al*., 2013b).

Along with chenopodolin, from the organic extract of the liquid culture of *P. chenopodiicola* were also isolated three novel tetrasubstituted furopyrans, named chenopodolans A–C (Cimmino *et al*., 2013c). The structures of chenopodolans A–C (**68-70**, Fig. 1.8.2) were established by spectroscopic and chemical methods as 2-(3-methoxy-2,6-dimethyl-7a*H*-furo[2,3-b]pyran-4-yl)-butane-2,3-diol, 1-(3-methoxy-2,6-dimethyl-7a*H*-furo[2,3-b]pyran-4-yl)ethanol and 3-methoxy-2,6-dimethyl-4-(1-methylpropenyl)-7a*H*furo[2,3-b]pyran, respectively. The absolute configuration *R* to the hydroxylated secondary carbon (C-11) of the side chain at C-4 of chenopodolan A was determined by applying the above cited advanced Mosher's method (Ohtani et al, 1991). Assayed

by leaf puncture on host and non-host weeds chenopodolans A and B, and the 11-*O*-acetylchenopodolan A showed a strong phytotoxicity. These results showed that the nature of the side chain attached at C-4 is an important feature for the phytotoxicity. A weak zootoxic activity was only showed by chenopodolan B (Cimmino *et al*., 2013c).

A further analysis of the organic extracts of the fungus, aimed both at re-isolating chenopodolans A–C to assign their absolute configuration, and to understand why the phytotoxicity of the extracts was higher than that expected by the content of chenopodolin and chenopodolans A–C, was undertaken. The isolation and chemical and biological characterization of further toxic metabolites from *P. chenopodiicola* represents one of the main topic of the present thesis.

2. OBJECTIVES

The first aim of the present thesis is the isolation and characterization by spectroscopic technique and chemical methods of the phytotoxic metabolites produced in liquid culture form *Diaporthe gulyae* and *Diaporthe kongii*, two novel plant phatogenic fungal species, associated with the stem canker of sunflower in Australia, and proposed as potential mycoherbicides for *Carthamus lanatus* biocontrol, which is an annual weed widely spread in Australia.

The second aim of the thesis is the isolation and characterization by spectroscopic technique and chemical methods of the phytotoxins produced in solid culture by *Alternaria sonchi*, a fungus proposed as mycoherbicides of *Sonchus arvensis*, a noxious perennial weed widely occurring in the temperate region of the world.

The third aim of the thesis is to isolate and characterize, through the use of spectroscopic techniques and chemical methods, the phytotoxins produced by *Phoma chenopodiicola*, a phatogenic Sphaeropsidales proposed for the control of *Chenopodium album* L., a worldwide weed of arable crop, sugar and maize.

The biological activity of the phytotoxins isolated as potential herbicides, carried out in collaboration with plant phatologist groups, is also reported.

3. MATERIALS AND METHODS

3.1 Fungi

The strains of *Diaporthe gulyae* and *Diaporthe kongii* used in this study were isolated from symptomatic saffron thistle (*C. lanatus*) plants in Australia (Thompson *et al*., 2011) and stored in the fungal collection of the Istituto di Scienze delle Produzioni Alimentari, CNR, Bari, Italy, with the codes ITEM 54025 and ITEM 17141, respectively. The DNA sequences of *D. gulyae* and *D. kongii* strains were previously reported by Ash *et al*. 2011. *D. gulyae* GenBank accession numbers are ITS, JF431299; TEF-1α, JN645803. The fungi were routinely grown on PDA plates at 25 °C as starting material for the production of culture filtrates.

The fungus *Aletrnaria sonchi* Davis was isolated from diseased leaves of *S. arvensis*, and monoconidial isolate (S-102) was deposited in the culture collection of All-Russian Research Institute of Plant Protection, Pushkin, Saint Petersburg, Russia. The isolate was maintained in sterile tubes containing potato dextrose agar.

The fungal strain of *Phoma chenopodicola* was isolated from diseased leaves of *Chenopodium album*. A monoconidial isolate was deposited in the culture collection of both the All-Russian Research Institute of Plant Protection, Pushkin, Saint-Petersburg, Russia (I-13.2), and the Istituto di Scienze delle Produzioni Alimentari, CNR, Bari, Italy (ITEM 12534). The isolate was routinely grown and kept in plates and slants containing potato-dextrose agar (PDA, Sigma-Aldrich, Chemik Gmbh, Buchs, Switzerland).

3.2 General procedures

Optical rotations were measured in $CHCl_3$/CH_3CN/MeOH solutions on Jasco P-1010 and Jasco DIP-370 digital polarimeters; absorption and ECD spectra were recorded at room temperature on a JASCO J815 spectropolarimeter, using 0.5 mm and 0.1 mm cells in the 180–400 nm range and a 2.0 mm cell in the 400–600 nm range and concentrations of about 1×10^{-3} M.

IR spectra were recorded as glassy film on a Perkin-Elmer Spectrum One FT-IR Spectrometer and UV spectra were recorded in MeOH solutions on a Perkin-Elmer Lambda 25 UV/Vis spectrophotometer.

^{1}H- and ^{13}C-NMR spectra were recorded at 600 and 400 MHz in $CDCl_3$ or MeOD on Bruker spectrometers. The same solvents were used as internal standard. Carbon multiplicities were determined by DEPT (Distortionless Enhancement by Polarization Transfer) spectra (Berger & Braun, 2004). DEPT, COSY-45 (Correlated Spectroscopy), HSQC (Heteronuclear Single Quantum Correlation), HMBC (Heteronuclear Multiple Quantum Correlation) and NOESY (Nuclear Overhauser Effect Spectroscopy) experiments (Berger & Braun, 2004), were performed using Bruker microprograms. Chemical shifts are in δ(ppm).

Coupling constants (*J*) are in Hertz. The following symbols were used: *s*: singlet; *br s*: broad singlet; *d*: doublet; *dd*: double doublet; *ddd*: doublet of double doublet; *t*: triplet; *q*: quartet; *m*: multiplet.

HRESI-MS (High Resolution ElectroSpray Ionization Mass Spectroscopy) and ESIMS (ElectroSpray Ionization) spectra were recorded on Waters Micromass Q-TOF Micro and Agilent Technologies 6120 Quadrupole LC/MS instruments, respectively.

Analytical and preparative thin-layer chromatography (TLC) were performed on silica gel plates, Kieselgel 60 F254, 0.25 and 0.5 mm, respectively (Merck, Darmstadt, Germany). The spots were visualized by either exposure to UV radiation (254 nm) or by spraying first with 10% H2SO4 in MeOH and then with 5% phosphomolybdic acid in EtOH followed by heating at 110°C for 10 min. Column chromatography was performed on a silica gel column, Kieselgel 60, 0.063–0.200 mm (Merck).

4. EXPERIMENTAL

4.1. Production, extraction and purification of phytotoxins from *Diaporthe gulyae* culture filtrate.

The fungus *Diaporthe gulyae* was grown in 1 L Erlenmeyer flasks containing 300 mL of a defined mineral (Pinkerton & Strobel, 1976). Each flask was seeded with 5 mL of a mycelia suspension and then incubated at 25°C for 4 weeks in the dark. After mycelial removal by filtration, The culture filtrates (27.7 L, pH 4.5), having high phytotoxic activity on leaves of host and non host plants, were lyophilized, dissolved in distilled water (1/10 of its original volume), and then extracted by EtOAc (4 × 3 L) previously acidified to pH 2.5 with HCOOH. The organic extracts were combined, dehydrated with anhydrous Na_2SO_4, and evaporated under reduced pressure, yielding a brown solid (20.3 g), showing high phytotoxic activity. This extract was dissolved in EtOAc and then washed with a saturated solution of $NaHCO_3$ to remove 3-nitropropionic acid identified as the main metabolite (**75**, 18.4 g, 692 mg/L, Fig. 5.1.1). The organic phase was dehydrated with anhydrous Na_2SO_4 and evaporated under reduced pressure, affording a brown, oily residue (1.07 g), which showed phytotoxic activity, when tested on above reported. This oil was purified by CC, eluted with $CHCl_3$-*i*-PrOH (9:1), yielding eight groups of homogeneous fractions. The residue of the third fraction (51.8 mg) was further purified on silica gel TLC, eluted with $CHCl_3$−*i*- PrOH−acetone (93:5:2), giving four fractions. The residue of the second fraction obtained as a yellow oil was characterized, as below reported, as phomentrioloxin C (**74**, 2.7 mg, 0.10 mg/L, R*f* 0.49, Fig. 5.1.1). The residue of the third fraction (5.6 mg) was purified by TLC, eluted with $CHCl_3$-*i*-PrOH (95:5), giving a white, amorphous solid identified as 4-methylbenzoic acid (**76**, 5.4 mg, 0.20 mg/L, R*f* 0.54, Fig. 5.1.1). The residue of the fourth fraction of the first chromatographic column was purified by TLC eluted with $CHCl_3$-*i*-PrOH-acetone (93:5:2), giving four homogeneous fractions. The residue of the second fraction (10.3 mg) was further purified by TLC on reversed-phase, eluted with EtOH-H_2O (7:3). One metabolite was obtained as a yellow oil,

characterized as phomentrioloxin B (**73**, 3.3 mg, 0.12 mg/L, R*f* 0.57, Fig. 5.1.1) as reported below. The fifth fraction of the first chromatographic column (120.9 mg) was further purified by TLC, eluted with $CHCl_3$-*i*-PrOH (9:1). Two metabolites were obtained as homogeneous solids, one identified as gulypyrone A (**71**, 7.0 mg, 0.3 mg/L, R*f* 0.46, Fig. 5.1.1), as below reported, and the other one identified as phomentrioloxin (**47**, 23.0 mg, 0.85 mg/L, R*f* 0.32, Fig. 1.6.1) (Cimmino *et al.*, 2012). The sixth fraction (89.6 mg) of the first chromatographic column was purified by TLC, eluted with $CHCl_3$−*i*-PrOH (95:5), giving five homogeneous fractions. The residue of the third fraction (7.3 mg) was further purified by TLC on reversed-phase eluted with EtOH−H_2O (7:3). One metabolite was obtained as a white solid and characterized as gulypyrone B (**72**, 3.5 mg, 0.13 mg/L, R*f* 0.46, Fig. 5.1.1) as reported below.

4.1.1. Gulypyrone A (71), 6-((2*S*)-2-hydroxy-1-methylpropyl)-4-methoxy-5-methylpyran-2-one:

Gulypirone A, obtained as amorphous solid; $[\alpha]^{25}_D$: -46.5 (c 0.2); IR ν_{max} 3407, 1694, 1635, 1560, 1453, 1405, 1246 cm^{-1}; UV λ_{max} nm (log ε) 288 (3.94); ^1H and ^{13}C NMR see Table 5.1.1; HRESI-MS *m/z*: 447 $[2M + Na]^+$, 235 $[M + Na]^+$, 213.1146 (calcd for $C_{11}H_{17}O_4$ 213.1137, $[M + H]^+$).

4.1.2. 9-*O*-Acetyl Derivative of gulypyrone A (77):

Gulypyrone A (**71**, 0.5 mg) dissolved in pyridine (10 μL) was acetylated with acetic anhydride (10 μL) at room temperature for 1 h. The reaction was stopped by addition of MeOH, and the azeotrope, obtained by the addition of benzene, was evaporated by an N_2 stream. The oily residue (2.0 mg) was purified by preparative TLC eluted with $CHCl_3$-*i*-PrOH (97:3), to give 9-*O*-acetylgulypyrone as a homogeneous compound (**77**, R*f* 0.62, 0.8 mg, Fig. 5.1.1).

Derivative **77** had: IR ν_{max} 1731, 1643, 1563, 1541, 1245 cm^{-1}; UV λ_{max} nm (log ε) 283 (2.04); ^1H NMR, δ 5.44 (1H, *s*, H-3), 5.04 (1H, *m*, H-9), 3.81 (3H, *s*, OMe), 3.13 (1H, *quint*, *J* = 7.0 Hz, H-8), 1.97 (3H, *s*, MeCO), 1.94 (3H, *s*, Me-7), 1.30 (3H, *J* = 6.2 Hz, Me- 10), 1.22 (3H, *d*, *J* = 7.2 Hz,

Me-11); ESI-MS (+) *m/z*: 531 $[2M + Na]^+$, 293 $[M + K]^+$, 277 $[M + Na]^+$; APCI-MS, *m/z*: 255 $[M + H]^+$.

4.1.3. (*S*)-α-Methoxy-α-trifluoromethyl-α-phenylacetate Ester of Gulypyrone A (78).

Gulypyrone A (**71**, 0.5 mg) was converted into the corresponding MTPA ester (31) by reaction with (*R*)-(−)-MTPA-Cl (20 μL) in dry pyridine (20 μL). The usual reaction workup yielded **77** (Fig. 5.1.1) as a homogeneous solid (0.9 mg): IR ν_{max} 1744, 1713, 1648, 1566, 1454, 1248 cm^{-1}; UV λ_{max} nm (log ε) 286 (2.68); ^1H NMR see Table 5.1.2; ESI-MS (+) *m/z*: 879 $[2M + Na]^+$, 467 $[M + K]^+$, 451 $[M + Na]^+$; APCI-MS *m/z*: 429 $[M + H]^+$.

4.1.4. (*R*)-α-Methoxy-α-trifluoromethyl-α-phenylacetate Ester of Gulypyrone A (79).

Gulypyrone A (**71**, 0.5 mg) was converted into the (*R*)-MTPA ester of **71** (**79**) by reaction of (*S*)-(+)-MTPA-Cl. The reaction was carried out under the same conditions used for preparing **78** from **71**. **79** (Fig. 5.1.1) was obtained as a homogeneous solid (0.9 mg): IR ν_{max} 1745, 1711, 1648, 1566, 1454, 1245; UV λ_{max} nm (log ε) 286 (2.71); ^1H NMR see Table 5.1.2; ESI-MS (+) *m/z*: 879 $[2\times M + Na]^+$, 467 $[M + K]^+$, 451 $[M + Na]^+$; APCI-MS *m/z*: 429 $[M + H]^+$.

4.1.5. Gulypyrone B (72), 6-((1*E*)-3-hydroxy-1-methylpropenyl)-4-methoxy-3-methylpyran-2-one:

Obtained as amorphous solid; IR ν_{max} 3239, 1694, 1625, 1553, 1421, 1370, 1262 cm^{-1}; UV λ_{max} nm (log ε) 228 (4.55), 323 (4.12); ^1H and ^{13}C NMR see Table 5.1.1; HRESI-MS (+) *m/z*: 443 $[2M + Na]^+$, 249 $[M + K]^+$, 233 $[M + Na]^+$, 211.0985 (calcd for $C_{11}H_{15}O_4$ 211.0970, $[M + H]^+$), 189 $[M + Na - CO_2]^+$; ESI-MS (−) *m/z*: 209 $[M - H]^-$.

4.1.6. Phomentrioloxin B (73), 4,6-dihydroxy-5-methoxy-2-(7-methyl-3-methyleneoct-6-en-1-ynyl)cyclohex-2-enone:

Obtained as yellow oil; $[\alpha]^{25}_D$ +1.9 (c 0.2); IR ν_{max} 3862, 2207, 1734, 1695, 1458 cm^{-1}; UV λ_{max} nm (log ε) 223 (2.84), 278 (2.69), 399 (2.19); ^1H and ^{13}C NMR see Table 5.1.3; HRESI-MS (+)

m/z: 603 $[2M + Na]^+$, 329 $[M + K]^+$, 313.1427 (calcd for $C_{17}H_{22}NaO_4$ 313.1416, $[M + Na]^+$); ESI-MS (−) *m/z*: 289 $[M - H]^-$.

4.1.7. Phomentrioloxin C (74), 2,5-dihydroxy-6-methoxy-3-(7-methyl- 3-methyleneoct-6-en-1-ynyl)cyclohex-3-enone:

Obtained as yellow oil; IR ν_{max} 3831, 2214, 1752, 1673, 1424 cm^{-1}; UV λ_{max} nm (log ε) 231 (2.73) 276 (2.62), 397 (2.05); ^1H NMR see Table 5.1.3; ESIMS (+) *m/z*: 603 [2M + Na]+, 329 $[M + K]^+$, 313 $[M + Na]^+$; ESI-MS (−) *m/z*: 289 $[M - H]^-$, m/z 253 $[M - H - H2O]^-$; APCI-MS (+) *m/z*: 291$[M + H]^+$, 273 $[M + H - H_2O]^+$, 255 $[M + H - 2H_2O]^+$.

4.2. Production, extraction and purification of phytotoxins from *Diaporthe gulyae* grown in bioreactor.

The same strain of *D. gulyae* was also grown in a bioreactor (BIOSTAT C 30, Sartorius Stedim Biotech). Two 1 L Erlenmeyer flasks, each containing 500 mL of PDB (potato-dextrose broth), were inoculated with the actively growing mycelium obtained from six plates of PDA and kept for 2 days in shaking conditions (100 rpm) on a orbital rotary shaker. The whole culture containing the mycelium was then fragmented in sterile conditions with a homogenizer for 2 min. The suspension was injected into the bioreactor (filled with 30 L of *in situ* sterilized M1D medium) (Pinkerton & Strobel, 1991) with the aid of a peristaltic pump and maintained for 2 weeks at a temperature of 26 °C, 80 rpm, and 1 L/min air flux. The culture (30 L, pH 4.5) was then collected, filtered first through gauze and then through filter papers to remove mycelium, and lyophilized. The lyophilized culture filtrates were extracted in the same conditions as previously reported, yielding a brown solid (7.3 g), which was highly phytotoxic. The extract was dissolved in EtOAc and then washed with a saturated solution of $NaHCO_3$ to remove acid compounds using the same procedure as previous reported, giving the mixture of acid compounds as a brown solid (6.4 g) and the neutral and/or basic compounds as a yellow oil (340.0 mg). The acid mixture was washed with small aliquots of EtOAc

to separate as white solids succinic acid (5.8 g, 190 mg/L, Fig. 5.1.2) and 4-hydroxybenzoic acid (**80** and **81**, 82.5 mg, 2.75 mg/L, R*f* 0.32, Fig. 5.1.2). The fraction containing neutral and/or basic compounds has been purified by CC eluted with $CHCl_3$-*i*-PrOH (9:1), yielding eight groups of homogeneous fractions. The residue of the second fraction (109.3 mg) was further purified by CC, eluted with $CHCl_3$-*i*-PrOH−acetone (94:3:3), giving five homogeneous fractions. The residue of the second fraction obtained as a homogeneous white solid was identified as nectriapyrone (**82**, 7.2 mg, 0.10 mg/L, R*f* = 0.45, Fig. 5.1.2). The residue of the third fraction (15 mg) of the first CC was purified by TLC, eluted with *n*-hexane−EtOAC (50:50), giving four fractions. The residue of the fourth fraction obtained as a white solid was characterized as 4- hydroxybenzaldehyde (**83**, 2.1 mg, 0.10 mg/L, R*f* 0.49, Fig. 5.1.2).

4.3. Production, extraction and purification of phytotoxins from *Diaporthe kongii* culture filtrate.

The strain of *Diaporthe kongii* used in this study was grown on a mineral defined liquid media M1-D as previously reported for *D. gulyae*. The culture filtrates (7 L, pH 4.3), having high phytotoxic activity on leaves, were lyophilized, dissolved in distilled water (1/10 of its original volume), and then extracted by EtOAc (4 x 700 mL). The organic extracts were combined, dehydrated with anhydrous Na_2SO_4, and evaporated under reduced pressure, yielding a brown solid (6.0 g), showing high phytotoxic activity. This latter was dissolved in EtOAc and extracted with a saturated solution of $NaHCO_3$ to remove 3-nitropropionic acid, which was identified as the main metabolite (13.2 g). The residue obtained from the organic phase (605.7 mg), still phytotoxic, was bioassay-guided purified by column chromatography, eluted with $CHCl_3$-*i*-PrOH (93:7), yielding six groups of homogeneous fractions. The residue of the second fraction (46.3 mg), showing phytotoxic activity, was further purified by preparative TLC on silica gel, eluted with CHCl3-i-PrOH (93:7) giving three fractions. The residue of the first fraction was obtained as a homogeneous

white solid identified as nectriapyrone (**82**, 4.2 mg, 0.14 mg/L, R*f* =0.43, Fig. 5.1.2). The residue of the second fraction appeared as a brown homogeneous solid (15.7 mg, 0.77 mg/L R*f* 0.58, Fig. 5.2.1) and was named kongiidiazadione (**84**) on the basis of its structural features reported below.

4.3.1. Kongiidiazadione (84). (-)-(*R*)-5-diazenyl-3-hydroxymethyl-cyclopent-3- en-1,2-dione.

Compound **84** had: $[\alpha]^{25}{}_{D}$ = -12.0 (c = 0.06, MeOH); IR, ν_{max} 3440, 1680, 1630, 1214 cm^{-1}; UV λ_{max} nm (log ε), 258 (3.7); ^{1}H- and ^{13}C-NMR spectra: see Table 5.2.1; HRESI-MS *m/z*,: 307.0689 (calcd for $C_{12}H_{11}N_4O_6$, 307.0679, $[2M-H]^-$), 153.0311 (calcd for $C_6H_5N_2O_3$, 153.0300, $[M-H]^-$).

4.3.2 6.-*O*-Acetylkongiidiazadione (85).

To kongiidiazadione (**84**) (0.5 mg), dissolved in pyridine (10 μL), was added acetic anhydride (10 μL). The reaction was carried out at room temperature for 1 h. The reaction was stopped by addition of MeOH and the azeotrope, obtained by the addition of benzene, was evaporated by an N_2 stream. The oily residue (2.0 mg) was purified by preparative TLC, eluted with $CHCl_3$-*i*-PrOH (99:1), to give **85** (R*f* 0.77, 0.5 mg, Fig. 5.2.1) as a homogeneous compound.

85 had: IR, ν_{max} 1742, 1242 cm^{-1}. ^{1}H-NMR spectrum: see Table 5.2.1; ESI-MS (-), *m/z*: 195 $[M - H]^-$.

4.3.3. Computational methods.

Preliminary conformational analysis was performed by Spartan02 package (SPARTAN O2) employing MMFF94s molecular mechanics (MM) force field with Monte Carlo searching and assuming the 5*R* absolute configuration for **84**. All possible conformers were searched, considering the degrees of freedom of the system within a range of 30 kcal/mol and retaining only the structures in an energy range of 10 kcal/mol with respect to the most stable one. The minimum energy conformers found by MM were further fully optimized by Gaussian09 package (Frisch *et al*., 2009) using the Density Functional Theory (DFT) at the DFT/B3LYP/TZVP level both in gas phase and in methanol by IEFPCM solvation model and at DFT/M062X/TZVP level in methanol by IEFPCM. All conformers are real minima, no imaginary vibrational frequencies were found, and the free

energy values were calculated and used to get the Boltzmann population of conformers at 298.15 K. The DFT geometries were then employed as input for time dependent DFT (TDDFT) calculations of UV and ECD spectra, both in gas phase and by IEFPCM (methanol) implicit solvation model, using either CAM-B3LYP (Yanai *et al*., 2004) or M062X (Zhao & Truhlar, 2008) functionals and aug-cc-pVDZ basis set and taking into account the lowest 30 states. The theoretical UV and ECD spectra were obtained as averages over the conformers Boltzmann populations. The ECD spectra were obtained from calculated excitation energies and rotational strengths, as a sum of Gaussian functions centred at the wavelength of each transition, with a parameter σ (width of the band at ½ height) of 0.4 eV using SpecDis v1.60 program (Bruhn *et al*., 2013). To evaluate the quality of the molecular wave functions employed ECD spectra calculated both in the length and velocity formalism were compared. In all cases the velocity/length calculated spectra were almost coincident, indicating a good level of calculation (Moscowitz, 1965). Therefore, in all figures only the velocity-form predicted spectra are reported.

4.4. Production, extraction and purification of phytotoxins from *Diaporthe kongii* grown in bioreactor.

The same strain of *D. kongii* was also grown in a bioreactor (BIOSTAT C 30 – Sartorius Stedim Biotech). Two 1-L Erlenmeyer flasks, each containing 500 mL of PDB (potato-dextrose broth), were inoculated with the actively growing mycelium obtained from six plates of PDA, and kept for 2 days in shaking conditions (100 rpm) on a orbital rotary shaker. The whole culture containing the mycelium was then fragmented in sterile conditions with a homogenizer for 2 min. The suspension was injected into the bioreactor (filled with 30 L of in-situ sterilized M1D medium) with the aid of a peristaltic pump and maintained for 2 weeks at a temperature of 26°C, 80 rpm, and 1 L/min air flux. The culture (30 L, pH 4.5) was then collected, filtered first by gauze, and then by filter papers to remove mycelium, and lyophilized. The lyophilized culture filtrates was extracted in the same conditions as previously reported yielding a brown solid (2.4 g), which was highly phytotoxic. The

extract was dissolved in EtOAc and then washed with a saturated solution of $NaHCO_3$ to remove acid compounds using the same procedure above described. This resulted in succinic acid (1.6 g), which is the main metabolite.

The fraction containing neutral and/or basic compounds (800 mg) was purified by column chromatography on silica gel eluted with $CHCl_3$-*i*-PrOH (92:8), yielding five groups of homogeneous fractions. The residue of the second fraction (46.3 mg) was further purified by TLC, eluted with $CHCl_3$-*i*-PrOH-acetone (93:5:2) giving four homogeneous fractions. The residue of the second fraction was further purified through two successive TLC, eluted with *n*-hexane-acetone (6:4), giving a white solid identified as 4-hydroxybenzaldehyde (3.7 mg, 0.12 mg/L, R*f* 0.69).

4.5. Production, extraction and purification of phytotoxins from *Alternaria sonchi* solid culture filtrate.

The fungus was grown on autoclaved pearl barley, and the solid culture (1.3 kg) was extracted with Me_2CO-H_2O (50:50) according to the procedure previously reported (Evidente *et al*., 2009). After evaporation of the Me_2CO, the H_2O phase was passed through a column containing 20 g of Diaion HP-20, and then was washed with H_2O, MeOH, EtOAc, and CH_2Cl_2. The dry residue (5.2 g) of the MeOH extract showed phytotoxic activity. It was then subjected to bioassay-guided fractionation through column chromatography on silica gel, eluted with CH_2Cl_2-MeOH (100:0 (800 mL), 95:5 (800 mL), 90:10 (800 mL), and 80:20 (800 mL)) affording four homogeneous fractions. The residue of the second fraction (3.3 g), showing both phytotoxic and antimicrobial activity, was further purified by CC on silica gel eluted with $CHCl_3$-*i*-PrOH (90:10) giving five homogeneous fractions. The residue of the fourth fraction (244 mg) was further purified by MPLC (medium pressure liquid chromatografy) on silica gel, eluted with *n*-hexane-Me_2CO (100:0 to 50:50), yielding alternethanoxin B, **57** (Fig. 1.7.1) (R*f* 0.37, toluene-EtOAc-glacial CH_3COOH (70:30:0.1), R*f* 0.35, H_2O-MeOH (20:80), 8.5 mg), and alternethanoxin E, **88** (Fig. 4.5.1) (R*f* 0.45 toluene-EtOAc-glacial CH_3COOH (70:30:0.1), R*f* 0.24, H_2O-MeOH (20:80), 5.0 mg) as a pale yellow

homogeneous amorphous solid. The residue of the fifth fraction (470 mg) was further purified by reverse-phase MPLC eluted with MeOH/H_2O (20:80 to 100:0) and finally by preparative TLC on silica gel eluted with toluene-EtOAc-glacial CH_3COOH (70:30:0.1) affording alternethanoxin A, **56** (Fig. 1.7.1) (R*f* 0.39, toluene-EtOAc-glacial CH_3COOH (70:30:0), R*f* 0.72, H_2O-MeOH (20:80) 25.0 mg), alternethanoxin C, **86** (Fig. 4.5.1) (R*f* 0.59, toluene-EtOAc-glacial CH_3COOH (70:30:0.1), R*f* 0.65, H_2O-MeOH (20:80), 16.0 mg) as a pale rose homogeneous amorphous solid, and alternethanoxin D, **87** (Fig. 4.5.1) (R*f* 0.39, toluene-EtOAc-glacial CH_3COOH (70:30:0.1), R*f* 0.36 H_2O-MeOH (20:80), 7.0 mg), as a pale yellow homogeneous amorphous solid.

4.5.1. Alternethanoxin C (86).

Pale rose amorphous solid, UV λ_{max} nm (log ε) 345 (0.1), 280 (0.65), 250 (0.40), 210 (1.75); ^1H and ^{13}C NMR, see Table 5.3.1; HRESI-MS (+) spectrum *m/z*: 695 $[2M + Na]^+$; 375 $[M + K]^+$, 359.0845 (calcd for $C_{16}H_{16}NaO_8$, 359.0743, $[M + Na]^+$).

4.5.2. Alternethanoxin D (87).

Pale yellow amorphous solid, UV λ_{max} nm (log ε) 365 (0.17), 300 (0.50), 243 (1.00); ^1H and ^{13}C NMR, see Table 5.3.1; HRESI-MS (+) spectrum *m/z*: 691 $[2M + Na]^+$; 373 $[M + K]^+$, 357.0574 (calcd for $C_{16}H_{14}NaO_8$, 357.0586, $[M + Na]^+$).

4.5.3. Alternethanoxin E (88).

Pale yellow amorphous solid, UV λ_{max} nm (log ε) 352 (0.16), 305 (0.60) 252 (0.75); 235 (1.14); ^1H and ^{13}C NMR, see Table 5.3.1; HRESI-MS (+) spectrum *m/z*: 623 $[2M + Na]^+$; 339 $[M + K]^+$, 323.0521 (calcd for $C_{16}H_{12}NaO_6$, 323.0532, $[M + Na]^+$).

4.6. Production, extraction and purification of phytotoxins from *Phoma chenopodiicola* culture filtrate.

The fungus was grown in 1 L Erlenmeyer flasks containing 300 mL of M-1-D medium.29 Each flask was seeded with several small fragments of the mycelium obtained by cutting Petri plates fully

colonized by the fungus. Flasks were then incubated in shaken conditions on an orbital shaker (100 rpm) at 25 °C for 2 weeks in the dark. After separating the mycelia by filtration, the culture filtrates (4.6 L) were lyophilized, dissolved in distilled water (1/10 of its original volume) and then extracted by EtOAc (4 x 1 L). The organic extracts were combined, dehydrated by Na_2SO_4, and evaporated under reduced pressure, giving a brownish-red oil residue (780 mg) which showed a high phytotoxic activity on host and non-host plants. The organic extract was then fractionated by CC eluted with $CHCl_3$-*i*-PrOH (97:3). Six homogeneous fractions were collected. The residue (43.3 mg) of the fourth fraction was further purified by preparative TLC, eluted with $CHCL_3$-*i*-PrOH (97:3), giving five fractions. The residue of the second fraction, obtained as a yellow oil, was identified, as below reported, as chenisocumarin (**90**, R*f* 0.24, 7.8 mg, 1.69 mg/L, Fig. 4.6.1). The residue (11 mg) of the third fraction was further purified by reverse phase TLC, eluted with EtOH-H_2O (6:4), yielding a yellow oil identified, as below reported, as chenopodolan D (**89**, R*f* 0.66, 4.5 mg, 0.98 mg/L, Fig. 4.6.1). The residue (138.7 mg) of the second fraction of the original column was purified by CC eluted with $CHCl_3$-*i*-PrOH (97:3), yielding five homogeneous fractions. The residue (67.6 mg) of the second fraction was washed with *n*-hexane followed by $CHCl_3$ to separate 6-hydroxymellein. The residue (4.9 mg) was further purified by preparative TLC, eluted with *n*-hexane-Me_2CO (7:3), giving a white amorphous solid, which was identified, as below reported, as chenopodolin B (**91**, R*f* 0.41, 4 mg, 0.85 mg/L, Fig. 4.6.1).

4.6.1. Chenopodolan D (89):

Compound **89** had: $[\alpha]^{25}_D$: -6.8 (c = 0.19); IR ν_{max} 3324, 1733, 1656, 1622, 1545, 1465, 1354, 1243 cm^{-1}; UV λ_{max} nm (log ε) 337 (3.6), 252 (sh); ^1H and ^{13}C NMR spectra: see Table 5.4.1; HRESI-MS (+) *m/z*: 539 $[2M+K]^+$, 523 $[2M+Na]^+$, 501 $[2M+H]^+$, 289 $[M+K]^+$, 273 $[M+Na]^+$, 251.1217 (calcd for $C_{14}H_{19}O_4$, 251.1208, $[M+H]^+$).

4.6.2. Chenisocoumarin (90):

Compound **90** had: $[\alpha]^{25}_{D}$: -1.6 (c = 0.36, MeOH); IR ν_{max} 3153, 1625, 1500, 1461, 1374 cm^{-1}; UV λ_{max} nm (log ε) 303 (3.6), 266 (4.1), 229 (sh); ^{1}H and ^{13}C NMR spectra: see Table 5.4.3; HRESI-MS (+) *m/z*: 233 $[M+Na]^+$, 211.1218 (calcd for $C_{10}H_{11}O_5$, 211.1208, $[M+H]^+$).

4.6.3. Chenopodolin B (91):

Compound **91** had: $[\alpha]^{25}_{D}$: -55.5 (c = 0.20); IR ν_{max} 1798, 1719, 1460, 1368, 1269, 1233 cm^{-1}; UV λ_{max} nm (log ε) 277 (3.2), 229 (3.8); ^{1}H and ^{13}C NMR spectra: see Table 5.4.5; HRESI-MS (+) *m/z*: 999 $[2M+Na]^+$, 511.1953 (calcd for $C_{26}H_{32}NaO_9$, 511.1944, $[M+Na]^+$).

4.6.4. 11-*O*-acetylchenopodolan D (92):

Chenopodolan D (**89**, 2.5 mg) was acetylated with pyridine (50 µL) and Ac_2O (50 µL) at room temperature for 1 h. The reaction was stopped by the addition of MeOH and the azeotrope, obtained by the addition of benzene, was evaporated by an N_2 stream. The oily residue (5.0 mg) was purified by preparative TLC and eluted with *n*-hexane-Me_2CO (1:1) to get the 11-*O*-acetyl derivative of chenopodolan D (**92**, Fig. 4.6.1) as a homogeneous compound (R*f* 0.62, 2.4 mg).

Derivative **92** had: IR ν_{max} 1732, 1689, 1622, 1551, 1459, 1370, 1232 cm^{-1}; UV λ_{max} nm (log ε) 336 (3.4), 253 (3.6); ^{1}H and ^{13}C NMR spectra: see Table 5.4.1. HRESI-MS (+) *m/z*: 623 $[2M+K]^+$, 607 $[2M+Na]^+$, 585 $[2M+H]^+$, 331 $[M+K]^+$, 293 $[M+H]^+$.

4.6.5. 5,7-*O*,*O*'-dimethylchenisocoumarin (93):

To chenisocoumarin (**90**, 4 mg), dissolved in CH_3OH (2 mL), was added an ethereal solution of diazomethane (200 µL). The reaction was carried out overnight at room temperature in the dark. The reaction was stopped by evaporation under N_2. The residue (7.6 mg) was purified by TLC, eluted with $CHCl_3$-*i*-PrOH (97:3), yielding the 5,7-*O*,*O'*-demethyl derivative of **90** (**93**, Fig. 5.4.1) as a homogeneous compound (2.6 mg, R*f* 0.46).

Derivative **93** had: IR ν_{max} 3406, 1698, 1604, 1560 cm^{-1}; UV λ_{max} nm (log ε) 299 (3.5), 262 (4.2), 230 (sh); ^{1}H and ^{13}C NMR spectra: see Table 5.4.3. ESI-MS (+) *m/z*: 515 $[2M+K]^+$, 499 $[2M+Na]^+$, 277 $[M+K]^+$, 261 $[M+Na]^+$, 239 $[M+H]^+$.

4.6.6. 4-*O*-(*S*)-α-methoxy-α-trifluoromethyl-α-phenylacetate (MTPA) ester of 93 (94):

To **93** (1.0 mg) dissolved in dry pyridine (20 μL) was added R)-(-)-MPTA-Cl (20 μL). The mixture was kept at room temperature for 1 h and the reaction stopped by adding MeOH. Pyridine was removed by a N_2 stream. The residue (2.5 mg) was purified by preparative TLC, eluted with *n*-hexane/Me_2CO, yielding **94** (Fig. 5.4.1)as a homogeneous oil (R*f* 0.71, 1.2 mg).

Derivative **94** had: IR ν_{max} 1722, 1606, 1581 cm^{-1}; UV λ_{max} nm (log ε) 301 (3.9), 261 (4.3), 232 (sh); ^1H NMR spectrum: see Table 5.4.4; ESI-MS (+) *m/z*: 947 $[2M+K]^+$, 931 $[2M+Na]^+$, 493 $[M+K]^+$, 477 $[M+Na]^+$, 455 $[M+H]^+$.

4.6.7. 4-*O*-(*R*)-α-methoxy-α-trifluoromethyl-α-phenylacetate (MTPA) ester of 93 (95):

To **93** (1.0 mg) dissolved in dry pyridine (20 μL) was added (*S*)-(+)-MPTA-Cl (20 μL). The reaction was carried out under the same conditions used for preparing **94** from **93**. The purification of the crude residue (2.2 mg) by preparative TLC, eluted with *n*-hexane-Me_2CO, gave **95** (Fig. 5.4.1) as a homogeneous oil (R*f* 0.71, 1.2 mg).

Derivative **95** had: IR ν_{max} 1720, 1605, 1581 cm^{-1}; UV λ_{max} nm (log ε) 303 (3.9), 262 (4.2), 229 (sh); ^1H NMR spectrum: see Table 5.4.4; ESI-MS (+) *m/z*: 947 $[2M+K]^+$, 931 $[2M+Na]^+$, 493 $[M+K]^+$, 477 $[M+Na]^+$, 455 $[M+H]^+$.

4.6.8. Computational methods.

Preliminary conformational analysis was performed by Spartan02 package (SPARTAN 02) employing MMFF94s molecular mechanics (MM) force field with Monte Carlo searching and assuming the (*R*) absolute configuration for **89**. All possible conformers were searched, considering the degrees of freedom of the system within a range of 30 kcal/mol and retaining only the structures in an energy range of 10 kcal/mol with respect to the most stable one. The minimum energy conformers found by MM were further fully optimized by Gaussian09 package (Frisch *et al*., 2009) using the Density Functional Theory (DFT) at the DFT/B3LYP/TZVP level either in gas phase or in

THF and CHCl3 by the IEFPCM solvation model (Tomasi *et al*., 2005). All conformers are real minima, no imaginary vibrational frequencies have been found and the free energy values have been calculated and used to obtain the Boltzmann population of conformers at 298.15 K. The DFT geometries were then employed as input for Time Dependent DFT (TDDFT) calculations of UV, ECD, and ORD spectra both in gas phase and by IEFPCM implicit solvation model in THF and CHCl3. Optical rotations were computed by using the TDDFT/B3LYP/aug-cc-pVDZ level on the DFT optimized geometries. The latter were also employed as input geometries for calculation of UV and ECD spectra at the TDDFT/CAM-B3LYP/aug-cc-pVDZ level and taking into account the lowest 30 states. TDDFT calculations employing the long-range corrected CAM-B3LYP functional (Yanai *et al*., 2004) provided good reproduction of Cotton effects observed in the theoretical ECD spectra (Evidente *et al*., 2011). The theoretical ORD, UV, and ECD spectra were obtained as average over the conformers Boltzmann populations. The ECD spectra were obtained from calculated excitation energies and rotational strengths, as a sum of Gaussian functions centered at the wavelength of each transition, with a parameter r (width of the band at 1/2 height) of 0.2 eV using SpecDis v1.60 program (Bruhn *et al*., 2013). The ECD spectrum was also calculated both in the length and velocity formalisms to guarantee origin independence and to evaluate the quality of the molecular wave functions employed (Moscowitz, 1965). These calculated spectra were almost coincident, indicating a good level of calculation. Therefore, in all figures only the velocity-form predicted spectra are reported.

4.7. Biological assays

4.7.1. Biological assays on *D. gulyae, D. kongii, A. sonchi* and *P. chenopodiicola*.

The assessment of phytotoxicity of culture filtrates, organic extracts, chromatographic fractions and pure metabolites were assayed by using a leaf-puncture assay on the suitable host and non host wild or cultivated plants. The pure metabolite, as well as extracts and fractions, were first dissolved

in a small amount of suitable solvent (frequently MeOH) and then diluted to the desired final concentrations with distilled water. The assays were carried out by Dr. M. Vurro, Institute of Food Production Sciences, CNR, Bari, Italy, or by Dr. A. Berestetskiy, All-Russian Institute of Plant Protection, St. Petersburg, Russia.

4.7.2. Biological assays on gulypyrone A and B, and phomontrioloxin B.

4.7.2.1. Phytotoxic bioassays.

In order to evaluate the presence of specific toxins, culture filtrates, organic extracts, and samples were assayed on punctured detached leaves of *Helianthus annuus*, one of the hosts of the pathogen. This bioassay was then used to guide all of the purification steps. The pure metabolites (except phomentrioloxin C, which was not available in sufficient amounts) were assayed at 5 mM on 15 plant species (see Result and Discussion section), both cultivated and weedy. Leaf disks (diameter 9 mm) were obtained by using a cork borer, placed on wet filter paper in polycarbonate boxes, and punctured in the middle by using a syringe needle. A droplet (15 μL) of the toxin solution was applied on each punctured disk. Boxes were kept at 25 °C under continuous light for 3 days. Four replications were prepared for each metabolite and for each plant species. Control disks were prepared with the same procedure but were added with water droplets. Effects were evaluated as necrosis appearance after 3 days by using a visual empiric scale from 0 (= no necrosis) to 4 (necrosis 8−10 mm).

4.7.2.2. Antimicrobial assays.

For the antibacterial activity pure compounds were tested on *Bacillus amyloliquefaciens* and *Pseudomonas fluorescens*, whereas the antifungal activity was tested on *Geotrichum candidum* as described elsewhere.

4.7.3. Biological assays on kongiidiazadione.

4.7.3.1. Phytotoxic Bioassays.

The phytotoxic activity of kongiidiazadione was tested on 15 plant species (see Result and Discussion section) as reported in paragraph 4.7.2.1.

4.7.3.2. Antimicrobial Bioassays.

The antimicrobial activity of kongiidiazadione was preliminarily tested as reported in paragraph 4.7.2.2.

4.7.4. Biological assays on alternethanoxins C, D and E.

4.7.4.1. Phytotoxic Activity.

Leaf segments of *Elytrigia repens* (couch-grass) 2 cm length and leaf discs of *Sonchus arvense* (perennial sowthistle) 1 cm in diameter were punctured with a sharp needle in the center. The diameter of necrotic spots was measured after 48 h of incubation at 24°C under alternating artificial illumination (12 h per day). Prior to performing biological tests, the compounds were dissolved in a small volume of 96% ethanol. The final concentration of ethanol, at which it exhibited no phytotoxicity, was 5%. The efficiency of the compounds was assessed at a concentration of 5 mg/mL; The specificity of the compounds was assessed at a concentration of 2 mg/mL.

Typically, for this bioassay samples of isolated compounds (400 μg) were dissolved in EtOH (10 μL) ultrasonically, and then water (190 μL) was added and the samples were vortexed. At least 10 replicate leaf segments or discs were used for each treatment.

4.7.4.2. Antimicrobial Activity.

The antimicrobial activity of the isolated compounds was tested against a Gram positive bacterium (*Bacillus subtilis*) and a yeast fungus (*Candida tropicalis*) by using an agar diffusion assay according to the protocol previously reported (Bottalico *et al*., 1990). Briefly, both microorganisms were grown on potato-dextrose agar. Up to 100 μg of each metabolite was applied

per disc (6 mm diam) (Macherey-Nagel, Duören, Germany). The cultures were incubated at 30 °C for 24 h before activity was determined by minimum inhibitory concentration (MIC) defined as the lowest concentration of antibiotic that inhibited visible growth (Onishi *et al*., 1996).

4.7.4.3. Statistical Analysis.

All bioassays were performed twice with at least three replicates. When appropriate, standard deviation was determined.

4.7.5. Biological assays on chenopodolan D, chenisocumarine and chenopodolin B.

4.7.5.1. Leaf puncture assay.

Each metabolite was first dissolved in MeOH and then diluted with distilled water to the desired concentrations (final concentration of methanol: 2%). The compounds were tested by using a leaf puncture assay on 6 different plant species, namely *Stellaria media*, *Urticadioica*, *Sonchus arvensis*, *Parietaria officinalis*, *Lactuca serriola*, *Helianthus annuus*, with the weedy plants (the first four in the list) collected in local open fields, and the crop plants grown in pots. Pure compounds were tested at 4 x 10^{-3} M by applying a droplet (20μL) of solution to detached leaves previously punctured with a needle. Five replications were used for each metabolite and for each plant species tested. Leaves were kept in a moistened chamber under continuous fluorescent lights. Symptoms were estimated visually between three to five days after droplet application, by using a visual scale from 0 (no symptoms) to 4 (necrosis wider than 1 cm). Control treatments were carried out by applying droplets not containing the metabolites.

5. RESULTS AND DISCUSSION

5.1.1. Chemical characterization of pure metabolites produced by *Diaporthe gulyae*, potential mycoherbicide for *Carthamus lanatus* biocontrol.

The organic extract obtained from the culture filtrates of a new strain of *D. gulyae* grown in static culture proved to be highly phytotoxic. As reported in detail in the experimental section, its bioassay guided-purification revealed two new trisubstituted α-pyrones, named gulypyrones A and B (**71** and **72**, Fig. 5.1.1, 0.3 and 0.13 mg/L, respectively), and two new analogues of phomentrioloxin (**47**, Fig. 1.6.1, 0.85 mg/L,), named phomentrioloxins B and C (**73** and **74**, Fig. 5.1.1, 0.12 and 0.10 mg/L, respectively). The same culture filtrates also contained the well known 3-nitropropionic and 4-methylbenzoic acids (**75** and **76**, Fig. 5.1.1, 600 and 0.2 mg/L, respectively). 3-Nitropropionic acid was the main phytotoxic metabolite.

When the same fungus was grown in a bioreactor, the phytotoxic organic extract obtained from the culture filtrates yielded succinic acid (**80**, Fig. 5.1.2, 193 mg/L) and 4-hydroxybenzoic acid, nectriapyrone, and 4-hydroxybenzaldehyde (**81-83**, Fig. 5.1.2; 2.72, 0.10 and 0.10 mg/L, respectively).

The identification of the already known metabolites 3-nitropropionic, succinic, 4-hydroxy- and 4-methylbenzoic acids, and 4-hydroxybenzaldehyde was confirmed by comparison of their TLC behaviour and ^{1}H NMR spectra with those of the corresponding commercial samples. The structures of phomentrioloxin and nectriapyrone were confirmed by comparing their physical and spectroscopic data (OR, IR, UV, ^{1}H and ^{13}C NMR, ESI MS) with those reported in the literature for **47** (Cimmino *et al*., 2012) and **82** (Evidente *et al*., 2011b), respectively.

Gulypyrone A (**71**) had a molecular formula of $C_{11}H_{16}O_4$ with four hydrogen deficincies, as deduced by its HRESI-MS. The IR spectrum (Fig. 5.1.11) showed the presence of hydroxy and *α,β*-unsaturated carbonyl groups (Nakanishi & Solomon, 1977) in agreement with the absorption maximum at 288 recorded in the UV spectrum (Fig. 5.1.10) and typical of a substituted α-pyrones

(Scott, 1964). These results were in agreement with its ^{1}H and ^{13}C NMR spectra (Table 5.1.1; Fig. 5.1.4 and 5.1.5). In particular, the ^{1}H NMR spectrum showed a singlet at δ 5.45 typical of an olefinic proton of a 4,5,6-trisubstituted α-pyrone ring (Pretsch *et al*., 2000). The substituents appeared to be a methoxy, a vinyl methyl, and 1-methyl-2-hydroxypropyl residues. The methyl and the methoxy groups resonated as two singlets at δ 1.92 and 3.82, respectively. The protons of the 1-methyl-2-hydroxypropyl side chain, attributed on the basis of the couplings observed in the COSY spectrum (Fig. 5.1.6) (Berger & Braun, 2004), appeared as a quintet at δ 4.05 (J = 7.0 Hz), and two doublets (J = 6.2 and 7.0 Hz, respectively) at δ 1.27 and 1.19, respectively, and were attributed to H-9, H-8, Me-10 and Me-11, respectively (Pretsch *et al*., 2000). The couplings observed in the HSQC spectrum (Fig. 5.1.7) (Berger & Braun, 2004) allowed the assignment of the corresponding carbons at δ 87.9, 56.1, 9.2 68.8, 42.7, 21.3 and 14.8 for C-3, OMe, C-7, C-9, C-8, C-10 and C-11, respectively (Breitmaier & Voelter, 1987). The couplings observed in the HMBC spectrum (Table 5.1.1 and Fig. 5.1.8) (Berger & Braun, 2004) also allowed the assignment of the four quaternary carbons of the pyrone ring at δ 170.9, 165.1, 164.3 127.8 to C-4, C-6, C-2 and C-5, respectively. Thus, the chemical shifts of all the protons and the corresponding carbons of **70** were assigned as reported in Table 5.1.1.

The couplings observed in the same HMBC spectrum also allowed the positioning of the substituents on the α-pyrone ring. In particular, the $J^{3}_{C,H}$ and the $J^{4}_{C,H}$ couplings observed between OMe and C-4, Me-7 with C-4, C-5 and C-6, in agreement with the literature (Pretsch *et al*., 2000; Berger & Braun, 2004; Breitmaier & Voelter, 1987), allowed their placement to C-4 and C-5, whereas the couplings between Me-11 and C-6 located the 2-hydroxy-1-methyl-propyl side chain at C-6. These results were in agreement with the long-range coupling (<1 Hz) observed in the COSY spectrum between H-3 and both OMe and Me-7. On the basis of these results gulypyrone was formulated as 6-(2-hydroxy-1-methylpropyl)-4-methoxy-5-methylpyran-2-one.

The structure assigned to **71** was supported by the other couplings observed in the HMBC spectrum and from the HRESI-MS and NOESY data. The HRESI-MS (Fig. 5.1.12) showed the dimeric sodiated form $[2M+Na]^+$, the sodiated cluster $[M+Na]^+$ and the pseudomolecular ion $[M + H]^+$ at *m/z* 447, 235, 213.1146, respectively. As expected the NOESY spectrum (Fig. 5.1.9) (Berger & Braun, 2004) showed correlations between OMe and H-3, H-9 and Me-10, and H-8 with both Me-7 and Me-11.

The structure assigned to gulypyrone A was confirmed by preparing its 9-*O*-acetyl derivative (**77**). The IR spectrum of **77** showed the lack of the hydroxy group bands while its ^{1}H NMR spectrum (Fig. 5.1.14) differed from that of **71** only by the downfield shift ($\Delta\delta$ 0.99) of H-9 resonating as a multiplet at δ 5.04 and the presence of the singlet of the acetyl group at δ 1.97. Its ESI-MS showed the dimeric sodiated form $[2M+Na]^+$ and the potassium $[M+K]^+$ and sodium $[M+Na]^+$ clusters at *m/z* 531, 293 and 277, respectively. The APCI mass spectrum showed the pseudomolecular ion at *m/z* 255.

The absolute configuration of the secondary hydroxylated carbon (C-9) of the 2-hydroxy-1-methy-propyl residue attached to C-6 was determined by applying a modified Mosher's method (Ohtani *et al*., 1991). By reaction with *R*-(-)-α-methoxy-α-trifluoromethylphenylacetyl (MTPA) and *S*-(+)-MTPA chlorides, gulypyrone A (**71**) was converted into the corresponding diastereomeric *S*-MTPA and *R*-MTPA monoesters at C-9 (**78** and **79**, respectively, Fig. 5.1.1), whose spectroscopic data were consistent with the structure assigned to **47**. Subtracting the proton chemical shifts (Table 5.1.2; Fig. 5.1.15 and Fig. 5.1.16) of the 9-*O*-*R*-MTPA (**79**) from that of 9-*O*-*S*-MTPA (**78**) esters, the $\Delta\delta$ (**78-79**) values for all of the protons were determined as reported in Fig. 5.1.3. The positive $\Delta\delta$ values were located on the right side, and those with negative values on the left side of the model A as reported by Othani *et al.* (1991). This model allowed the assignment of the *R* configuration to C-9. **71** was formulated as 6-((2*R*)-2-hydroxy-1-methyl-propyl)-4-methoxy-5-methyl-pyran-2-one.

Gulypyrone B (**72**) had a molecular formula of $C_{11}H_4O_4$ with five hydrogen deficiencies, as deduced by its HRESI-MS. Preliminary ^1H and ^{13}C NMR investigations, supported by the data from IR (Fig. 5.1.21) and UV spectra, showed that **72** is closely related to nectriapyrone (**82**, Fig. 5.1.2), a phytotoxin recently isolated from culture filtrates of *Diaporthe angelicae* (anamorph *Phomopsis foeniculi*) a pathogen of fennel (*Foeniculum vulgare*) in Bulgaria (Evidente *et al*., 2011b). The ^1H NMR spectrum (Table 5.1.1; Fig. 5.1.17) showed a singlet at δ 6.20 typical of an olefinic proton of a 3,4,6-trisubstituted α-pyrone ring (Pretsch *et al*., 2000), and three further singlets at δ 3.91, 1.94 and 1.93, attributable to a methoxy and two vinyl methyl groups, respectively. Moreover ^1H NMR, COSY and NOESY data proved that the two α-pyrones (**72** and **82**) differed only in the substitution of the 1-methyl-propenyl side chain. The ^1H NMR spectrum of **72** showed the presence of a triplet (J = 5.5 Hz) at δ 6.69 assigned to the olefinic proton H-9, which in the COSY spectrum (Fig. 5.1.18) coupled with a hydroxymethylene group (H_2C-10), that resonated as two doublet of doublets (J= 5.5 and 1 Hz) at δ 4.41 and 4.39, respectively. **72** differed from nectriapyrone by the presence of a hydroxy group at C-10 (Table 5.1.1) as also confirmed by the couplings observed in the HMBC spectrum (Fig. 5.1.19).

The structure assigned to **72** was also supported by NOESY data spectrum (Fig. 5.1.20) in which a significant coupling was observed between H-5 with the methoxy group and Me-11. In the same spectrum a clear correlation was also observed between H_2-10 and Me-11, allowing the assignment of *E* stereochemistry to the trisubstituted double bond located between C-8 and C-9.

The structure assigned to **72** was supported by the data of the HRESI-MS (Fig. 5.1.22 and 5.1.23). The dimeric sodiated form, the sodium cluster and the pseudomolecular ion were observed at *m/z* 443 $[2M+Na]^+$, 233 $[M+Na]^+$, 211 $[M+H]^+$, respectively; the ESI-MS spectrum also showed a significant fragmentation peak $[M+Na-CO_2]+$ at *m/z* 189 generated from the sodium cluster by loss of CO_2, a fragmentation mechanism typical of the α-pyrones (Pretsch *et al*., 2000). **72** was

named, according to IUPAC nomenclature, 6-[(1*E*)-3-hydroxy-1-methylpropenyl]-4-methoxy-3-methylpyran-2-one.

Phomentrioloxin B (**73**) had a molecular formula of $C_{17}H_{22}O_4$ as deduced by its HRESI-MS which is consistent with seven hydrogen deficiencies and therefore differed from phomentioloxin (Cimmino *et al*., 2012) by two hydrogen atoms. The IR spectrum (Fig. 5.1.31) of **73** differed from that of **47** essentially for the presence of the band of a conjugated carbonyl group at 1734 cm^{-1}. The ^1H NMR spectrum (Table 5.1.3 and Fig. 5.1.24) of **73** differed from that of **47** by the lack of H-1 and HO-1 signals, while H-2 appeared as a double doublet (J = 10 and 2.0 Hz) at δ 4.57. Furthermore, the downfield shift ($\Delta\delta$ 0.98) of H-5, was observed as this proton resonated as a doublet (J =6.0 Hz) at δ 7.14, the typical chemical shift of a proton of an α,β-unsaturated carbonyl group (Pretsch *et al*., 2000). Considering these findings, the structure of a 1,*O*-dehydrophomentrioloxin might be suggested for phomentrioloxin B. The ^{13}C NMR data (Table 5.1.3 and Fig. 5.1.25) confirmed this hypothesis. The signals of the α,β-unsaturated carbonyl group appeared at δ 194.9 (C-1), 124.4 (C-6) and 146.4 (C-5) for the carbonyl group and the two carbons of the trisubstituted double bond, respectively (Breitmaier & Voelter, 1987). Finally, the couplings observed in the COSY (Fig. 5.1.26) and HSQC (Fig. 5.1.27) spectra and the correlation observed in the NOESY spectrum (Fig. 5.1.29) between the Me-9´ and H-6´allowed us to assign the chemical shifts to all the protons and their corresponding carbons (Table 5.1.3), and to phomentrioloxin B the structure 4,6-dihydroxy-5-methoxy-2-(7-methyl-3-methylene-oct-6-enynyl)-cyclohex-2-enone (**73**).

This structure was supported by the long-range couplings observed in the HMBC spectrum (Table 5.1.3 and Fig. 5.1.28) and by the HRESI-MS data (Fig. 5.1.32). The latter, recorded in positive mode showed in addition to the dimeric sodiated form $[2M+Na]^+$, the potassium $[M+K]^+$and sodium $[M+Na]^+$ clusters at *m/z* 603, 329 and 313.1427, respectively. The ESI-MS spectrum (Fig. 5.1.33) was recorded in negative mode and showed the pseudomolecular ion $[M-H]^-$ at *m/z* 289.

As depicted in Fig. 5.1.1, the relative configuration of the chiral carbons of phomentriloxin B was deduced by the comparison of the coupling constants measured in its ^{1}H NMR spectrum with those of **47** and by the correlations observed in the NOESY spectrum (Fig. 5.1.29) between H-4 and both H-3 and H-5, as well as the lack of correlation between H-2 and H-3 (Cimmino *et al*., 2012).

Phomentrioloxin C (**74**) had the same molecular weight as phomentrioloxin B as deduced by its HRESI and APCI-MS spectra, but its ^{1}H NMR spectrum (Table 5.1.3 and Fig. 5.1.34) differed from those of phomentrioloxin (Cimmino *et al*., 2012) and phomentrioloxin B. In particular, it differed from that of **47** essentially by the absence of the H-2 and HO-2 signals, while H-1 appeared as a doublet of doublets (J= 11.0 and 2.0 Hz) at δ 4.95. Compared to **73,** the spectrum did not show the same downfield shift observed for the signal of H-5 that resonated as a doublet of doublets (J =6.0 and 2.0 Hz) at δ 6.74.

Considering these findings, the structure of a 2,*O*-didehydrophomentrioloxin might be suggested for phomentrioloxin C. This structure was supported by the HRESI and APCI-MS data. The ESI-MS spectrum (Fig. 5.1.35) recorded in positive mode showed the dimeric sodiated form $[2M+Na]^+$ and the potassium $[M+K]^+$and sodium clusters $[M+Na]^+$ at *m/z* 603, 329 and 313, respectively. The ESI-MS spectrum (Fig. 5.1.36), recorded in negative mode, showed the pseudomolecular ion $[M-H]^-$ at *m/z* 289 and the ion it generated by loss of H_2O $[M-H-H_2O]^-$ at *m/z* 253. The APCI spectrum, recorded in positive modality, showed the pseudomolecular ion $[M+H]^+$ at *m/z* 291, and the ions originating from this latter by the loss of one or two H_2O molecules $[M+H-H_2O]^+$ and $[M+H-2H_2O]^+$ at *m/z* 273 and 255, respectively.

The relative configuration of phomentrioloxin C, as depicted in Fig. 5.1.1, was deduced by comparing the coupling constants measured in its ^{1}H NMR spectrum with those of **47** and the IUPAC name to 2,5-dihydroxy-6-methoxy-3-(7-methyl-3-methylene-oct-6-en-1-ynyl)-cyclohex-3-enone was given to phomentrioloxin B.

Gulypyrone A and B belong to a group of naturally occurring compounds which are broadly distributed, being produced by plants, animals, marine organisms and microorganisms, and having

interesting biological properties (Dean, 1963; Thomson, 1985; Moreno-Manas & Pleixats, 1992). These include metabolites containing the pyran-2-one moiety produced by fungi belonging to several genera and showing antibiotic, antifungal, cytotoxic, neurotoxic, and phytotoxic activities (Dickinson, 1993). Other bioactive fungal α-pyrones have been isolated, including viridepyronone produced by *Trichoderma viride* (Evidente *et al*., 2003), having antifungal activity against *Sclerotium rolfsii*, the causal agent of crown and stem rot of artichoke. 3-Nitropropionic acid was previously isolated as a phytotoxin from other fungi pathogenic to weeds (Evidente *et al*., 2011c). *p*-Hydroxybenzaldehyde is a known phytotoxic metabolite of pathogenic fungi of important crops and forest plants. This metabolite was also isolated together with known cytochalasins from the liquid and solid cultures of two strains of *Phoma exigua var exigua*, a pathogenic fungus that has been proposed for the biocontrol of *Cirsium arvense* and *Sonchus arvensis* (Cimmino *et al*., 2008). *p*-Hydroxybenzoic acid, identified as a phytotoxin produced by *Rhizoctonia oryzae*, induced brown spots typical of disease on plant tissue (Takuo & Kimiharu, 1988). *p*-Methylbenzoic acid was isolated from cultures of the fungus *Cladosporium cladosporioides* isolated from a marine sponge (San-Martin, 2005).

5.1.2. Biological activity of the metabolites isolated from *D. gulyae*.

In the leaf disk bioassay, 3-nitropropionic acid proved to be quite active, being able to produce small but clear necroses on several weedy and crop plant species, in particular to *Papaver rhoes, Ecballium elaterium, Urtica dioica* and *Hedysarum coronarium*. Smaller necroses were also visible on *Mercurialis annua, Lactuca serriola, Ailanthus altissima and Inula viscosa.* Moreover, considering that the compound is present at higher concentrations, it is probably the principal compound responsible for the high phytotoxicity of the culture filtrates and the organic extract. Tested at the same concentration, phomentrioloxin B proved to have a weaker toxicity, causing necrosis on *P. rhoeas* and *U. dioica*, and even smaller necrosis on *M. annua, L. serriola, A. altissima, Picris echioides, I. viscosa, H. coronarium, H. annuus, Aster* sp. Assayed at 5 mM by

stem immersion on *H. annuus* plantlets, gulypyrone A caused the rapid appearance of clear and very expanded necrosis on leaves; interestingly, the lack of symptoms on the stems suggest that the compound can be easily translocated through the vascular system, accumulating in the leaf tissues. Even weaker activity was observed in case of 4-methylbenzoic acid which caused small necrosis only to *M. annua, U. dioica*, *Solanum nigrum* and *Aster* sp. All the other compounds were very weakly or not at all toxic. Considering the high toxicity of the culture filtrate, an additive or synergistic activity of all the weakly active metabolites could be hypothesized.

None of the compounds showed significant antibacterial or antifungal activity.

5.2.1. Chemical characterization of pure metabolites produced by *Diaporthe kongii*, potential mycoherbicide for *Carthamus lanatus* biocontrol.

A new 3-substituted-5-diazenylcyclopentendione named kongiidiazadione (**84,** Fig. 5.2.1) was isolated from the culture filtrates of *Diaporthe kongii* through a bio-guided purification of the organic extract, as reported in detail in the experimental section. From the same culture filtrates were also isolated the well known 3-nitropropionic, identified as the main metabolite, and the fungal metabolite nectriapyrone (**82**, Fig. 5.1.2).

When the same fungus was grown in a bioreactor yielded succinic acid, as the main metabolite, and 4-hydroxybenzaldehyde. This latter compounds were identified as previously reported when they were isolated from *D. gulyae* (Andolfi *et al*., 2015).

In the HRESI-MS spectrum recorded in negative mode (Fig. 5.2.13) kongiidiazadione exhibited a molecular weight of 154 corresponding to the molecular formula $C_6H_6N_2O_3$ consistent with five hydrogen deficiencies. Its IR spectrum (Fig. 5.2.11) showed bands typical of hydroxy group at 3440 cm^{-1}, conjugated carbonyl group at 1680 cm^{-1}, conjugated double bond at 1630 cm^{-1}, and the *trans*-diazenyl group at 1214 cm^{-1} (Nakanishi & Solomon, 1977; Pretsch *et al*., 2000). The UV spectrum (Fig. 5.2.10) showed an absorption maximum typical of an extended conjugated chromophore (Scott, 1964). The ^1H NMR spectrum (Table 5.2.3 and Fig. 5.2.3) showed a double triplet (J = 1.9

and 1.5 Hz) at δ 6.68 typical of a proton H-C(4) of a trisubstituted olefinic group (Pretsch *et al*., 2000). In the COSY spectrum (Fig. 5.2.6) (Berger & Braun, 2004) H-C(4) coupled with the proton of the adjacent methine group H-C(5) which give an overlapped multiplet at δ 3.84 with the proton of a monosubstituted diazenyl group as confirmed by the integration of the ^{1}H NMR spectrum. H-C(4) also appeared allylic coupled with both protons of the hydroxymethylene group H_2-C(6) resonating as two broad doublets (J= 17.4 Hz) at δ 4.58 and 4.07, respectively (Pretsch *et al*., 2000). These latter, in turn, coupled with the germinal hydroxy group present as a broad singlet at δ 1.88. The ^{13}C NMR spectrum (Fig. 5.2.4) showed the presence of signals of two conjugated ketone carbonyl groups and the quaternary olefinic carbon at δ 192.0, 191.1 and 147.9, respectively (Breitmaier & Voelter, 1987). Also on the basis of the couplings observed in the HMBC spectrum (Fig. 5.2.8) (Berger & Braun, 2004) they were assigned to C(1), C(2) and C(3), respectively. Furthermore, the ^{13}C-NMR spectrum (Fig. 5.2.4) showed the signals of two methine and one hydroxy methylene carbons at δ 131.2, 59.6, 54.2, respectively, which, on the basis of the couplings observed in the HSQC spectrum (Fig. 5.2.7), were assigned to C(4), C(5) and C(6) (Breitmaier & Voelter, 1987). Taking into account these structural features and the total number of unsaturations, a cyclopentendione skeleton bearing a hydroxymethylene and a diazenyl groups was hypothesized for **84**. The location of the diazenyl and the hydroxymethylene groups at C(5) and C(4), respectively, was deduced by the couplings recorded in the COSY spectrum (Fig. 5.2.6) and confirmed by those observed in the HMBC spectrum (Fig. 5.2.8) between C(5) and NH, and C(3) and H_2-C(6) and OH.

On the basis of these results kongiidiazadione was formulated as 5-diazenyl-cyclopent-3-en-1,2-dione.

This structure was supported by the other couplings observed in the HMBC spectrum (Table 5.2.1 and Fig. 5.2.8) and for the data of the HRESI-MS (Fig. 5.2.13) and NOESY spectra (Fig. 5.2.9). Indeed, beside the pseudomolecular ion above cited, the HRESI-MS spectrum, recorded in negative mode (Fig. 5.2.13), showed also the corresponding dimer $[2M-H]^-$ at *m/z* 307.0689. When the spectrum was recorded in positive mode any useful spectrum was obtained. This was in

agreement to the structure assigned to kongiidiazadione. When the spectrum was recorded in negative mode the probable anion was generated at C-5 as H-5 resulted to be the more acid proton. In fact, this anion was stabilized by several resonance structures generated by its conjugation with both the double bond and the carbonyl groups as reported in Fig. 5.2.2. Moreover, the NOESY spectrum (Fig. 5.2.9) showed the expected correlation between H-C(4) and both protons of $H_2C(6)$.

The structure assigned to kongiidiazadione was confirmed by preparing the corresponding acetyl derivate by reaction carried out with pyridine and acetic anhydride. The usual work-up of the reaction gave a residue which was purified by preparative TLC on silica gel affording the 6-*O*-acetyl derivate, **85** (Fig. 5.2.1) as homogeneous solid (R_f 0.77). Its IR spectrum (Fig. 5.2.16) showed the absence of the significant bands of hydroxy groups while those significant for the ester carbonyl and the diazenyl groups were present. The ^{1}H NMR of **85** (Fig. 5.2.14) differed from that of **84** for the expected downfield shift ($\Delta\delta$ 0.40 and 0.76) of two protons of the hydroxymethylene group $H_2C(6)$, which appeared as two double doublets (J= 17.0 and 1.6 Hz) at δ 4.98 and 4.83, respectively, and for the presence of the singlet of the acetyl group at δ 2.13. Its ESIMS spectrum, recorded in negative mode, showed the pseudomolecular ion $[M-H]^-$ at *m/z* 195 and the fragmentation ion at *m/z* 153 $[M-H-CH_2CO]^-$, generated by the loss of a ketene.

The *trans* stereochemistry of the diazenyl group was deduced by the typical IR absorption value at 1214 cm^{-1} which substantially differed from that of the *cis*-stereoisomer (1425-1385 cm^{-1}) (Nakanishi & Solomon, 1977).

The absolute configuration at C(5) of (-)-**84** was determined by *ab initio* computational analysis of its ECD spectrum (Autschbach, 2009; Autschbach 2012). Such approach has in fact recently emerged as one of the most powerful and practical methods for stereochemical analysis of natural products (Mazzeo *et al*., 2013; Santoro *et al*., 2013). The UV and ECD spectra of (-)-**84** (Fig. 5.2.17) were recorded in the 180-600 nm spectral range in $1.95\cdot10^{-3}$ M (CH_3OH) solution. The UV spectrum shows broad absorption bands with two visible maxima at 209.8 nm (ε = 9800) and 258.0 nm (ε = 3600), a shoulder at 229.4 nm and a very weak signal around 400 nm. The ECD spectrum

shows a weak positive Cotton effect (CE) at 190.1 nm ($\Delta\varepsilon$ +2.2), a negative one at 214.2 nm ($\Delta\varepsilon$ -3.0), a positive band at 245.0 nm ($\Delta\varepsilon$ +2.5) and a very broad negative CE around 370 nm. First, on arbitrarily chosen (5*R*)-**84**, a conformational analysis was carried out by Monte Carlo search at Molecular Mechanics (MM) level by MMFF94 force field, obtaining ten appreciably populated conformers (Table 5.2.2). The latter were then further optimized in gas phase at DFT/B3LYP/TZVP level and, taking into account methanol solvent effects by the implicit IEF-PCM solvation model (Tomasi *et al*., 2005), at both DFT/B3LYP/TZVP and DFT/M062X/TZVP level of theory (Zhao & Truhlar, 2008). The three approaches provided different conformers populations but only minor changes in conformers geometries (Table 5.2.2 and Fig. 5.2.18). The ten populated conformers differed essentially in the rotations of the H-C(5)-N=N and C(4)-C(3)-C(6)-OH dihedral angles. Interestingly, the five most populated conformers **84a-e** which, depending on the calculation level, accounted for 70÷90% of the overall population, show the same disposition of the *trans*-N=NH moiety, which lies in plane with an angle of 110° in respect to the ring plane. Only in the minor conformers **84d**, **84e**, and **84i** the OH group and the adjacent carbonyl moiety have a distance minor than 2.5 Å, making possible the presence of an intramolecular hydrogen bonding (Anslyn & Dougherty, 2006). Taking into account conformer structures coming from calculations with both B3LYP and M062X functionals and TZVP basis set in the IEFPCM (methanol) solvation model, UV and ECD spectra for (5*R*)-**84** were calculated by TDDFT/CAM-B3LYP/aug-cc-pVDZ/IEFPCM(MeOH) and TDDFT/M062X/aug-cc-pVDZ/IEFPCM (MeOH) levels of theory, respectively. Interestingly, with both approaches the ten most populated conformers display very similar ECD profiles (Fig. 5.2.19 and 5.2.20) showing that, in this case, the accuracy of the conformers population description does not much affect the quality of the overall spectral reproduction but only, to a minor extent, its shape. After Boltzmann averaging over conformer populations the averaged spectra (Fig. 5.2.17) were compared with experimental data. Comparison between experimental spectrum for (-)-**84** and calculated ones for (5*R*)-**84** shows better agreement with the TDDFT/M062X/aug-ccpVDZ//DFT/M062X/TZVP/ IEFPCM (MeOH) calculated

spectrum. This spectrum displays a good agreement in position, sign, and intensity of the main ECD bands, suggesting to assign (5*R*) absolute configuration to (-)-1. Comparison of experimental ECD spectrum with the one calculated in gas phase (Fig. 5.2.21) confirmed the same configurational assignment, but showed a worse spectral agreement, pointing out that a more reliable description of conformers population is provided taking into account solvation effects. A MOs (Molecular Orbital) analysis of the electronic transitions allied to the main ECD spectral features (Table 5.2.3 and Fig. 5.2.22) shows that the three high energy Cotton effects (CEs) below 300 nm are determined by transitions involving the conjugated usaturated dicarbonyl chromophore, while the high energy CE at 506 nm is allied to the diazo chromophore. The latter positive CE is however not detectable in the experimental ECD spectrum.

In the above calculations conformers populations were obtained from Gibbs free energies calculated in the standard harmonic approach. However, in this molecule the vibration of the -OH and -N=N-H groups around a single bond could have a very broad potential energy and the harmonic approach could not perform well. Therefore, the assignment should be confirmed using energy derived populations. Actually, the latter (Table 5.2.4) show somehow different conformers distribution with respect to the free energy derived (Table 5.2.2). However, ECD spectra calculated taking into account either energy or Gibbs free energy derived populations show only minor differences that do not affect the configurational assignment (Fig. 5.2.17 and Fig. 5.2.23).

5.2.2. Biological activity of kongiidiazadione.

When assayed on both cultivated and weedy plants, the toxin caused small but well defined necrotic spots (3-5 mm) on some of them, in particular to *Helianthus annuus* and *Trifolium campestre*. Smaller necrosis were visible on *Urtica dioica*, *Solanum nigrum* and *Aster* sp. No symptoms were detectable on *Lolium italicum*, *Avena fatua*, *Papaver rhoeas*, *Mercurialis annua*, *Ecballium elaterium*, *Lactuca serriola*, *Ailanthus altissima*, *Picrisechioides*, *Inula viscosa*, *Hedysarum coronarium*. Interestingly, the most sensitive plant species proved to be *H. annuus*

(sunflower), one of the hosts of the pathogen producing the toxin, and also *Aster* sp., belonging to the same plant family (Asteraceae). Moreover, no necrosis could be observed on plant belonging to the Poaceae representatives, as well as on other plant species having leaves particularly suitable to uptake to metabolite (e.g. with succulent tissues and hairy leaf blades). Thus the compound, could be in some way involved in the interactions between the host and the pathogen. Studies in this direction are in progress.

In preliminary tests for its antibiotic properties, kongiidiazadione caused clear inhibition halos on *Bacillus amyloliquefaciens* (gram-positive), but only at concentration higher than 100 µg/diskette, whereas it was inactive at 25 µg/diskette. Assayed on *Pseudomonas fluorescens* (gram-negative) the compound proved to be only slightly bacteriostatic at the highest concentration tested. No antifungal activity was observed against *Geotrichum candidum* applied up to 50 µg/diskette.

5.3.1. Chemical characterization of pure metabolites produced by *Alternaria sonchi*, potential mycoherbicide for *Sonchus arvensis* biocontrol.

The organic extract of the *A. sonchi* solid culture was purified by a combination of column and TLC chromatography, yielding three homogeneous amorphous solids that were closely related to alternethanoxins A and B (**56** and **57**, Fig. 1.7.1) as deduced by preliminary investigation of the ^{1}H and ^{13}C NMR spectra, and were named alternethanoxins C−E (**86-88,** Fig. 5.3.1).

Alternethanoxin C, **86** has a molecular formula of $C_{16}H_{16}O_8$ as deduced from its HRESI-MS spectrum, which is associated with ten hydrogen deficiencies. In particular, its ^{1}H NMR spectrum (Table 5.3.1) differed from that of **56** in the presence of two aromatic protons (H-8 and H-9), which were *ortho*-coupled in the COSY spectrum (Fig. 5.3.4) (Berger & Braun, 2004) instead of the typical systems of a 1,2,3-substituted benzene ring (Pretsch *et al*., 2000). H-8 and H-9 resonated as two doublets (J = 7.3 Hz) at δ 7.51 and 7.45 together with the singlets of H-3 and H-6, which appeared as an overlapped signal as in **56**, the methoxy and the methylcarbonyl signals at δ 6.21, 3.70, and 2.20. Probably, the phenolic hydroxy group at C-1 was hydrogen bonded with the acetyl

group at C-2 generating a stable six membered ring as shown by the singlet observed at the typical chemical shift value of δ 12.19 as in **56** (Evidente *et al*., 2011c; Evidente *et al*., 2009; Berger & Braun, 2004; Pretsch *et al*., 2000). The couplings observed in the HMBC spectrum (Fig. 5.3.5) (Berger & Braun, 2004) allowed the assignment of the signals of the protonated carbons in the ^{13}C NMR spectrum (Table 5.3.1 and Fig. 5.3.3) at δ 129.4, 122.1, 110.1 (an overlapped signal), 53.8, and 21.9 to C-8, C-9, C-3, and C-6, OMe and MeCO. The signals observed in the ^{13}C NMR spectrum at δ 166.2, 162.8 (an overlapped signal), 149.8, 136.3, and 127.7 were assigned to C-7, C-4 and C-5, C-10, and C-10a (Breitmaier & Voelter, 1987) also on the basis of the couplings observed in the HMBC spectrum (Fig. 5.3.6) (Berger & Braun, 2004) between the C-4 and C-5, which gave an overlapped signal, with H-3, C-6a with H-8, C-7 with H-9, H-8 and OMe, and C-10 and C-10a with H- 9 and H-8. The signals at δ 148.9, 126.2, and 110.0 were assigned to C-1, C-2, and C-10b by comparison with the values reported for the same carbons in **56** (Evidente *et al*., 2011c). Finally, the carbonyl group appeared at the typical chemical shift value of δ 199.2 (Breitmaier & Voelter, 1987). The chemical shifts of all protons and corresponding carbons of **86** were assigned and reported in Table 5.3.1.

On the basis of these results, alternethanoxin C appeared to be close to **56**, differing in the hydrolytic opening of the hemiacetal bond between C-6 and C-5 and the hydroxylation of C-10. The structure assigned to **86** was confirmed from the other couplings observed in the HMBC spectrum (Fig. 5.3.6) and from the data of its HRESI-MS spectrum (Fig. 5.3.8). This latter spectrum showed the sodiated dimeric form $[2M + Na]^+$ and the potassium and sodium clusters $[M + K]^+$ and $[M + Na]^+$, at *m/z* 695, 375, and 359.0845, respectively. Moreover, a correlation was observed in the NOESY spectrum between H-3 and MeCO. Therefore, **86** was formulated as 2′-dihydroxymethyl-2,5,6,6′- tetrahydroxy-3′-methoxy-biphenyl-3-carboxylic acid methyl ester.

Alternethanoxin D, **87**, has a molecular formula of $C_{16}H_{14}O_8$ as deduced from its HRESI-MS spectrum (Fig. 5.3.16) consistent with nine hydrogen deficiencies. The investigation of its ^{1}H and ^{13}C NMR spectra (Table 1; Fig. 5.3.10 and Fig. 5.3.11) showed that **87** was also very closely related

to **56**. In fact, the ^{1}H NMR spectrum differed from that of **56** in the presence of a proton (H-8) of a pentasubstituted benzene ring appearing as a singlet at δ 7.06; the two carbons adjacent to C-8 (C-10 and C-9) were hydroxylated and resonated in the ^{13}C NMR spectrum at the typical chemical shifts values of δ 165.0 and 156.9 (Breitmaier & Voelter, 1987). The singlets of H-3, H-6, MeO, and MeCO resonated at the expected δ values of 6.66, 6.93, 3.90, and 2.50. Furthermore, the singlet at δ 12.19 was due to the phenolic hydroxy group at C-6 hydrogen bonded with the methoxy group at C-7 as in **57**, indicating for C-6 the same relative stereochemistry assigned to alternethanoxin B. The couplings observed in the HMQC spectrum (Fig. 5.3.13) allowed the assignment of the chemical shifts to the hydrogenated carbons and the signals at δ 112.4, 111.6, 106.3, 53.3, and 22.6 to C-8, C-6, C-3, OMe, and MeCO. In addition, the couplings observed in the HMBC spectrum (Table 5.3.1 and Fig. 5.3.14) between C-1 and MeCO, C-2 and C-4 with H-3, C-3 with H-6 and MeCO, C-5 with H-6, and C-7 with H-9 and OMe allowed the assignment of the chemical shifts at δ 149.3, 128.9, 153.0, 161.4, and 168.6 to C-1, C-2, C-4, C-5, and C-7. The signals at δ 155.3, 133.2, and 112.7 were assigned to C-6a, C-10a and C-10b by comparison with the values reported for the same carbons in **56** (Evidente *et al*., 2011c). Finally, the acetyl group appeared at the typical chemical shift value of δ 179.8 (Breitmaier & Voelter, 1987).

The chemical shifts were attributed to all of the protons and the corresponding carbons as reported in Table 5.3.1, and alternethanoxin D, **87** was formulated as 1,4,6,9,10-pentahydroxy-7-methoxy-6*H*-benzo[c]chromene-2-carboxylic acid methyl ester. This structure was confirmed by the other long range couplings observed in the HMBC spectrum (Table 5.3.1 and Fig. 5.3.14) and from the data of its HRESI-MS spectrum (Fig. 5.3.16). This latter spectrum showed the sodiated dimeric form $[2M + Na]^{+}$, and potassium and sodium clusters $[M + K]^{+}$ and $[M + Na]^{+}$ at *m/z* 691, 373, and 357.0574, respectively. Furthermore, a correlation was observed in the NOESY spectrum (Fig. 5.3.15) between H-3 and MeCO.

The absolute configuration at C-6 as depicted in Fig. 5.3.1, established by comparing the chemical shifts of H-6 and H-3, which in **57** differed in respect to **56**, where they gave an

overlapped signal. This was confirmed by the signal at δ 12.10 due to the hemiacetalic hydroxy group at C-6, which was probably hydrogen bonded with the methoxy at C-7 generating a stable six-membered cycle.

Alternethanoxin E, **88**, showed the molecular formula of $C_{16}H_{12}O_6$ deduced from its HRESI-MS (Fig. 5.3.24) and consistent with 11 hydrogen deficiencies. The preliminary investigation of ^{1}H and ^{13}C NMR spectra (Fig. 5.3.18 and Fig. 5.3.19) showed that **88** is closely related to **57**. In fact, its ^{1}H NMR spectrum (Table 5.3.1) differed from that of **57** only in the location of the methoxy group that was attached to C-8 instead of C-7. This generated the typical system of two meta-coupled aromatic protons (H-7 and H-9), resonating as two doublets (J = 2.2 Hz) at δ 6.99 and 6.91 (Pretsch *et al*., 2000). Their carbons resonated in the ^{13}C NMR spectrum (Table 5.3.1) at the typical chemical shift values of δ 168.4, 112.6, and 103.3 for C-8, C-9, and C-7. As expected, H-3, H-6, MeO, and MeCO were all observed as singlets at δ 6.84, 6.64, 3.92, and 2.45, respectively (Pretsch *et al*., 2000). The couplings observed in the HMQC spectrum (Fig. 5.3.21) allowed the assignment of the chemical shifts to the other protonated carbons at δ 111.2, 107.2, 52.0, and 21.5 to C-6, C-3, OMe, and MeCO. The couplings observed in the HMBC (Table 5.3.1 and Fig. 5.3.22) between C-1 and C-2 with H-3, C-4 with MeCO, C-5 and C-6a with H-6, C-8 with OMe, and C-10 with H-9 allowed the assignment of the signals at δ 155.9, 106.2, 148.9, 158.2, 161.2, 168.4, and 168.8 to C-1, C-2, C-4, C-5, C-6a, C-8, and C- 10. The signals at δ 135.9 and 110.1 were assigned to C-10a and C-10b by comparison with the values reported for the same carbons in **56** (Evidente *et al*., 2011c). Finally, the acetyl group appeared at the typical chemical shift value of δ 179.6 (Breitmaier & Voelter, 1987).

The chemical shifts were attributed to all of the protons and the corresponding carbons as reported in Table 5.3.1, and alternethanoxin E, **88** was formulated as 7,9-dihydroxy-2-methoxy-9*H*-4,8-dioxa-cyclopenta[def]phenanthrene-5-carboxylic acid methyl ester. This structure was confirmed by the other long-range couplings observed in the HMBC spectrum (Fig. 5.3.22) and from the data of its HRESI-MS spectrum (Fig. 5.3.24). This latter spectrum showed the sodiated dimeric form $[2M + Na]^+$ and the potassium and sodium clusters $[M + K]^+$ and $[M + Na]^+$ at *m/z*

623, 339, and 323.0521, respectively. Furthermore, a correlation was observed in the NOESY spectrum (Fig. 5.3.23) between H-3 and MeCO.

The absolute stereochemistry at C-6 of alternethanoxin E, as depicted in Fig. 5.3.1, should be the same as **57** considering the chemical shift values of H3/C3 and H6/C6.

5.3.2. Biological activity of alternethanoxins C-E.

The three new alternethanoxins C−E were assayed together with alternethanoxins A and B for their phytotoxic and antimicrobial activity (Table 5.3.2). Among the five compounds tested, only alternethanoxins A and C were toxic to the host plant of the fungus *S. arvensis*. Alternethanoxin C was more active than alternethanoxin A. Couch-grass was sensitive to 4 of 5 compounds tested. Alternethanoxins A and C caused significantly stronger necrotic reaction than alternethanoxins B and D. Alternethanoxin E was non-toxic to both plants (Table 5.3.2). Alternethanoxins A and B showed low antibiotic activity against *B. subtilis*. The yeast fungus was insensitive to them. In the previous study (Evidente *et al*., 2011c), the absence of this kind activity was reported for Alternethanoxins A and B. As compared to them, alternethanoxins C and D had notable antimicrobial activity against both *B. subtilis* and *C. tropicalis*. Alternethanoxin E was not active at all (Table 5.3.2).

5.4.1. Chemical characterization of pure metabolites produced by *Phoma chenopodiicola*, potential mycoherbicide for *Chenopodium album* biocontrol.

Three new phytotoxins, named chenopodolan D (**89**), chenisocumarine (**90**), and chenopodolin B (**91**), were obtained from the purification of the organic extract of *P. chenopodiicola* as reported in details in the Experimental.

Chenopodolan D (**89**, Fig. 5.4.1) has the molecular formula $C_{14}H_{18}O_4$ as deduced from its HRESI-MS spectrum (Fig. 5.4.8), which is consistent with six hydrogen deficiencies (rings or double bonds). Compared to chenopodolans A-C (Cimmino *et al*., 2013c), chenopodolan D ^{1}H and

^{13}C NMR spectra (Table 5.4.1) showed proton and carbon signals very similar to that of their 2,3,4,6-tetrasubstituted furopyran moiety. The signals of the methoxy and the two methyl groups at C-3 , C-2 and C-6, respectively, were very similar to those of the other chenopodolans A-C, while the signals of the side chain attached to C-4 differed substantially. In particular, the ^{1}H (Fig. 5.4.3) and ^{13}C NMR spectra showed a broad singlet and a triplet typical of a hydroxymethylene group (HO-CH_2-11) at δ 4.38 (2H)/59.8 (*t*) (Pretsch *et al*., 2000; Breitmaier & Voelter 1987), in respect to the signals of the terminal vinylic methyl group (Me-11) of chenopodolan C (Cimmino *et al*., 2013c). The presence of a hydroxymethylene is also consistent with the hydroxy group band observed in the IR spectrum (Fig. 5.4.9) (Nakanishi & Solomons, 1977). These findings suggested for **89** the structure of 11-hydroxychenopodolan C, which was confirmed by the assignment of all the protons and the corresponding carbon chemical shifts based on the couplings observed in the COSY and HSQC spectra (Fig. 5.4.4 and Fig. 5.4.5, respectively) (Berger & Braun, 2004). Furthermore, the quaternary carbons C-3, C-3a, C-4, C-6, C-7a and C-9 as reported in Table 5.4.1 were assigned by the long range couplings observed in the HMBC spectrum (Table 5.4.1 and Fig. 5.4.6) (Berger & Braun, 2004). Thus chenopodolan D was formulated as 3-(3-methoxy-2,6-dimethyl-7a*H*-furo[2,3-*b*]pyran-4-yl)-but-2-en-1-ol.

This structure was confirmed by all the long range couplings observed in the HMBC spectrum (Table 5.4.1 and Fig. 5.4.6) and in particular those between H_2-11 with both C-9 and C-10. Further support for the structure assigned to **89** was obtained from its HRESI-MS spectrum (Fig. 5.4.8) which showed: the potassium $[2M + K]^+$, sodium [2M + Na] and protonated $[2M + H]^+$dimer forms at *m/z* 539, 523 and 501, respectively; the potassium $[M + K]^+$ and sodium $[M + Na]^+$clusters at *m/z* 289 and 273, respectively; the pseudomolecular ion $[M + H]^+$ *m/z* at 251.1217.

The structure assigned to **89** was finally confirmed by preparing its 11-*O*-acetyl derivative (**92**, Fig. 5.4.1) by acetylation with pyridine and acetic anhydride. The IR spectrum of **92** showed the absence of any hydroxy group band while its ^{1}H NMR spectrum (Table 5.4.1 and Fig. 5.4.11) differed from that of **89** essentially for the downfield shift ($\Delta\delta$ 0.41 and 0.39) of the H_2C-11 signals

resonating as two broad singlets at δ 4.73 and 4.71, respectively, and for the presence of the singlet of the acetyl group at δ 2.08. Its ESI-MS spectrum (Fig. 5.4.12) showed potassium $[2M + K]^+$, sodium $[2M + Na]^+$ and protonated $[2M + H]^+$ dimer forms, potassium cluster $[M + K]^+$ and the pseudomolecular ion $[M + H]^+$ at *m/z*: 623, 607, 585, 331, 293, respectively.

The absolute configuration of (-)-**89** was determined by *ab initio* computational analyses of its ORD and ECD spectra (Autschbach, 2009, 2012). This approach was demonstrated to be particularly straightforward and reliable for the absolute configuration assignment of natural products (Mazzeo *et al*., 2013; Santoro *et al*., 2013; Santoro *et al*., 2014), allowing analyses in solution and sometimes on a microscale, using very dilute solutions (Berova *et al.*, 2010). To this end, conformational analysis was carried out on the randomly chosen (*R*)-**89** stereoisomer. The conformational search was first carried out at MM level with MMFF94s force field, then refined by optimization at DFT/B3LYP/TZVP level of theory in gas phase, providing 15 appreciably populated conformers (Fig. 5.4.32 and Table 5.4.2). The conformers differ in the rotation of the OCH_3 moiety and of the C4-C9 bond which affect the relative position of the exocyclic double bond with respect to the bicyclic system. UV and ECD spectra of (-)-**89** were recorded in THF in the 210-350 nm range (Fig. 5.4.30). The UV spectrum shows a maximum at 210 nm (ε 44600), followed by a shoulder at 229 nm (ε 29900), two weak broad bands at 254 nm (ε 11500) and 286 nm (ε 6090) and a very broad band centered at 326 nm (ε 7800). The ECD spectrum shows a relatively intense negative Corron effect (CE) at 220 nm ($\Delta\varepsilon$ -6.0) followed weaker bands in the low energy spectral range: two positive CEs at 232 nm ($\Delta\varepsilon$ +0.4)and 254 ($\Delta\varepsilon$ +1.1), a negative band at 272 nm ($\Delta\varepsilon$ -0.4) and a broad positive one centred at 288 nm ($\Delta\varepsilon$ +0.62).

The UV and ECD spectra of (*R*)-**89**, were then calculated in gas phase at the TDDFT/CAM-B3LYP/aug-cc-pVDZ level on previously found conformers and Boltzmann averaged over conformers populations. Computed ECD spectrum for (*R*)-**89** was then compared with the experimental one for (-)-**89** (Fig. 5.4.30). Such comparison shows that, although the low energy range of the theoretical spectrum is not in full agreement with the experimental, computations

correctly reproduced the strongest Cotton effect at 231 nm in sign and position, suggesting the (*R*) absolute configuration for (-)-**89**. A close look into the ECD spectra of single conformers (Fig. 5.4.33) reveals that, although they show quite different ECD spectra, most of them display a negative Cotton effect between 210 and 230 nm, pointing out that the sign of this band can be considered as a reliable probe for absolute configurational assignment of this compound. In order to get a better agreement between computed and experimental ECD spectra, both conformational analysis and ECD calculations were carried out taking into account solvation effects by the IEFPCM implicit solvation model (Tomasi *et. al*., 2005). For this purpose, the outcome from MM conformational analysis on (*R*)-**89** was submitted to optimization at DFT/B3LYP/TZVP theory level by IEFPCM model (THF) leading again to 15 significantly populated conformers (Fig. 5.4.32 and Table 5.4.2). As inferred from Table 5.4.2 solvent effects give rise to a redistribution of conformers population with decreasing of the most populated conformer 2 and increasing of population of conformers 8 and 11. The UV and ECD spectra for (*R*)-**89** were then calculated at the TDDFT/CAM-B3LYP/aug-cc-pVDZ/IEFPCM(THF) level and Boltzmann averaged over conformer populations. Comparison of the computed ECD spectrum for (*R*)-**89** with the experimental one for (-)-**89** (Fig. 5.4.30) shows a better agreement than that with the spectrum computed in the gas phase. In fact the IEFPCM computed spectrum better reproduces the low energy spectral range. Thus, when the solvent effects are taken into account the ECD spectral analysis does allow one to clearly establish the (*R*) absolute configuration for natural (-)-**89**. The good agreement in position and relative intensity of the ECD CEs with experimental spectrum supports also the accuracy in the theoretical reproduction of conformer population.

To further confirm the configurational assignment, computational analysis of the ORD curve was then undertaken. The ORD data of (-)-**89** were recorded in $CHCl_3$ at c = 0.2 g/100ml obtaining a plane negative curve (Fig. 5.4.31). ORD data for (*R*)-**89** were then calculated on previously found conformers at the TDDFT/B3LYP/aug-cc-pVDZ level in gas phase and Boltzmann averaged over all conformer populations. Comparison of computed and experimental data shows (Fig. 5.4.31) an

agreement in sign, both giving rise to a negative plane curve, thus confirming the assignment of the (*R*) absolute configuration for (-)-**89**. However, a difference in one order of magnitude of optical rotation values was observed. To obtain a better numerical agreement between computed and experimental data, the ORD spectrum was calculated also taking into account chloroform solvent effects. Therefore, conformational analysis was carried out by DFT/B3LYP/TZVP/IEFPCM($CHCl_3$) computations, obtaining 14 stable conformers with populations quite similar to those found in THF. For each conformer, ORD data were computed at the TDDFT/B3LYP/aug-cc-pVDZ/IEFPCM($CHCl_3$) level of theory and Boltzmann averaged over all populations, which led to the ORD curve in Fig. 5.4.31. As inferred from Fig. 5.4.31, computations in solution allow one to obtain a slightly better numerical agreement with experimental, although with data still one order of magnitude greater than experimental. In conclusion, both ECD and ORD analyses indicate the same assignment of the (*R*) absolute configuration for (-)-**89**. However, the computed ORD curve does not match (both in gas phase and solvent) the experimental data in order of magnitude.

Chenisocoumarin (**90,** Fig. 5.4.1) has the molecular formula $C_{10}H_{10}O_5$, as deduced from its HRESI MS (Fig. 5.4.19) and consistent with six sites of unsaturation (rings or double bonds). Its IR spectrum (Fig. 5.4.20) showed bands typical for hydroxy, ester carbonyl and aromatic groups (Nakanishi & Solomons, 1977). Compared to that of 6-hydroxymellein, which was previously isolated as the main phytotoxic metabolite from the culture filtrates of the same fungus (Cimmino *et al*., 2013c), the ^1H and ^{13}C NMR spectra (Table 5.4.3) of **90** showed very similar signal systems. Indeed, the ^1H NMR (Fig. 5.4.14) and COSY (Fig. 5.4.14) spectra showed the presence of two *meta*-coupled aromatic protons (H-6 and H-8) resonating as two doublets (J = 1.7 Hz) at δ 6.35 and 6.33, respectively. Their corresponding carbons were observed at δ 106.8 and 99.2, respectively, and were also assigned for their couplings observed in the HSQC spectrum (Fig. 5.4.16). Furthermore, the significant signal of the phenolic protons at C-8 hydrogen bonded with the carbonyl group at C-1, previously observed in the ^1H NMR spectrum of 6-hydroxymellein, was

absent in **90**. Thus, the two hydroxy phenolic groups were located at C-5 and C-7 also on the basis of the chemical shifts of their corresponding quaternary carbons resonating as two singlets at δ 164.1 and 155.3 (C-7 and C-5, respectively) (Breitmaier & Voelter, 1987). These latter signals were assigned on the basis of the couplings observed in the HMBC spectrum (Fig. 5.4.17) (see Table 5.4.3), as well as the other quaternary carbons at δ 142.5, 135.8 and 169.0, which were assigned to C-4a, C-8a and the carbonyl group C-1, respectively. Furthermore, the signal systems typical for 4-hydroxymellein were observed in the ^{1}H and ^{13}C NMR spectra (Table 5.4.3) at δ 4.57 (H-3, *dq*, *J* = 6.6 and 1.8 Hz)/67.2 (C-3, *d*), 4.38 (H-4, *d*, *J* = 1.8 Hz)/77.5 (C-4, *d*) and 1.48 (Me-9, *d*, *J* = 6.6 Hz)/15.8 (Me-19, *q*).

Based on these findings, **90** was formulated as 4,5,7-trihydroxy-3-methyl-isochroman-1-one. This structure was supported from all the couplings observed in the HMBC spectrum (Table 5.4.3 and Fig. 5.4.17) and the data obtained from its HRESI-MS spectrum (Fig. 5.4.19). This latter showed the sodium cluster $[M + Na]^+$ and the pseudomolecular ion $[M + H]^+$ at *m/z* 233 and 211.1218, respectively. The *trans* relative configuration was assigned to **90** on the basis of the significant correlation observed in its NOESY spectrum (Fig. 5.4.18) between H-3 and Me-9 (Berger & Braun, 2004).

The absolute configuration of **90** was assigned by applying an advanced Mosher's method (Othani *et al*, 1991). Besides the suitable secondary hydroxyl group at C-3, **90** also contained two phenol hydroxy groups at C-5 and C-7. First, **90** was converted into the corresponding 5,7-*O,O'*-dimethyl derivative **93** (Fig. 5.4.1) by treatment with an ethereal solution of diazomethane. **93** showed the significant presence of the hydroxy group signal into the IR spectrum (Nakanishi & Solomon, 1987), while its ^{1}H NMR spectrum differed from that of **90** for the presence of the two singlets typical of methoxy groups at δ 3.92 and 3.89, respectively (Pretsch *et al*., 2000). Its ESI-MS spectrum (Fig. 5.4.19) showed: the potassium $[2M + K]^+$ and the sodium $[2M + Na]^+$ dimeric forms at *m/z* 515, 499, respectively; the potassium $[M + K]^+$ and sodium $[M + Na]^+$ clusters at *m/z* 277, 261, respectively; and the pseudomolecular ion $[M + H]^+$ at *m/z* 239. By reaction with *R*-(-)-α-

methoxy-α-trifluoromethylphenylacetyl- (MTPA) and *S*-(+)MTPA chlorides, **93** was converted into the corresponding diastereomeric *S*-MTPA and *R*-MTPA monoesters at C-4 (**94** and **95**, Fig. 5.4.1, respectively), whose spectroscopic data were consistent with the structure assigned to **90**. Subtracting the chemical shift of the protons (Table 5.4.4) of the 3-*O*-*R*-MTPA (**95**) from that of 3-*O*-*S*-MTPA (**94**) esters, the $\Delta\delta$ (**94-95**) values for all of the protons were determined as reported in Fig. 5.4.2. The positive $\Delta\delta$ values were located on the right-hand side, and those with negative values on the left-hand side of the model A as reported in Othani *et al*. (1991). This model allowed the assignment of the *R* configuration at C-4. Considering the relative configuration assigned by NMR as reported above, **90** was then formulated as (4*R*,3*S*)-4,5,7-trihydroxy-3-methyl-isochroman-1-one.

Chenopodolin B (**91**, Fig. 5.4.1) had a molecular formula of $C_{26}H_{32}O_9$ as deduced from its HRESI-MS spectrum (Fig. 5.4.27) which is consistent with eleven hydrogen deficiencies (rings or double bonds). The preliminary investigation of its ^{1}H (Fig. 5.4.22) and ^{13}C NMR spectra (Table 5.4.5) showed that they are very similar to those of chenopodolin (Cimmino et al., 2013b). Indeed, **91** showed the signal systems typical of the tetracyclic *ent*-pimaradiene lactone and also those corresponding to the *α,β*-unstaturated ketone at C(6)-C(8), the vinylic and the tertiary methyl both bonded to C-13, as well as the acetoxy groups at C-1 and C-12. The only difference observed by the comparison of the above cited spectra was the downfield shift ($\Delta\delta$ 1.07) of the C-3 proton appearing as a broad singlet at δ 5.21 while its corresponding carbon resonated at δ 78.1. The signals of a further acetyl group was observed at δ 2.10 (MeCO, *s*)/174.8 (MeCO,s) and 20.7 (MeCO,*q*). Thus, **91** appeared to be the 3-*O*-acetyl chenopodolin for which the chemical shifts of all the protons and the corresponding carbons were assigned on the basis of the couplings observed in the COSY (Fig. 5.4.23), HSQC (Fig. 5.4.24), HMBC (Table 5.4.5 and Fig. 5.4.25) and NOESY (Fig. 5.4.26) spectra. In fact, in this latter spectrum significant correlations were observed between H-15 with both H_2-16 and Me-17, H-9 with H-3, H-12, H_2-11, and Me-17. The structure assigned to **91** was supported by the data obtained from its HR ESIMS spectrum (Fig. 5.4.27), which showed the

sodium dimer form $[2M + Na]^+$ and the sodium cluster $[M + Na]^+$ at *m/z* 999 and 511.1953, respectively. When compared to the chenopodolin 3-*O*-acetyl derivative prepared by acetylation with pyridine and acetic anhydride (Cimmino *et al.*, 2013b), **91** showed the same chromatographic behaviour by TLC analysis of a mixture of the two samples with solvent systems A and C, and the same ^{1}H NMR data as previously reported (Cimmino *et al.*, 2013b). Thus, **91** was formulated as (1*S*,2*S*,3*S*,4*S*,5*S*,9*R*,10*S*,12*S*,13*S*)-1,3,12-triacetoxy-2,-6-oxo-*ent*-pimara-7(8),15-dien-18-oic acid 2,18-lactone. This is the first isolation of **91** as a naturally occurring compound. It was not an artefact generated by the transesterification of chenopodolin with ethyl acetate during the extraction process because chenopodolin remained unaltered when dissolved and left in EtOAc (the solvent used to extract the fungal culture filtrates) for 2-3 days at room temperature.

5.4.2. Biological activity of chenopodolan D (89), chenisocumarine (90) and chenopodolin B (91).

Assayed at $4x10^{-3}$ M on punctured detached leaves, chenopodolin B (**91**) proved to be active in particular on *Sonchus arvensis*, causing the fast appearance of wide necrosis (scored +++) and on *Urtica dioica* and *Parietaria officinalis*, with smaller but still evident necrosis (+). This result differed from the not toxic activity previously observed when chenopodolin B was tested on different plants *(Mercurialis annua*, *Cirsium arvense* and *Setaria viride*) using the same bioassay (Cimmino *et al*., 2013b). The different behaviour could be due to different plant sensitivity. Furthermore, it is also important to consider that when chenopodolin B crosses the plant cell membrane it could be partially or fully hydrolized at the physiological pH, according to the well know lethal metabolism (Hassal, 1990), into chenopodolin. Chenopodolan D (**89**) was less toxic compared to chenopodolin B, as it caused medium-size necrosis (++) on *Stellaria media* and *U. dioica*, whereas was inactive against other plants. Finally, both 9-*O*-acetyl chenopodolan D (**92**) and chenisocoumarin (**90**) proved to be inactive on all the tested plants. The phytotoxicity observed for Chenopodolan D was in agreement with the results previously obtained testing chenopodolans A-C

(Cimmino *et al*., 2013c) confirming that the nature of the side chain at C-4, and in particular its hydroxylation, is an important feature to impart biological activity. Its 9-*O* acetyl derivative probably is inactive because it is not completely hydrolized into **89**.

6. CONCLUSION

1) A virulent strain of *Diaporthe gulyae*, isolated from stem cankers of sunflower and known to be pathogenic to saffron thistle, has been shown to produce both known and previously undescribed metabolites when grown in either static liquid culture or in a bioreactor. Together with phomentrioloxin, a phytotoxic geranylcyclohexenetriol recently isolated from a strain of *Phomopsis* sp., two new phytotoxic trisubstituted α-pyrones, named gulypyrones A and B (7**1** and 7**2**), and two new 1,*O*- and 2,*O*-dehydro derivatives of phomentrioloxin, named phomentrioloxins B and C (7**3** and 7**4**) were isolated from the liquid culture filtrates of *D. gulyae*. These four metabolites were characterized through the use of spectroscopic and spectrometric methods (essentially ^{1}H and ^{13}C NMR and HRESI-MS). When assayed using a 5 mM concentration on punctured leaf disks of weedy and crop plants, apart from 3-nitropropionic acid (the main metabolite responsible for the strong phytotoxicity of the culture filtrate), phomentrioloxin B caused small, but clear, necrotic spots on a number of plant species, whereas gulypyrone A caused leaf necrosis on *Helianthus annuus* plantlets. All other compounds were weakly active or inactive.

2) From the organic extracts of the *D. kongii* culture filtrates a new natural 3-substituted diazenylcyclopentendione, named kongiidiazadione (**84**) was isolated. Its structure was determined by extensive HRESI-MS, NMR and IR analysis and its absolute configuration was assigned by computational analysis of its ECD spectrum. It showed a toxicity effect when assayed on different weeds. While there are no natural compounds containing a cyclopentenedione moiety, only one compound was found to contain the diazenyl group, i.e a bacterial antibiotic produced by *Alcaligeness faecalis* (Fujio *et al*., 1993). However, there are no natural compounds having both diazenyl and cyclopentenedione groups. Thus, kongiidiazadione is the first example of a natural compound containing both these functional groups. Diazo compounds are very well known as intermediates in organic synthesis (Pryor, 1966). Their ability to act as powerful and selective

reducing agents and as a source of free radicals was also previously reported (Zolliger, 1994; Regit, 1986).

3-Nitropropionic and succinic acids, *p*-Hydroxybenzaldehyde and nectriapyrone were previously isolated as phytotoxins from other fungi pathogenic to weeds crops and forest plants as also recently reported when they were also isolated as phytotoxic metabolites from *D. gulyae* (Andolfi *et al*., 2015).

3) Three new polycyclic ethanones, named alternethanoxins C−E (**86-88**), were isolated together with the well-known and closely related alternethanoxins A and B, from the solid culture of *Alternaria sonchi*, a fungal pathogen proposed for perennial sowthistle (*Sonchus arvensis* L.) biocontrol. Alternethanoxins C−E were characterized by spectroscopic methods (essentially NMR and HRESI-MS). When assayed on leaf segments of weeds (*Sonchus arvensis* and *Elytrigia repens*), alternethanoxins A and C showed phytotoxic activity inducing notable necrotic lesions Alternethanoxins C and D possess notable antimicrobial activity when tested against *Bacillus subtilis* (MIC 10 μg/disc) and *Candida tropicalis* (MIC 25 μg/disc). Alternethanoxins A and B had low activity against these microbes, while alternethanoxin E was inactive.

4) A new furopyran, named chenopodolan D (**89**), a new isocoumarin, named chenisocoumarin (**90**) and a new unrearranged *ent*-pimaradiene, named chenopodolin B (**91**), were isolated from *P. chenopodiicola*, a fungal pathogen proposed for the biocontrol of *C. album*. The absolute configuration of chenopodolan D was established by quantum mechanical calculations of ECD and ORD spectra, while that of chenisocumarine by applying an advanced Mosher's method (Ohtani *et al*., 1989). Both **89** and **91** showed phytotoxic activity. Thus, it is possible also hypothesised a synergism between them and chenopodolin and chenopodolans B and C which contribute to the phytoxicity showed by the culture filtrates of *P. chenopodiicola* and its organic extracts. This could be an important finding in the view of a practical application as herbicides of these phytotoxic metabolites in the management of *C. album* .

REFERENCES

Abbas, H.K., & Duke, S.O. **1995**. Phytotoxins from Plant Pathogens as Potential Herbicides. *J Toxicol, Toxin Rev*., *14*, 523-543.

Allard, R. **1965**. *The genetic of colonizing species*, ed. H. Baker and G. Stebins, Academic Press, New York, pp. 49-76.

Alstrom, S. **1990**. Weeds in Human Affairs in Sub-Saharan Africa: Implication for Sustainable Food Production. *Weed Technol*, *5*, 680-690.

Andolfi, A., Boari, A., Evidente, M., Cimmino, A., Vurro, M., Ash, G., Evidente, A. **2015**. Gulypyrones A and B, and Phomentrioloxins B and C, Produced by *Diaporthe gulyae*, a Potential Mycoherbicide for Saffron Thistle (*Carthamus lanatus*). *J. Nat. Prod*., *78*, 623-629

Andreatta, R. H., Nair, V., Robertson A. V., Simpson, W.R.J. **1967**. Synthesis of the *Cis* and *Trans* Isomers of 4-Chloro-*L*-proline, 4-Bromo-*L*-proline, and 4-Amino-*L*-proline *Aust. J. Chem.*, *20*, 1493-1509.

Anslyn, E.V., Dougherty D.A. **2006**. Modern Physical Organic Chemistry, University Science Books, Sausalito, CA.

Ash, G. J., Stodart, B., Sakuanrungsirikul, S., Anshaw, E., Crump, N. **2010**. Genetic Characterization of a Novel *Phomopsis* sp., a Putative Biocontrol Agent for *Carthamus lanatus*. *Mycologia*, 102, 54−61.

Autschbach, J. **2009**. Computing Chiroptical Properties with First-Principles Theoretical Methods: Background and Illustrative Examples. *Chirality*; *21*, E116-E152.

Autschbach, J. **2012**. *Ab initio* Electronic Circular Dichroism and Optical Rotatory Dispersion: from Organic Molecules to Transition Metal Complexes. In: Berova, N., Polavarapu, P.L., Nakanishi, K., Woody, R.W., (Eds.), Comprehensive Chiroptical Spectroscopy: Applications in

Stereochemical Analysis of SyntheticCcompounds, Natural Products, and Biomolecules. John Wiley & Sons, Inc. Hoboken, NJ, USA.. Vol. 1, Chapter 21, pp. 593–642.

Avolio, F., Andolfi, A., Zonno, M. C., Boari, A., Vurro M., Evidente, A. **2011**. Large-Scale Production and Purification of *Ascochyta caulina* Phytotoxins and a New HPLC Method for their Analysis. *Chromatographia, 74*, 633-638.

Ayer, W. A., Fukazawa Y., Orszanska, H. **1993**. . Scytolide, a New Shikimate from the Fungus *Scytalidium urendicola*. *Nat. Prod. Lett.*, *2*, 77-82.

Baker, H. 1974. The Evolution of Weeds. *Annu. Rev. Ecol. Syst*, *5*, 1-24.

Baltazar, A.M. & DeDatta, S.K. **1992**. Weed Management in Rice. *Weed Abstracts*, *41*, 495-507.

Bassarello, C., Bifulco, G., Evidente, A., Riccio, R., Gomez-Paloma, L. **2001**. Stereochemical Studies on Ascaulitoxin: a *J*-based NMR Configurational Analysis of a Nitrogen Substituted System. *Tetrahedron Lett*. 42, 8611−8613.

Berestetskiy, A.O. **2008**. A review of Fungal Phytotoxins: from Basic Studies to Practical Use. *Appl Biochem Micro*, *44*, 453–465.

Berestetskiy, A. O., Yuzikhin, O. S., Katkova, A. S., Dobrodumov, A. V., Sivogrivov, D. E., Kolombet, L. V. **2010**. Isolation, Identification, and Characteristics of the Phytotoxin Produced by the Fungus *Alternaria cirsinoxia*. *Appl. Biochem. Microbiol*., *46*, 75−79.

Berger, S., Braun, S. **2004**. 200 and More Basic NMR Experiments: a Practical Course. Wiley-VCH: Weinheim, Germany;. p 838.

Blair, B.D., Parochetti, J.V. **1982**. Extension and Implentation of Integrated Pest Management Systems. *Weed Sci*, *30*, pp. 48-53.

Bottalico, A.; Capasso, R.; Evidente, A.; Randazzo, G.; Vurro, M. 1990. Cytochalasins: Structure-Activity Relationships. *Phytochemistry*, *29*, 93−96.

Bottiglieri, A., Zonno, M. C., Vurro, M. **2000**. I Bioerbicidi Contro le Piante Infestanti. *L'informatore agrario*, *13*, 69-73.

Breitmaier, E., Voelter, W. **1987**. Carbon-13 NMR Spectroscopy; VCH: Weinheim, pp. 183-280

Briese, D. T. **1988**. Weed Status of Twelve Thistle Species in New South Wales. *Plant Prot. Q, 3*, 135.

Bruhn, T., Schaumloeffel, A., Hemberger, Y., Bringmann, G. **2013.** SpecDis Quantifying the Comparison of Calculated and Experimental Electronic Circular Dichroism Spectra. *Chirality 25*, 243–249

Bruzzese, E. **1990**. Protocols for Biological Control of Weeds and Current Victorian Priorities. *Plant Prot. Q, 5*, 98-99.

Burnside, O.C., **1993**. Weed Science: the Step Child. *Weed technol*, *7*, 515-518.

Charudattan, R. & DeLoach, C.J., **1988**. Management of Pathogens and Insects for Weed Control in Agroecosystems. Weed Management in agroecosystems: ecological approaches, eds M. A. Altieri and M. Liebman. CRC press. Boca Raton: Florida. pp. 245-264.

Cimmino, A., Andolfi, A., Berestetskiy, A., Evidente A. **2008.** Production of Phytotoxins by *Phoma exigua* var.*exigua*, a Potential Mycoherbicide against Perennial Thistles. *J. Agr. Food Chem., 56*, 6304-6309.

Cimmino, A., Andolfi, A., Zonno, M. C., Troise, C., Santini, A., Tuzi, A., Vurro, M., Ash, G., Evidente, A. **2012**. Phomentrioloxin: A Phytotoxic Pentasubstituted Geranylcyclohexentriol Produced by *Phomopsis* ssp., a Potential Mycoherbicide for *Carthamus lanatus* Biocontrol. *J. Nat. Prod*, *75*, 1130−1137.

Cimmino, A., Andolfi, A., Zonno, M. C., Boari, A., Troise, C., Motta, A., Vurro, M., Ash, G., Evidente, A. **2013a**. Phomentrioloxin, a Fungal Phytotoxin with Potential Herbicidal Activity, and its Derivatives: A Structure-Activity Relationship Study. *J. Agric. Food Chem*, *61*, 9645−9649.

Cimmino, A., Andolfi, A., Zonno, M.C., Avolio, F., Santini, A., Tuzi, A., Berestetskyi, A., Vurro, M., Evidente, A. **2013b**. Chenopodolin: a Phytotoxic Unrearranged *ent*-pimaradiene Diterpene Produced by *Phoma chenopodiicola*, a Fungal Pathogen for *Chenopodium album* Biocontrol. *J. Nat. Prod*, *76*, 1291–1297.

Cimmino, A., Andolfi, A., Zonno, M.C., Avolio, F., Berestetskiy, A., Vurro, M., Evidente, A., **2013c**. Chenopodolans A–C: Phytotoxic Furopyrans Produced by *Phoma chenopodiicola*, a Fungal Pathogen of *Chenopodium album*. *Phytochemistry*, *96*, 208–213.

Cimmino, A., Masi, M., Evidente, M., Superchi, S., Evidente, A. **2015**. Fungal Phytotoxins with Potential Herbicidal Activity: Chemical and Biological Characterization. *Nat. Prod. Rep.*, *39*, 1629-1653.

Chisaka, H., 1977. Weed Damage to Crops: Yield Loss Due to Weed Competition. Integrated Control of Weeds, eds J. D. Fryer and S. Matsunaka. Japan Scientific Society Press: Tokyo, pp. 1-16.

Cole, R. J., Cox, R. H. 1981. Handbook of Toxic Fungal Metabolites; Academic Press: New York, Chapter 12, pp 614-645.

Crump, N. S., Ash, G. J., Nickandrow, A. **1996a**. *Phomopsis* spp. Associated with Die-back of Saffron Thistle (*Carthamus lanatus*). *Australas. Plant Pathol*., *25*, 143.

Crump, N. S., Ash, G. J., Nickandrow, A. **1996b**. The Potential of Native Pathogens for the Control of Saffron Thistle. *Plant Prot. Q*, *11*, 254−255.

Dayan, F. E. Cantrell, C. L. Duke, S. O. **2009**. Natural Products in Crop Protection. *Bioorg. Med. Chem*, *17*, 4022−4034.

Dean, F. M. **1963**. Naturally Occurring Oxygen Ring Compounds. Butterworth: London, UK,; pp 82-134.

Dellow, J. J., Wilson, G. C., King, W. M., Auld, B. A. **2002**. Occurrence of Weeds in the Perennial Pasture Zone of New South Wales. *Plant Prot. Q*, 17, 12−16.

Dickinson, J. M. **1993.** Microbial Pyran-2-ones and Dihydropyran-2-ones. *Nat. Prod. Rep*., *10*, 71-98.

Donald, W. W. **1990**. Management and control of Canada thistle (*Cirsium arvense*). *Rev. Weed Sci*., *5*, 193–250.

Evans, G., Rowland, P.C., McLean, G.D., **1996**. Herbicide Dependent Agriculture: Have we Gone too far? Proceedings of the 11th Australian weed conference, R.C.H. Shepherd. Weed Science Society of Victoria, pp. 506-510.

Evidente, A., Capasso, R., Cutignano, A., Taglialatela-Scafati, O., Vurro, M., Zonno, M. C., Motta, A. **1998**. Ascaulitoxin, a Phytotoxic bis-aminoacid *N*-glucoside from *Ascochyta caulina*. *Phytochemistry*, *48*, 1131−1137.

Evidente, A., Andolfi, A., Vurro, M., Zonno, M. C., Motta, A. **2000**. *Trans*-4-aminoproline, a Phytotoxic Metabolite with Herbicidal Activity Produced by *Ascochyta caulina*. *Phytochemistry*, *53*, 231−237.

Evidente, A., Andolfi, A., Vurro, M., Zonno, M. C. **2001a**. Determination of *Ascochyta caulina* Phytotoxins by High Performance Anion Exchange Chromatography and Pulsed Amperometric Detection. *Phytochem. Anal*, 12, 383−387.

Evidente, A.; Motta, A. **2001b**. Phytotoxins from Fungi Pathogenic for Agrarian, Forestal and Weedy Plants. In Bioactive Compounds from Natural Source; Tringali, C., Ed.; Taylor and Francis: London, U.K., pp 473-525.

Evidente, A., Andolfi, A., Vurro, M., Zonno M. C., Motta, A. **2002**. Cytochalasins Z1, Z2 and Z3, Three 24-oxa [14] Cytochalasans Produced by *Pyrenophora semeniperda*. *Phytochemistry, 60*, 45-53.

Evidente, A., Andolfi, A., Abouzeid, M., Vurro, M., Zonno M. C., Motta, A. **2004**. Ascosonchine, the Enol Tautomer of 4-Pyridylpyruvic Acid with Herbicidal Activity Produced by *Ascochyta sonchi*. *Phytochemistry, 65,* 475-480.

Evidente, A. **2006**. Chemical and Biological Characterization of Toxins Produced by Weed Pathogenic Fungi as Potential Natural Herbicides. Rimando A.M. and Duke S.O. (Ed.) Natural Products for Pest Managements, ACS Symposium Series 927, Oxford University Press, Washington DC, pp. 62-75.

Evidente, A., Cimmino, A., Berestetskiy, A., Mitina, G., Andolfi A., Motta, A. **2008a**. Stagonolides B-F, Nonenolides Produced by *Stagonospora cirsii*, a Potential Mycoherbicide of *Cirsium arvense. J. Nat. Prod., 71,* 31-34.

Evidente, A., Cimmino, A., Berestetskiy, A., Andolfi A., Motta, A. **2008b**. Stagonolides G-I and Modiolide A, Nonenolides Produced by *Stagonospora cirsii*, a Potential Mycoherbicide for *Cirsium arvense*. *J. Nat. Prod., 71,* 1897-1901.

Evidente, A., Cimmino, A., Andolfi, A., Vurro, M., Zonno, M. C., Cantrell, C. L., Motta, A. **2008c**. Phyllostictines A–D, Oxazatricycloalkenones Produced by *Phyllosticta cirsii*, a Potential Mycoherbicide for *Cirsium arvense* Biocontrol. *Tetrahedron, 64,* 1612-1619.

Evidente, A., Cimmino, A., Andolfi, A., Vurro, M., Zonno, M. C., Motta, A. **2008d**. Phyllostoxin and Phyllostin, Bioactive Metabolites Produced by *Phyllosticta cirsii*, a Potential Mycoherbicide for *Cirsium arvense* Biocontrol. *J. Agric. Food Chem., 56,* 884-888.

Evidente, A., Punzo, B., Andolfi, A., Berestetskiy, A., Motta, A. **2009**. Alternethanoxin A and B, Polycyclic Ethanones Produced by *Alternaria sonchi*, Potential Mycoherbicides for *Sonchus arvenis* Biocontrol. *J. Agric. Food Chem, 57,* 6656−6660.

Evidente, A., Cimmino, A., Andolfi, A., Berestetskiy A., Motta, A. **2011a**. Phomachalasins A-D, 26-oxa[16] and [15]cytochalasans Produced by *Phoma exigua* var. *exigua*, a potential Mycoherbicide for *Cirsium arvense* Biocontrol. *Tetrahedron*, *67*, 1557-1563.

Evidente, A., Abouzeid, M. A., Andolfi, A., Cimmino, A. **2011b**. Recent Achievements in the Bio-ontrol of Orobanche Infesting Important Crops in the Mediterranean Basin. *J. Agric. Sci. Technol*., *A1*, 461-483.

Evidente, A., Superchi, S., Cimmino, A., Mazzeo, G., Mugnai, L., Rubiales, D., Andolfi, A., Villegas-Fernández, A.M., **2011c**. Regiolone and Isosclerone, Two Enantiomeric Phytotoxic Naphthalenone Pentaketides: Computational Assignment of Absolute Configuration and its Relationship with Phytotoxic Activity. *Eur. J. Org. Chem*., 5564–5570.

Evidente, A., Rodeva, R., Andolfi, A., Stoyanova, Z., Perrone, C., Motta, A. **2011d.** Phytotoxic Polyketides Produced by *Phomopsis foeniculi*, a Strain Isolated from Diseased Bulgarian Fennel. *Eur. J. Plant Pathol.*, *130*, 173-182 (and references therein cited).

Evidente, A., Andolfi, A., Cimmino, A. **2011e**. Fungal Phytotoxins for Control of *Cirsium arvense* and *Sonchus arvensis*. *Pest Technol*., *5*, 1−17.

Fischer A.J., Lozano, J., Ramirez, A., Sanint, L.R. **1993**. Yield Loss Prediction for Integrated Weed Management in Rice. *Int. J. Pest Manage*, *39*, 175-180.

Frisch M. J., Trucks G. W., Schlegel H. B., Scuseria G. E., Robb M. A., Cheeseman J. R., Scalmani G, Barone V, Mennucci B, Petersson G. A., Nakatsuji H, Caricato M, Li X, Hratchian H. P., Izmaylov A. F., Bloino J, Zheng G, Sonnenberg J. L., Hada M, Ehara M, Toyota K, Fukuda R, Hasegawa J, Ishida M, Nakajima T, Honda Y, Kitao O, Nakai H, Vreven T, Montgomery J. A., Peralta J. E., Ogliaro F, Bearpark M, Heyd J. J., Brothers E, Kudin K. N., Staroverov V. N., Kobayashi R, Normand J, Raghavachari K, Rendell A, Burant J. C., Iyengar S. S., Tomasi J, Cossi M, Rega N, Millam J. M., Klene M, Knox J. E., Cross J. B., Bakken V, Adamo C, Jaramillo J, Gomperts R, Stratmann R. E., Yazyev O, Austin A. J., Cammi R, Pomelli C,

Ochterski J. W., Martin R. L., Morokuma K, Zakrzewski V. G., Voth G. A., Salvador P, Dannenberg J. J., Dapprich S, Daniels A. D., Farkas O, Foresman J. B., Ortiz J. V., Cioslowski J, Fox D. J. **2009**. Gaussian 09, Revision A.02. Wallingford, CT;

Fumagalli, P., Andolfi, A., Avolio, F., Boari, A., Cimmino A., Finizio, A. **2013**. Ecotoxicological Characterisation of a Mycoherbicide Mixture Isolated from the Fungus *Ascochyta caulina*. *Pest Manag. Sci., 69,* 850-856.

Fujio I, Michiko T, Toshiaki K, Akiko S, Hideyuki S, Masatoshi I, Akira I, Kentaro K, Hideyuki H, Terumi W. A new antibiotic, B-1015, produced by *Alcaligenesfaecalis*. *Sankyo Kenkyusho Nenpo* 1993;45:113-118.

Gannibal, Ph. B., Egorova, A. V., Berestetskiy, A. **2006**. Potential of the *Alternaria* fungi for biocontrol of sow thistle. In Proceedings of International Conference "Development of Environmentally Friendly Plant Protection", Puhajarve, Estonia, Sept 5-7,; p 27.

Graniti, A., Durbin, R.D., Ballio, A. **1989**. Phytotoxins and Plant Pathogenesis. NATO ASI Series, Series H, Vol 27, Springer-Verlag, Berlin.

Grekul, C.W., Cole, D.E., Bork, E.W. **2005**. Canada Thistle (*Cirsium arvense*) and Pasture Forage Responses to Wiping with Various Herbicides. *Weed Technol, 9,* 298–306.

Grime, J.P. **1979**. Plant Strategies and Vegetation Processes. John Wiley and Sons., New York.

Grekul, C. W., Cole, D. E., Bork, E. W. **2005**. Canada Thistle (*Cirsium arvense*) and Pasture Forage Responses to Wiping with Various Herbicides. *Weed Technol., 9,* 298–306.

Harlan, J. R., & deWelt, J. M. J. **1965**. Some Thoughts About Weeds. *Economic Botany* 19: 16-24.

Hassan, S. **1980**. Plant Pathogens and Biological Control of Weeds. *Rev Plant Pathol, 59,* 349.

Heap, I.M. **2005**. The International Survey of Herbicide Resistant Weeds. Available on line at www.weedscience.org/in.asp.

Holm, L. G., Pluckett, D. L., Pancho, J. V., Herberger, J. P. **1977**. The World's Worst Weeds (Distribution and Biology); University Press of Hawaii: Honoloulou, HI,; pp 84−91.

Holt, J.S. **1988**. Ecological and Physiological Characteristics of Weeds. Altieri M.A. and Liebman M. (Ed), Weed Management in Agroecosystems: Ecological Approaches. CRC Press, Boca Raton.

Hoppe H. H. **1998**. Fungal Phytotoxins In Resistance of Crop Plants Against Fungi; Hartleb, H., Heitefuss, R., Hoppe, H. H., Eds.; G. Fischer: Stuttgart, Germany, pp 54-82.

Hunter, O. F. **2010**. Use of Natural Products in the Crop Protection Industry. *Phytochem. Rev*, *10*, 185−194.

Kale S., & Bennett, J.W. **1992**. Handbook in Applied Mycology. Mycotoxins in Ecological Systems, Bhtnagar D., Lillehoj E.B., and Arora D.K. (Ed.), New York: Marcel Dekker, pp. 311–331.

Kempenaar, C. **1995**. Studies on the Biological Control of *Chenopodium album* by *Ascochyta caulina*. Doctoral Thesis, University of Wageningen, The Netherlands.

Kempenaar, C., Horsten, P. J. F. M., Scheepens, P. C. **1996**. Spore Germination and Disease Development After Apllication of Pycnidiospores of *Ascochyta Caulina* to *Chenopodium Album Plants*. *Eur. J. Plant Pathol*, *102*, 143−153.

Kenfield, D., Bunkers, G., Strobel, G., Sugawara, F. **1989**. Fungal Phytotoxins; Potential New Herbicides. In Phytotoxins and Plant Pathogenesis; Graniti, A., Durbin, R. D., Ballio, A., Eds.; Springer-Verlag Berlin, Germany,; pp 319-335.

Kent, J. M. **1994**. Plant Protection B – Notes and Readings: Weeds. Charles Sturt University. pp. 2.

Kloppenburg, D. J., Hall, J. C. **1990**. Efficacy of Five Different Formulations of Clopyrad on *Cirsium arvense* (L.) Scop. and Polygonum convolvulus. *Weed Res*., *30*, 227–234.

Kohli, R.K., Batish, D.R., Singh, H.P. **2006**. Weeds and Their Management: Rationale and Approaches. Handbook of Sustainable Weed Management. Singh P.H., Batish D.R. and Kohli R.K. (Ed.), The Harworth Press Inc., New York, pp. 1-19.

Kropff, M.J. **1993**. Eco-Physiological Models for Crop-Weed Competition. Modelling Crop-Weed Interactions, eds M. J. Kropff and Van Laar H. H. X: X, pp. 25-32.

Ichara, A., Tazaki, H., Sakamura, S. **1983**. Solanapyrones A, B and C, Phytotoxic Metabolites from the Fungus *Alternaria solani*. *Tetrahedron Lett*., 24, 5373–5376.

Lemna, W.K., & Messersmith, C.G. **1990**. The Biology of Canadian Weeds *Sonchus arvensis L*. *Can. J. Plant Sci, 70*, 509-532.

Lovett, J.V., & Knights, S.E. **1996**. Where in the World Is Weed Science Going?, Proceedings of 11th Australian weed conference, R. C. H. Shepherd. Weed Science Society of Victoria, pp. 2-13.

Masi, M., Meyers, S., Cimmino, A., Andolfi A., Evidente, A. **2014a**. Pyrenophoric Acid, a Phytotoxic Sesquiterpenoid Penta-2,4-dienoic Acid Produced by a Potential Mycoherbicide, *Pyrenophora semeniperda***.** *J. Nat. Prod., 77*, 925-930.

Masi, M., Meyers, S., Cimmino, A., Clement, S., Black, B., Evidente, A. **2014b**, Pyrenophoric Acids B and C, Two New Phytotoxic Sesquiterpenoids Produced by *Pyrenophora semeniperda*. *J. Agric. Food Chem., 62*, 10304-10311.

Masi, M., Meyers, S., Clement, S., Andolfi, A., Cimmino A., Evidente, A. **2014c**. Spirostaphylotrichin W, a Spirocyclic γ-Lactam Isolated from Liquid Culture of *Pyrenophora semeniperda*, a Potential Mycoherbicide for Cheatgrass (*Bromus tectorum*) Biocontrol. *Tetrahedron, 70*, 1497-1501.

Matsumori, N., Kaneno, D., Murata, M., Nakamura H., Tachibana K. **1999**. Stereochemical Determination of Acyclic Structures Based on Carbon-Proton Spin-Coupling Constants. A Method of Configuration Analysis for Natural Products. *J. Org. Chem. 64*, 866-876

Mazzeo, G., Santoro, E., Andolfi, A., Cimmino, A., Troselj, P., Petrovic, A.G., Superchi, S., Evidente, A., Berova, N. **2013**. Absolute Configurations of Fungal and Plant Metabolites by Chiroptical Methods. ORD, ECD, and VCD Studies on Phyllostin, Scytolide, and Oxysporone. *J. Nat. Prod*. *76*, 588-99.

Mohler, C.L. **1996**. Ecological Bases for the Cultural Control of Annual Weeds. *J. Prod Agric*, *9*, 468-474.

Moreno-Manas, M., Pleixats, R. **1992**. Dehydroacetic Acid, Triacetic Acid Lactone and Related Pyrones. In *Advances in Heterocyclic Chemistry*; Katritzky, A. R., Ed.; Academic Press: San Diego, CA,; Vol. 53, pp 1-84.

Moscowitz, A., **1965**. Action of Light and Organic Crystals. In: Sinanoglu, O. (Ed.), Modern Quantum Chemistry, Part III. Academic Press, London, p. 31.

Myers, M. G., Harvey R. G. **1993**. Triazine-Resistant Common Lambsquarters (*Chenopodium album* L.) Control in Field Corn (*Zea mays* L.) *Weed Technol*, *7***,** 884-889

Nakanishi, K., and Solomon, P.H. **1977**. Infrared Absorption Spectroscopy, second ed. Holden Day, Oakland, pp. 17–44.

Norris, R.F., **1992**. Have Ecological and Biological Studies Improved Weed Control Strategies?, Proceedings of the 7th Australian Weeds Conference. Vol. 1 pp. 129.

Ohtani, I. Kusumi, T., Ishitsuka M. O., Kakisawa H. **1989**. An Application of an Advanced Mosher's Method. *Tetrahedron*, *30*, 3147-3150.

Onishi, H. R., Pelak, B. A., Gerckens, L. S., Silver, L. L., Kahan, F. M., Chen, M. H., Patchett, A. A.,Galloway, S. M., Hyland, S. A., Derson, M. S., Raetz, C. R. **1996**. Antibacterial Agents that Inhibit Lipid A Biosynthesis. *Science*, *274*, 980−982.

Ostlie, M. H., Howatt, K. A. **2013**. Downy Brome (*Bromus tectorum*) Competition and Control in No-Till Spring Wheat. *Weed Technol.*, *27*, 502-508.

Parsons, W. T., & Cuthbertson, E. G. **1992**. Noxious Weed of Australia; Kata Press: Melbourne/Sidney; p 692.

Penner, D., **1982**. Integrated Approach to Teaching Integrated Pest Management. *Weed Sci*, *30*, 46-47.

Pinkerton, F., & Strobel, G. A. **1976**. Serinol as an Activator of Toxin Production in Attenuated Cultures of *Helminthosporium sacchari*. Proc. Natl. Acad. Sci. U. S. A. *73*, 4007−4011.

Portoghese, P. S., Mikhail, A. A. **1966**. Bicyclic Bases. Synthesis of 2, 5-Diazabicyclo [2.2. 1] heptanes1. *J. Org. Chem*, *3*, 1059-1062.

Pretsch, E.; Bühlmann, P.; Affolter, C. **2000**. Structure Determination of Organic Compounds – Tables of Spectral Data; 3rd ed.; Springer-Verlag: Berlin, pp. 161-243.

Pryor, A. **1966.** 'Free Radical', Mcgraw Hill, New York, NJ.

Regit, M. **1986.** 'Diazo Compounds-Properties and Synthesis', Academic Press Inc., Orlando FL.

Rimando, A.; Duke, S. O. **2006**. Natural Products for Pest Management. In Natural Products for Pest Management; Rimando, A., Duke, S. O., Eds.; American Chemical Society: Washington, DC, pp 2 21.

Ross, M.A., & Lembi, C.A., 1985. Applied Weed Science, Burgess Publishing Company: Minneapolis, Minnesota.

San-Martin, A., Painemal, K., Diaz, Y., Martinez, C., Rovirosa, J. **2005** Metabolites From The Marine Fungus *Cladosporium Cladosporioides. J. Arg. Chem Soc.*, *93*, 247-251.

Santoro, S., Superchi, S., Messina, F., Santoro, E., Rosati, O., Santi, C., Marcotullio, M.C. **2013.** A Garsenone, a Cadinane Sesquiterpenoid From *Commiphora erythraea*. *J. Nat. Prod*. *76*, 1254-1259.

Scherlach, K., Boettger, D., Remme N., Hertweck, C. **2010**. The Chemistry and Biology of Cytochalasans. *Nat. Prod. Rep*, *27*, 869-886.

Scott A.I. **1964**. Interpretation of Ultraviolet Spectra of Natural Products, Pergamon Press LTD: Oxford,; pp. 135-164.

Shaw, W.C., **1982**. Integrated Weed Management Systems for Pest Managemenet. *Weed Sci*, *30*, 3-11.

Shorten, C. Note Number LC0225, **2007**. http://www.dpi.vic. gov.au/agriculture/pests-diseases-and-weeds/weeds/other-declaredweeds/ saffron-thistle.

Sindel, B. **1996**. Glyphosate Resistance Discovered in Annual Ryegrass.*Resist. Pest Manage*, *8*, 5−6.

Smith, R.J., **1983**. Weeds of Major Economic Importance in Rice and Yield Losses Due to Weed Competition. Proceeding of the Conference on Weed Control in Rice, International Rice Research Institute, pp. 19-36.

Smith, R.J., **1991**. Integration of Biological Control Agents with Chemical Pesticides. Microbial Control of Weeds, ed. D. O. TeBeest. Champan and Hall Inc: London.

SPARTAN ’02; Wavefunction Inc.: Irvine, CA; <http://www.wavefunction.com>.

Stahlman P. W., Miller, S. D. **1990**. Downy Brome (*Bromus tectorum*) Interference and Economic Thresholds in Winter Wheat (*Triticum aestivum*). *Weed Sci.*, *38*, 224-228.

Strobel, G.A., **1991**. Il Controllo Biologico delle Erbe Infestanti. *Le Scienze*, *277*, 56-63.

Swanton, C.J., & Murphy, S.D., 1996. Weed Science Beyond the Weeds: the Role of Integrated Weed Management in Agroecosystem Health. *Weed Sci*, *44*, 437-445.

Takuo, A., Kimiharu, I. **1988**. Phytotoxin Produced by *Rhizoctonia oryzae* Ryker *et* Gooch. *Agr. Biol. Chem.*, *52*, 2625-.

Templeton, G.E., **1985**. Specific Weed Control with Mycoherbicides. British crop protection conference – weeds, pp. 601-608.

Tewari, J. P.; Bains, P. S. **1997**. Phytotoxins Produced by *Alternaria brassicae* and Bioassay of Dextrusin B. In Toxins in Plant Disease and Development and Evolving Biotechnology; Upadayay, R. K., Mukerji, K. G., Eds.; Oxford and IBH Publishing: New Delhi, India, pp 21-36.

Thompson, S. M., Tan, Y. P., Young, A. J., Neate, S. M., Aitken, E. A. B., Shivas, R. G. **2011**. Stem Cankers on Sunflower (*Helianthus annuus*) in Australia Reveal a Complex of Pathogenic *Diaporthe* (*Phomopsis*) Species. *Persoonia*, *27*, 80−89.

Thomson, R. H. **1985**. The Chemistry of Natural Products. Blackie: Glasgow, Scotland,; pp 107-153.

Tomasi J, Mennucci B, Cammi R. **2005**. Quantum Mechanical Continuum Solvation Models. *Chem Soc Rev*; *105*, 2999–3094.

Trumble, J.T., & Kok, L.T., **1982**. Integrated Pest Management Techniques in Thistle Suppression in Pastures of North America. *Weed res*, *22*, 345-359.

Turner, W. B.; Aldridge, D. C. **1983**. Fungal Metabolites; Academic Press: London, U.K.

Tuzi, A., Andolfi, A., Cimmino A., Evidente, A. **2010**. X-Ray Crystal Structure of Phyllostin, a Metabolite Produced by *Phyllosticta cirsii*, a Potential Mycoherbicide of *Cirsium arvense*. *J. Chem. Crystallogr.*, *40*, 15-18.

Vurro, M., Bottalico, A., Capasso R., Evidente, A. **1997**. in: *Toxins in Plant Disease Development and Evolving Biotechnology*, ed. R. K. Upadhyay and K. G. Mukerji, Oxford & IBH Publishing Co, New Delhi, India, pp. 127-147.

Vurro, M.; Evidente, A.; Andolfi, A.; Zonno, M. C.; Giordano, F.; Motta, A. **1998**. Brefeldin A and R,*β*-dehydrocurvularin, Two Phytotoxins from *Alternaria zinniae*, a Biocontrol Agent of *Xanthium occidentale*. *Plant Sci*., 138, 67–79.

Vurro, M., Zonno, M. C., Evidente, A., Andolfi, A., Montemurro, P. **2001**. Enhancement of Efficacy of *Ascochyta caulina* to Control *Chenopodium album* by Use of Phytotoxins and Reduced Rates of Herbicides. *Biol. Control, 21*, 182-190.

Waterhouse, D.F., **1978**. Biological Control. CSIRO Information Service. Sheet No. 1-14.

Yanai T, Tew D. P., Handy N. C. **2004**. A New Hybrid Exchange–Correlation Functional Using the Coulomb-Attenuating Method (CAM-B3LYP). *Chem Phys Lett*; *393*, 51.

Yuzikhin, O., Mitina G., Berestetskiy, A. **2007**. Herbicidal Potential of Stagonolide, a New Phytotoxic Nonenolide from *Stagonospora cirsii***.** *J. Agric. Food Chem., 55*, 7707-7711.

Zhao Y, Truhlar DG. **2008**. The M06 Suite of Density Functionals for Main Group Thermochemistry, Thermochemical Kinetics, Noncovalent Interactions, Excited States, and Transition Elements: Two New Functionals and Systematic Testing of Four M06-Class Functionals and 12 Other Functionals. *Theor Chem Acc*; *120*, 215–241.

Zolliger, H. **1994.** 'Diazo Chemistry', Verlag Chemie, Weinheim,.

Zonno, M. C., Vurro, M., Lucetti, S., Andolfi, A., Perrone C., Evidente, A. **2008**. Phyllostictine A, a Potential Natural Herbicide Produced by *Phyllosticta cirsii*: *in vitro* Production and Toxicity. *Plant Sci., 175*, 818-825.

Zoschke, A. **1990**. Yield Loss in Tropical Rice as Influenced by the Competition of Weed Flora and the Timing of its Elimination. Pest Management in Rice, eds B. T. Grayson, M. B. Green and L. G. Copping. Elsevier Science: London, pp. 301-313.

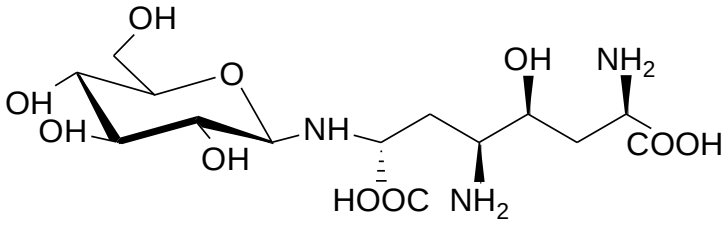

1

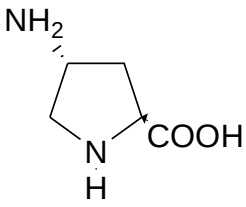

2

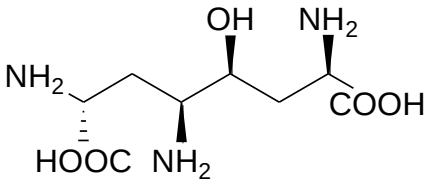

3

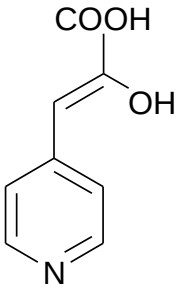

4

Figure 1.5.1 Structure of Ascaulitoxin (**1**), *trans*-4-aminoproline (**2**), 5-hydroxyoctandioic acid (**3**) ascosonchine (**4**) isolated from *Ascochyta caulina* culture filtrate.

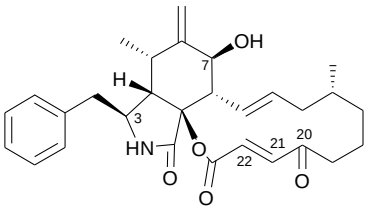

Cytochalasin A, **5**

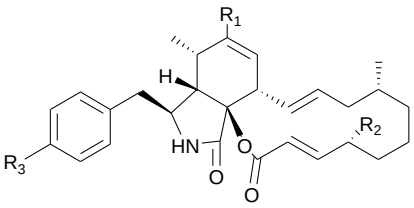

Cytochalasin Z2, **8**, R_1=CH_2OH, R_2=OH, R_3=H

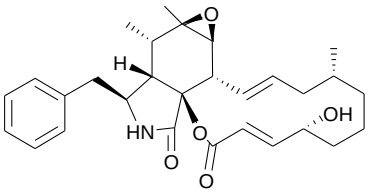

Cytochalasin F, **7**

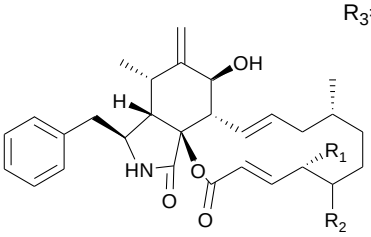

Cytochalasin B, **6**, R_1=OH, R_2=H
Cytochalasin Z3, **9**, R_1=H, R_2=OH

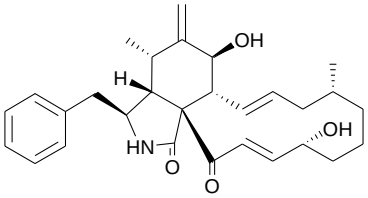

10 Deoxaphomin

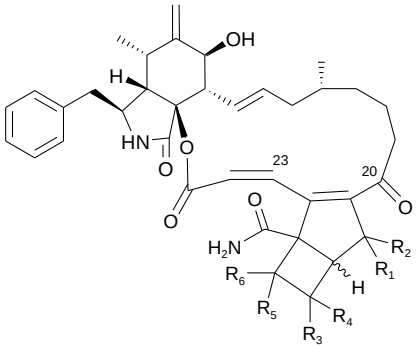

Phomachalasin A, **11**, R_1= OCH_3, R_2=R_3=R_5=H, R_4=R_6=OH
Phomachalasin C, **13**, R_1=OCH_3, R_2= R_4=R_6= H, R_3=R_5=OH
Phomachalasin D, **14**, R_1=OCH_3, R_2=R_3= R_6=H, R_4=R_5=OH

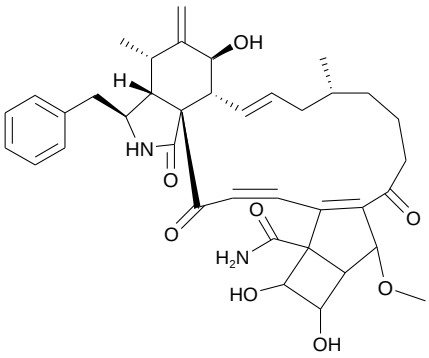

Phomachalasin B, **12**

Figure 1.5.2. Structure of Cytochalasins A, B, F, Z2, Z3 (**5**-**9**), deoxaphomin (**10**), phomachalasins A, B, C, D (**11**-**14**), isolated from two different strains (C-177 and S-9) of *Phoma exigua* var. *exigua* culture filtrate.

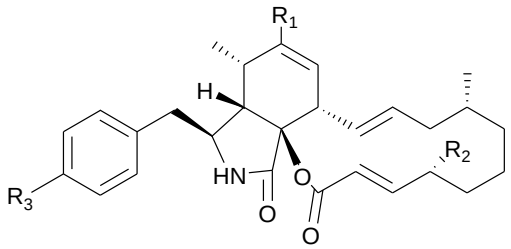

Cytochalasin T, **17**, R_1=CH_3, R_3=H, R_2=OH
Cytochalasin Z1, **18**, R_1= CH_3, R_2=H, R_3=OH

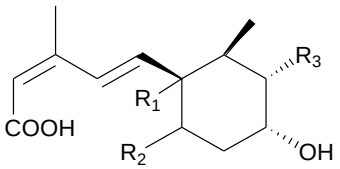

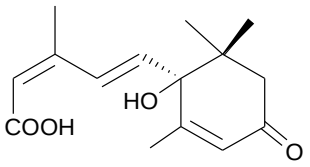

Pyrenophoric acid R_1=H, R_2=β-Me, R_3=OH, **19**
Pyrenophoric acid B R_1=OH, R_2=β-Me, R_3=H, **20**
Pyrenophoric acic C R_1=H, R_2=α-Me, R_3=OH, **21**

Abscisic acid, **22**

Figure 1.5.3. Structure of Cytochalasins T, Z1 (**17-18**), pyrenophoric acid (**19**), pyrenophoric acid B and C (**20-21**) and abscisic acid (**22**), isolated from *Pyrenophora semeniperda* solid culture filtrate.

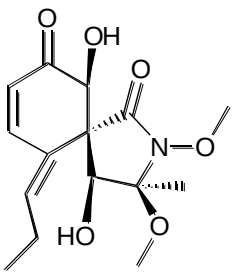

Spirostaphylotrichin W, **23**

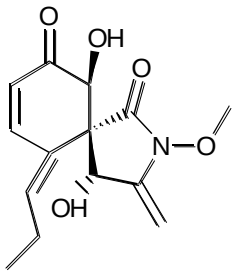

Spirostaphylotrichin A, **24**

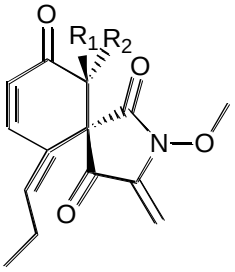

Spirostaphylotrichin C, **25**, R_1=OH R_2=H
Spirostaphylotrichin D, **26,** R_1=H R_2=OH

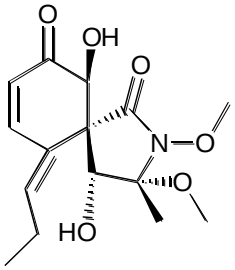

Spirostaphylotrichin V, **28**

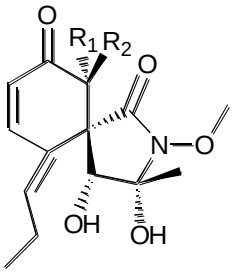

Triticone E, **29**, R_1=OH R_2=H
Spirostaphylotrichin R, **27**, R_1=H R_2=OH

Figure 1.5.4. Structure of spirostaphylotrichin W, A, C, D, R, V (**23-28**), and triticone E (**29**), isolated from *Pyrenophora semeniperda* liquid culture filtrate.

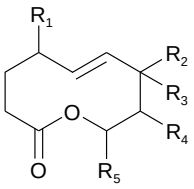

Stagonolide, **30**, R_1=H, R_2,R_3=O, R_4=α-OH, R_5=β-$CH_2CH_2CH_3$

Stagonolide B, **31**, R_1=β-OH, R_2=H, R_3=α-OH, R_4=α–OH, R_5=β-$CH_2CH_2CH_3$

Stagonolide C, **32,** R_1=α-OH, R_2=H, R_3=β–OH, R_4=H, R_5=β-CH_3

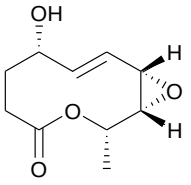

Stagonolide D, **33**

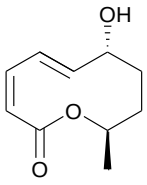

Stagonolide E, **34**

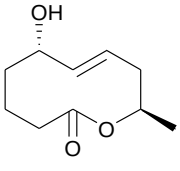

Stagonolide F, **35**

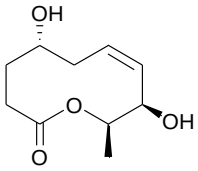

Stagonolide G, **36**

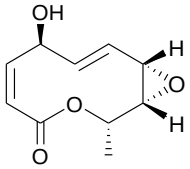

Stagonolide H, **37**

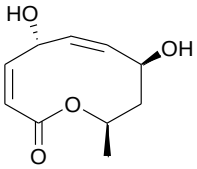

Stagonolide I, **38**

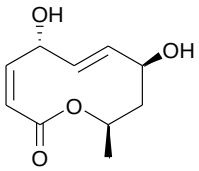

Modiolide A, **39**

Figure 1.5.5. Structures of staganolide (**30**), staganolide B-I (**31-38**), and modiolide A (**39**), isolated from *Stagonospora cirsii* culture filtrate.

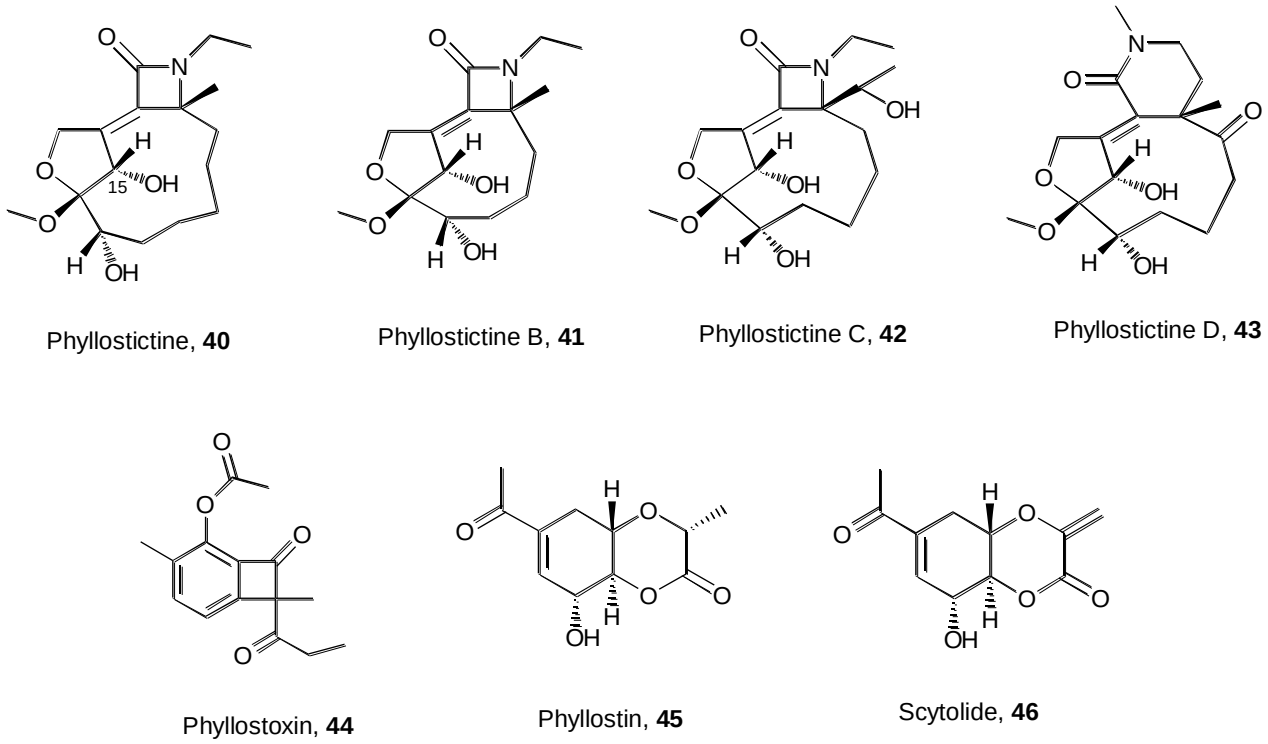

Figure 1.5.6. Structures of phyllostictine (**40**), phyllostictine B-D (**41**-**43**), phyllostoxin (**44**), phyllostin (**45**) and scytolide (**46**) isolated from *Phyllosticta cirsii* culture filtrate.

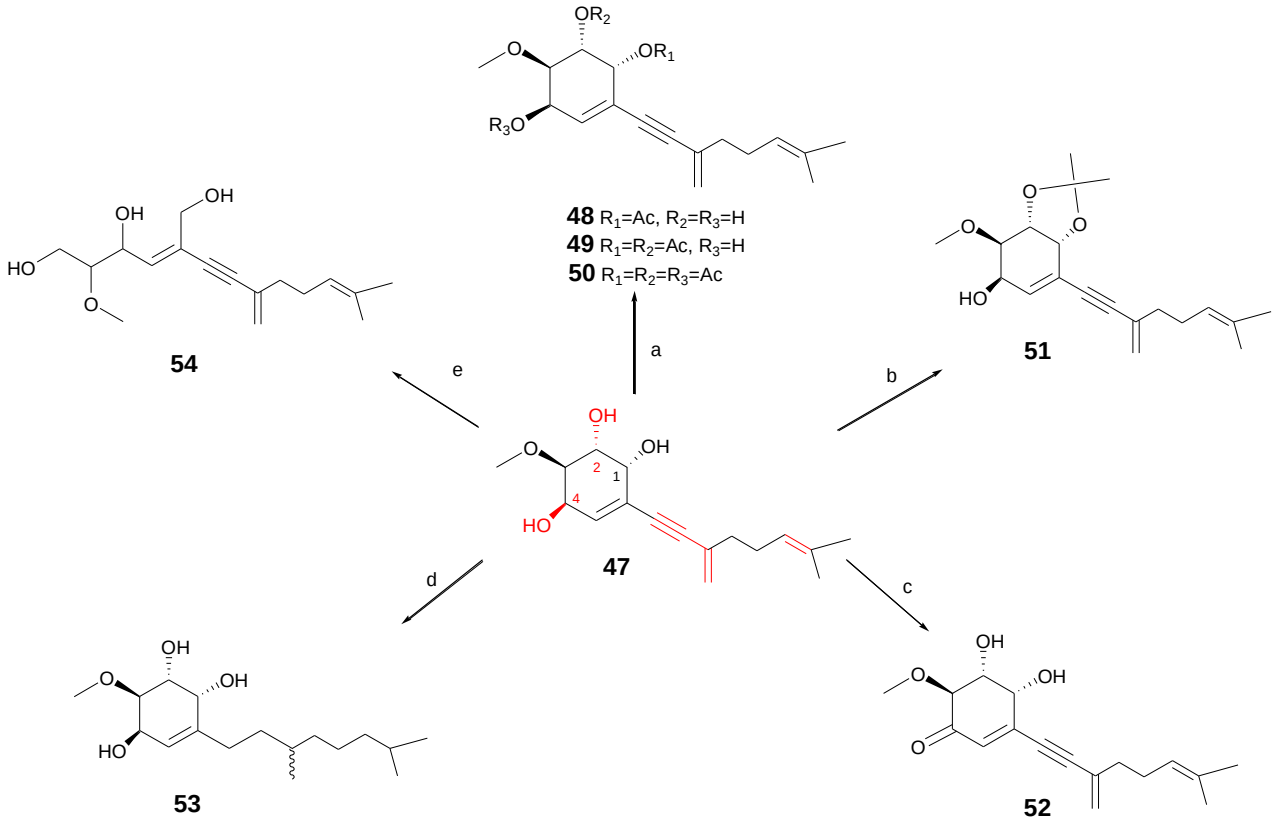

Reagents and conditions: (a) Ac_2O, pyridine, rt, 5 or 10 min; (b) dry Me_2CO, dry $CuSO_4$, rt, 2 h; (c) MnO_2, CH_2Cl_2, rt, 5 h; (d) H_2, 5%Pd/C, MeOH, rt, 15 min; (e) MeOH, $NaIO_4$ rt, 1 h; MeOH, $NaBH_4$ rt, 1 h;

Figure 1.6.1. Structures of phomentrioloxin (**47**) and its derivatives (**48-54**), isolated from *Diaporthe gulyae* culture filtrate.

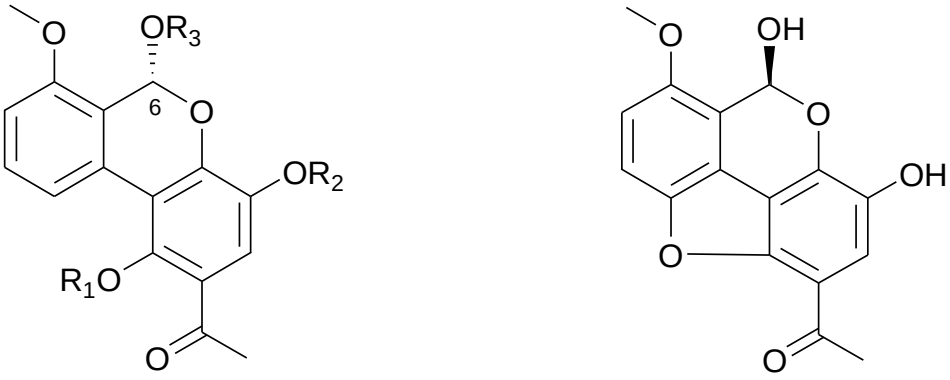

56 $R_1=R_2=R_3=H$
58 $R_1=R_2=R_3=Ac$
59 $R_1=H$ $R_2=R_3=Me$
60 $R_1=R_2=H$ $R_3=S$-MTPA
61 $R_1=R_2=H$ $R_3=R$-MTPA

57

Figure 1.7.1. Structures of alternethanoxin A (**56**), its triacetyl and 4,6-*O*,*O*′-dimethyl ether derivatives (**58**-**59**) and 6-*O*-*S*-MTPA and 6-*O*-*R*-MTPA esters derivatives (**60**-**61**) isolated from *Alternaria sonchi* culture filtrate.

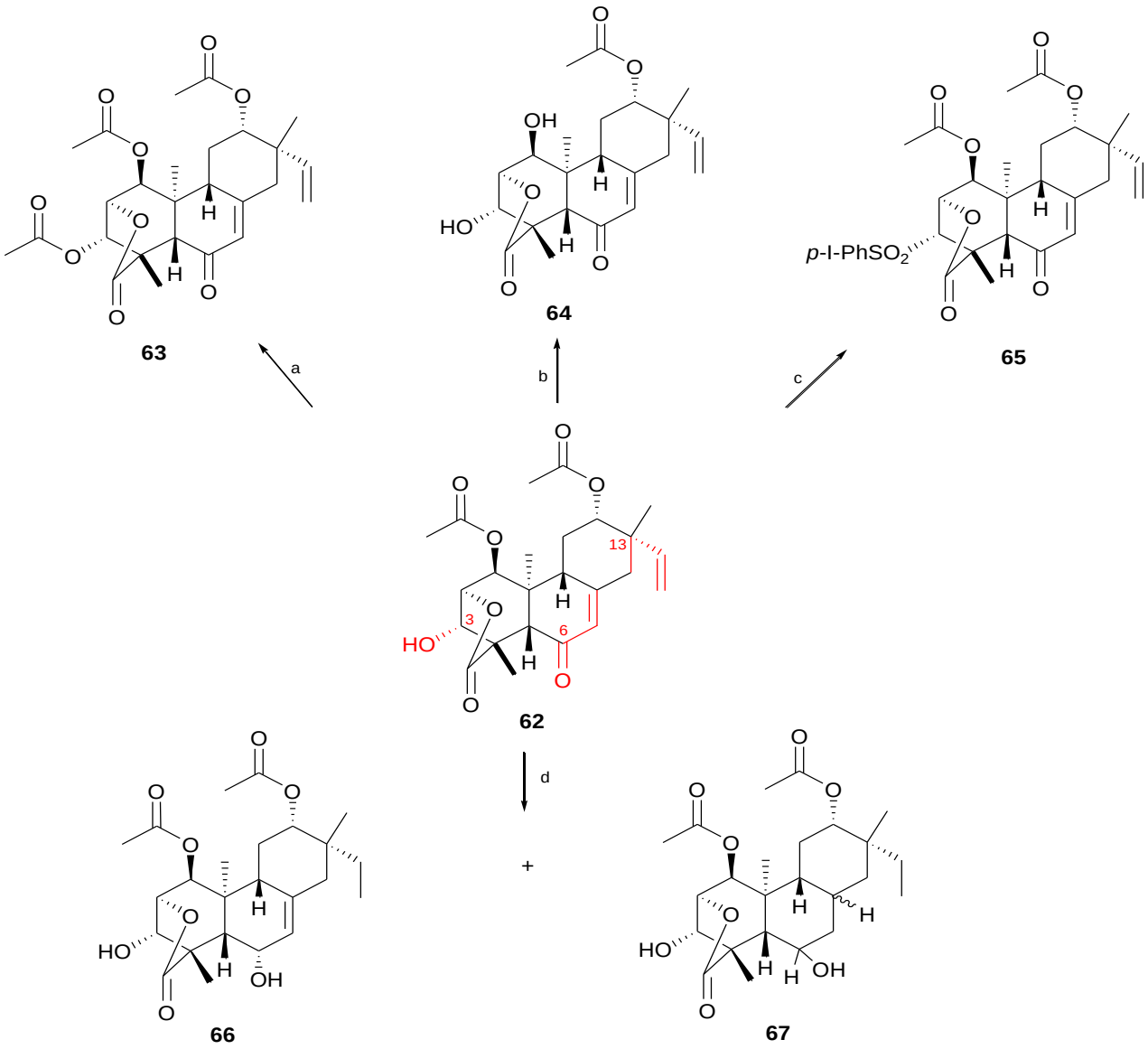

Figure 1.8.1. Structures of chenopodolin (**62**) and its derivatives (**63**-**67**) isolated from *Phoma chenopodiicola* culture filtrate.

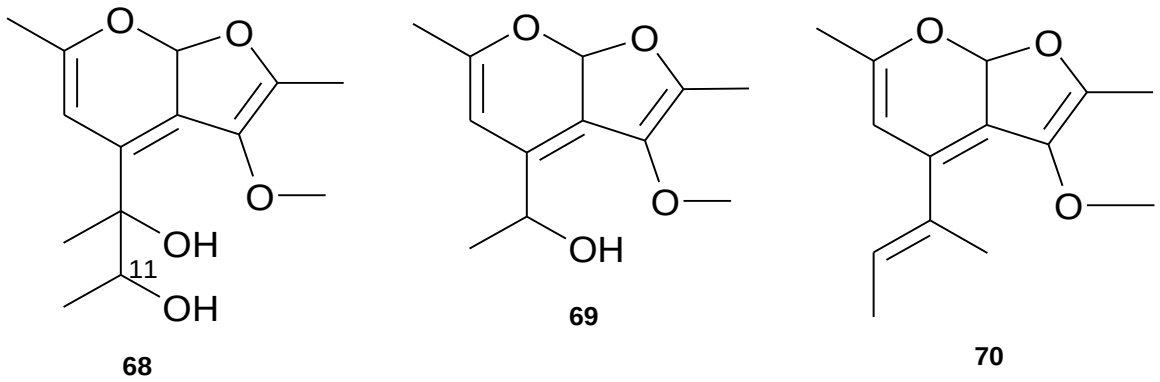

Figure 1.8.2. Structures of chenopodolan A-C (**68-70**), isolated from *Phoma chenopodiicola* culture filtrate.

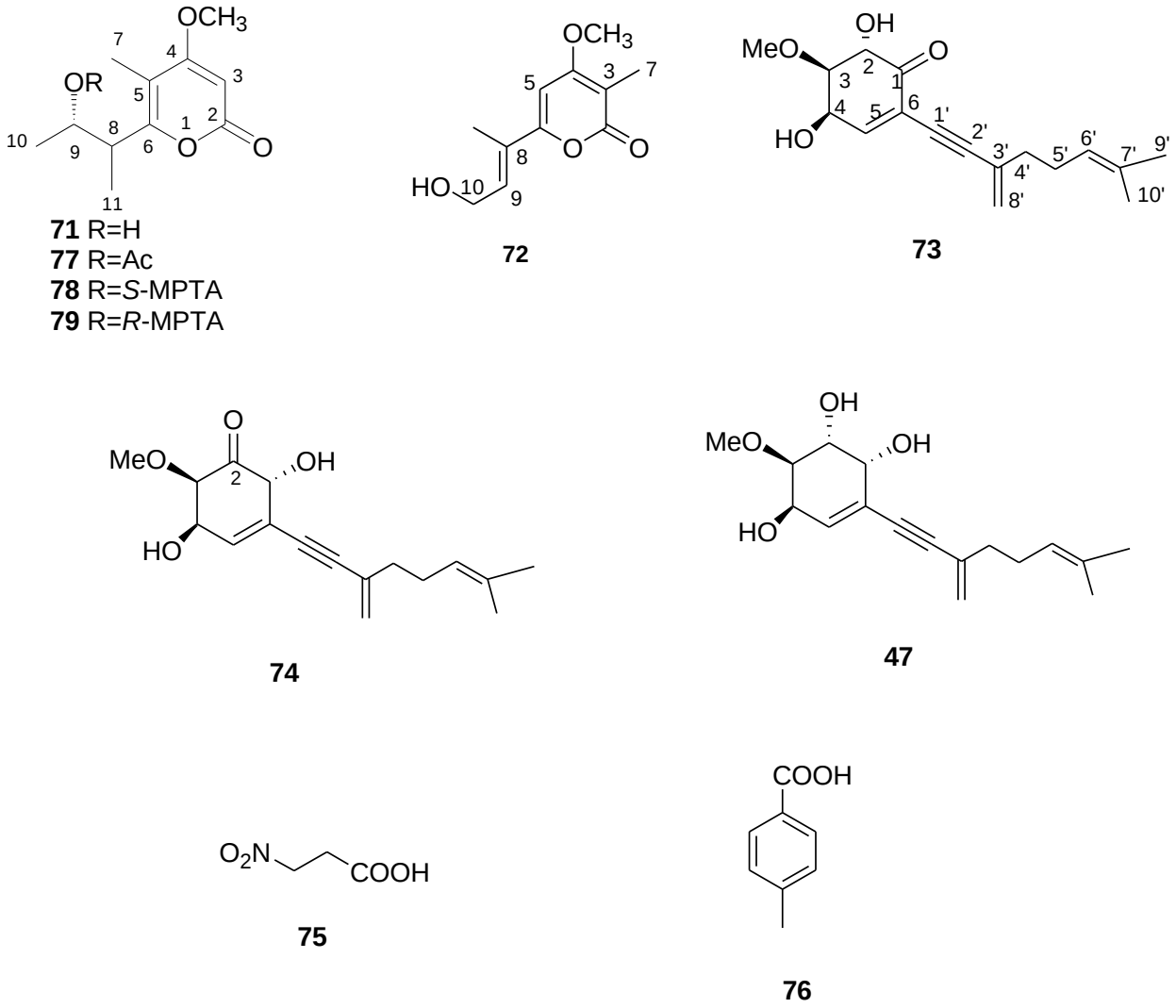

Figure. 5.1.1 Structures of: gulypyrone A (**71**); its 9-*O*-acetyl, 3-*O*-*S*-MTPA, 3-*O*-*R*-MTPA and 3-*O*-acetyl esters (**77**-**79**, respectively); gulypyrone B (**72**), phomentrioloxin B, C and phomentrioloxin (**73**, **74** and **47,** respectively), and 3-nitropropionic and 4-methylbenzoic acids (**75** and **76**, respectively) produced by *D. gulyae* grown in static culture.

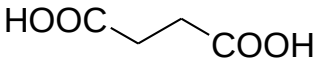

80

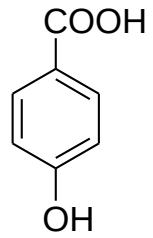

81

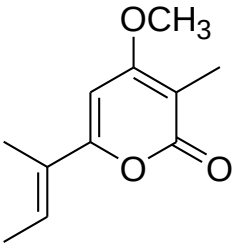

82

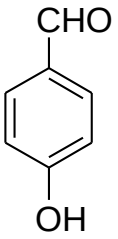

83

Figure. 5.1.2 Structures of succinic acid, 4-hydroxybenzoic acid, nectriapyrone and 4-hydroxybenzaldehyde (**80**-**83**) produced by *D. gulyae* grown in bioreactor.

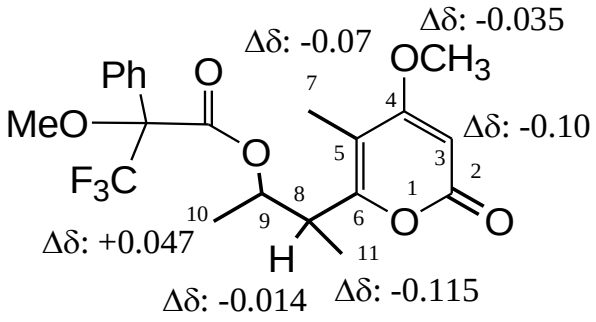

Figure. 5.1.3 Structures of 9-*O*-*S*- and 9-*O*-*R*-MPTA esters of gulypyrone A (**78** and **79**), reporting the $\Delta\delta$ value obtained by comparison of each proton system.

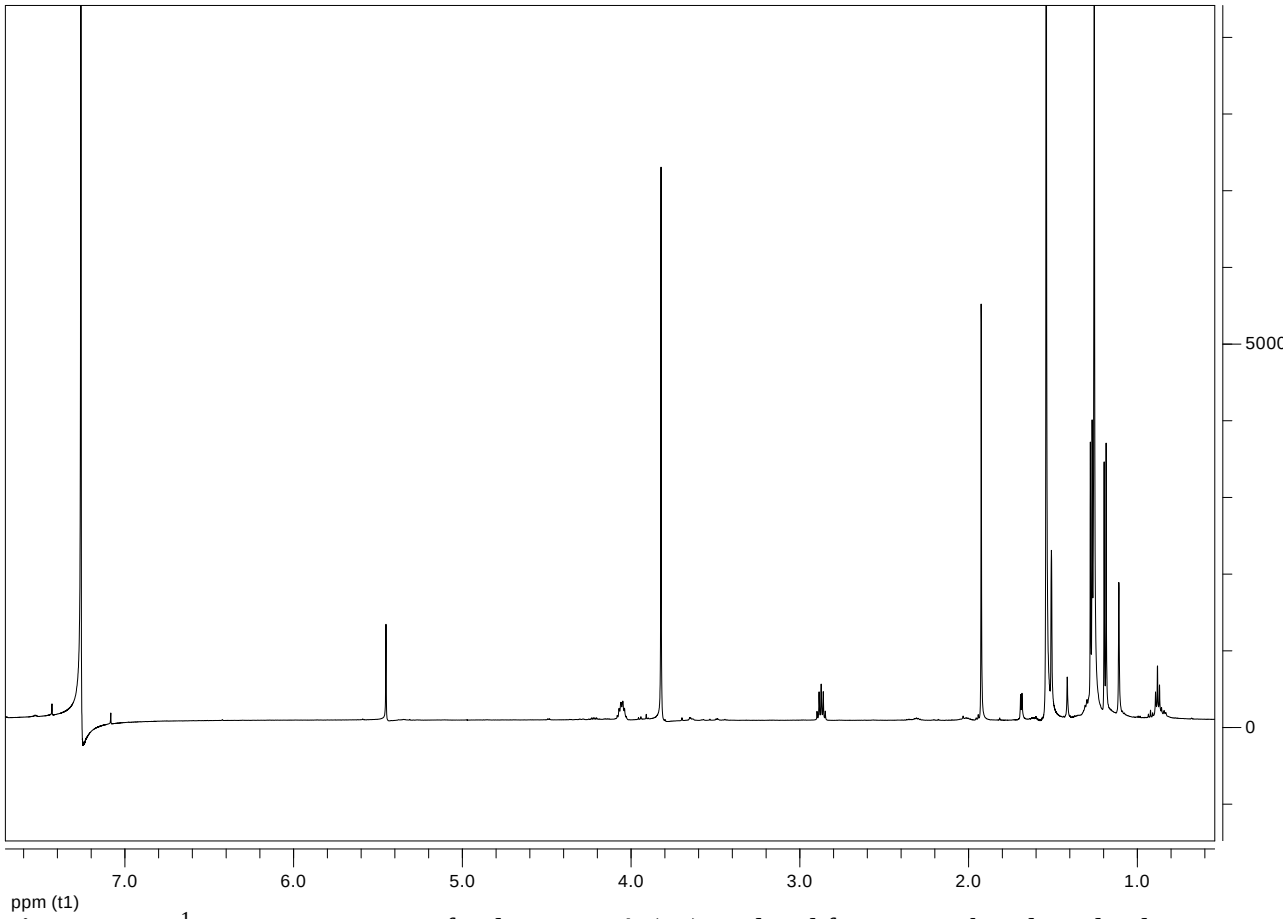

Figure. 5.1.4 ^{1}H NMR spectrum of gulypyrone A (**71**), isolated from *D. gulyae* liquid culture.

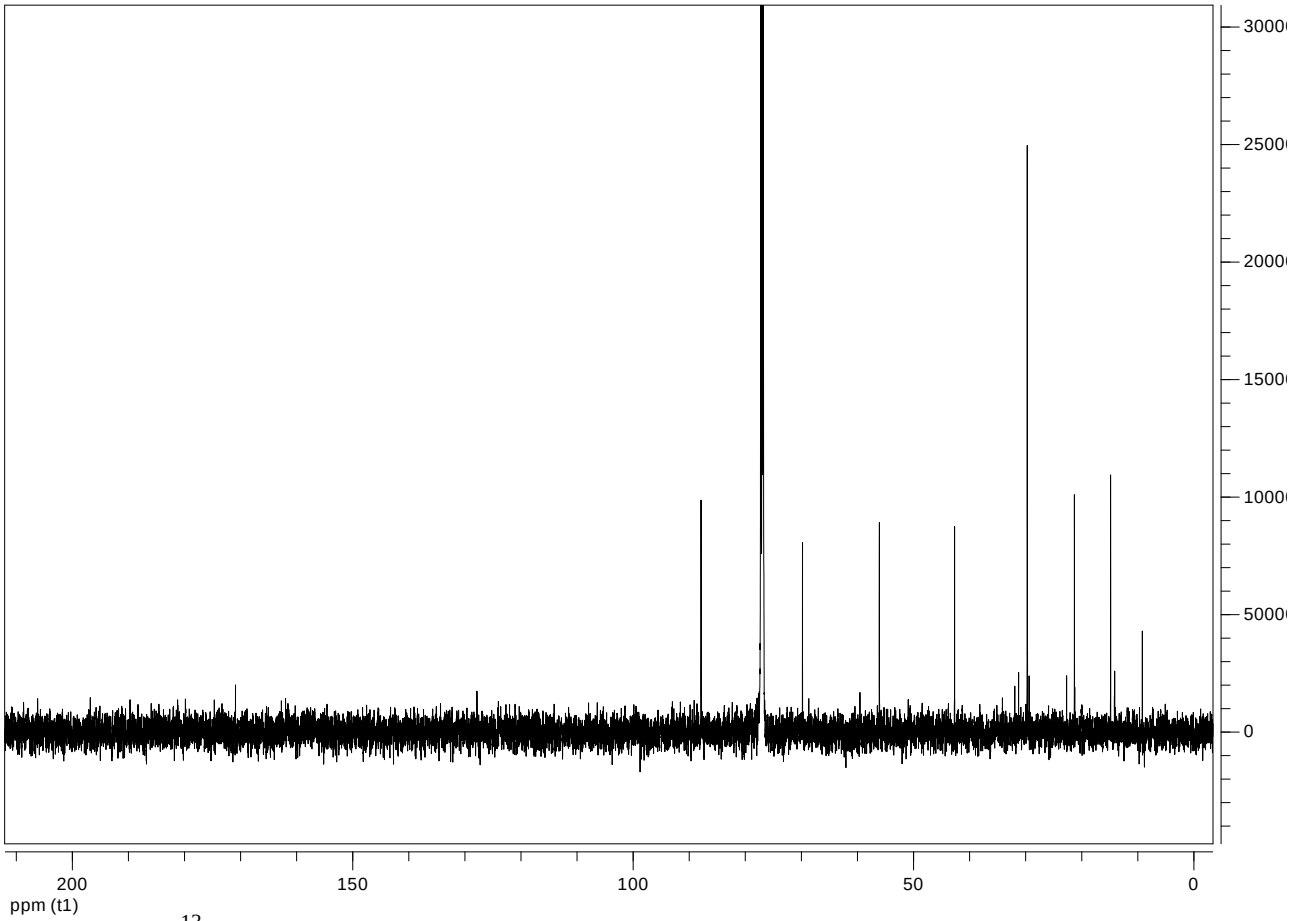

Figure. 5.1.5 ^{13}C NMR spectrum of gulypyrone A (**71**), isolated from *D. gulyae* liquid culture.

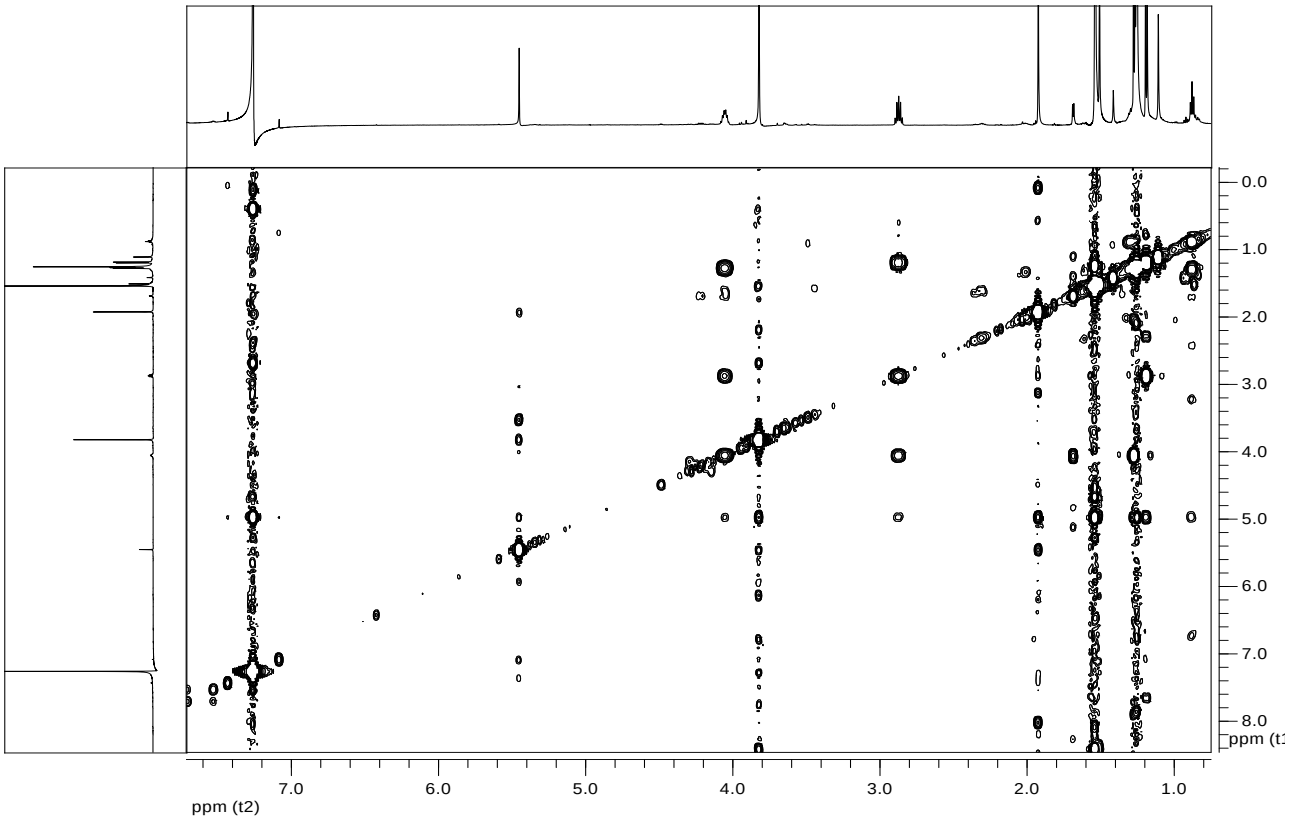

Figure. 5.1.6 COSY spectrum of gulypyrone A (**71**), isolated from *D. gulyae* liquid culture.

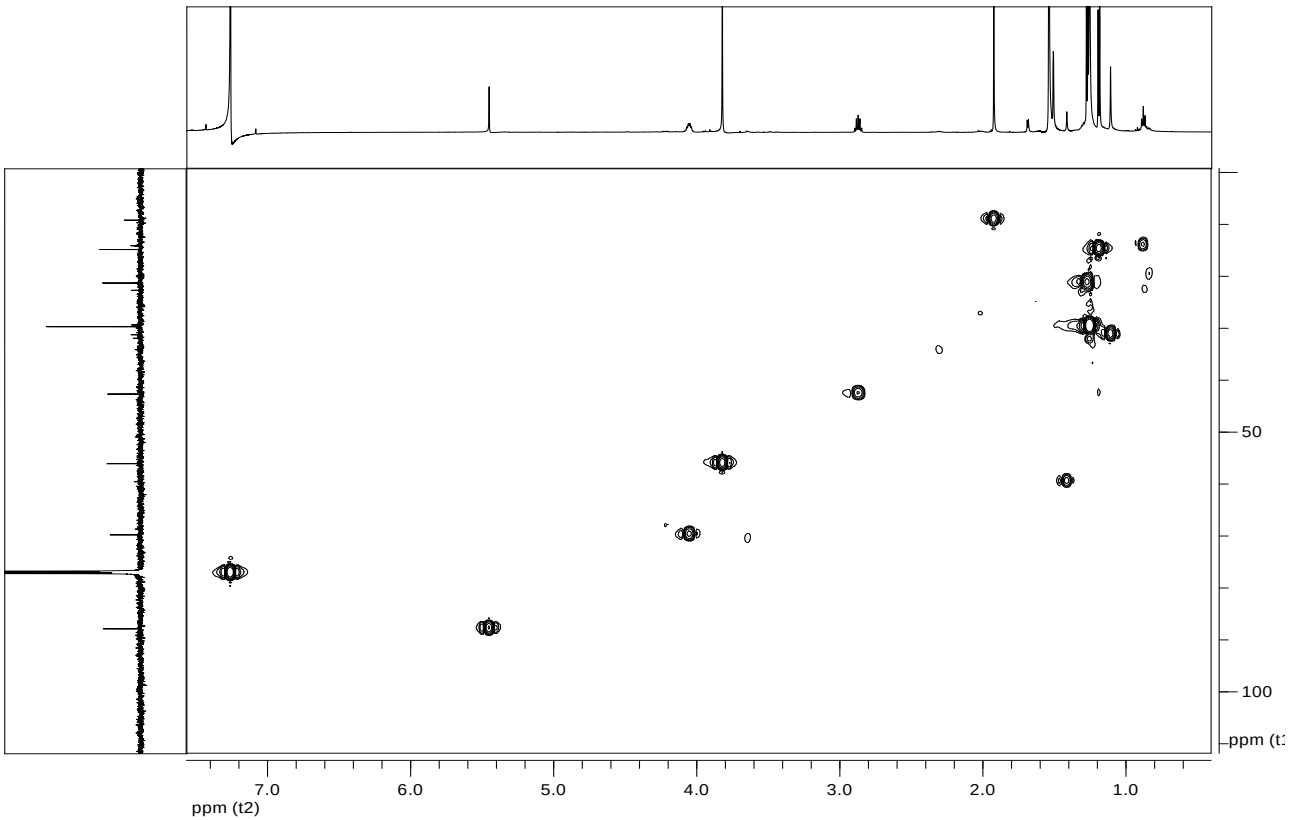

Figure. 5.1.7 HSQC spectrum of gulypyrone A (**71**), isolated from *D. gulyae* liquid culture.

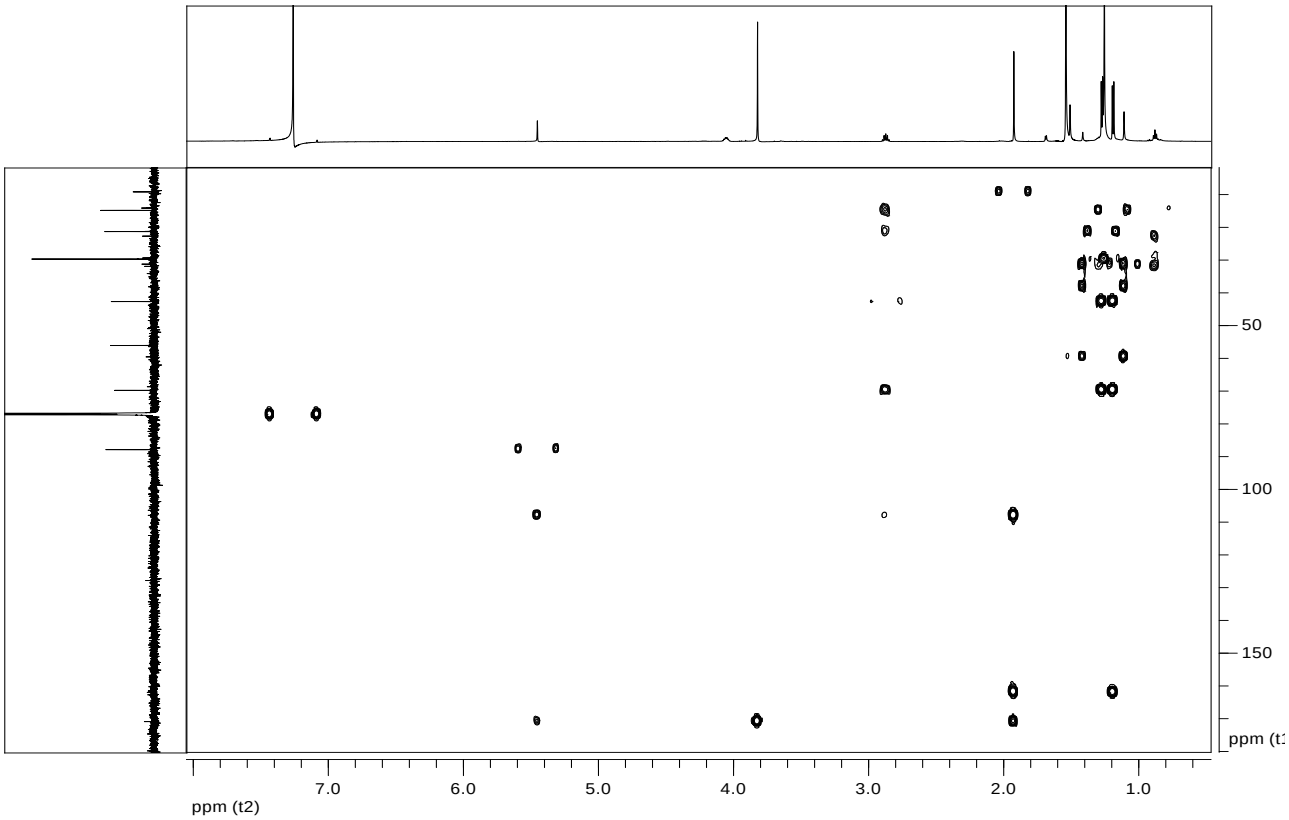

Figure. 5.1.8 HMBC spectrum of gulypyrone A (**71**), isolated from *D. gulyae* liquid culture.

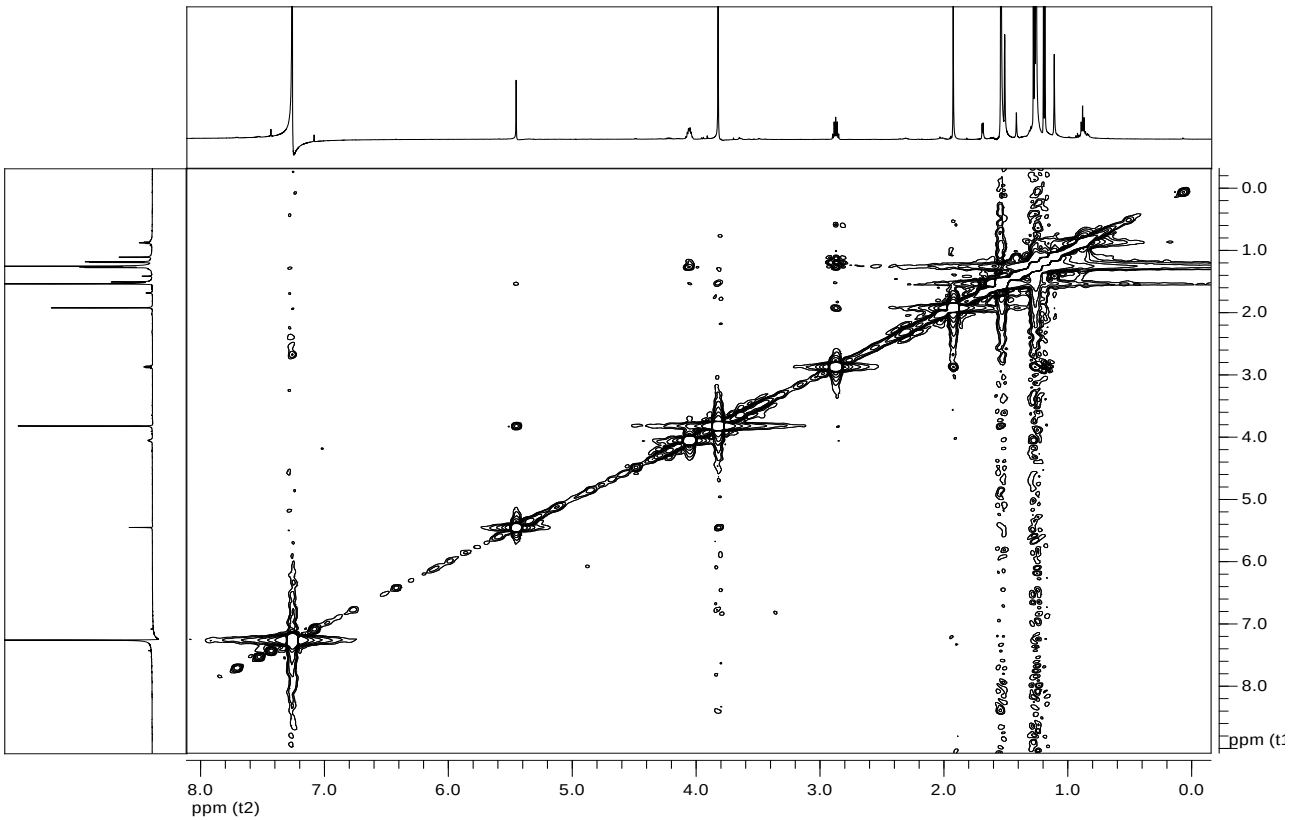

Figure. 5.1.9 NOESY spectrum of gulypyrone A (**71**), isolated from *D. gulyae* liquid culture.

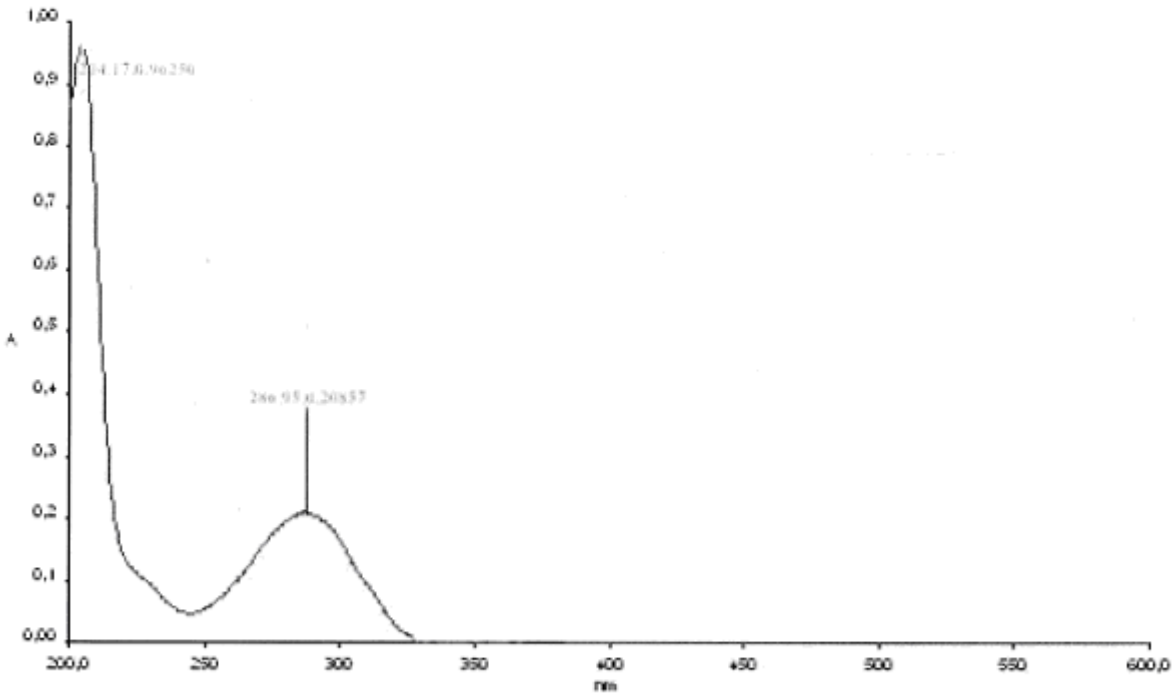

Figure. 5.1.10 UV spectrum of gulypyrone A (**71**), isolated from *D. gulyae* liquid culture.

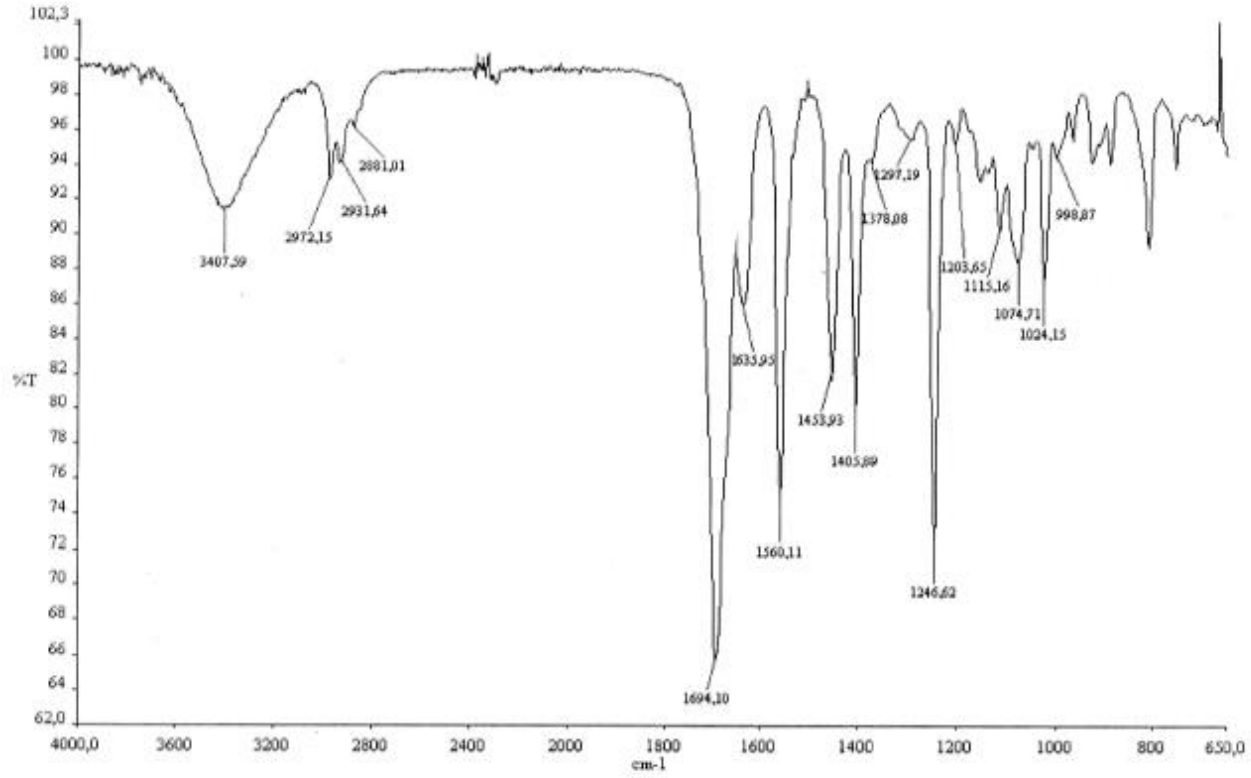

Figure. 5.1.11 IR spectrum of gulypyrone A (**71**), isolated from *D. gulyae* liquid culture.

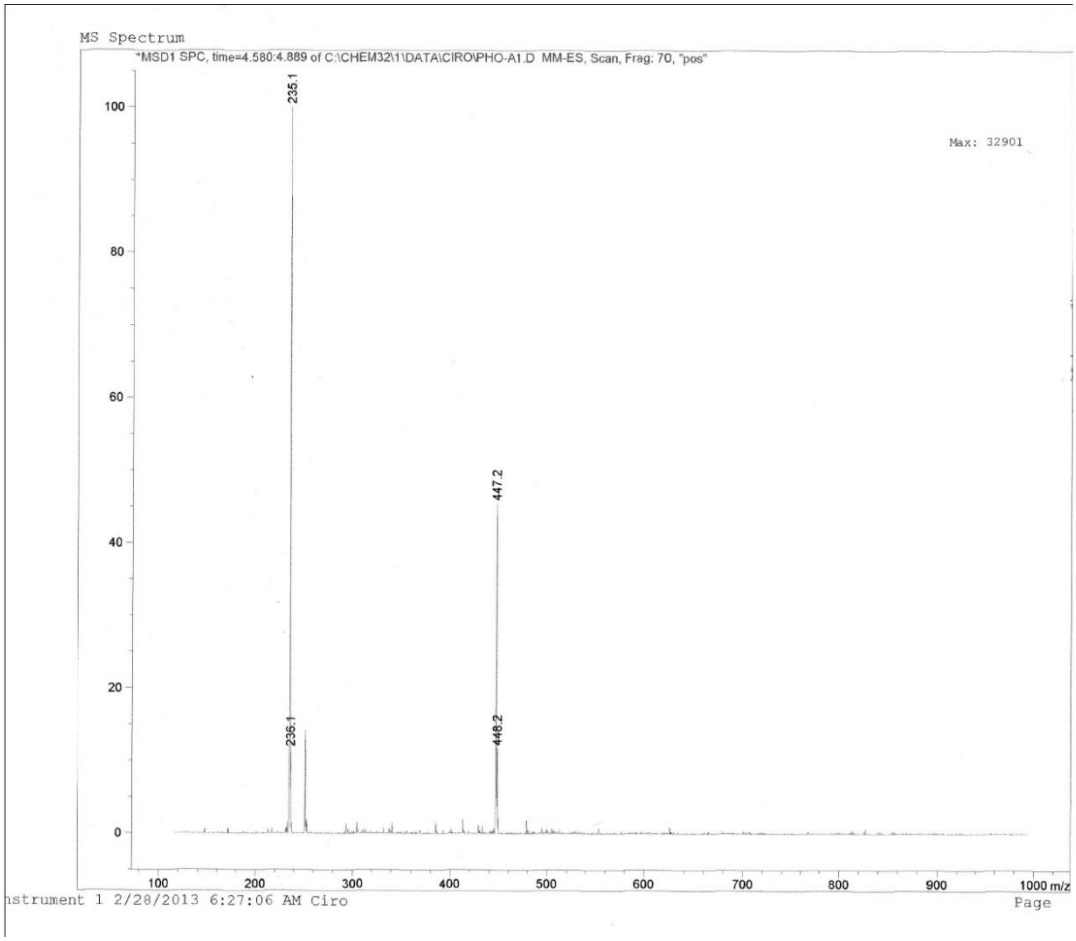

Figure. 5.1.12 ESIMS (+) spectrum of gulypyrone A (**71**), isolated from *D. gulyae* liquid culture.

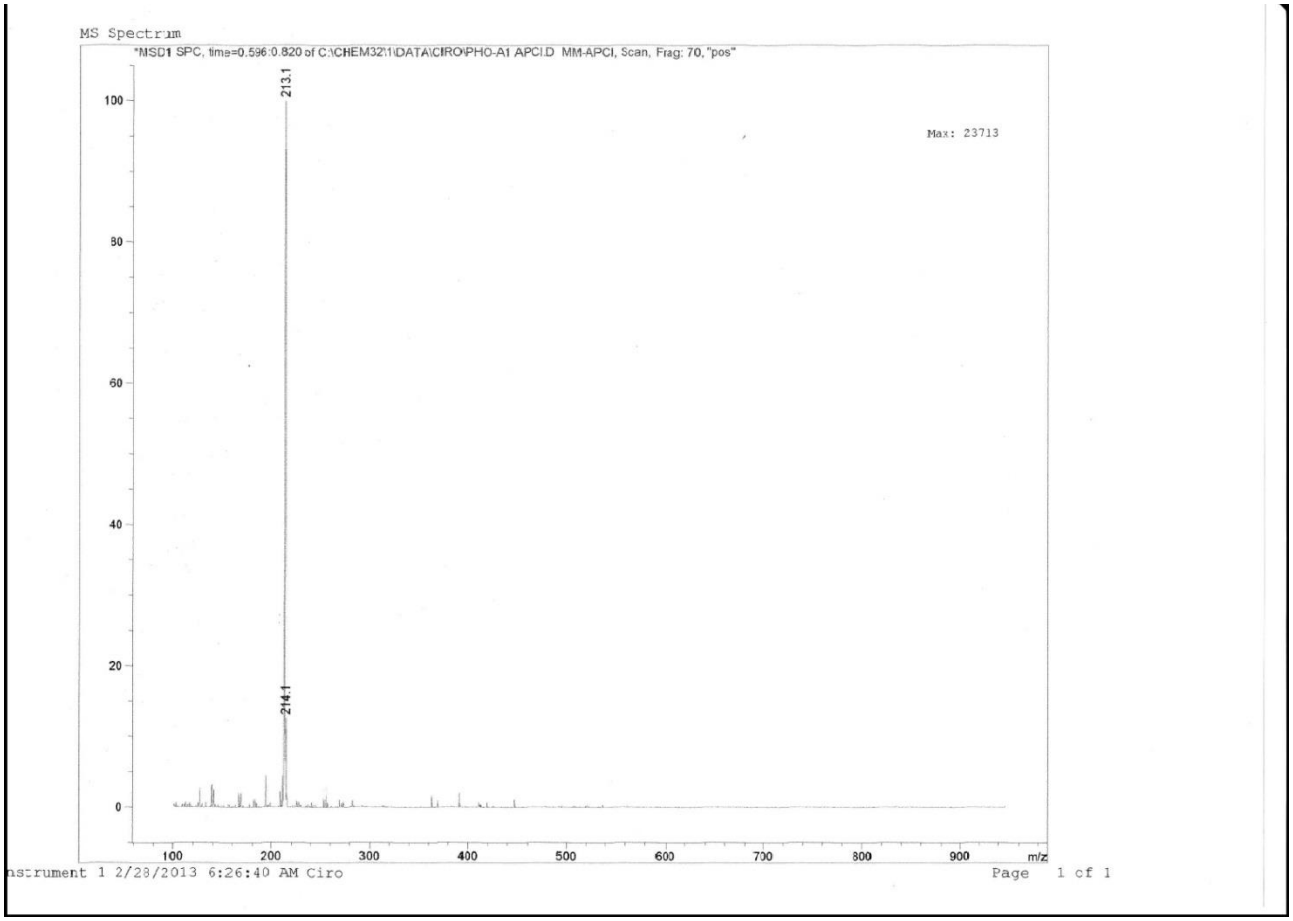

Figure. 5.1.13 APCIMS (+) spectrum of gulypyrone A (**71**), isolated from *D. gulyae* liquid culture.

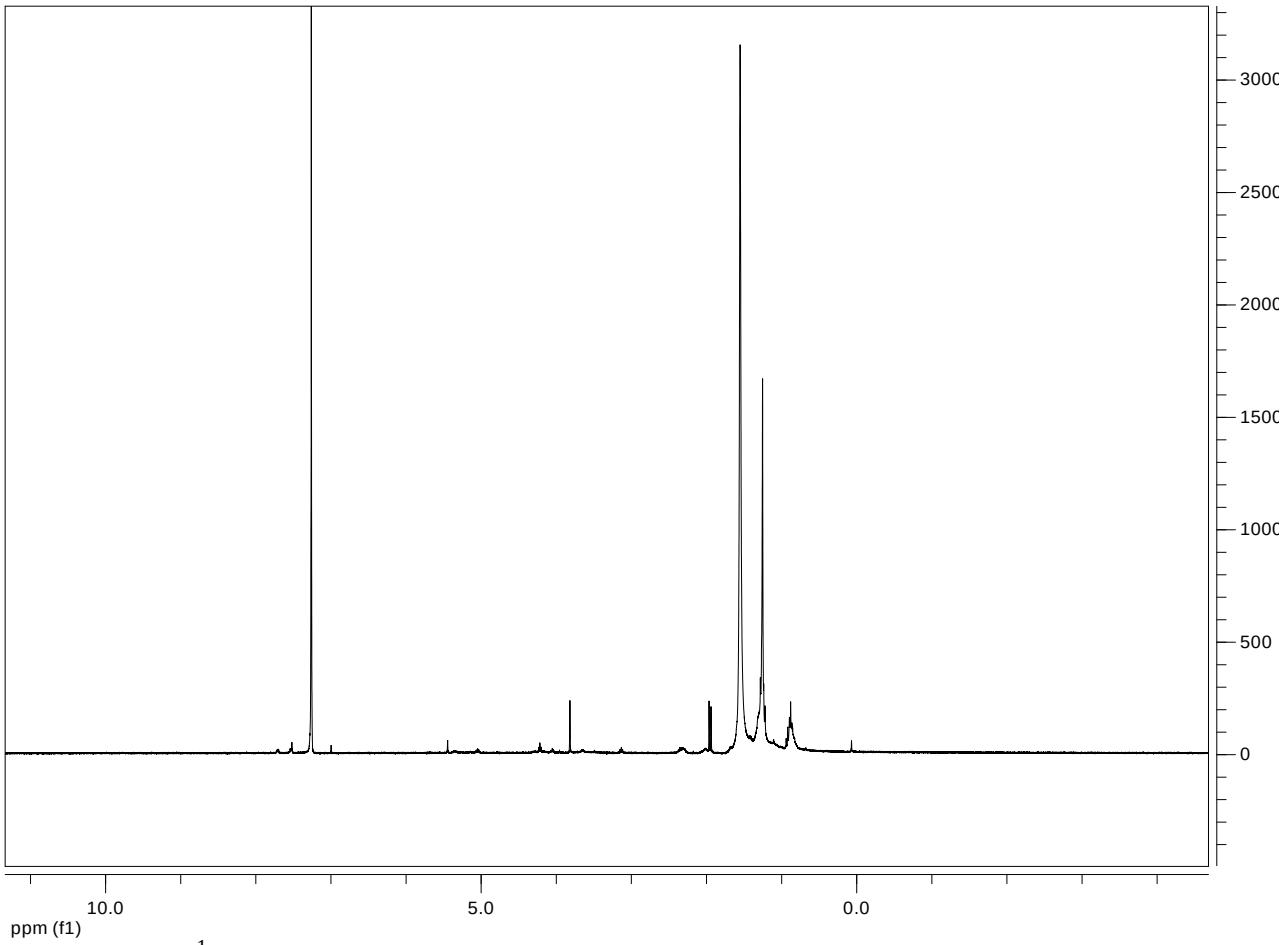

Figure. 5.1.14 ^{1}H NMR spectrum of 9-*O*-Acetyl derivative of gulypyrone A (**77**)

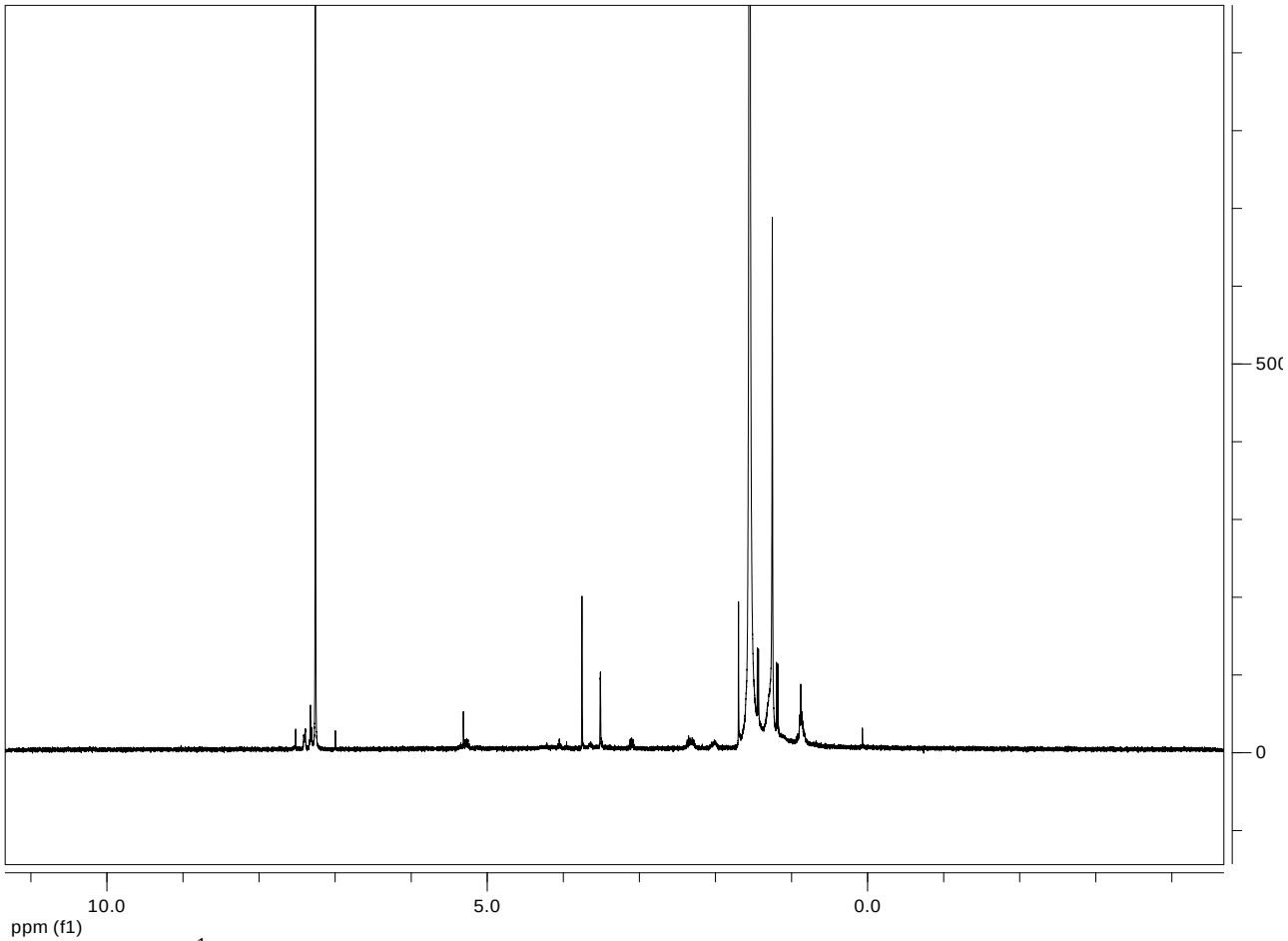

Figure. 5.1.15 ^{1}H NMR spectrum of (*S*)-α-Methoxy-α-trifluoromethyl-α-phenylacetate (MTPA) ester of gulypyrone A (**78**).

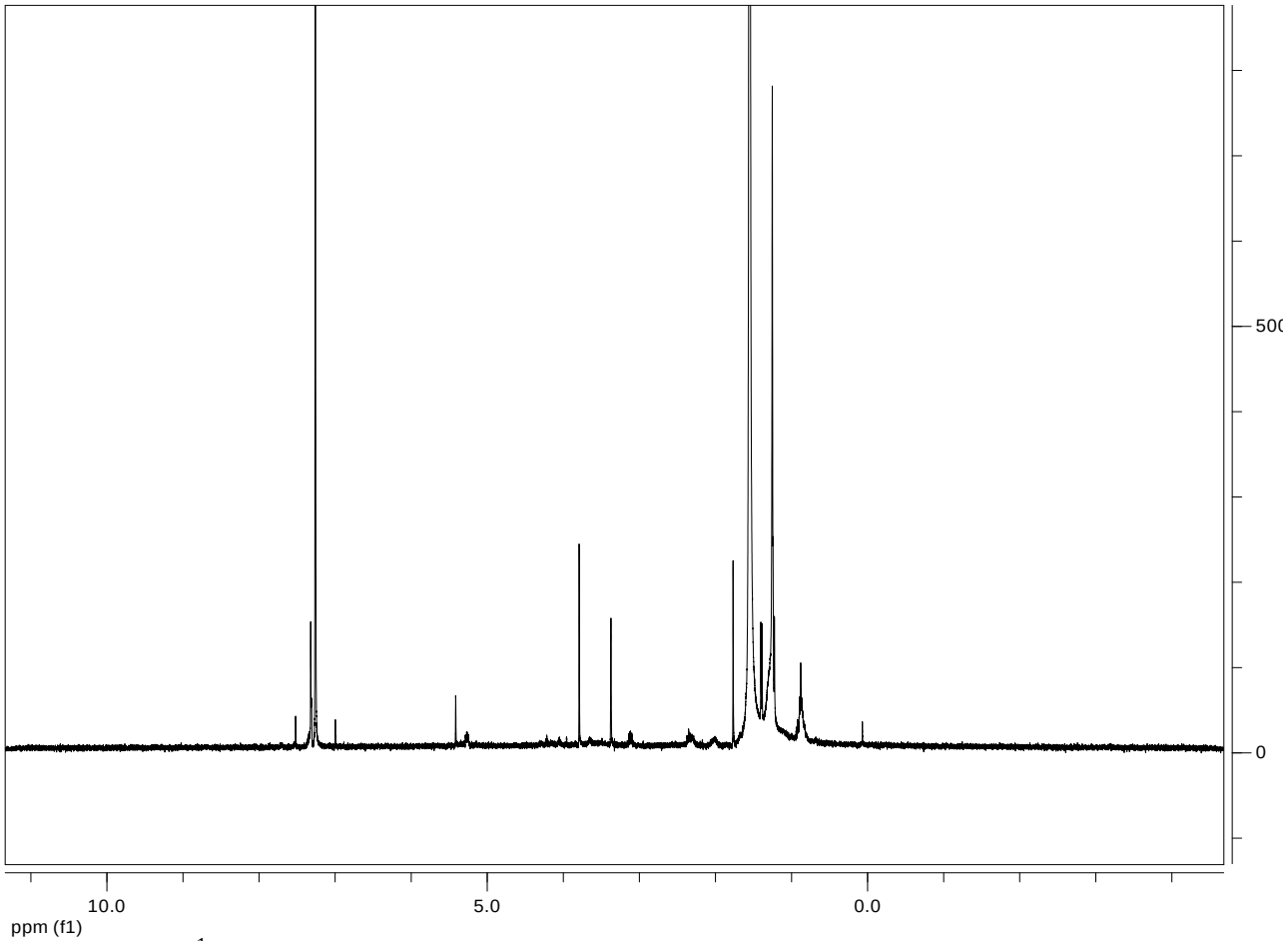

Figure. 5.1.16 ^{1}H NMR spectrum of (*R*)-α-Methoxy-α-trifluoromethyl-α-phenylacetate (MTPA) ester of gulypyrone A (**79**).

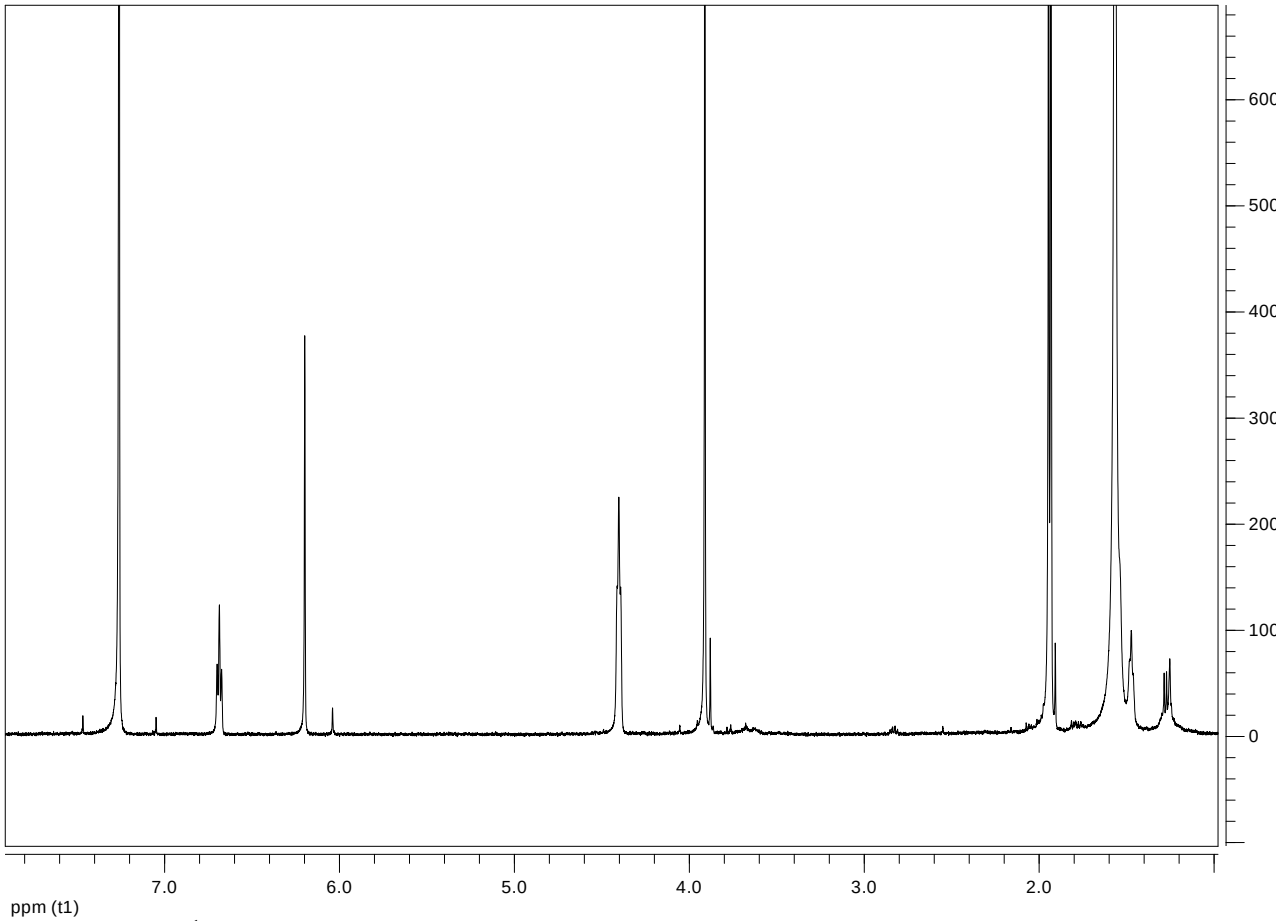

Figure. 5.1.17 ^{1}H NMR spectrum of gulypyrone B (**72**), isolated from *D. gulyae* liquid culture.

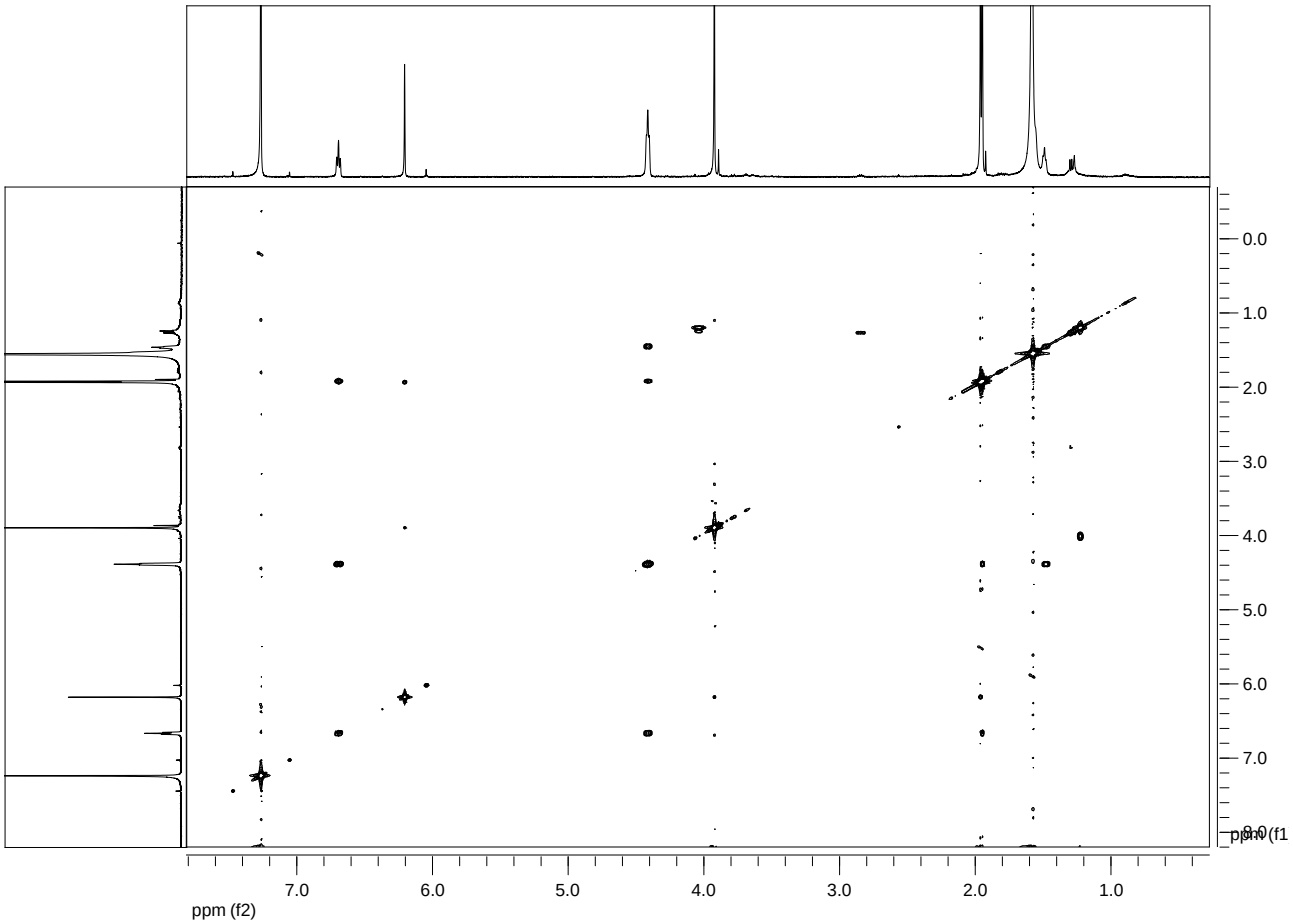

Figure. 5.1.18 COSY spectrum of gulypyrone B (**72**), isolated from *D. gulyae* liquid culture.

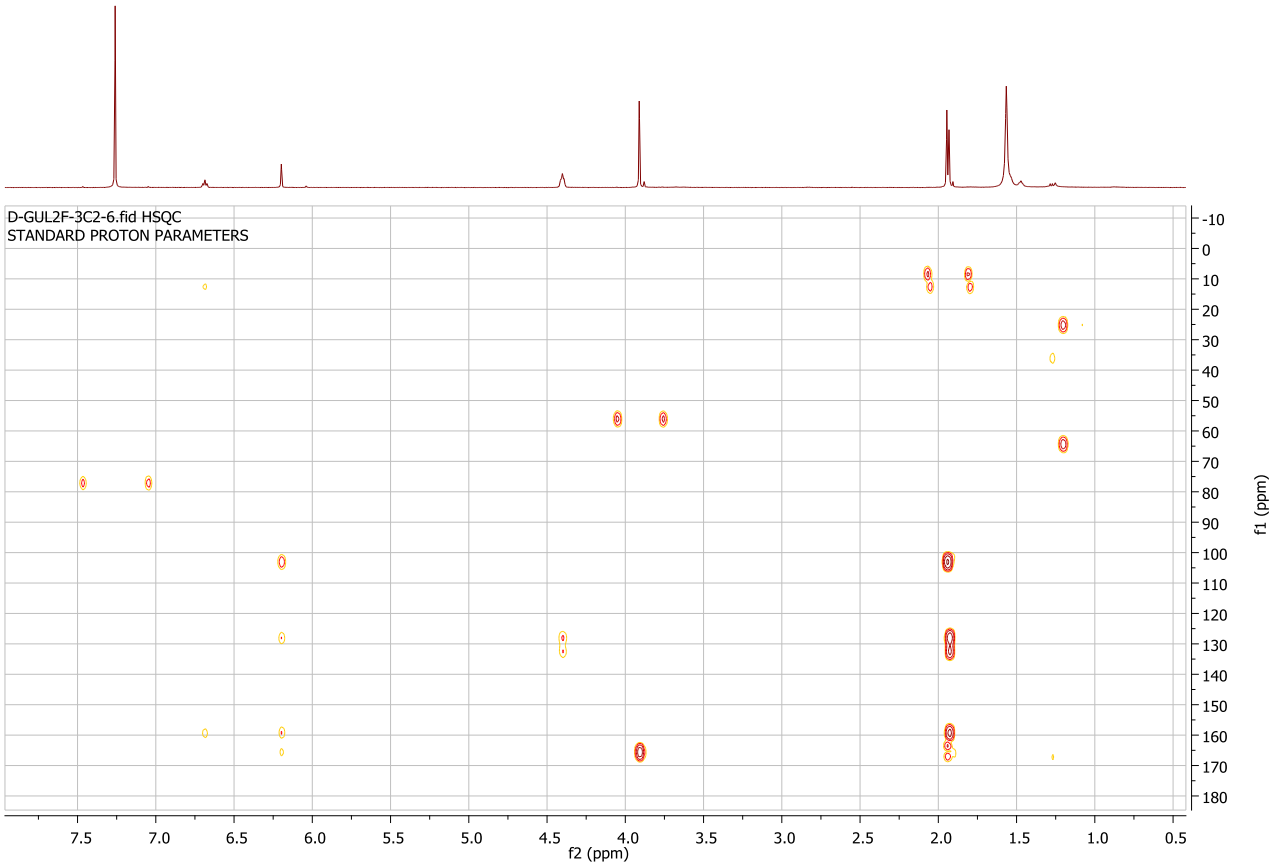

Figure. 5.1.19 HMBC spectrum of gulypyrone B (**72**), isolated from *D. gulyae* liquid culture.

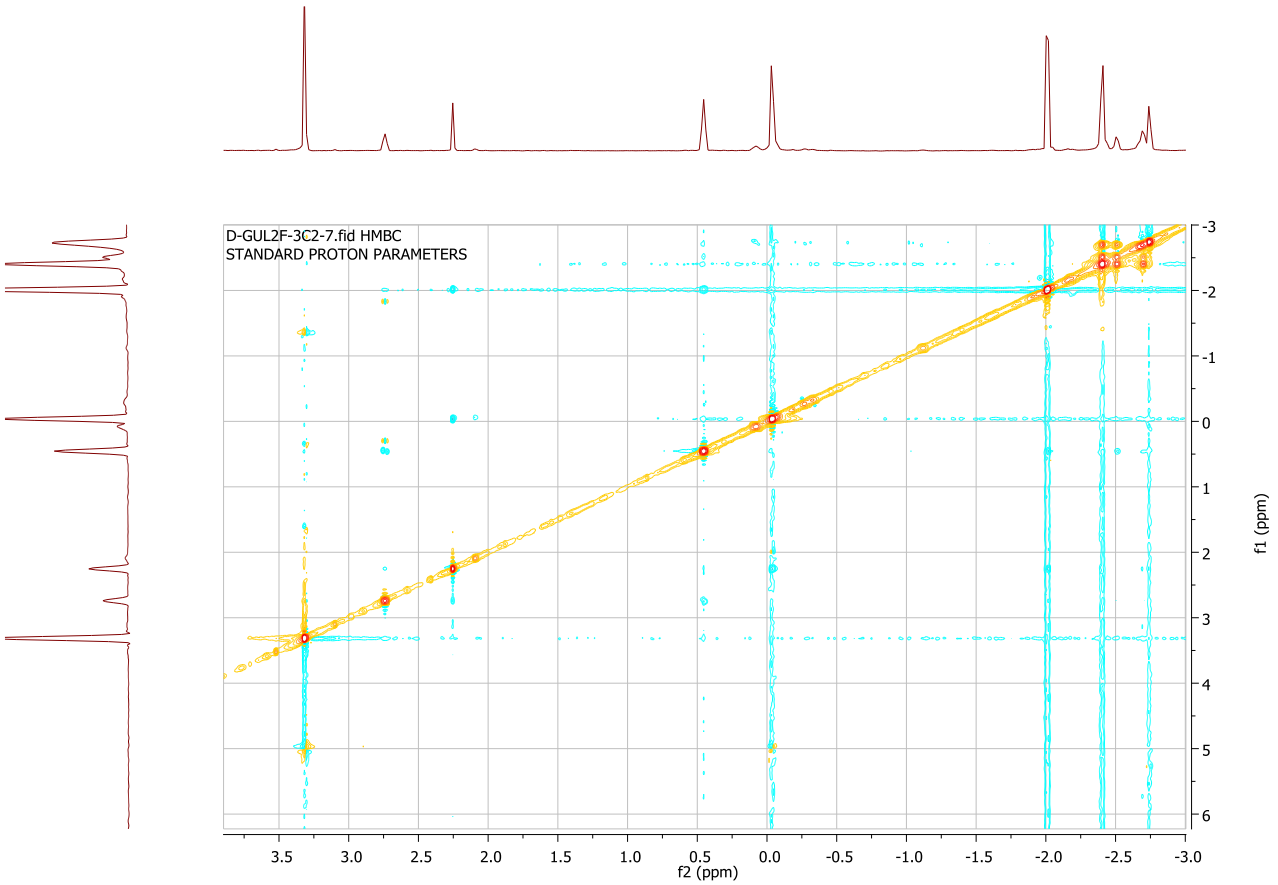

Figure. 5.1.20 NOESY spectrum of gulypyrone B (**72**), isolated from *D. gulyae* liquid culture.

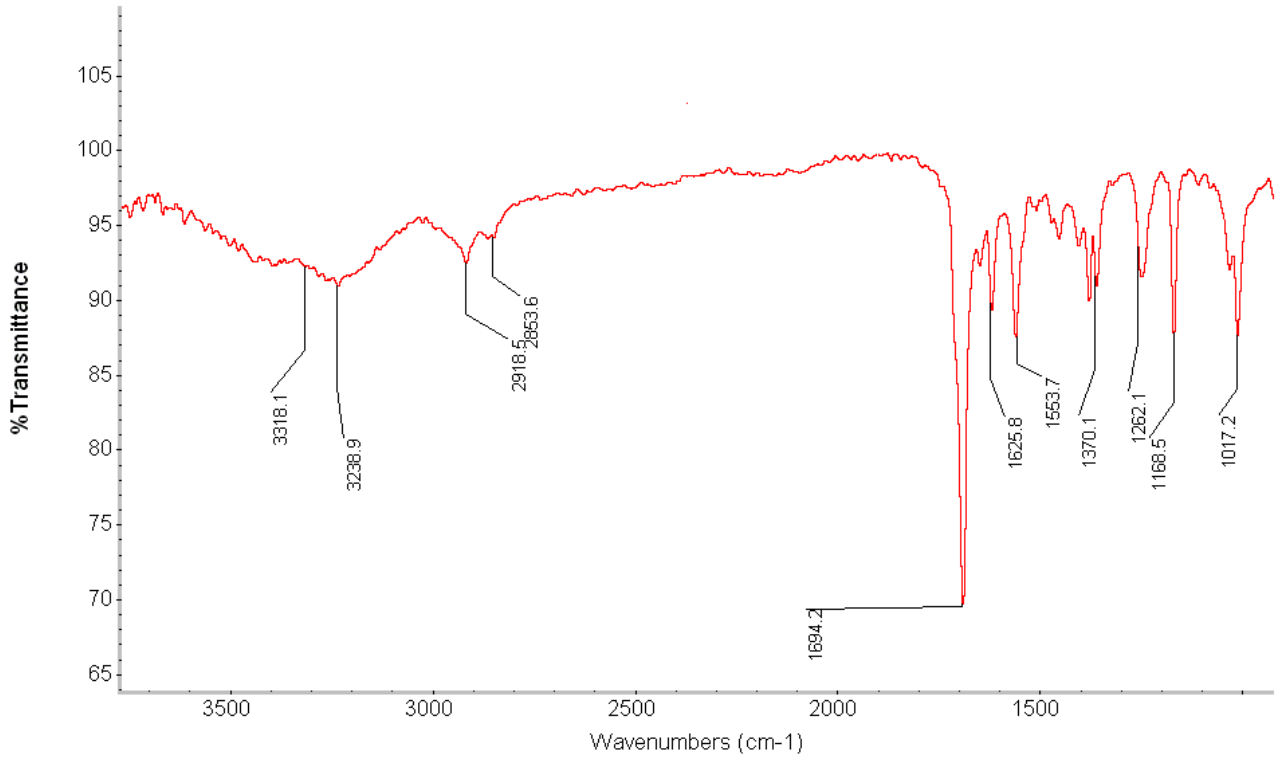

Figure. 5.1.21 IR spectrum of gulypyrone B (**72**), isolated from *D. gulyae* liquid culture.

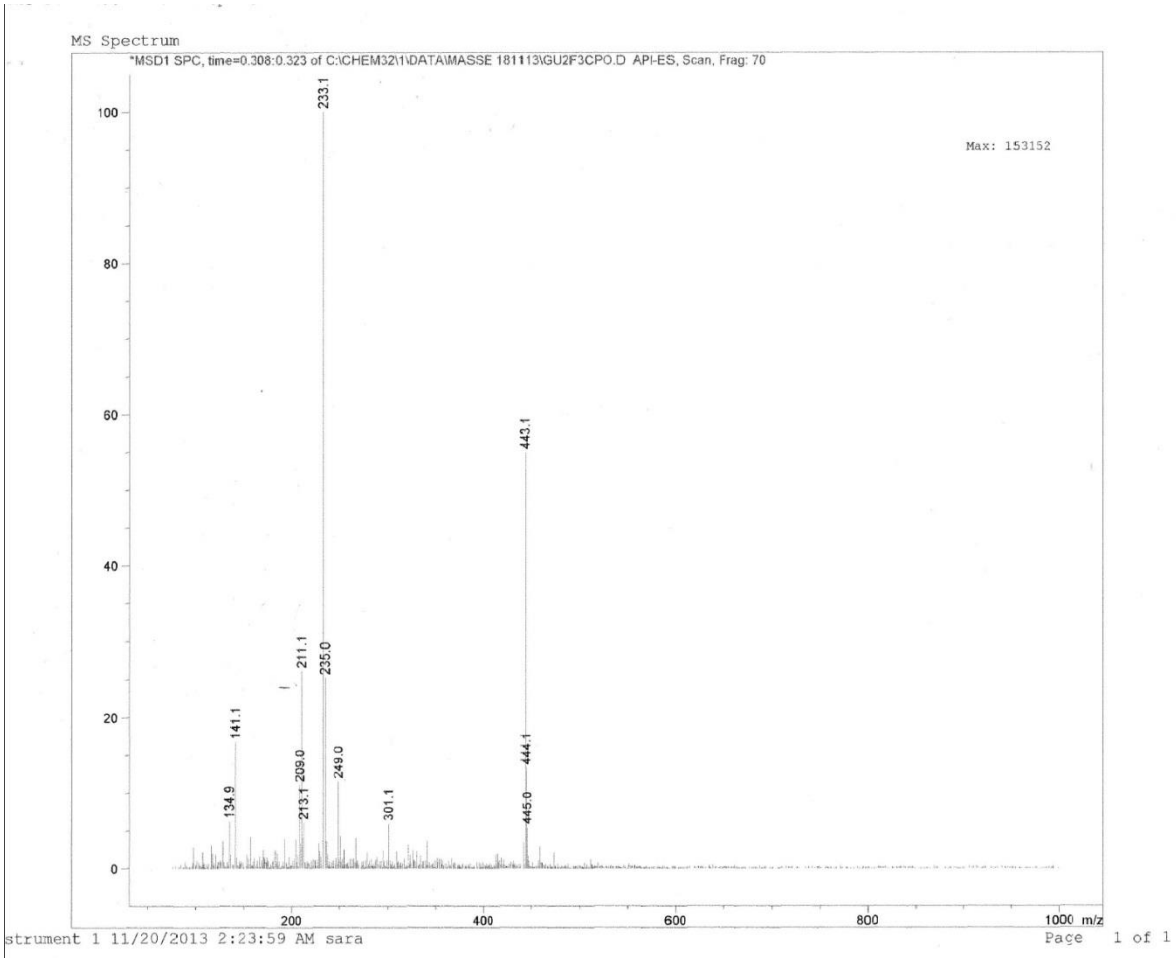

Figure. 5.1.22 ESIMS (+) spectrum of gulypyrone B (**72**), isolated from *D. gulyae* liquid culture.

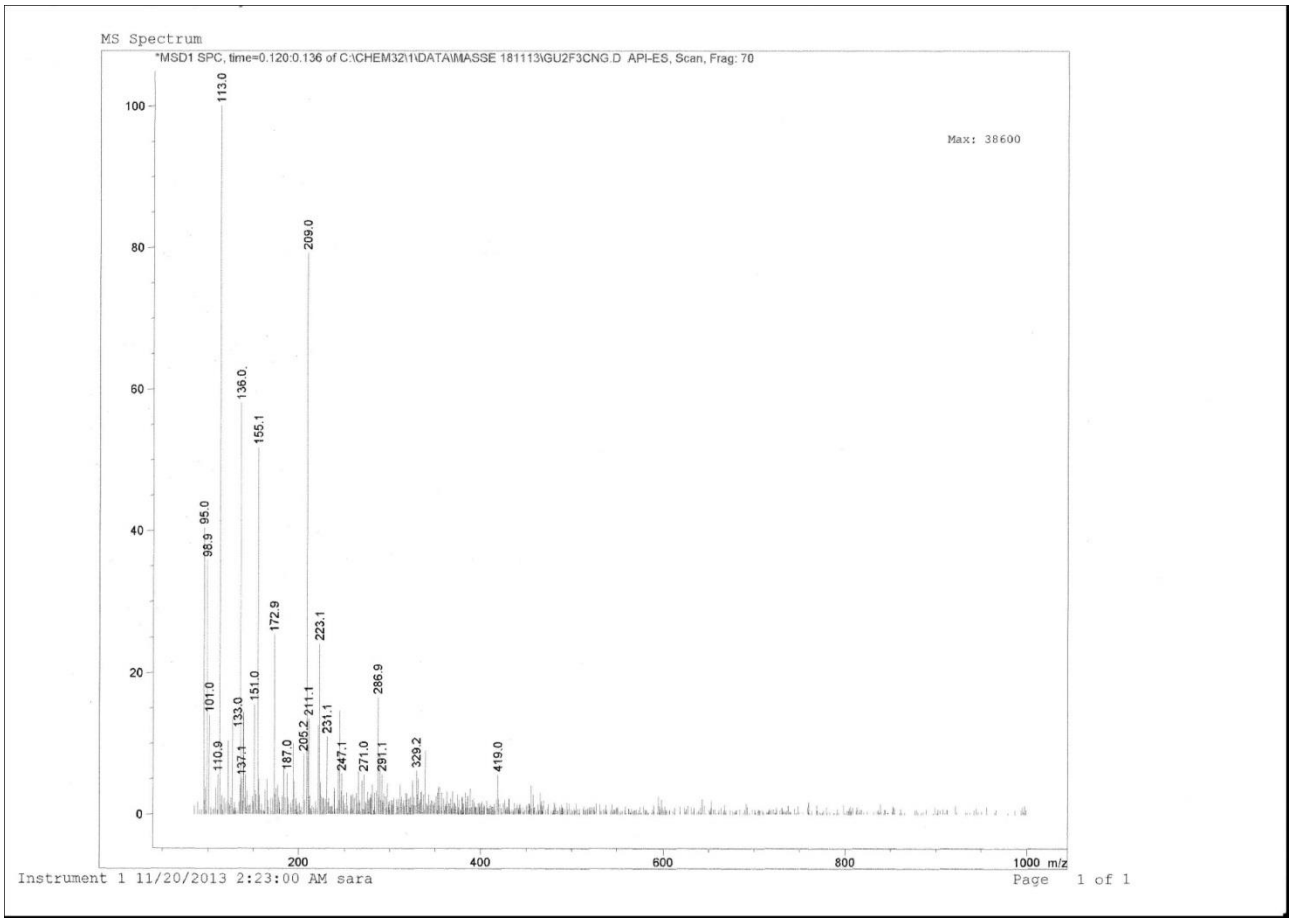

Figure. 5.1.23 ESIMS (-) spectrum of gulypyrone B (**72**), isolated from *D. gulyae* liquid culture.

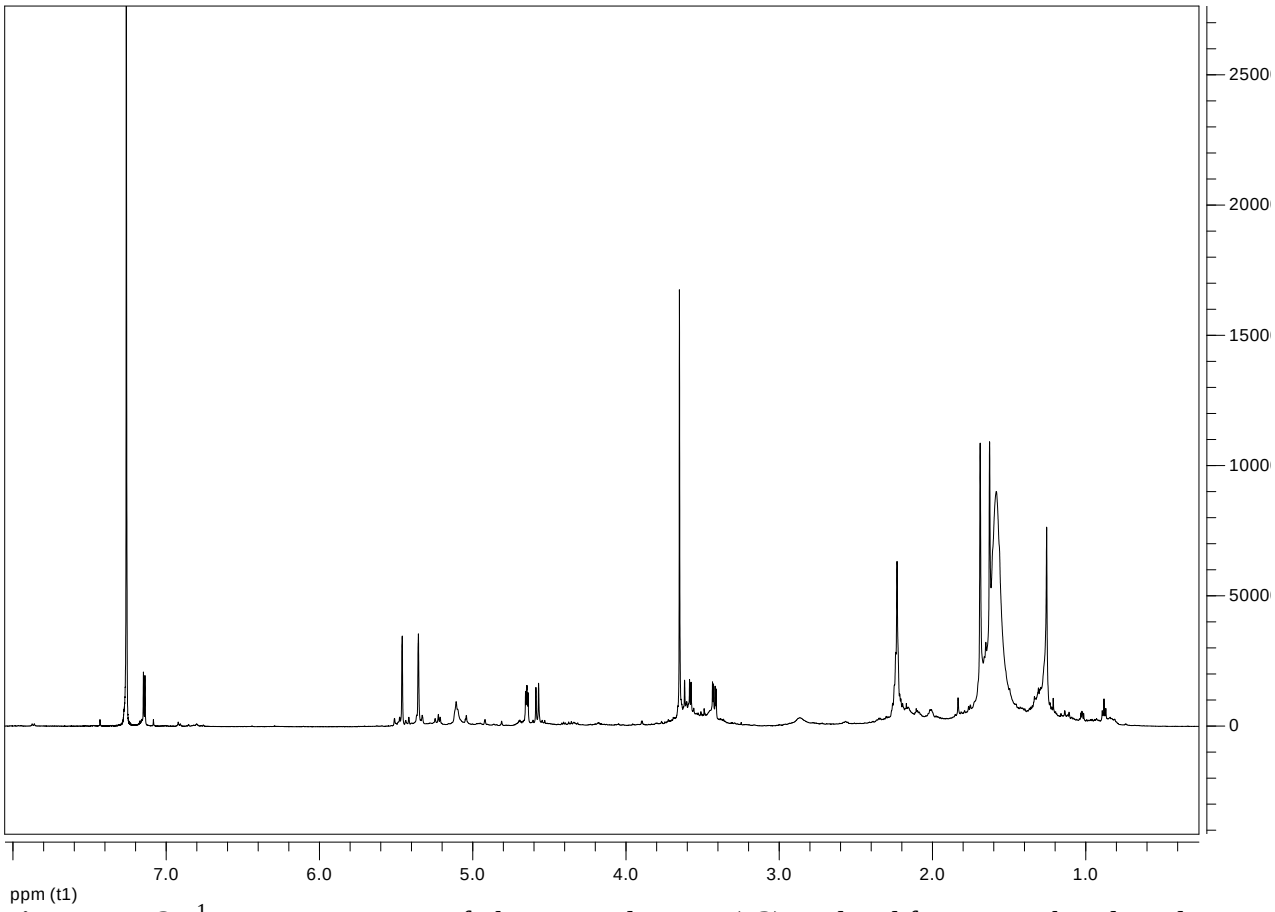

Figure. 5.1.24 ^{1}H NMR spectrum of phomentrioloxin B (**73**), isolated from *D. gulyae* liquid culture.

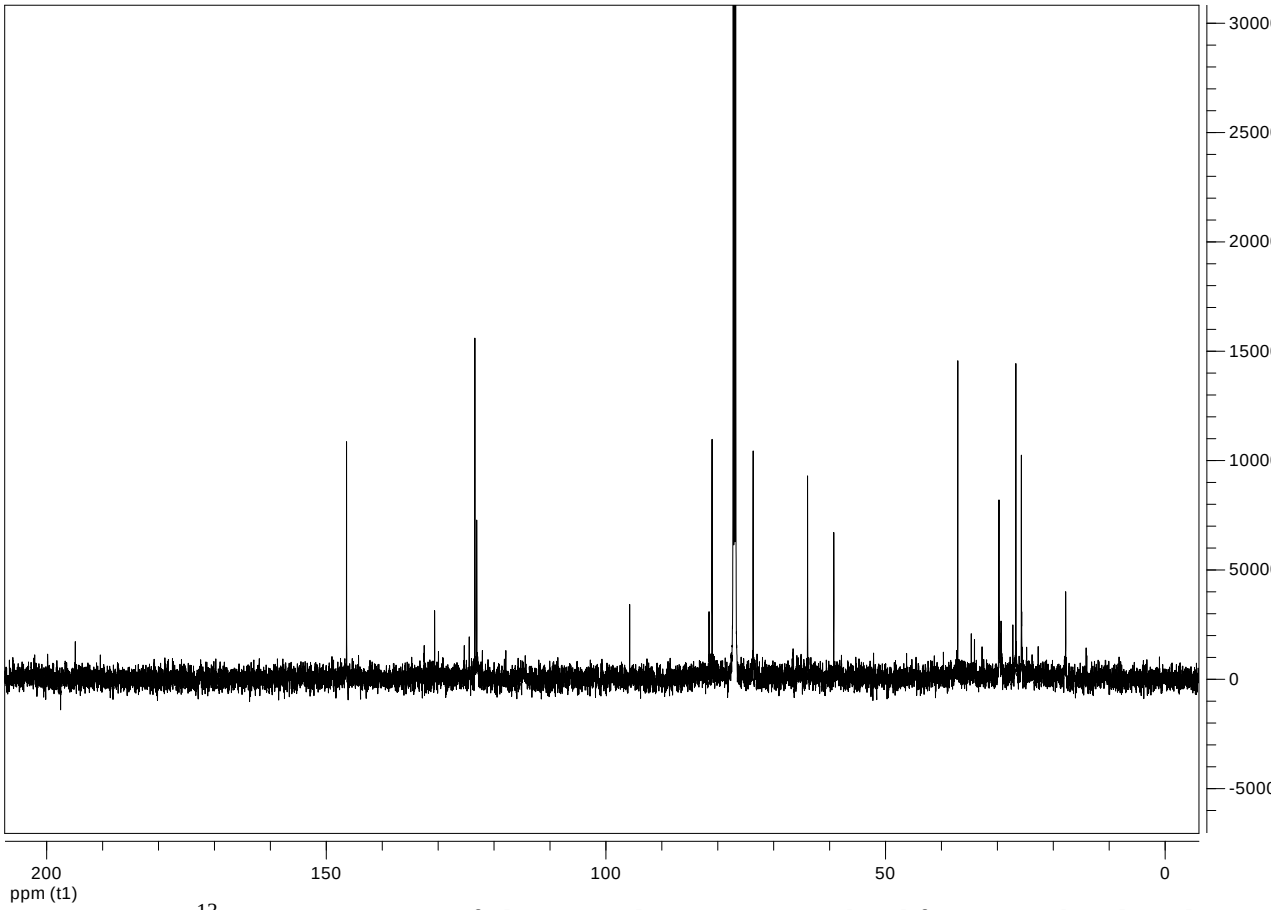

Figure. 5.1.25 ^{13}C NMR spectrum of phomentrioloxin B (**73**), isolated from *D. gulyae* liquid culture.

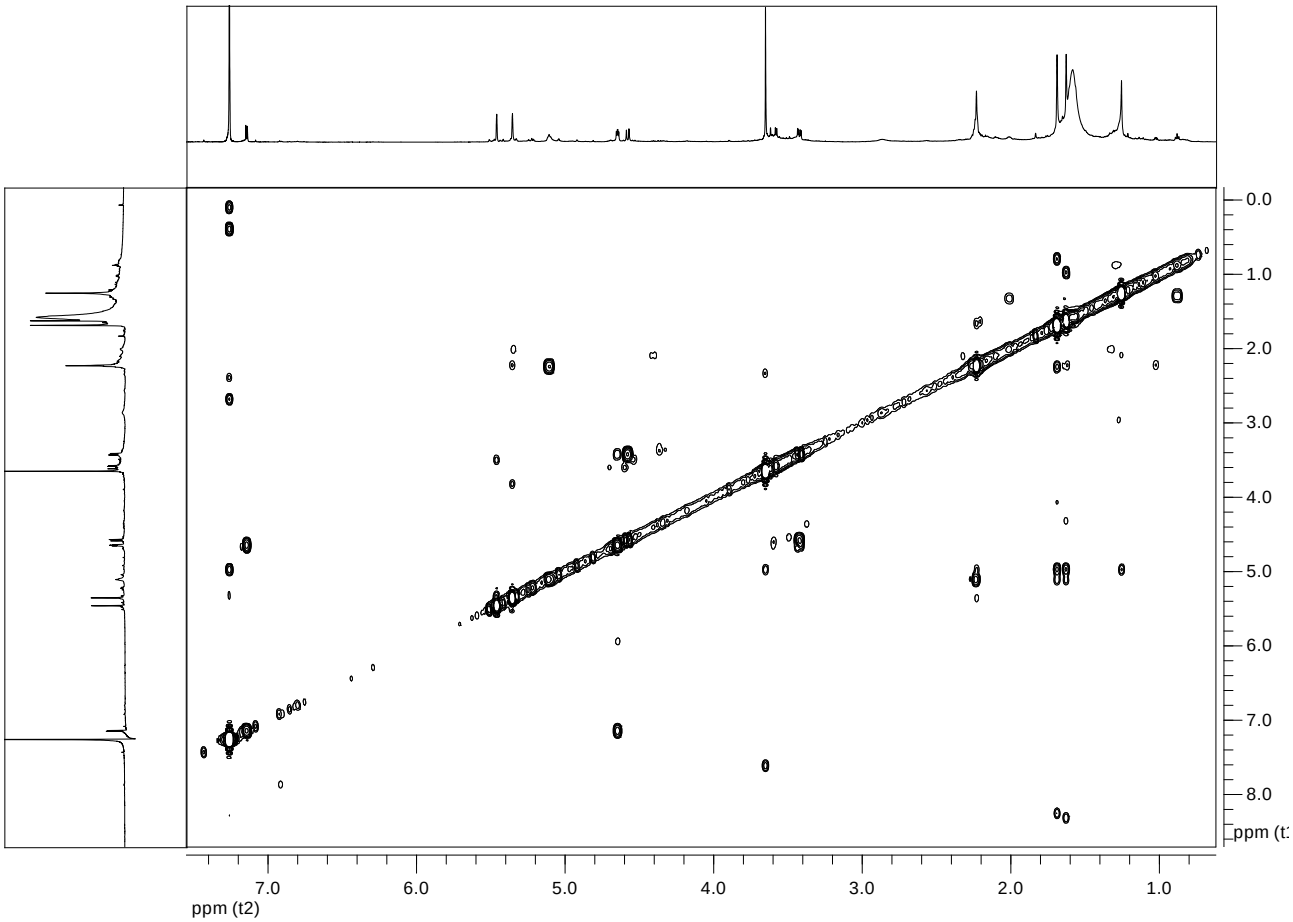

Figure. 5.1.26 COSYspectrum of phomentrioloxin B (**73**), isolated from *D. gulyae* liquid culture.

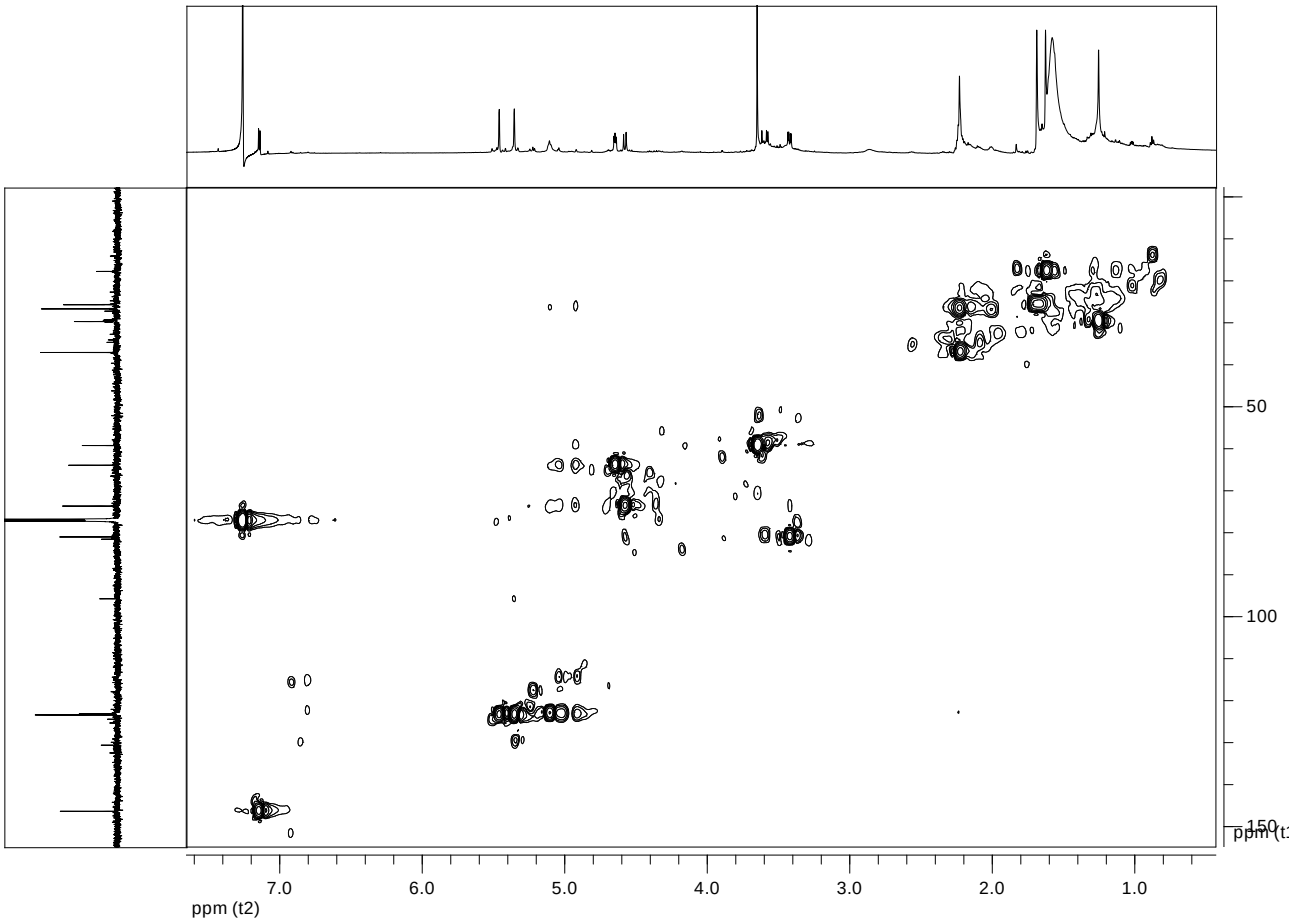

Figure. 5.1.27 HSQC spectrum of phomentrioloxin B (**73**), isolated from *D. gulyae* liquid culture.

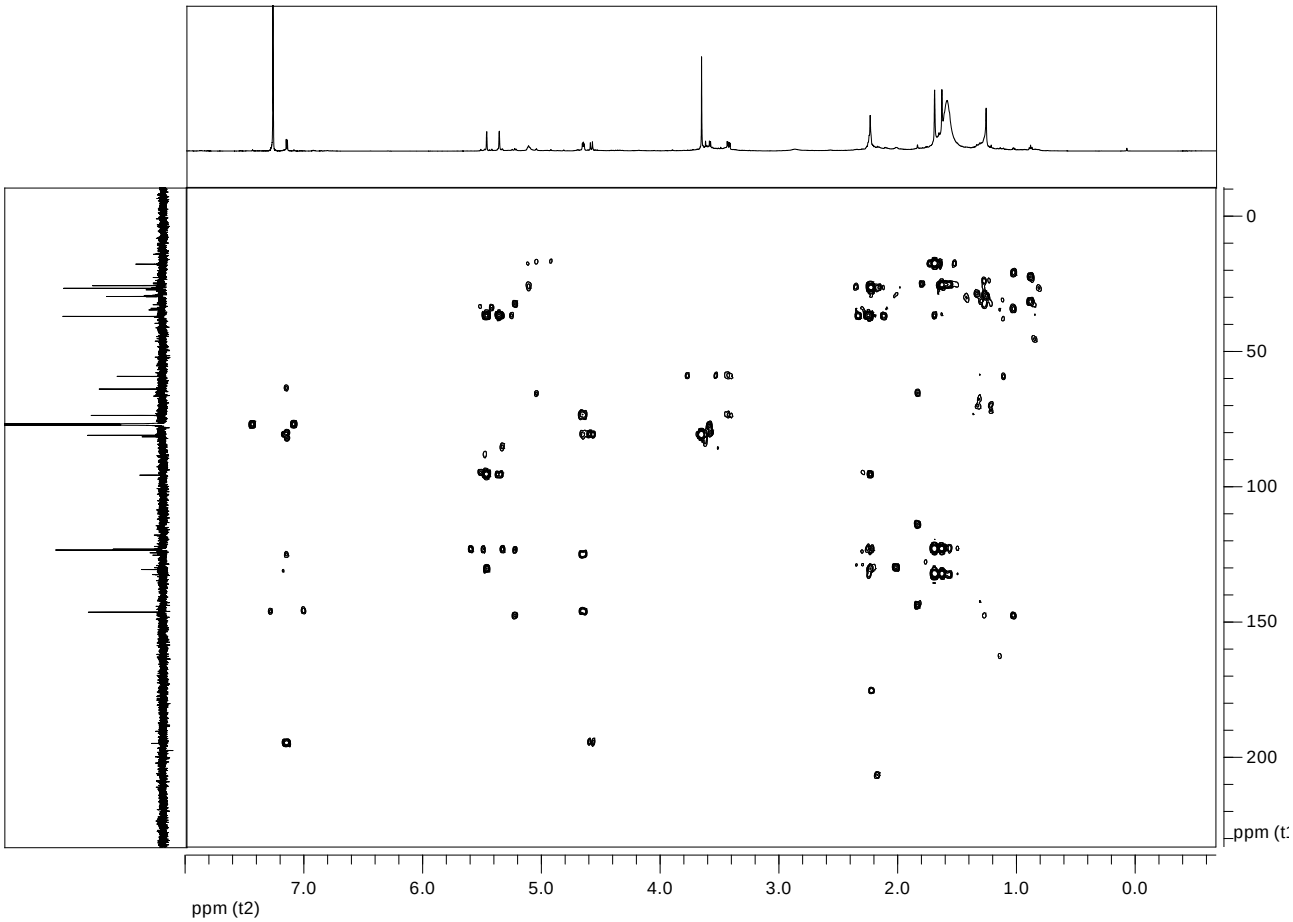

Figure. 5.1.28 HMBC spectrum of phomentrioloxin B (**73**), isolated from *D. gulyae* liquid culture.

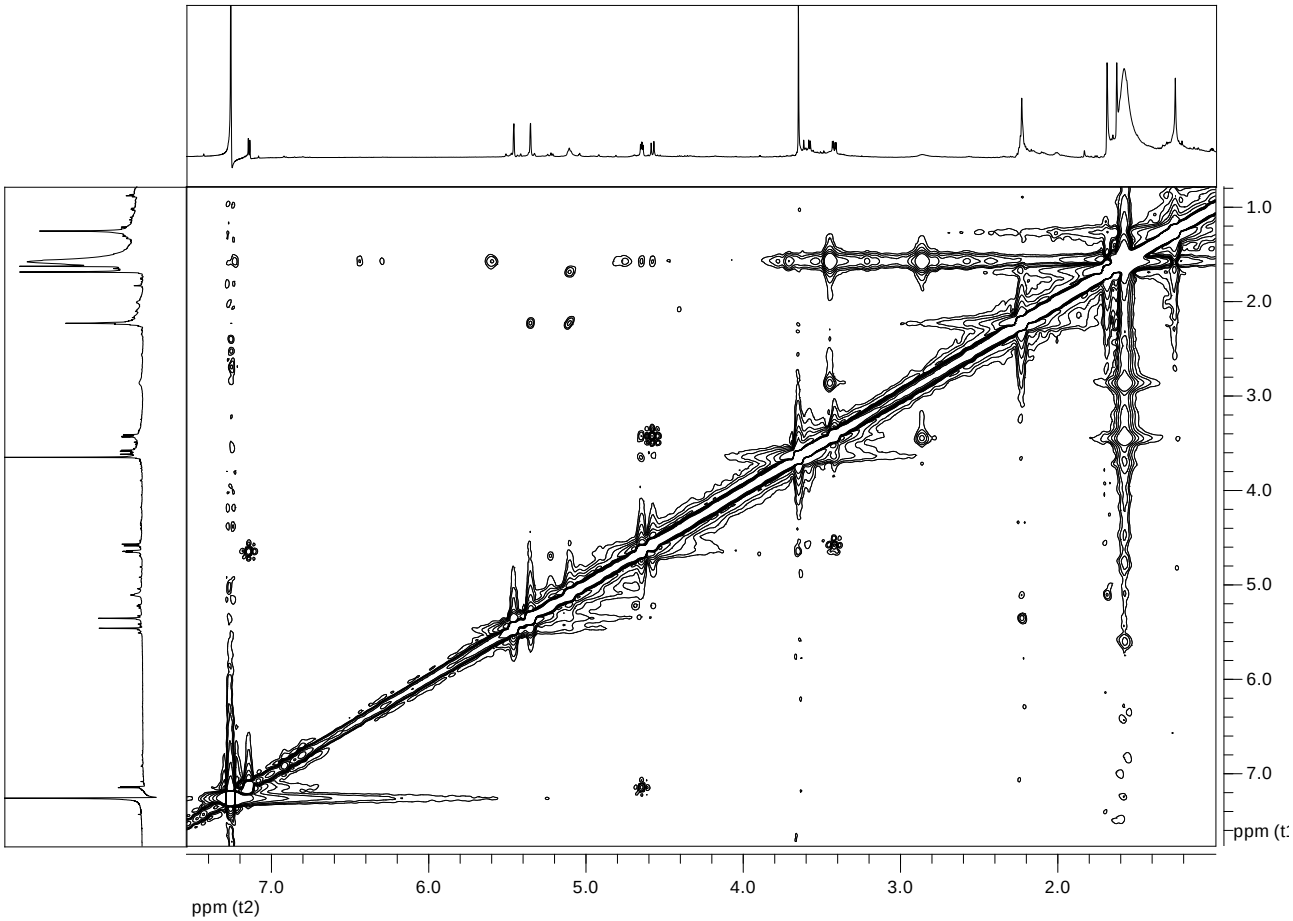

Figure. 5.1.29 NOESY spectrum of phomentrioloxin B (**73**), isolated from *D. gulyae* liquid culture.

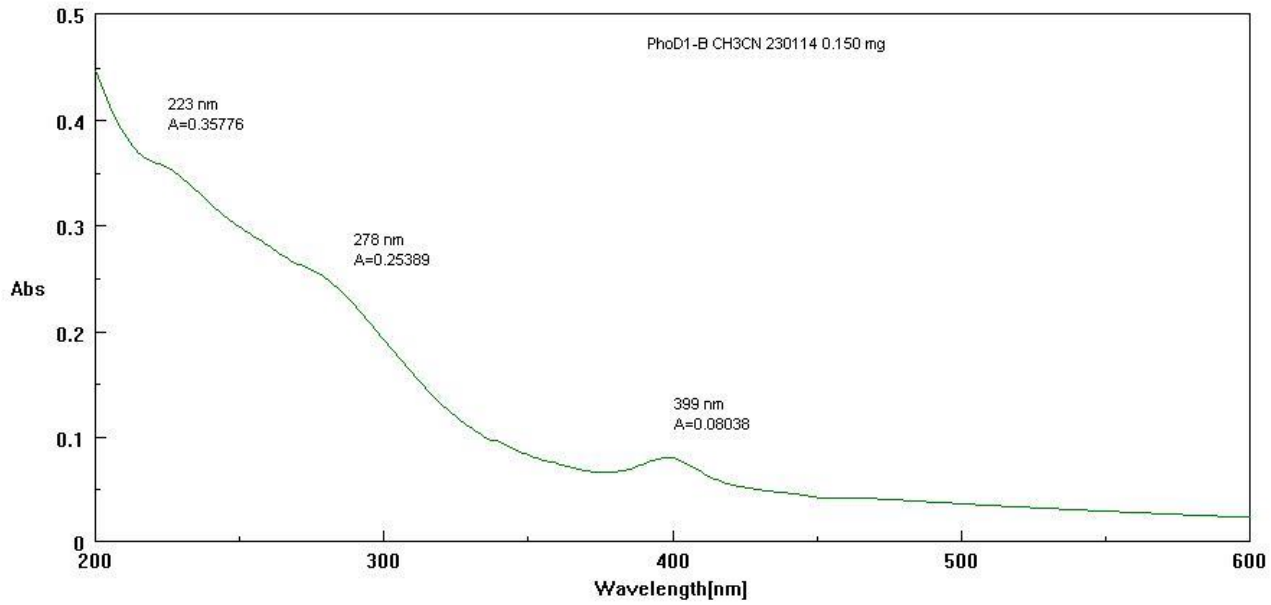

Figure. 5.1.30 UV spectrum of phomentrioloxin B (**73**), isolated from *D. gulyae* liquid culture.

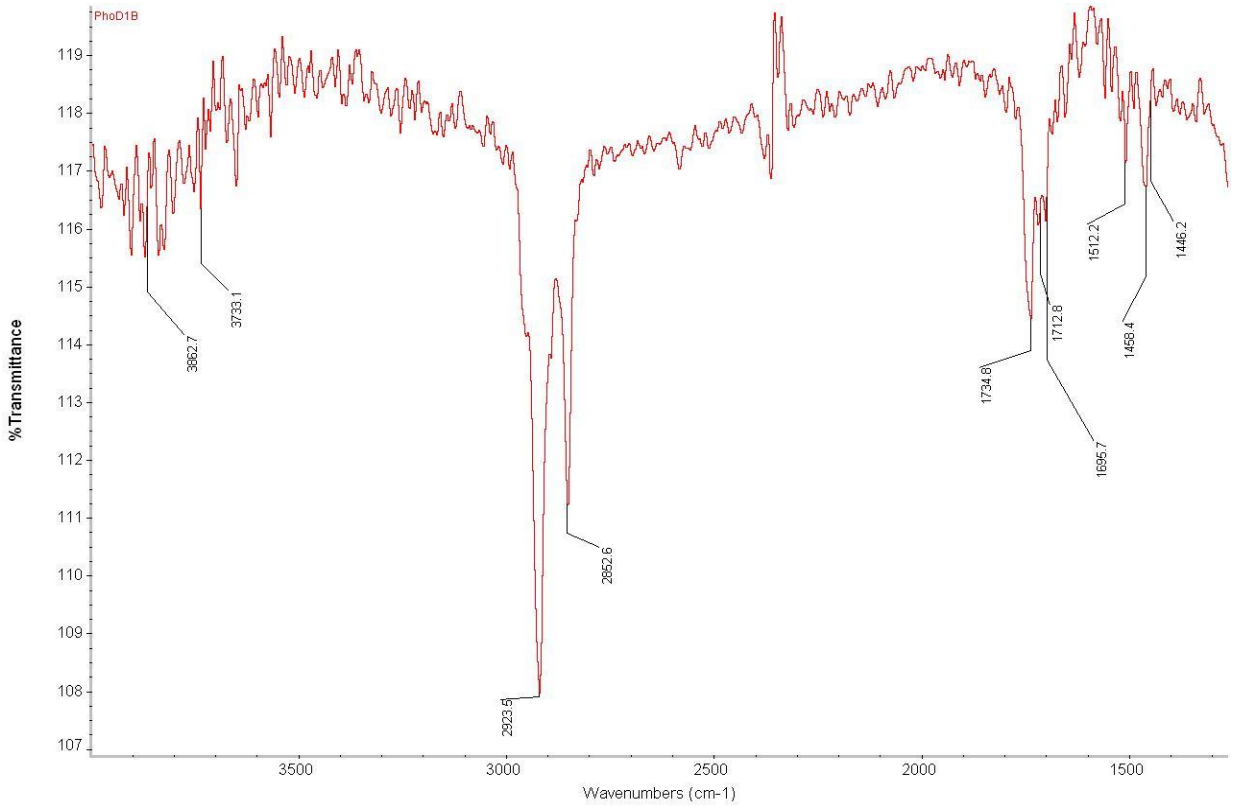

Figure. 5.1.31 IR spectrum of phomentrioloxin B (**73**), isolated from *D. gulyae* liquid culture.

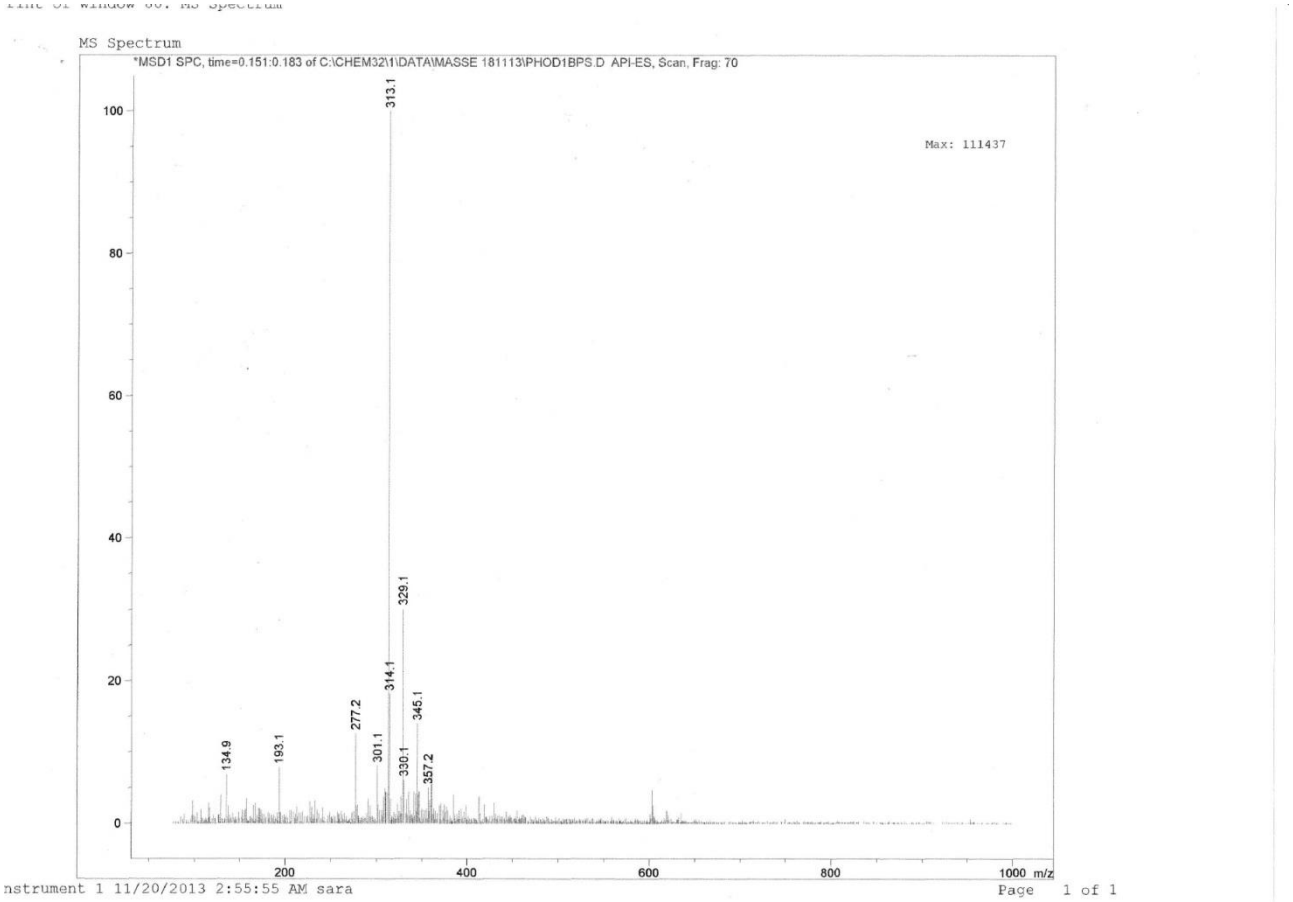

Figure. 5.1.32 ESIMS (+) spectrum of phomentrioloxin B (**73**), isolated from *D. gulyae* liquid culture.

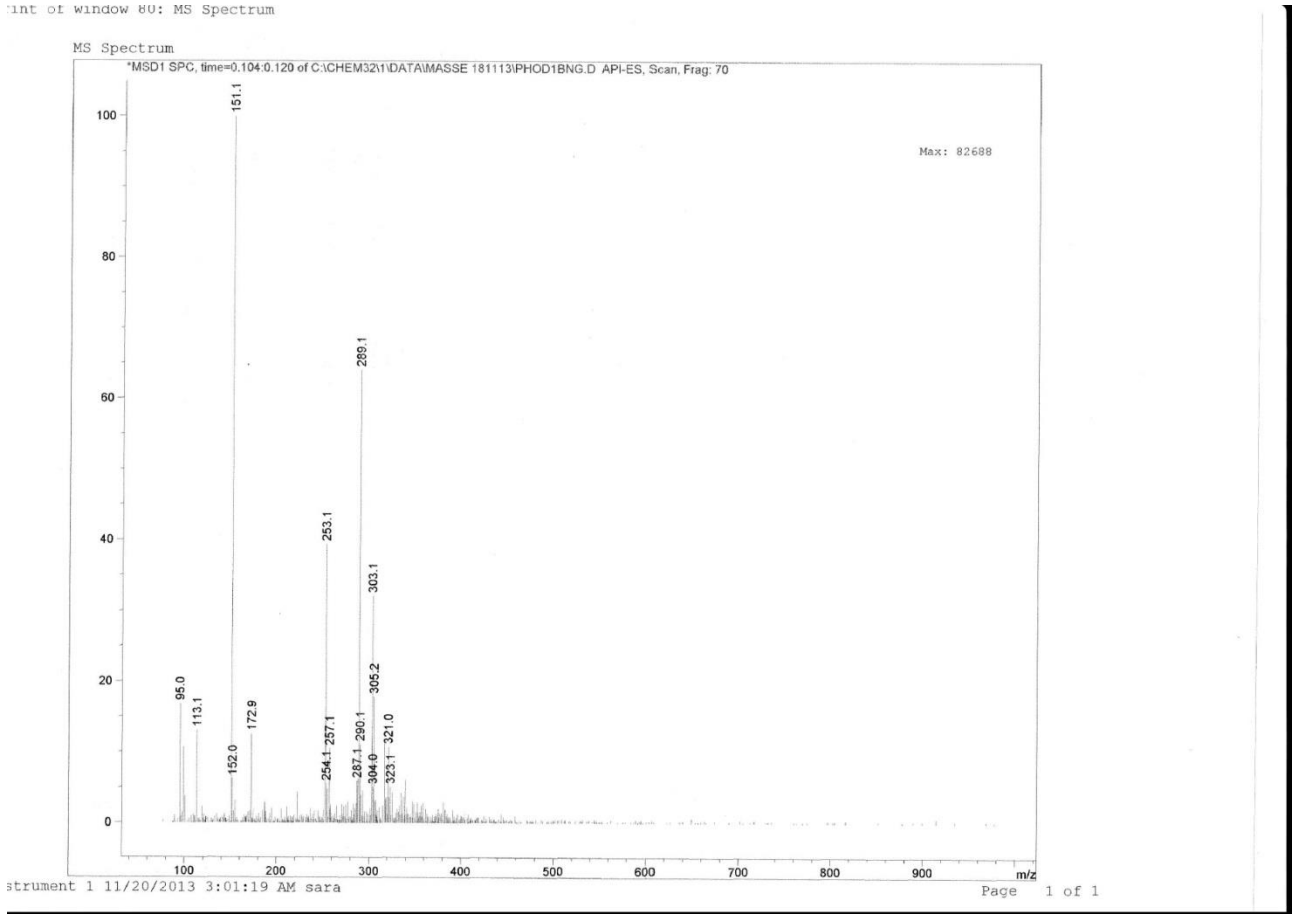

Figure. 5.1.33 ESIMS (-) spectrum of phomentrioloxin B (**73**), isolated from *D. gulyae* liquid culture.

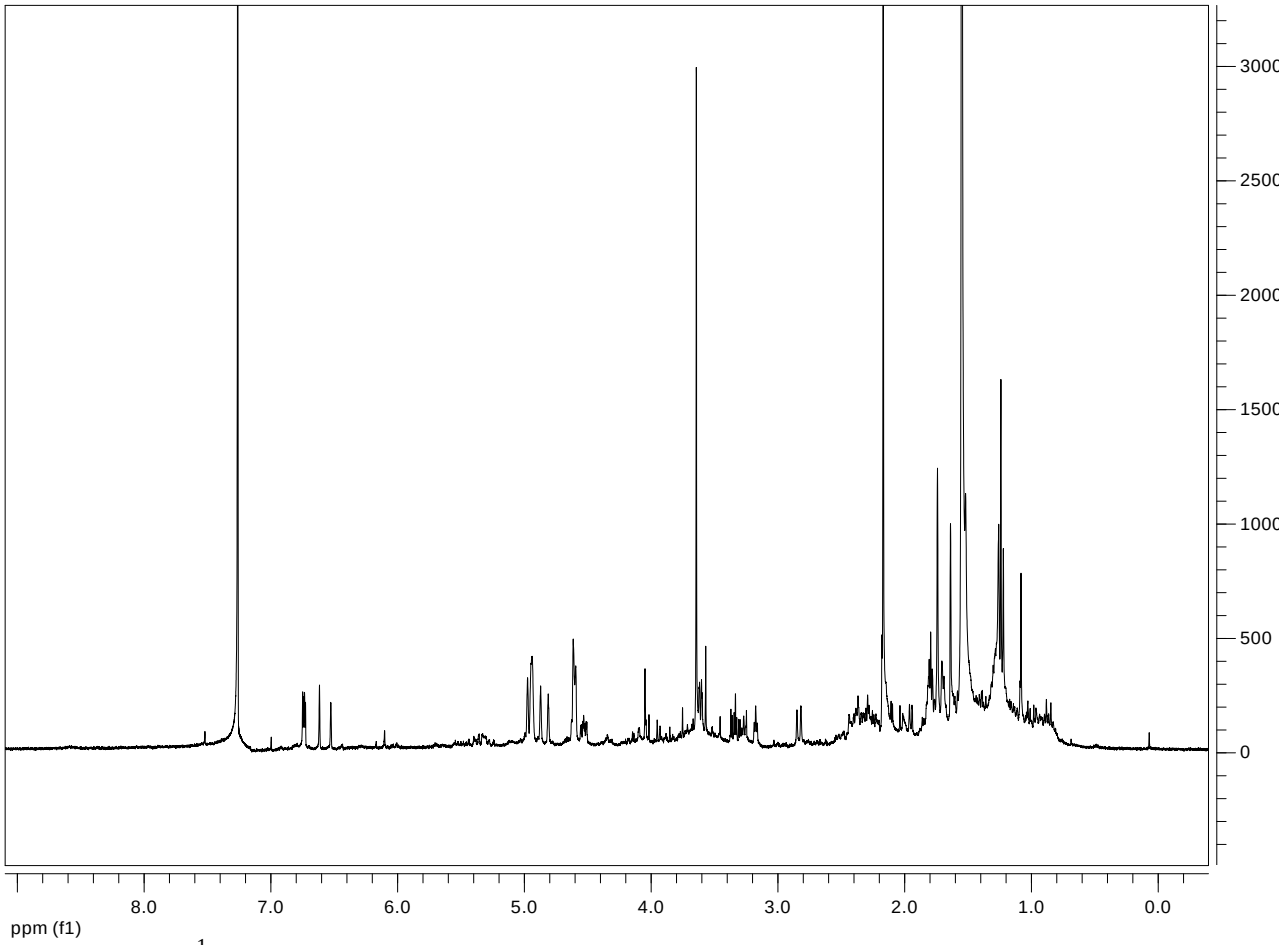

Figure. 5.1.34 ^{1}H NMR spectrum of phomentrioloxin C (**74**), isolated from *D. gulyae* liquid culture.

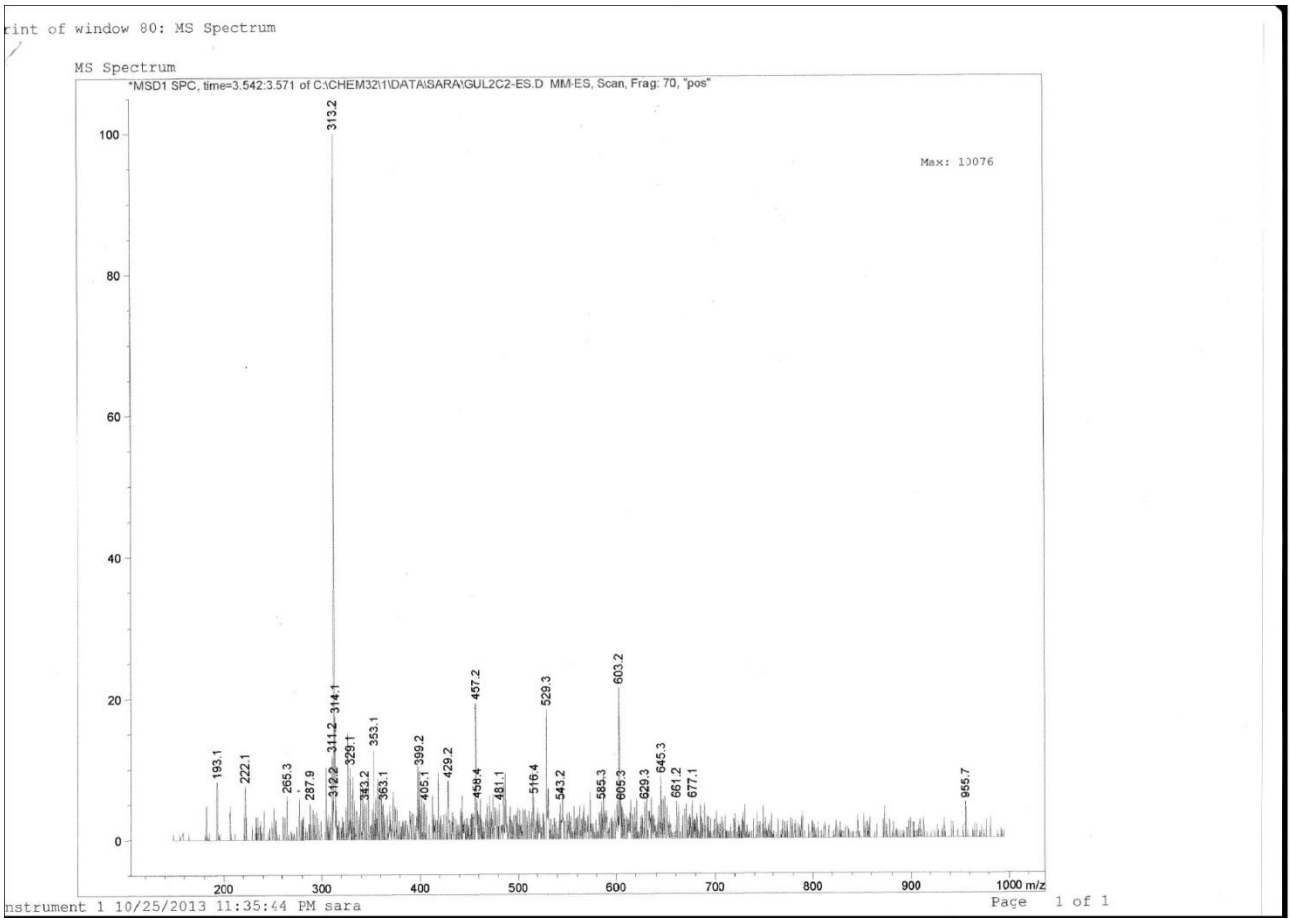

Figure. 5.1.35 ESIMS (+) spectrum of phomentrioloxin C (**74**), isolated from *D. gulyae* liquid culture.

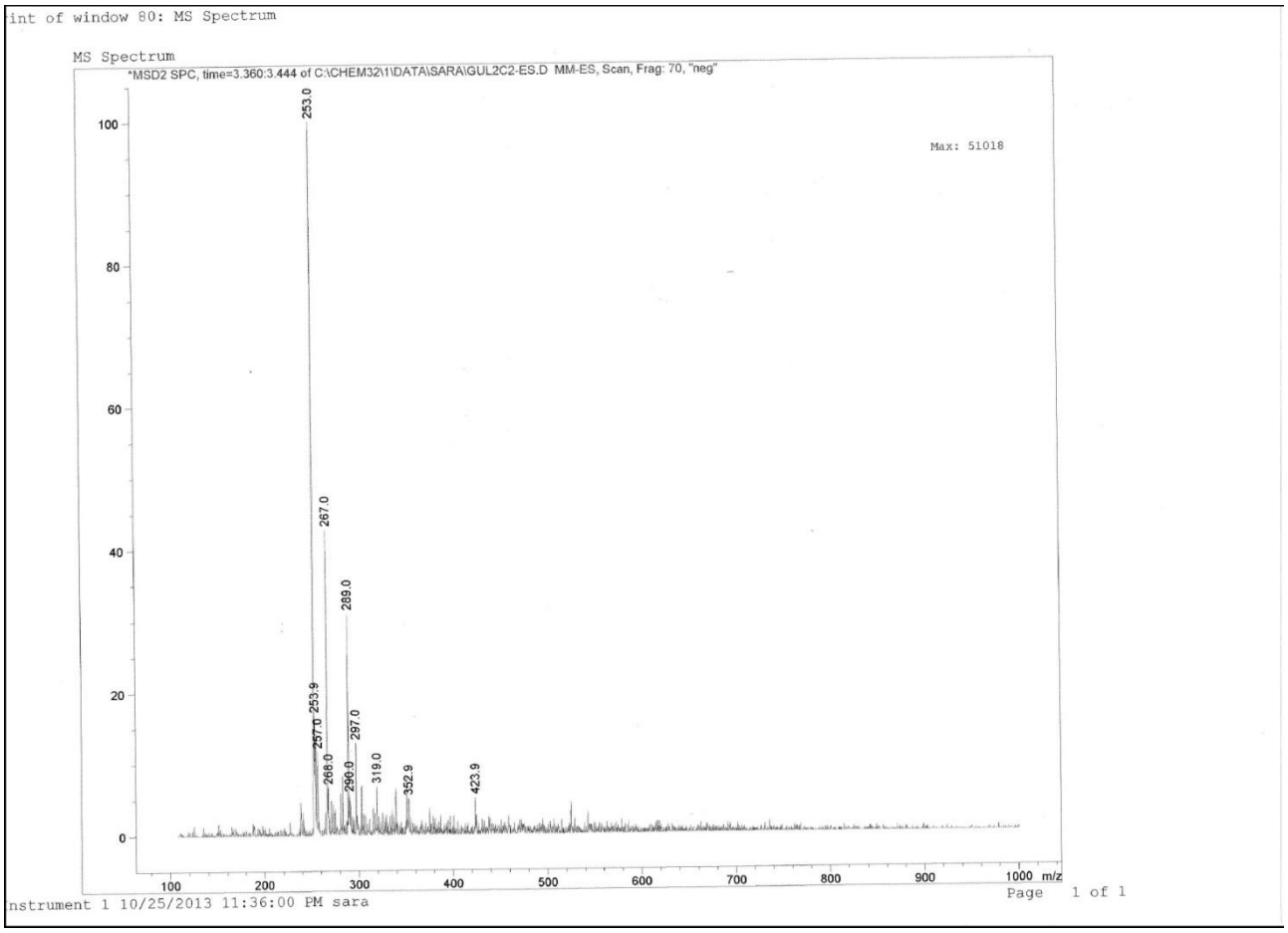

Figure. 5.1.36 ESIMS (-) spectrum of phomentrioloxin C (**74**), isolated from *D. gulyae* liquid culture.

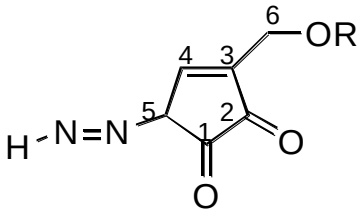

84 R=H
85 R=Ac

Figure 5.2.1. Structures of kongiidiazadione and its 6-*O*-acetylkongiidiazadione (**84** and **85**) produced by *D. kongii* growth in liquid culture.

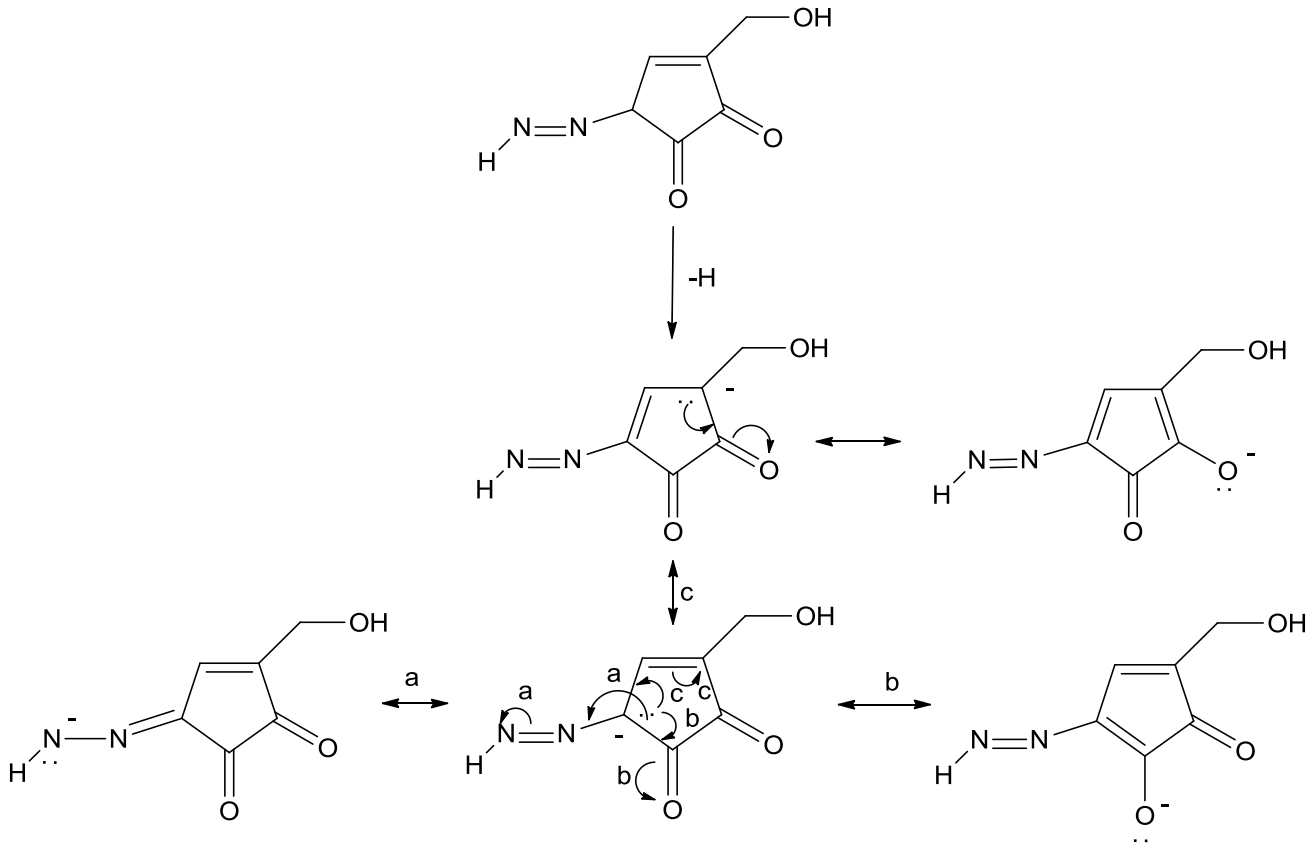

Figure 5.2.2. Possible resonance structures of kongiidiazadione (**84**) in ESI-MS analysis, recorded in negative mode.

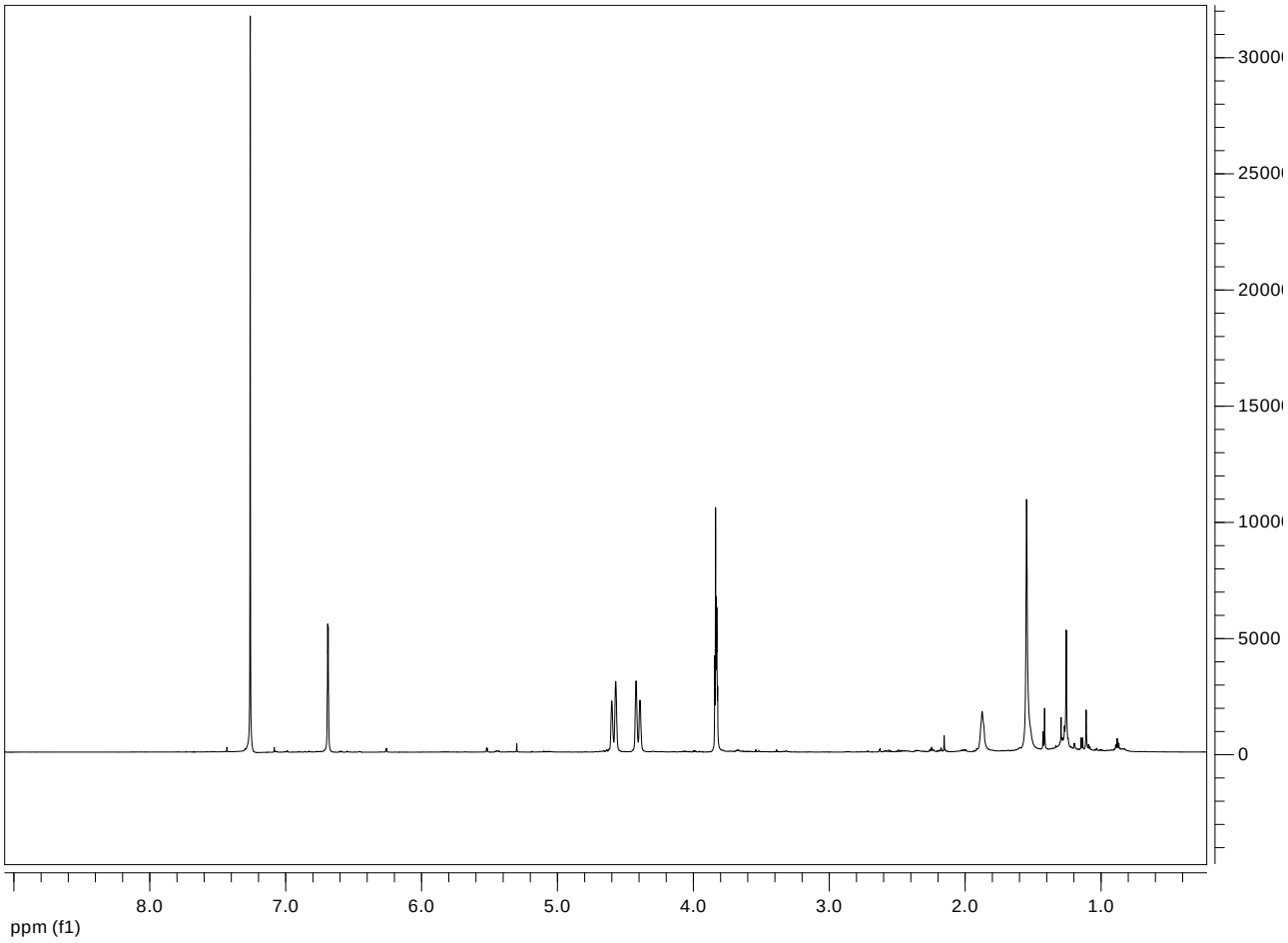

Figure 5.2.3. ^{1}H NMR spectrum of kongiidiazadione (**84**), isolated from *D. kongii* liquid culture.

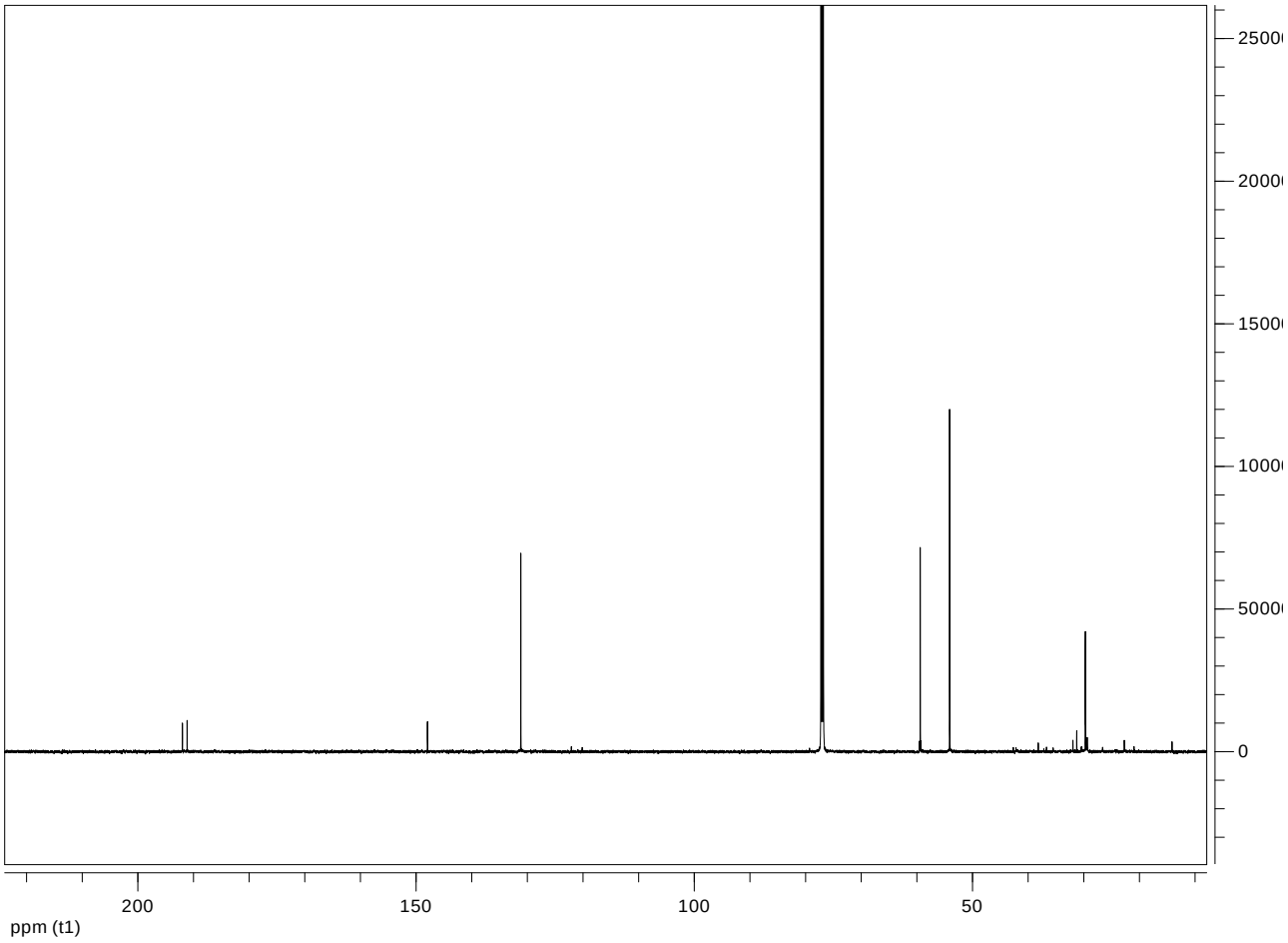

Figure 5.2.4. ^{13}C NMR spectrum of kongiidiazadione (**84**), isolated from *D. kongii* liquid culture.

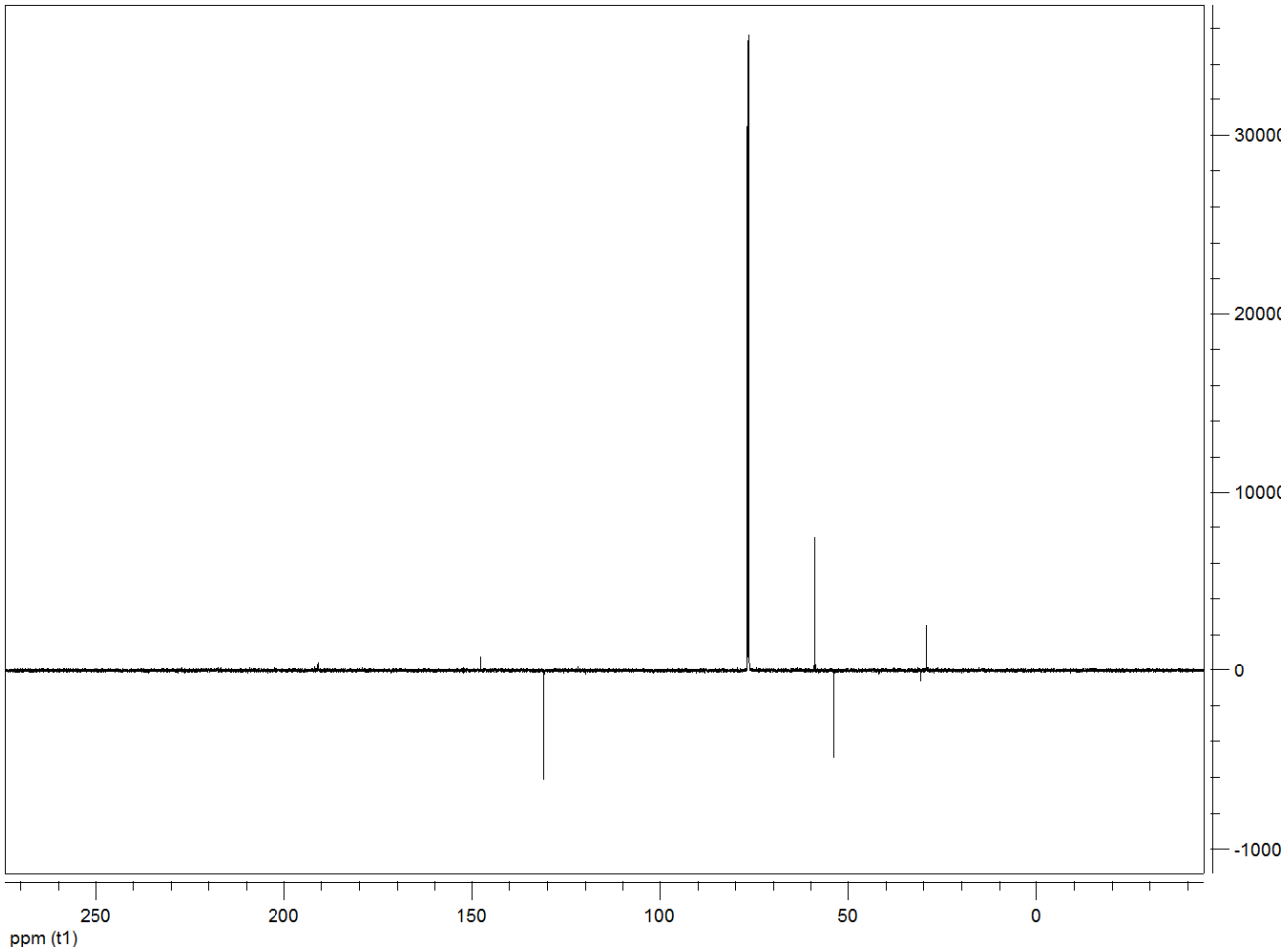

Figure 5.2.5. ^{13}C NMR DEPT spectrum of kongiidiazadione (**84**), isolated from *D. kongii* liquid culture.

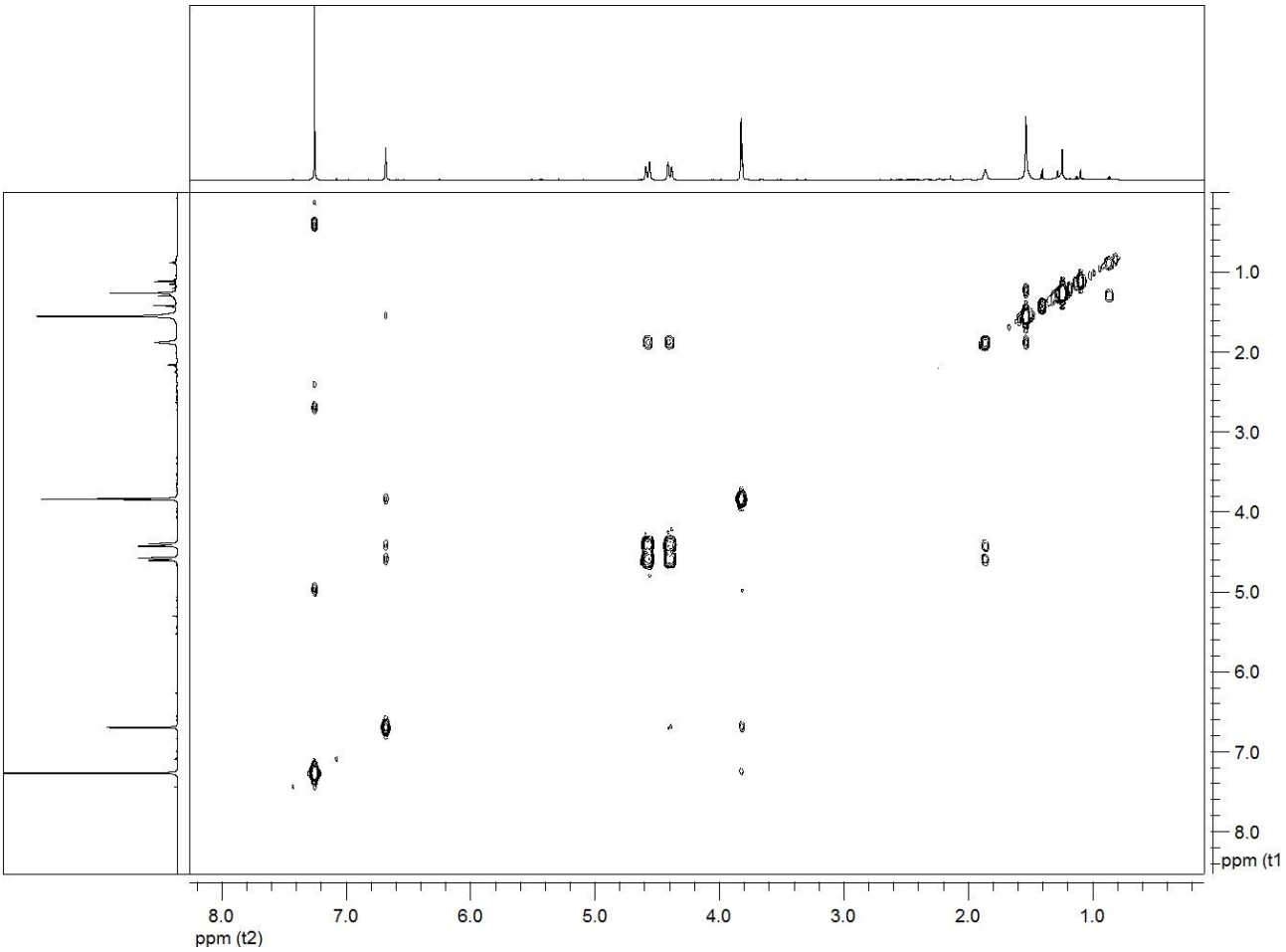

Figure 5.2.6. COSY spectrum of kongiidiazadione (**84**), isolated from *D. kongii* liquid culture.

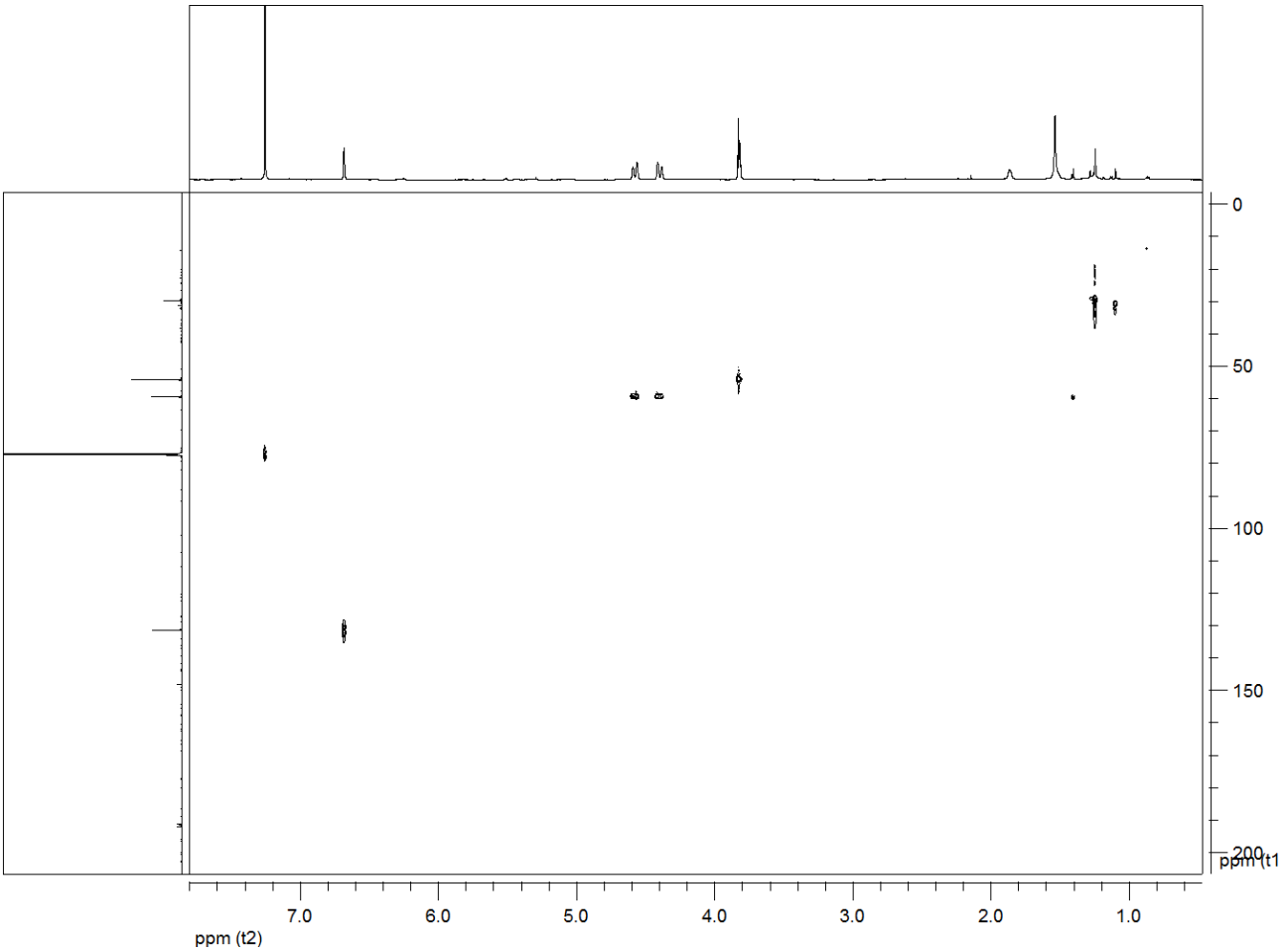

Figure 5.2.7. HSQC spectrum of kongiidiazadione (**84**), isolated from *D. kongii* liquid culture.

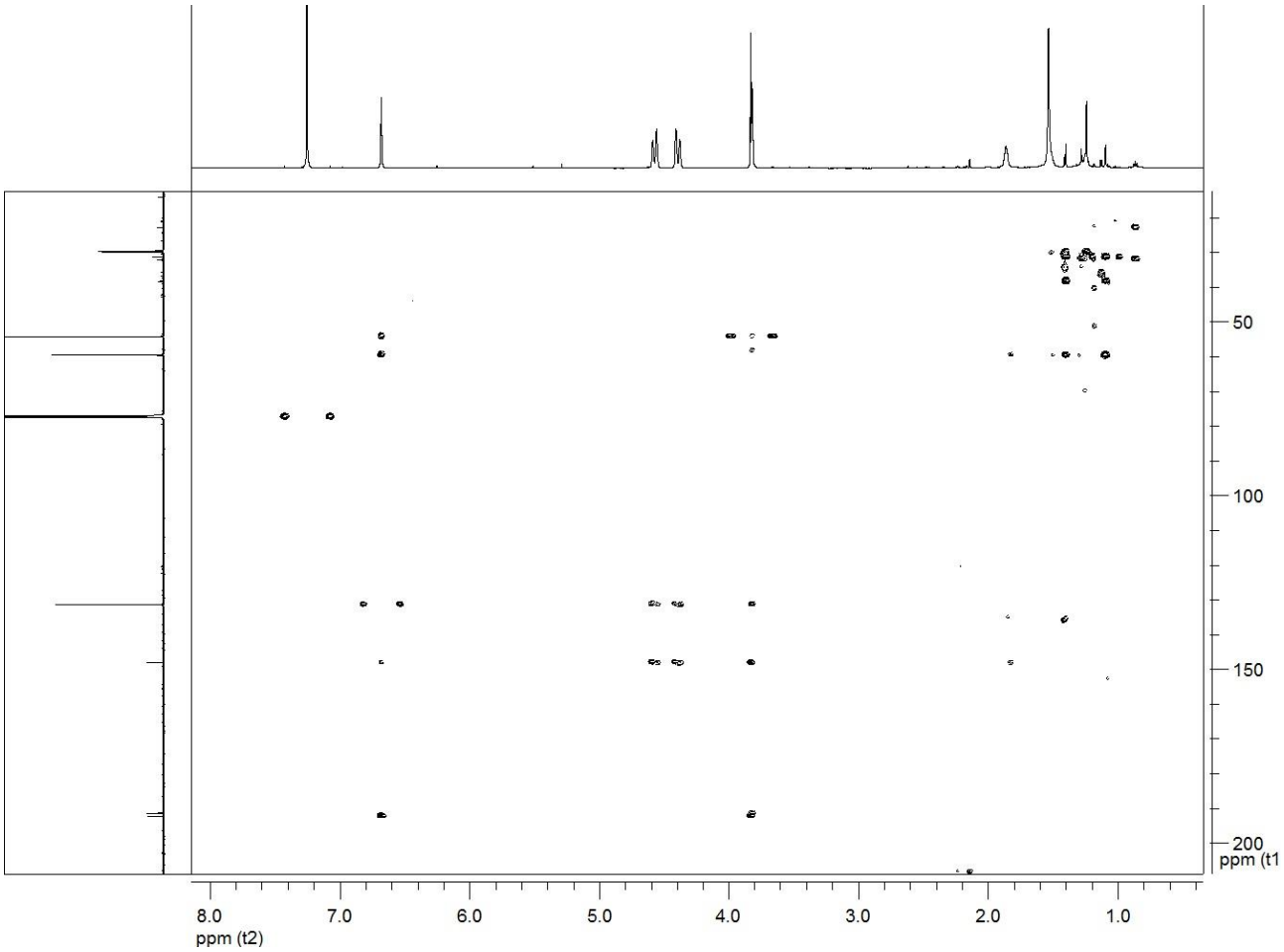

Figure 5.2.8. HMBC spectrum of kongiidiazadione (**84**), isolated from *D. kongii* liquid culture.

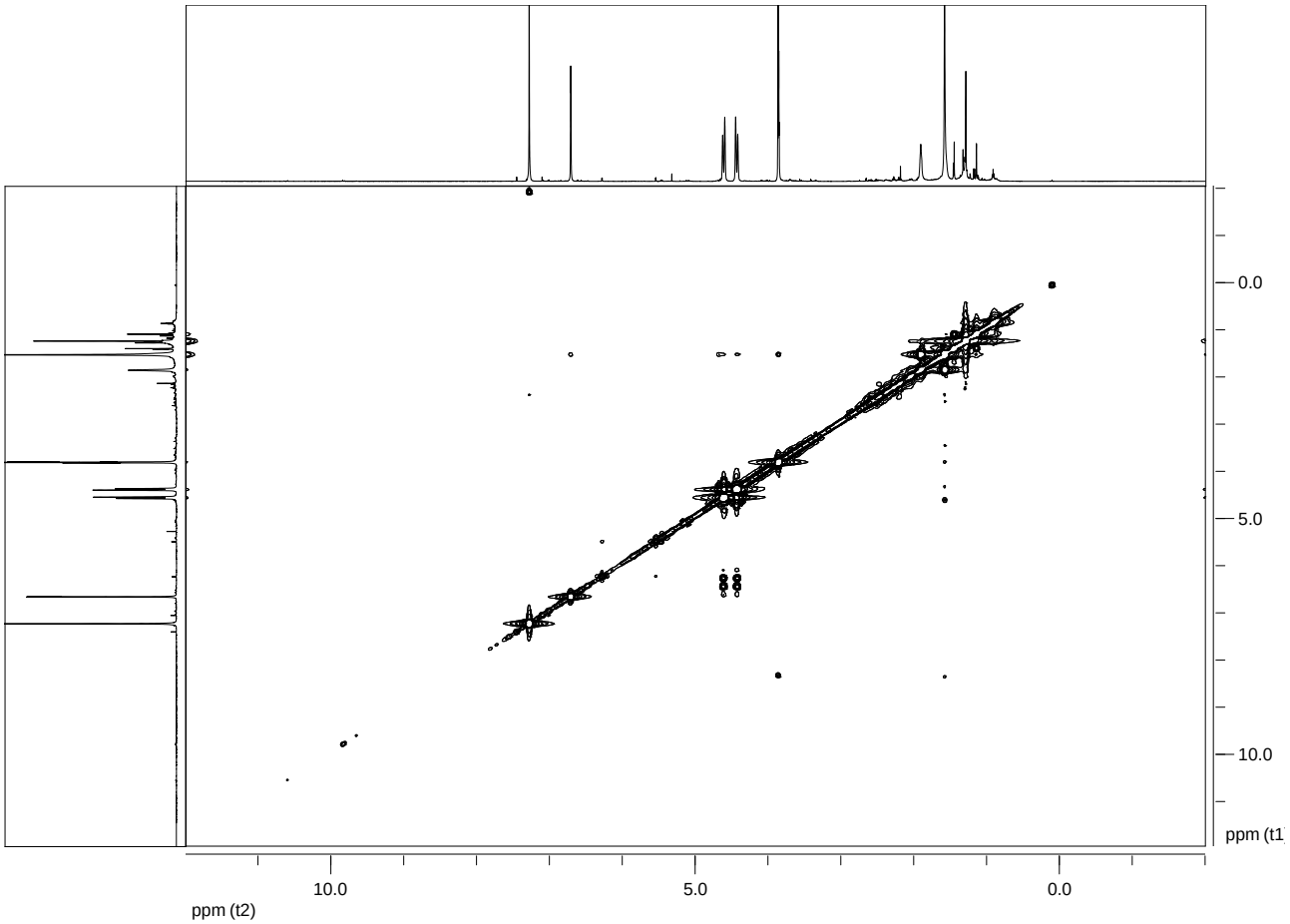

Figure 5.2.9. NOESY spectrum of kongiidiazadione (**84**), isolated from *D. kongii* liquid culture.

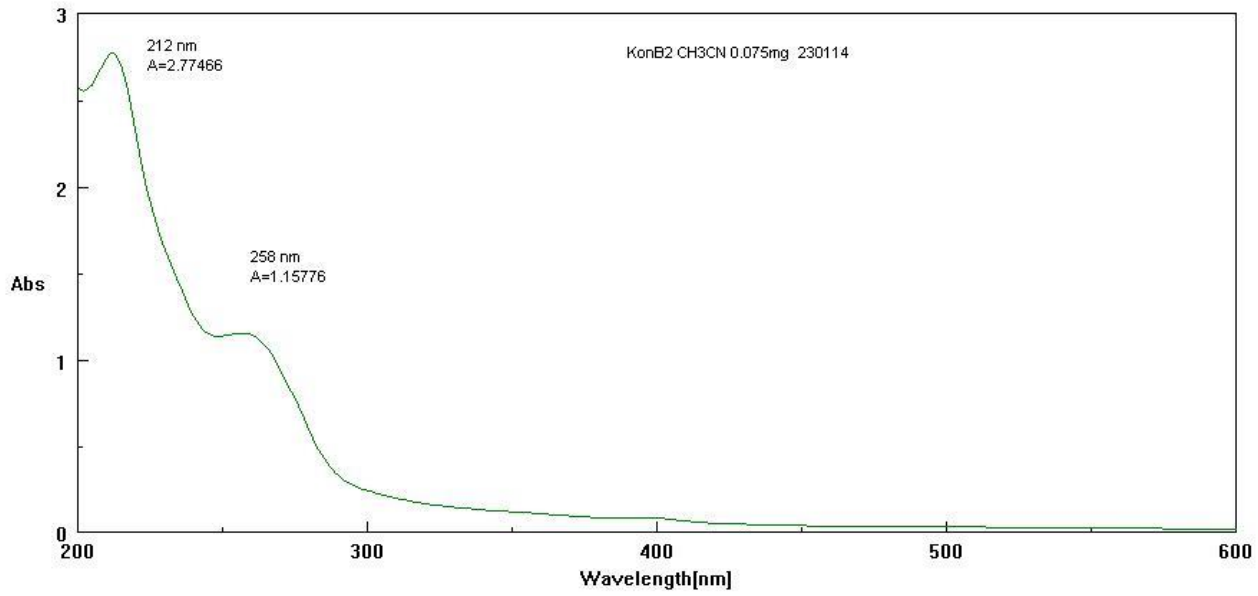

Figure 5.2.10. UV spectrum of kongiidiazadione (**84**), isolated from *D. kongii* liquid culture.

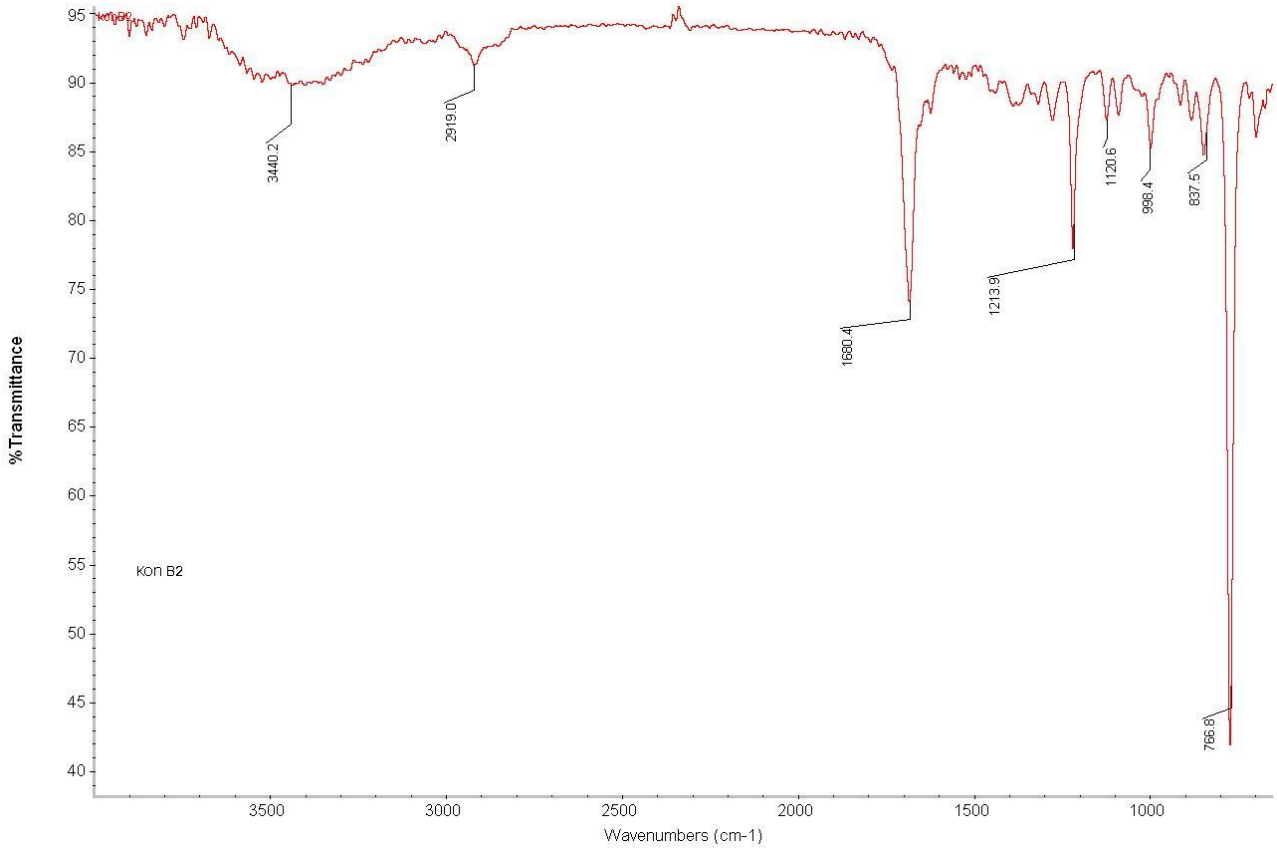

Figure 5.2.11. IR spectrum of kongiidiazadione (**84**), isolated from *D. kongii* liquid culture.

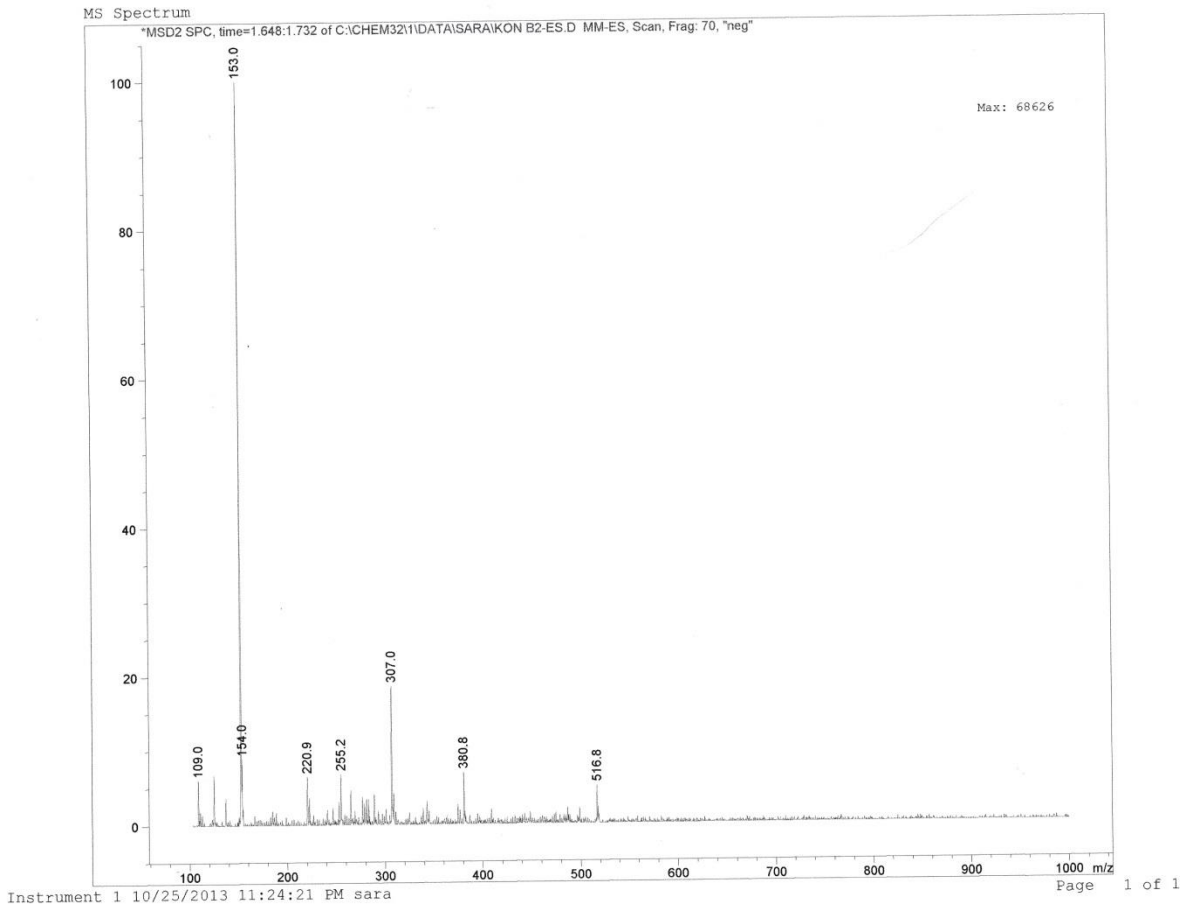

Figure 5.2.12. ESI-MS (-) spectrum of kongiidiazadione (**84**), isolated from *D. kongii* liquid culture.

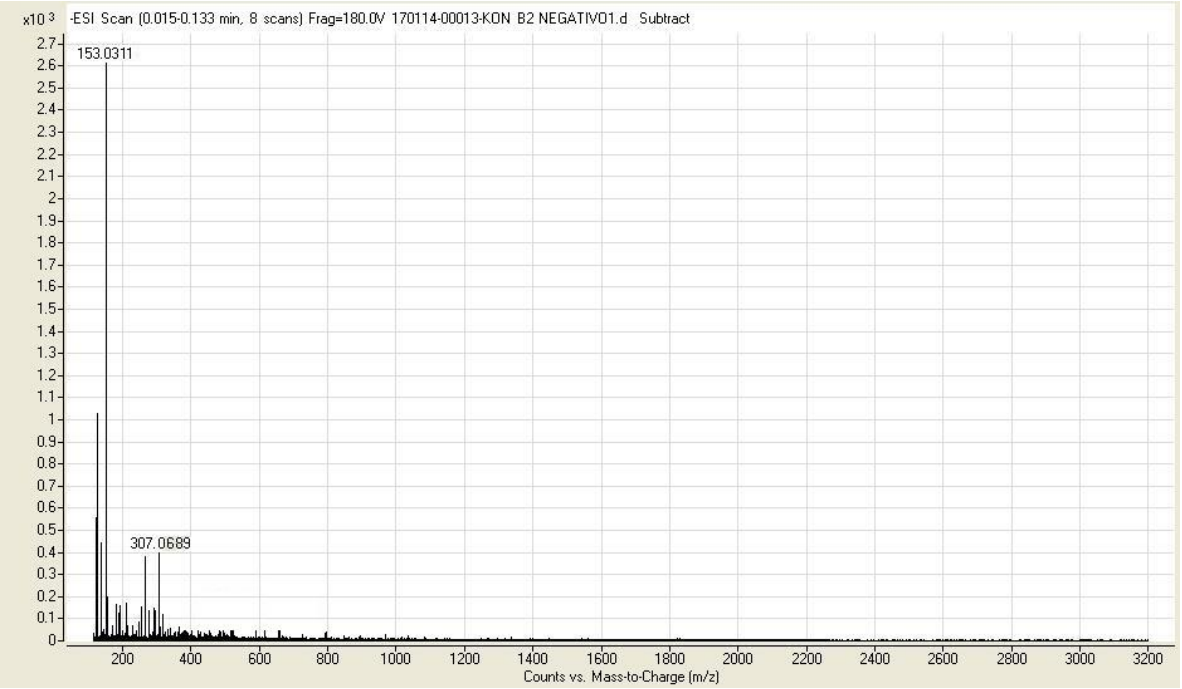

Figure 5.2.13. HRESI-MS (-) spectrum of kongiidiazadione (**84**), isolated from *D. kongii* liquid culture.

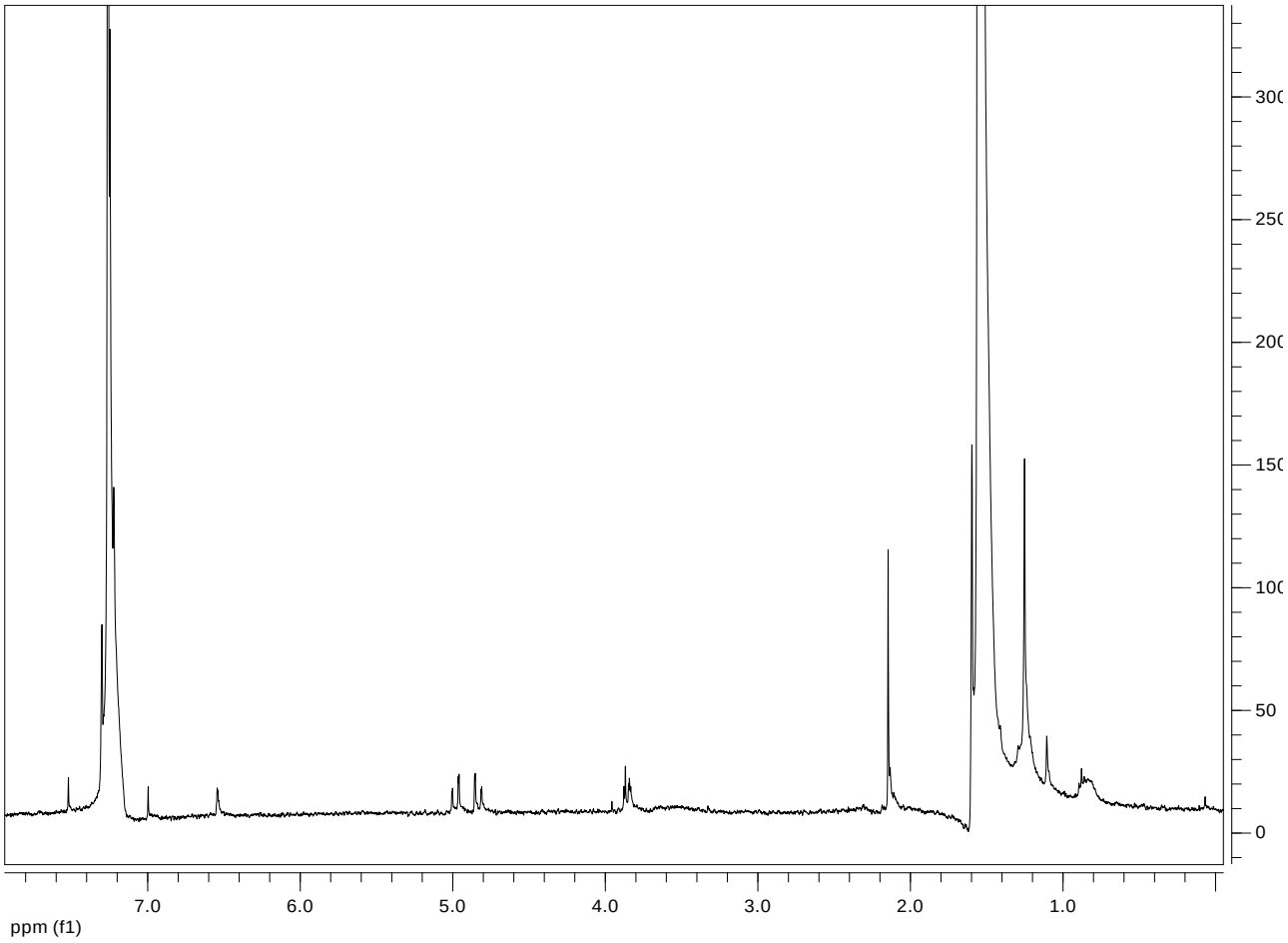

Figure 5.2.14. ^{1}H-NMR spectrum of 6-*O*-acetyl derivative of kongiidiazadione (**85**).

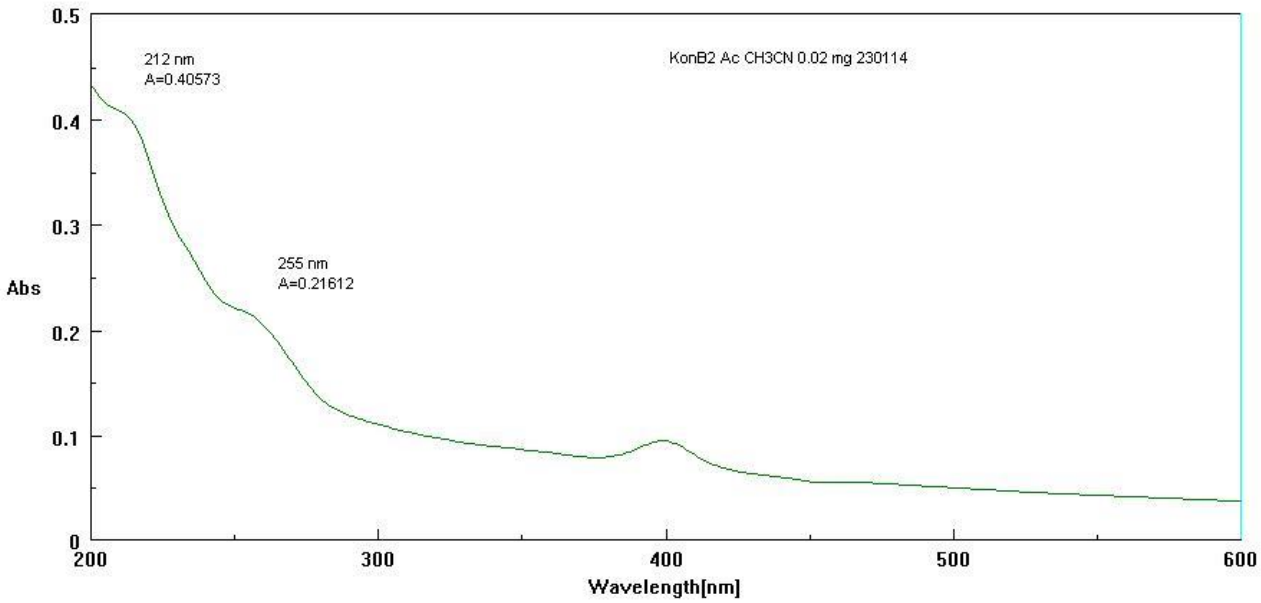

Figure 5.2.15. UV spectrum of 6-*O*-acetyl derivative of kongiidiazadione (**85**).

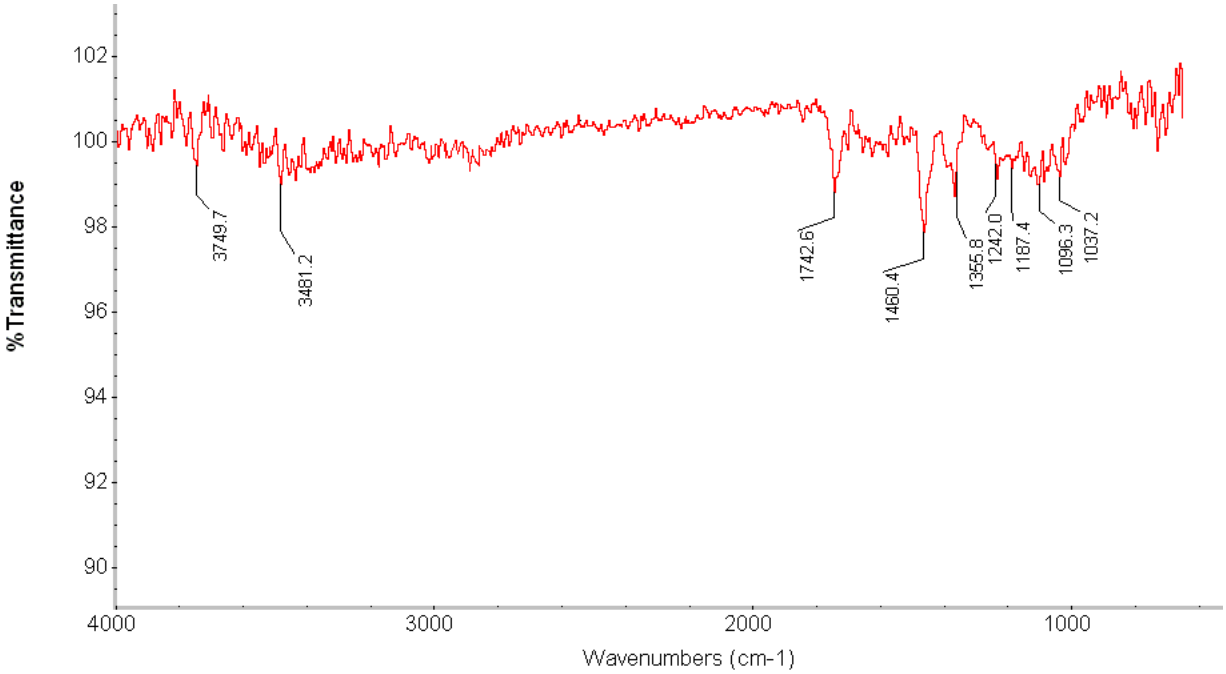

Figure 5.2.16. IR spectrum of 6-*O*-acetyl derivative of kongiidiazadione (**85**)

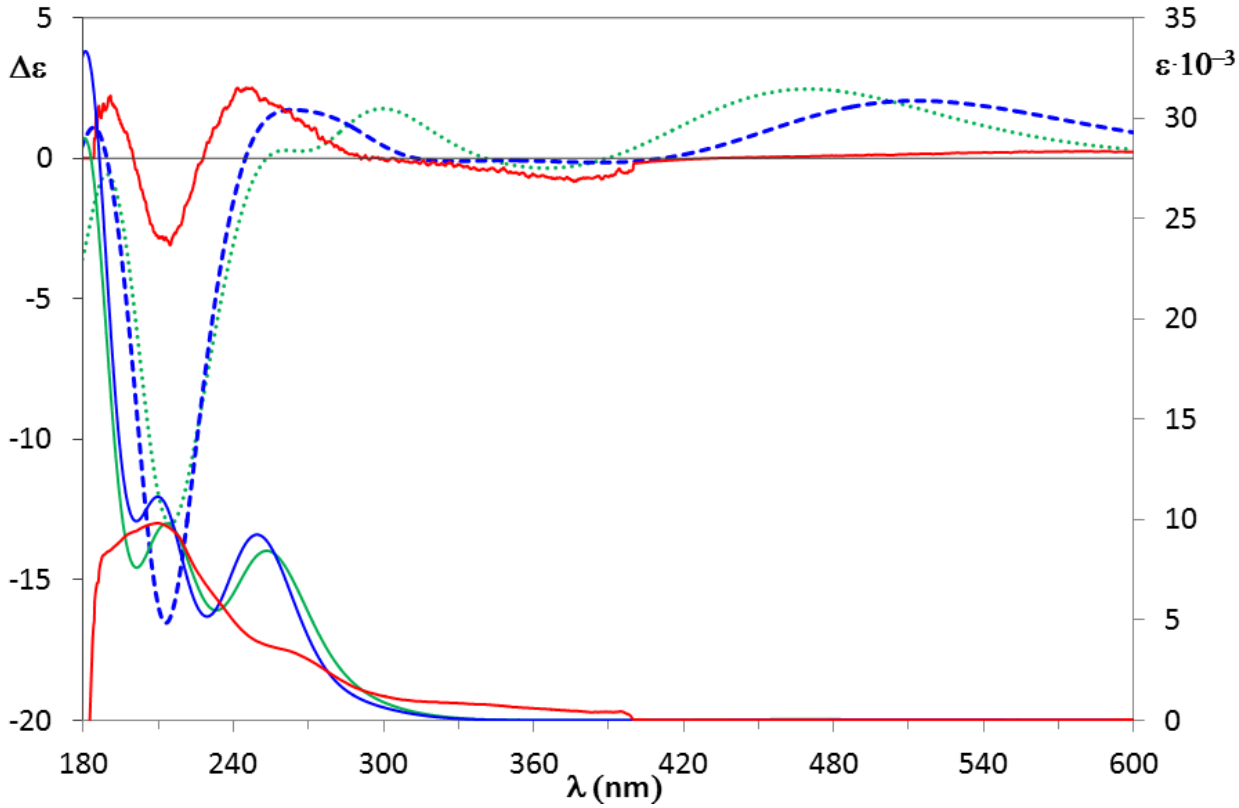

Figure 5.2.17. Experimental UV and ECD spectra of (-)-**84** [solid red line, methanol] and calculated UV and ECD spectra for (5*R*)-**84** [TDDFT/CAM-B3LYP/aug-cc-pVDZ//DFT/B3LYP/TZVP/IEFPCM (CH_3OH) solid and dotted green line; TDDFT/M062X/aug-cc-pVDZ//DFT/M062X/TZVP/IEFPCM (CH_3OH) solid and dashed blue line; 0.4 eV bandwidth]. M062X calculated UV and ECD spectra are red shifted of +5.0 nm.

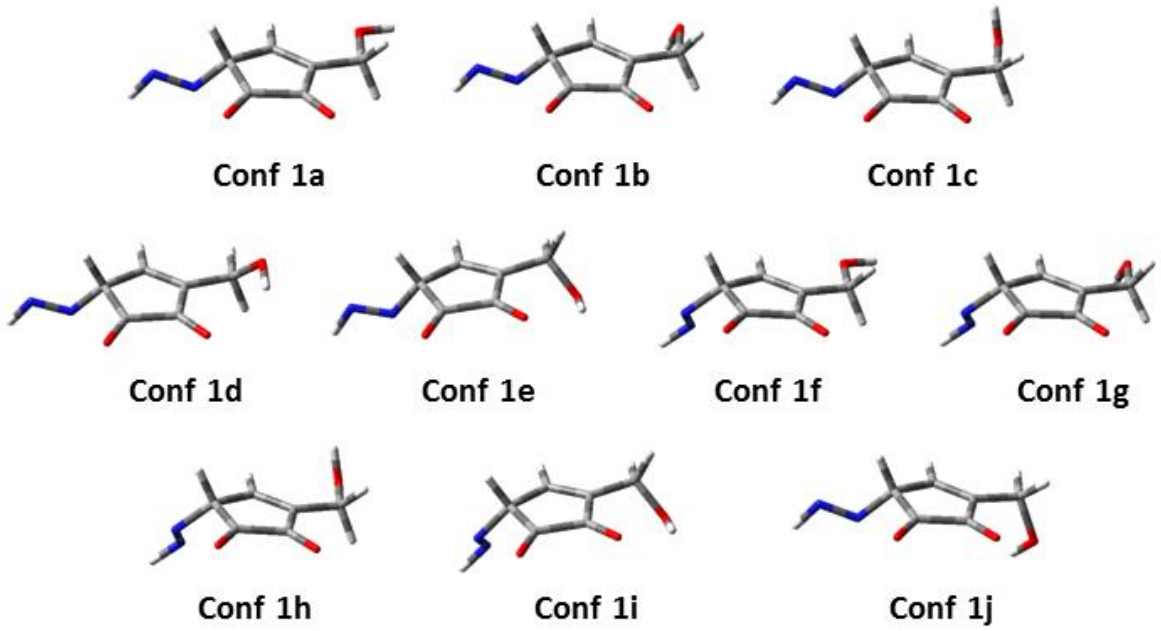

Fig. 5.2.18. Computed [DFT/M062X/TZVP/IEFPCM(CH3OH)] most stable conformers of (5*R*)-**84**.

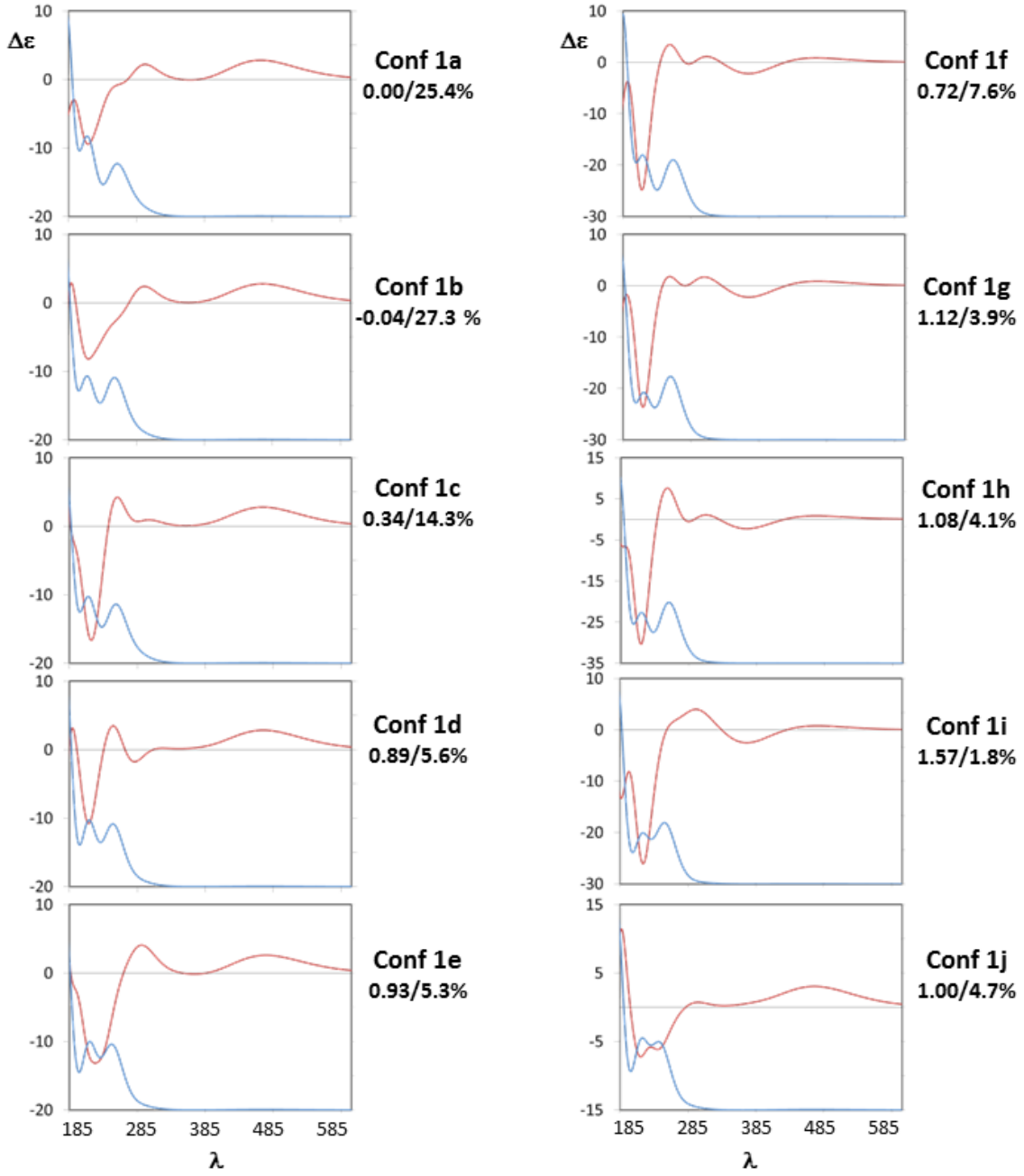

Figure 5.2.19. Computed single conformer ECD (red line) and UV (blue line) spectra for (5*R*)-**84** (TDDFT/CAM-B3LYP/aug-cc-pVDZ//DFT/B3LYP/TZVP/IEFPCM(MeOH). For each conformer ΔG (kcal mol^{-1})/population is reported.

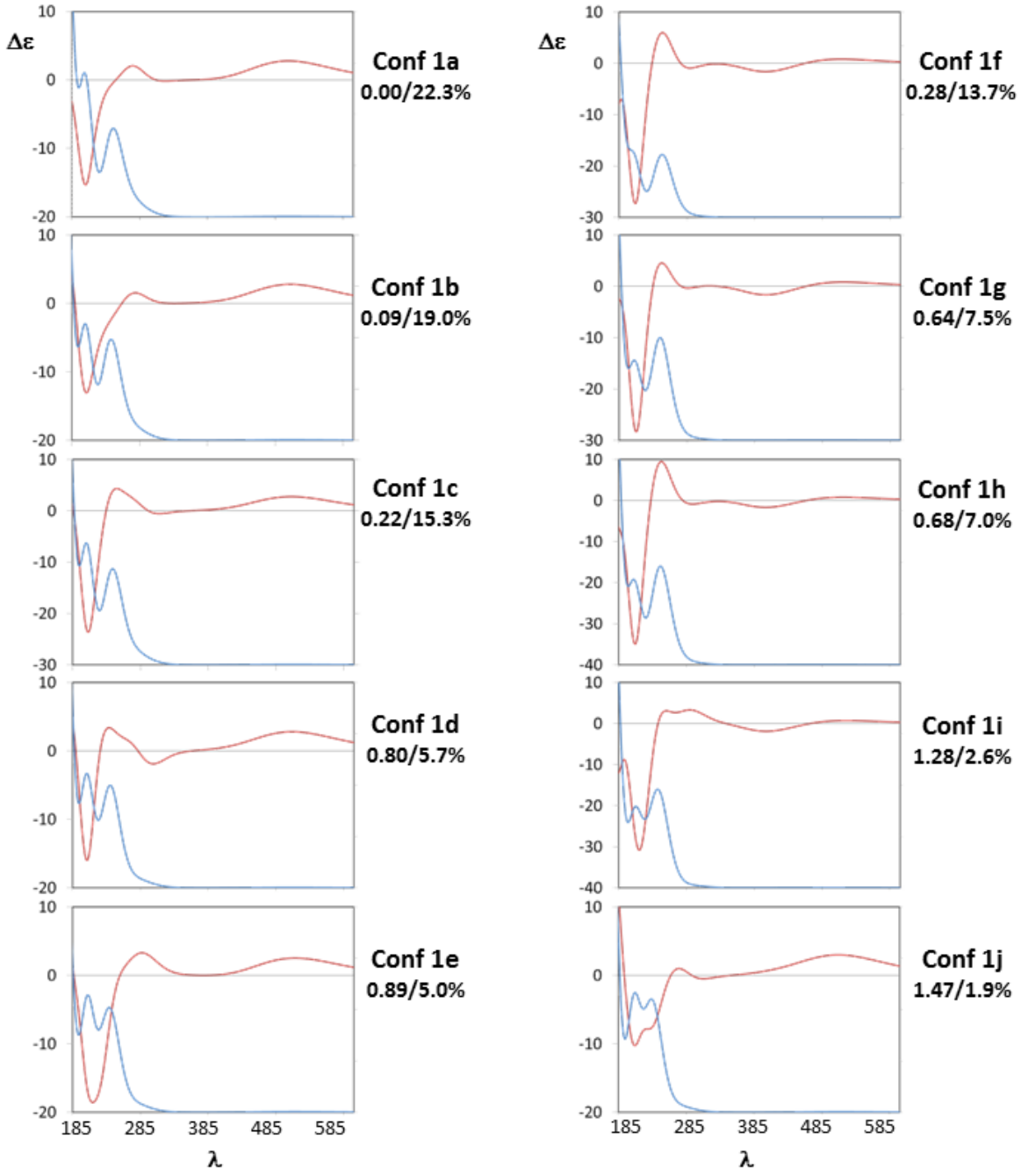

Figure 5.2.20. Computed single conformer ECD (red line) and UV (blue line) spectra for (5*R*)-**84** (TDDFT/M062X/aug-cc-pVDZ//DFT/M062X/TZVP/IEFPCM(MeOH). For each conformer ΔG (kcal mol^{-1})/population is reported.

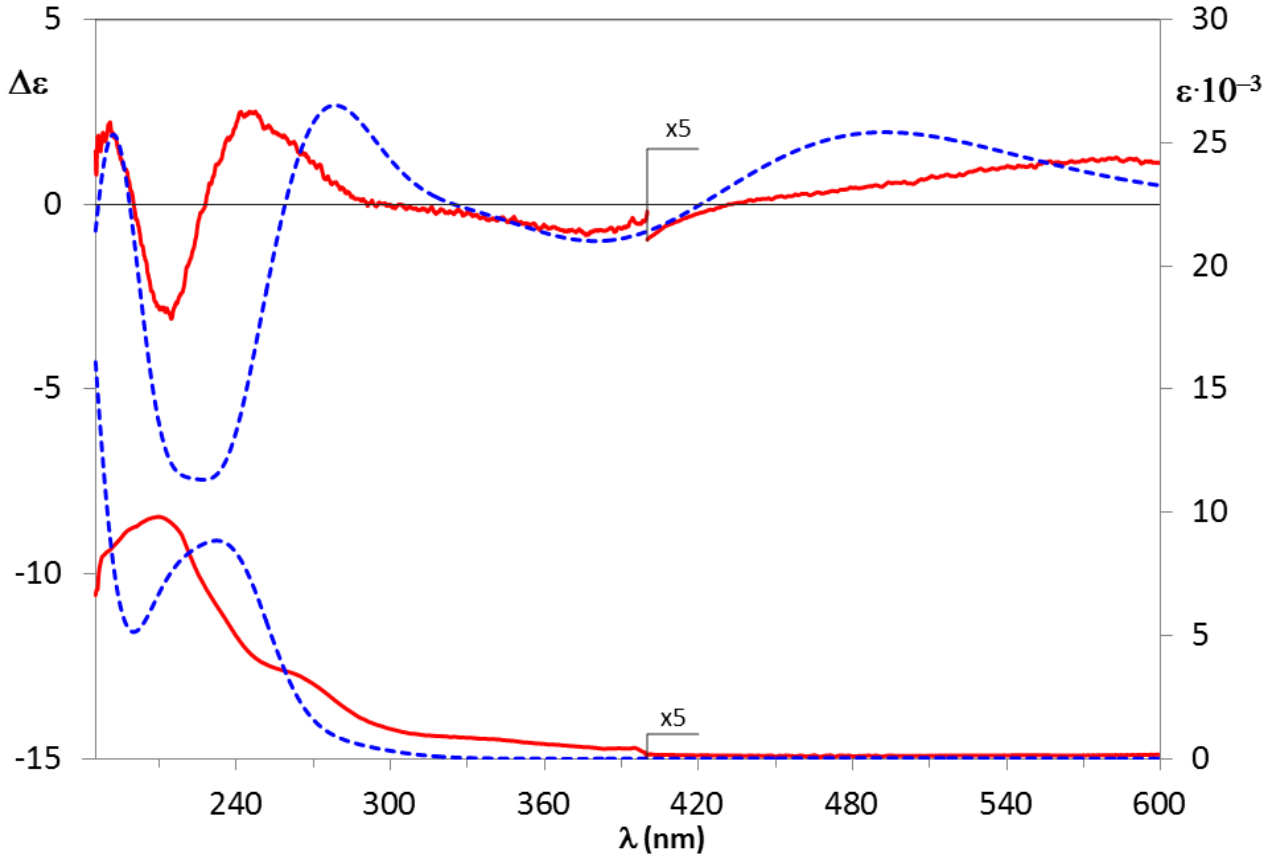

Figure 5.2.21. Experimental UV and ECD spectra of (-)-**84** [solid red line, methanol] and calculated UV and ECD spectra for (5*R*)-**84** [TDDFT/CAM-B3LYP/aug-cc-pVDZ// DFT/B3LYP/TZVP/IEFPCM (gas phase) dashed blue line; 0.4 eV bandwidth]. Experimental UV and ECD spectra are magnified five times above 400 nm.

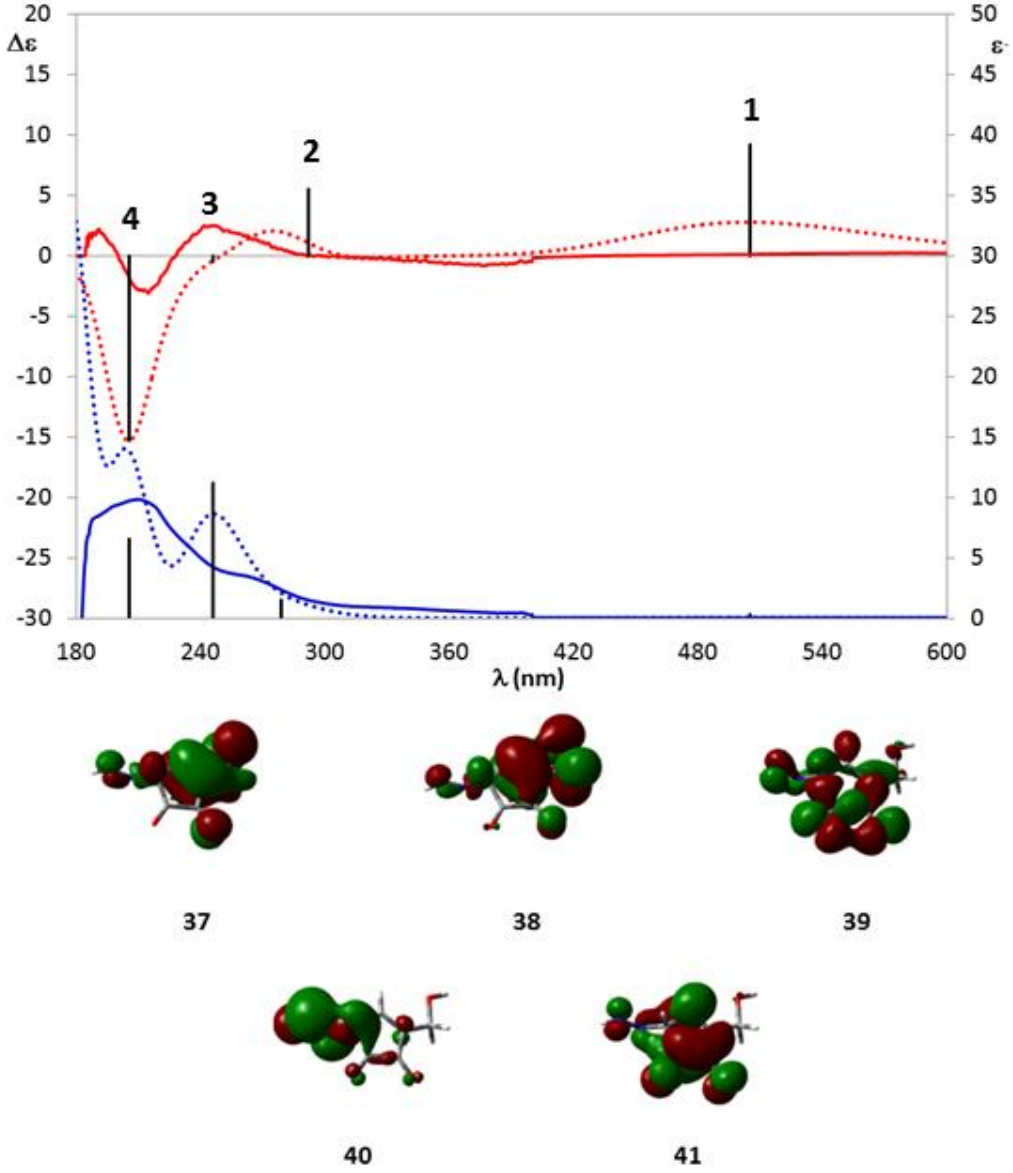

Figure. 5.2.22. Top: Experimental UV (solid blue line) and ECD (solid red line) spectra of (-)-**84** and calculated UV and ECD (dotted lines) spectra for (5*R*)-**84** [TDDFT/M062X/aug-cc-pVDZ// DFT/M062X/TZVP/IEFPCM (CH_3OH); 0.4 eV bandwidth]. Vertical bars relate to rotatory strength values (in arbitrary units), calculated in the velocity formalism. Bottom: Molecular orbitals allied to electronic transitions calculated for conformer (5*R*)-**84a** in the 180-600 nm range.

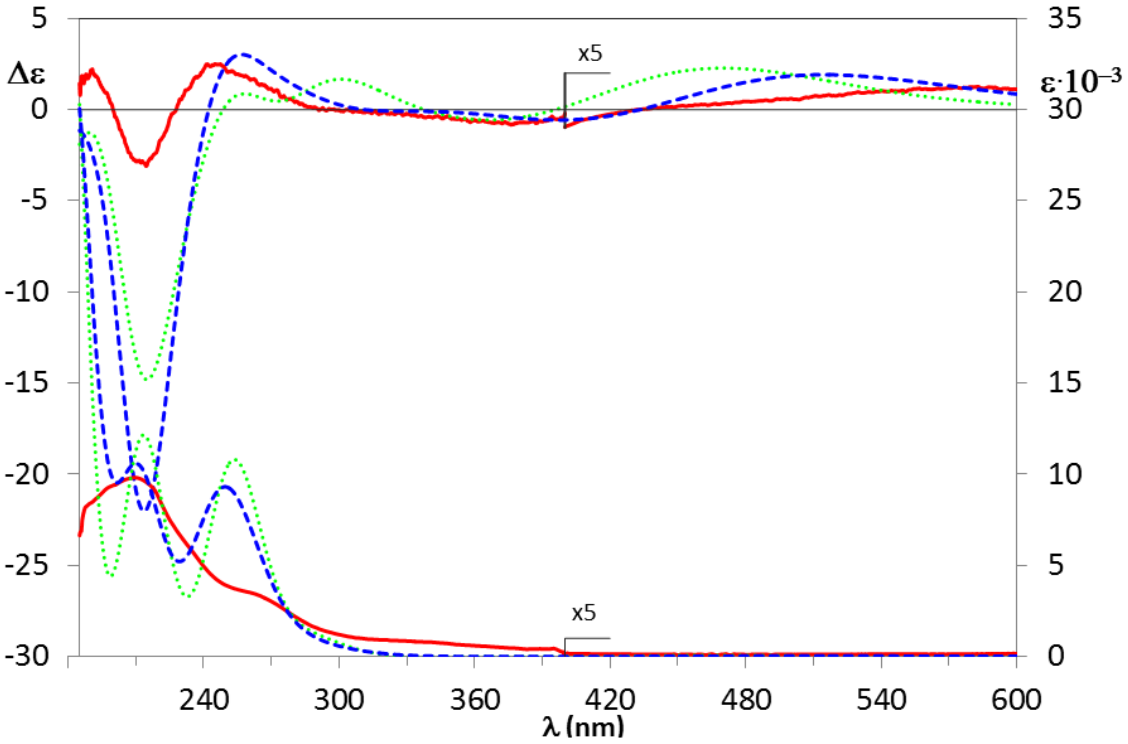

Fig. 5.2.23. Experimental UV and ECD spectra of (-)-**84** [solid red line, methanol] and calculated UV and ECD spectra for (5*R*)-**84** taking into account ΔE conformers populations [TDDFT/CAM-B3LYP/aug-cc-pVDZ//DFT/B3LYP/TZVP/IEFPCM (CH_3OH) dotted green line; TDDFT/M062X/aug-cc-pVDZ//DFT/M062X/TZVP/IEFPCM (CH_3OH) dashed blue line; 0.4 eV bandwidth]. M062X calculated UV and ECD spectra are red shifted of +5.0 nm. Experimental UV and ECD spectra beyond 400 nm are magnified five times.

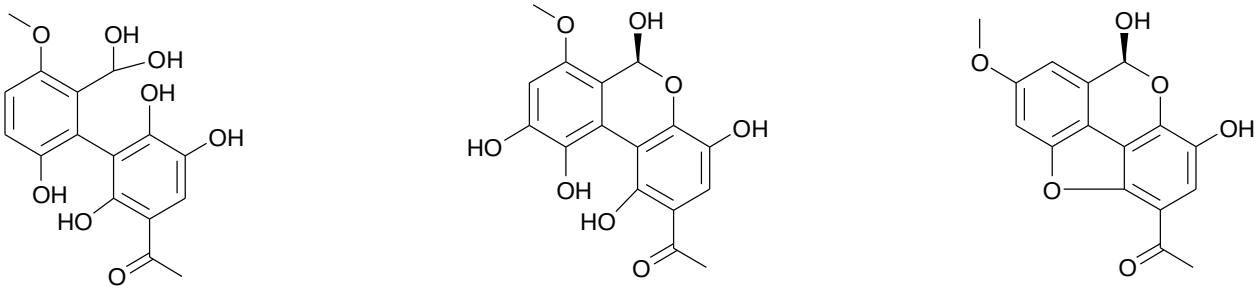

86 **87** **88**

Figure. 5.3.1 Structures of: alternethanoxin C-E (**86**-**88**) isolated from *A. sonchi* liquid culture.

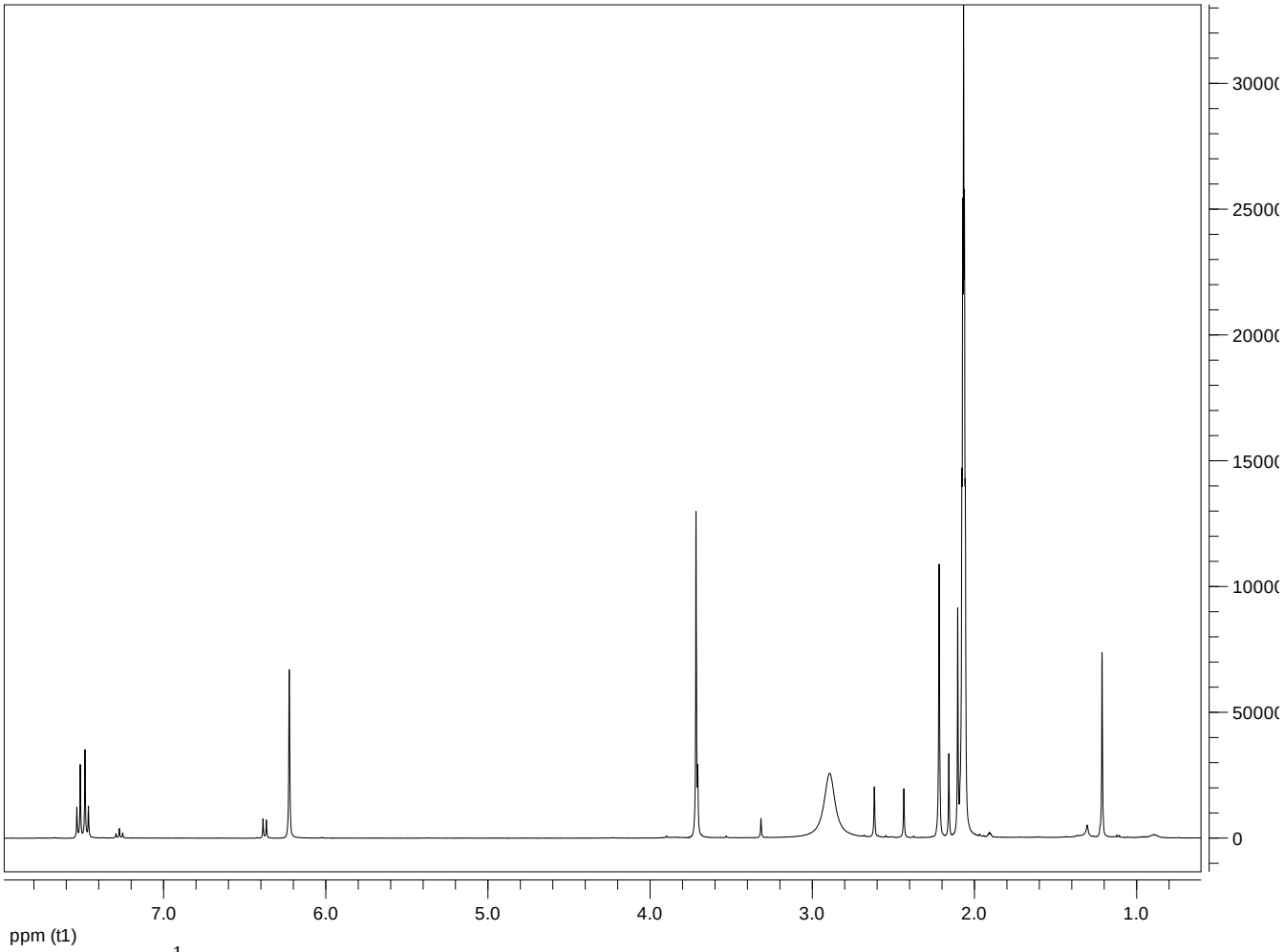

Figure. 5.3.2 ^{1}H NMR spectrum of alternethanoxin C (**86**), isolated from *A. sonchi* solid culture.

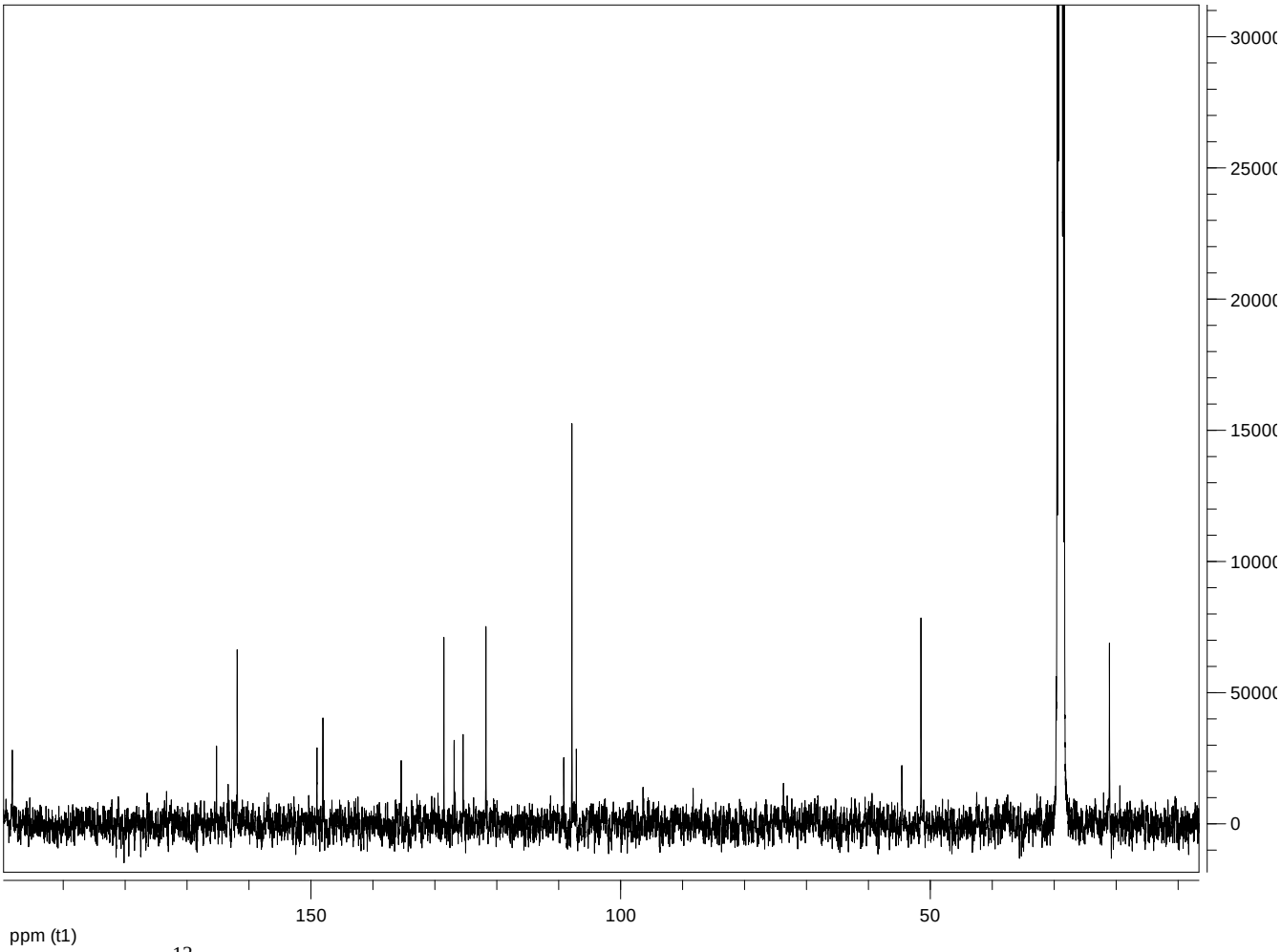

Figure. 5.3.3 ^{13}C NMR spectrum of alternethanoxin C(**86**), isolated from *A. sonchi* solid culture.

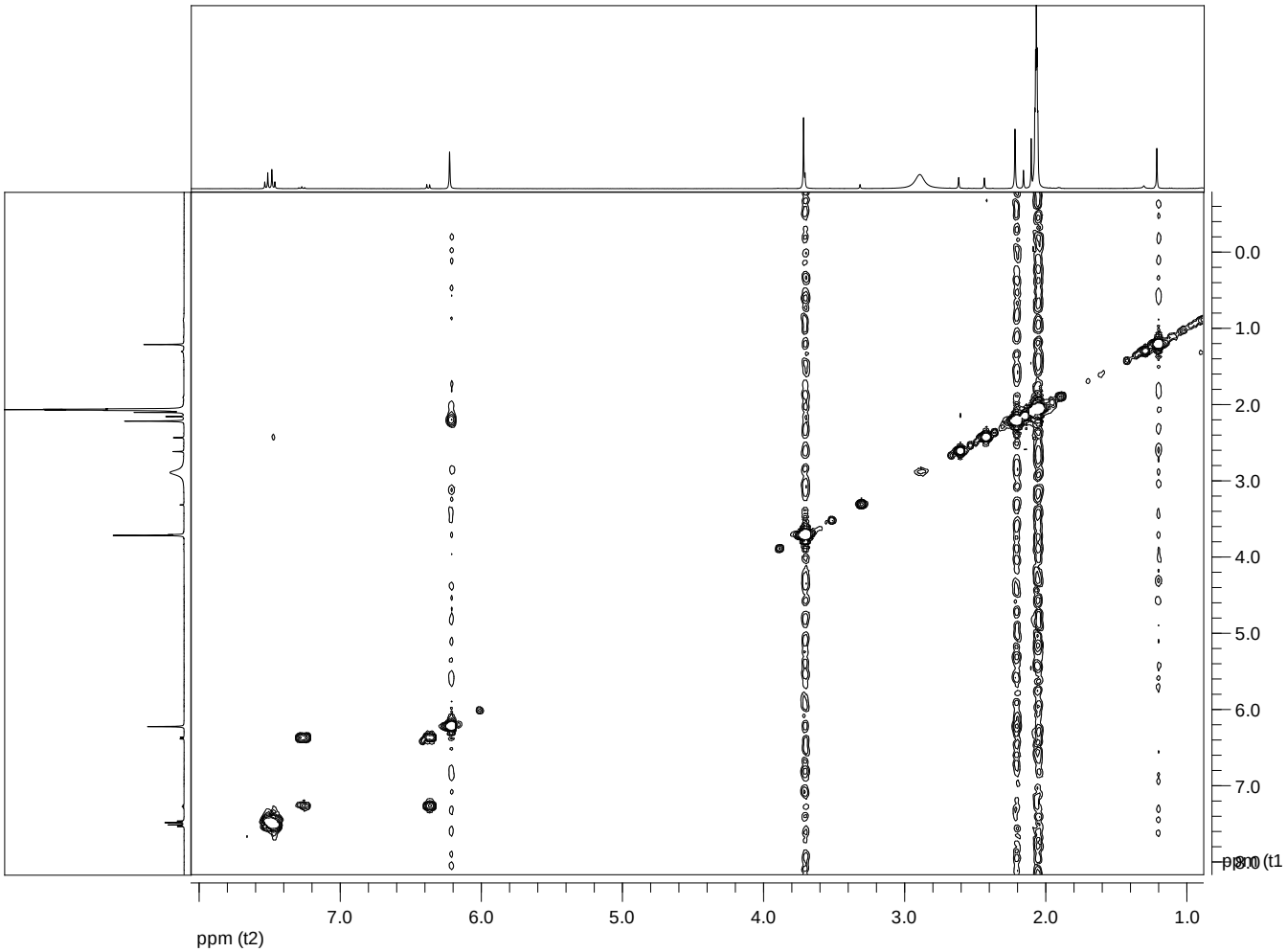

Figure. 5.3.4 COSY spectrum of alternethanoxin C (**86**), isolated from *A. sonchi* solid culture.

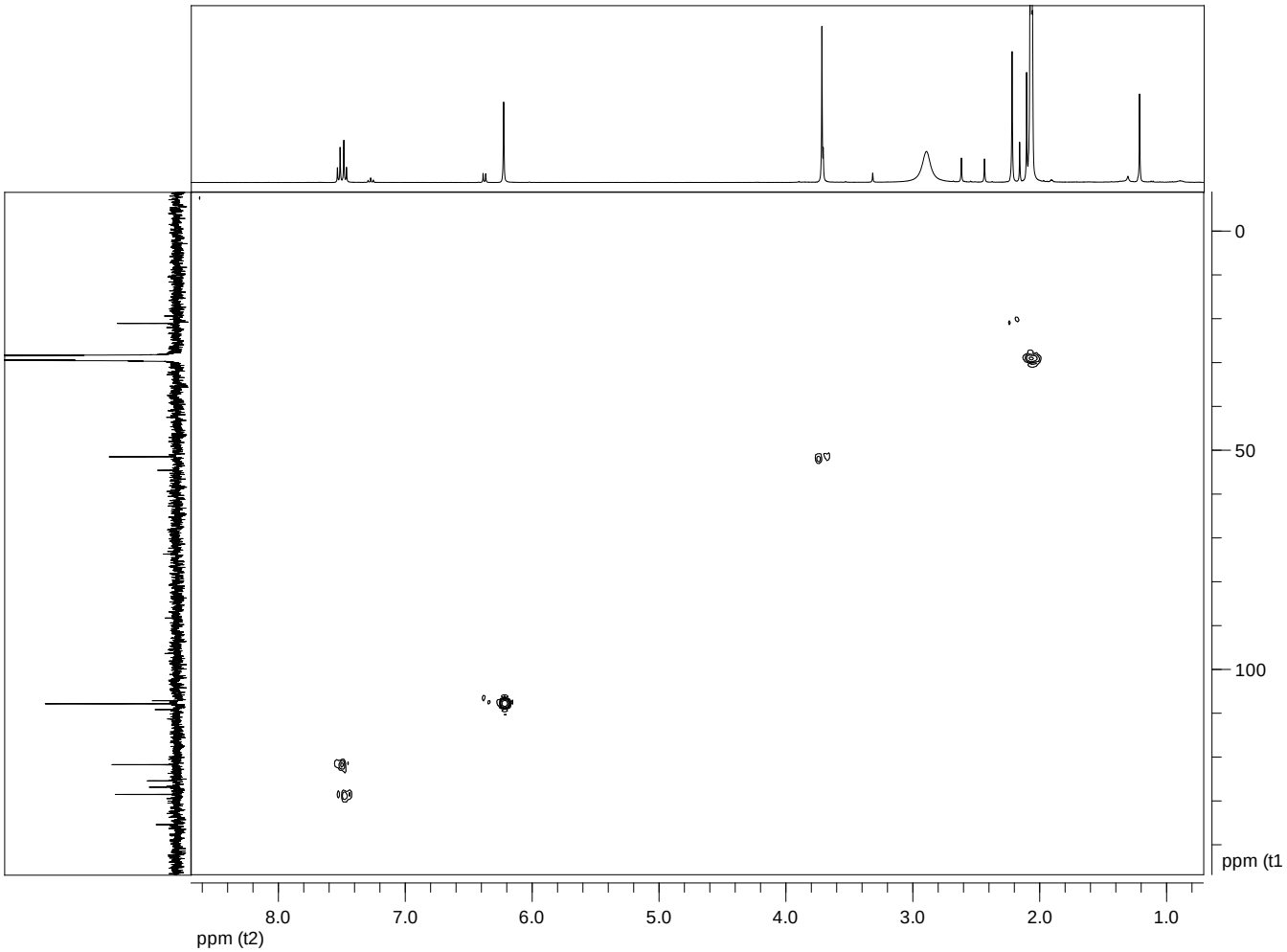

Figure. 5.3.5 HSQC spectrum of alternethanoxin C (**86**), isolated from *A. sonchi* solid culture.

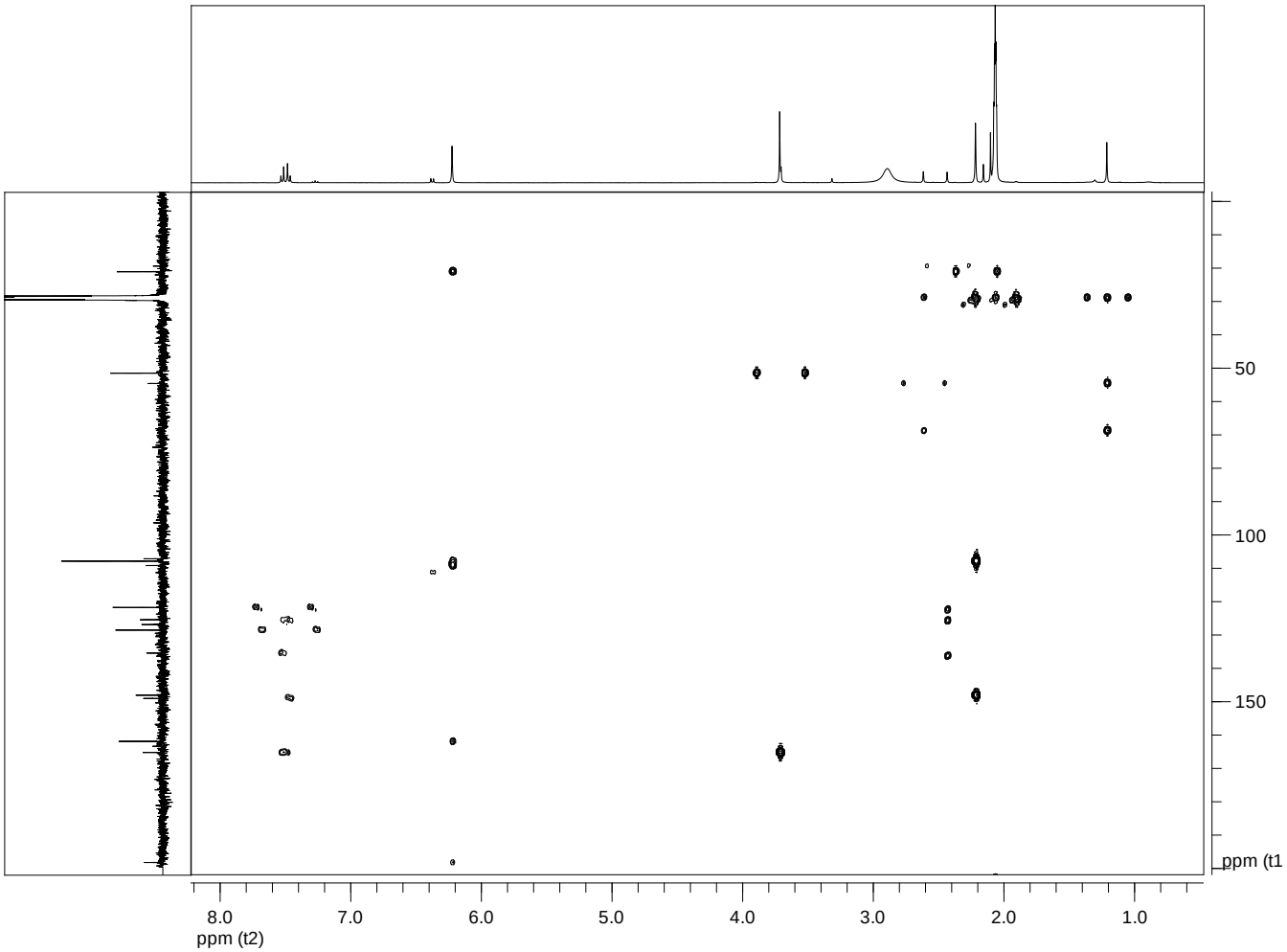

Figure. 5.3.6 HMBC spectrum of alternethanoxin C (**86**), isolated from *A. sonchi* solid culture.

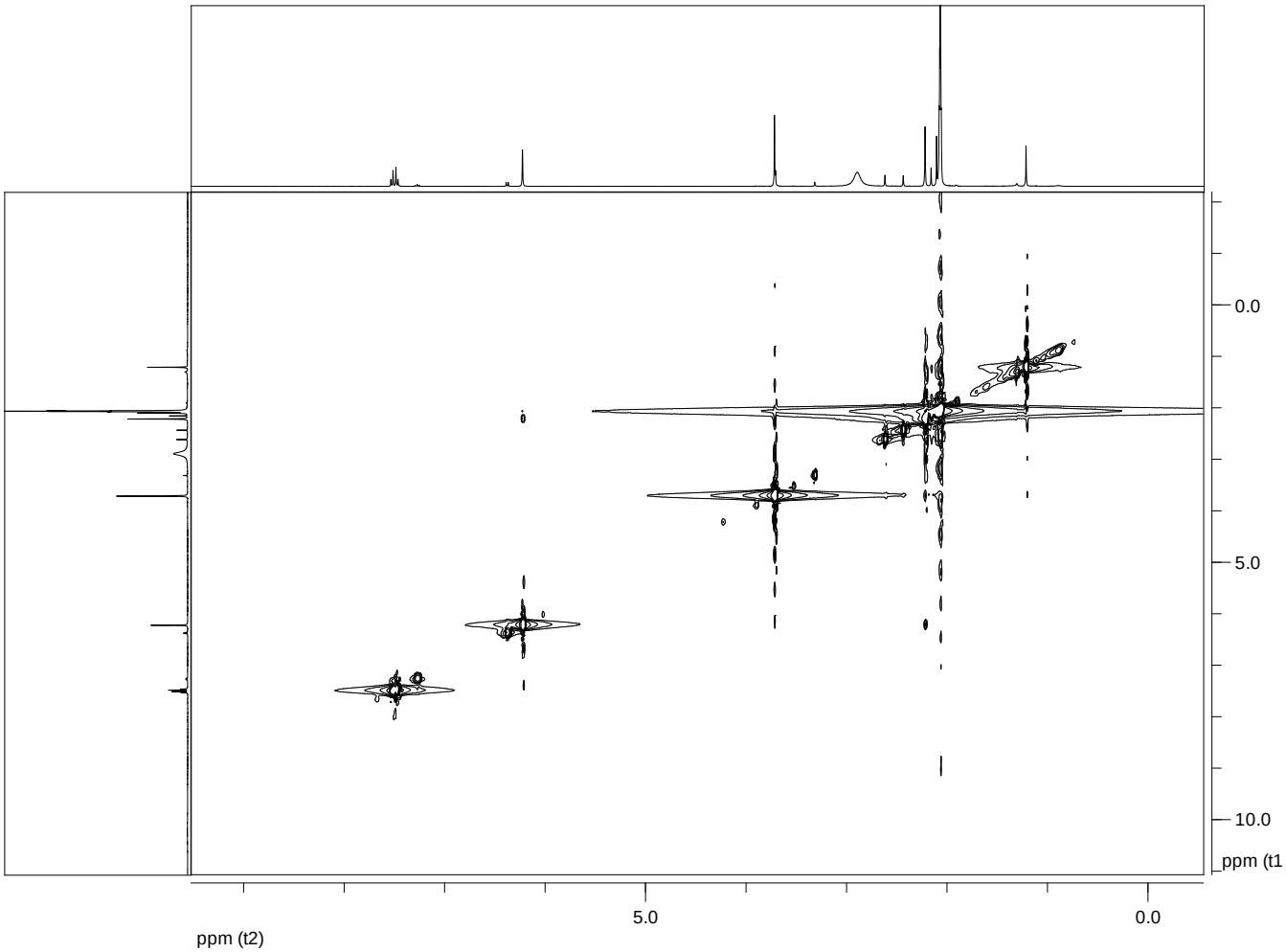

Figure. 5.3.7 NOESY spectrum of alternethanoxin C (**86**), isolated from *A. sonchi* solid culture.

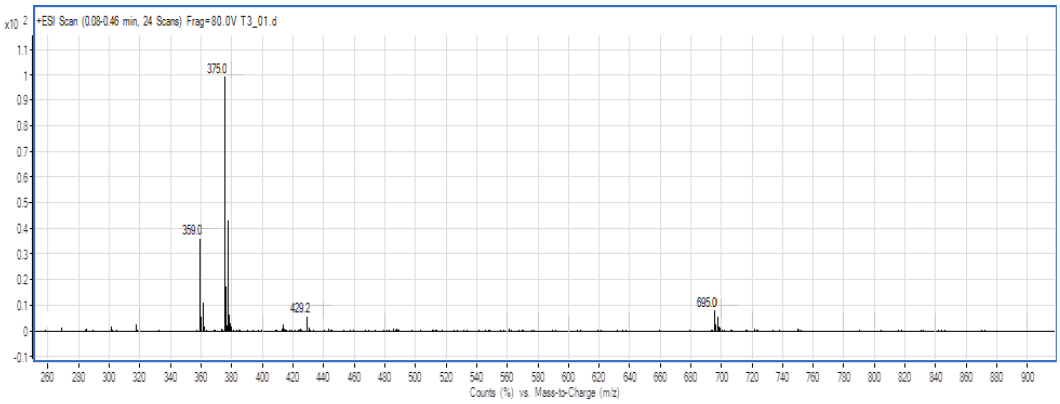

Figure. 5.3.8 ESI-MS spectrum of alternethanoxin C (**86**), isolated from *A. sonchi* solid culture.

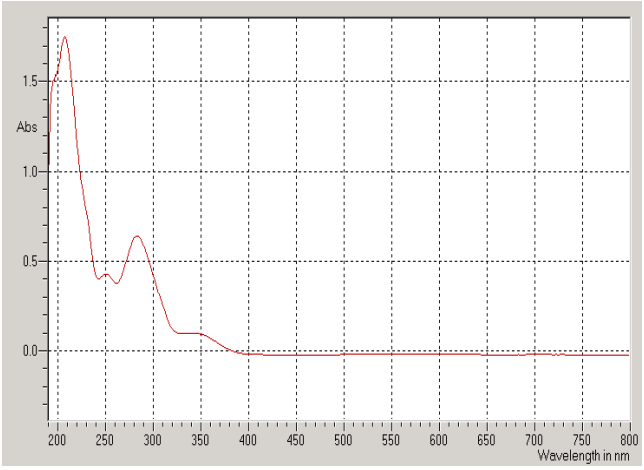

Figure. 5.3.9 ESI-MS spectrum of alternethanoxin C (**86**), isolated from *A. sonchi* solid culture.

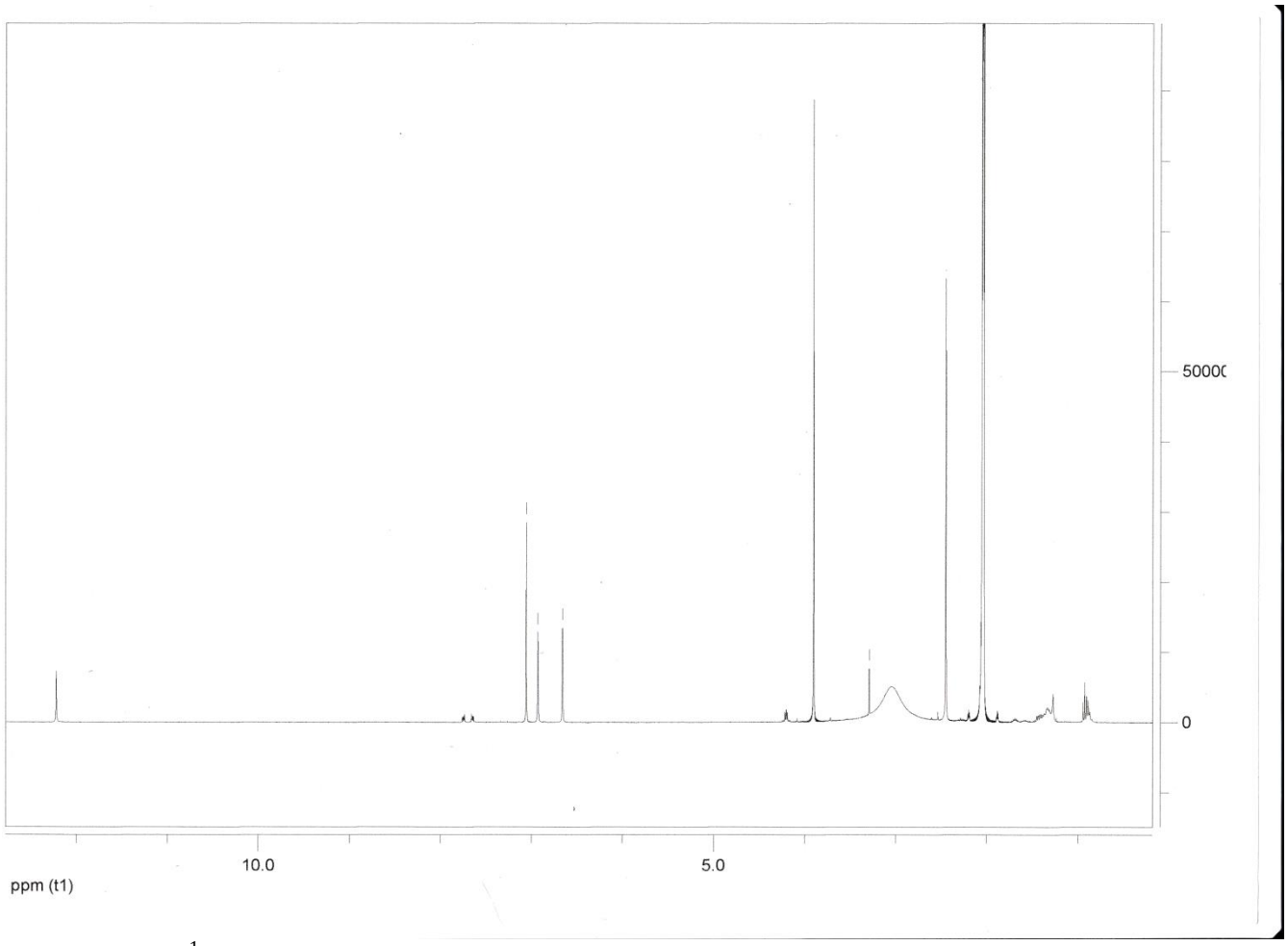

Figure. 5.3.10 ^{1}H-NMR spectrum of alternethanoxin D (**87**), isolated from *A. sonchi* solid culture.

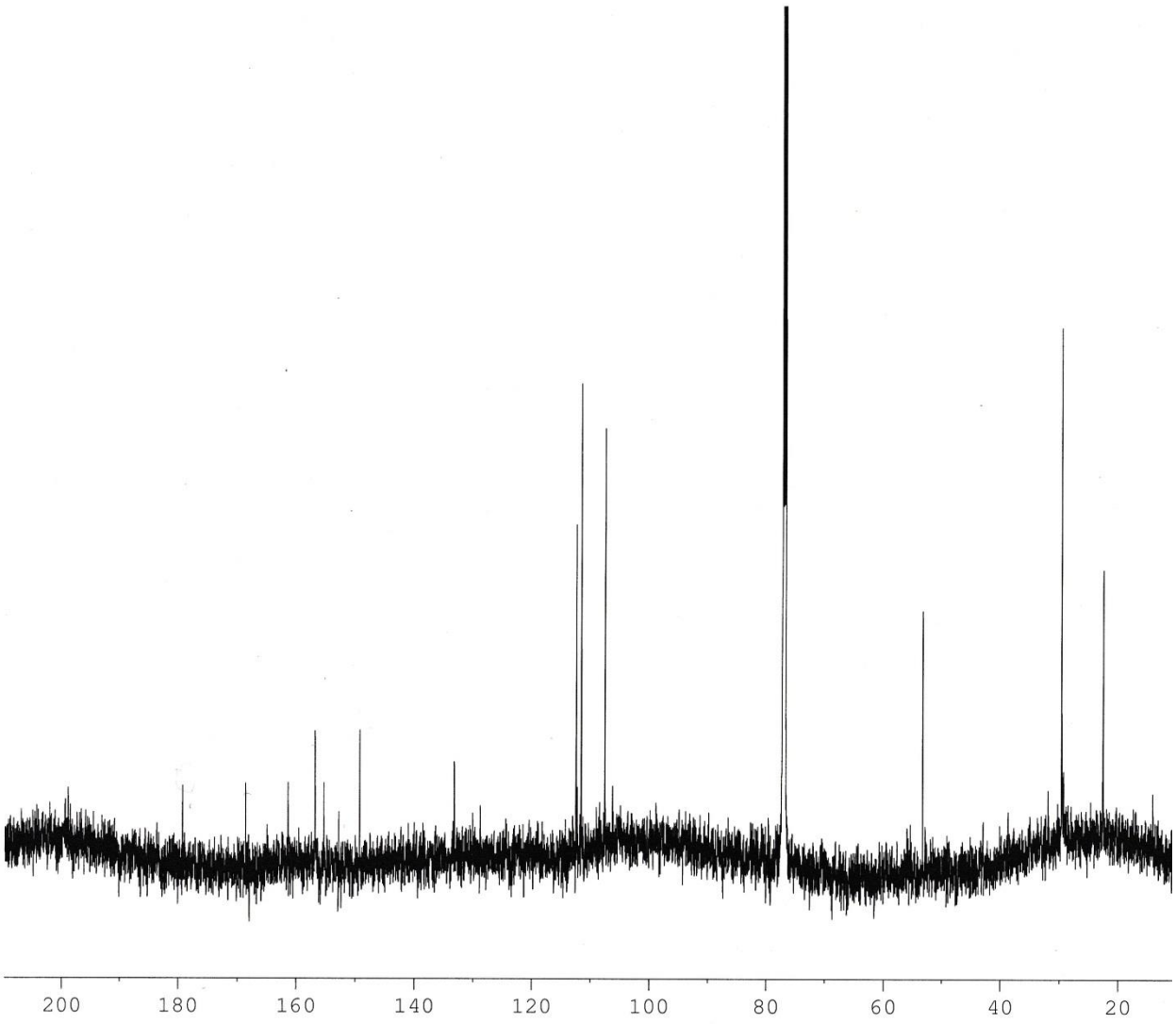

Figure. 5.3.11 ^{13}C-NMR spectrum of alternethanoxin D (**87**), isolated from *A. sonchi* solid culture.

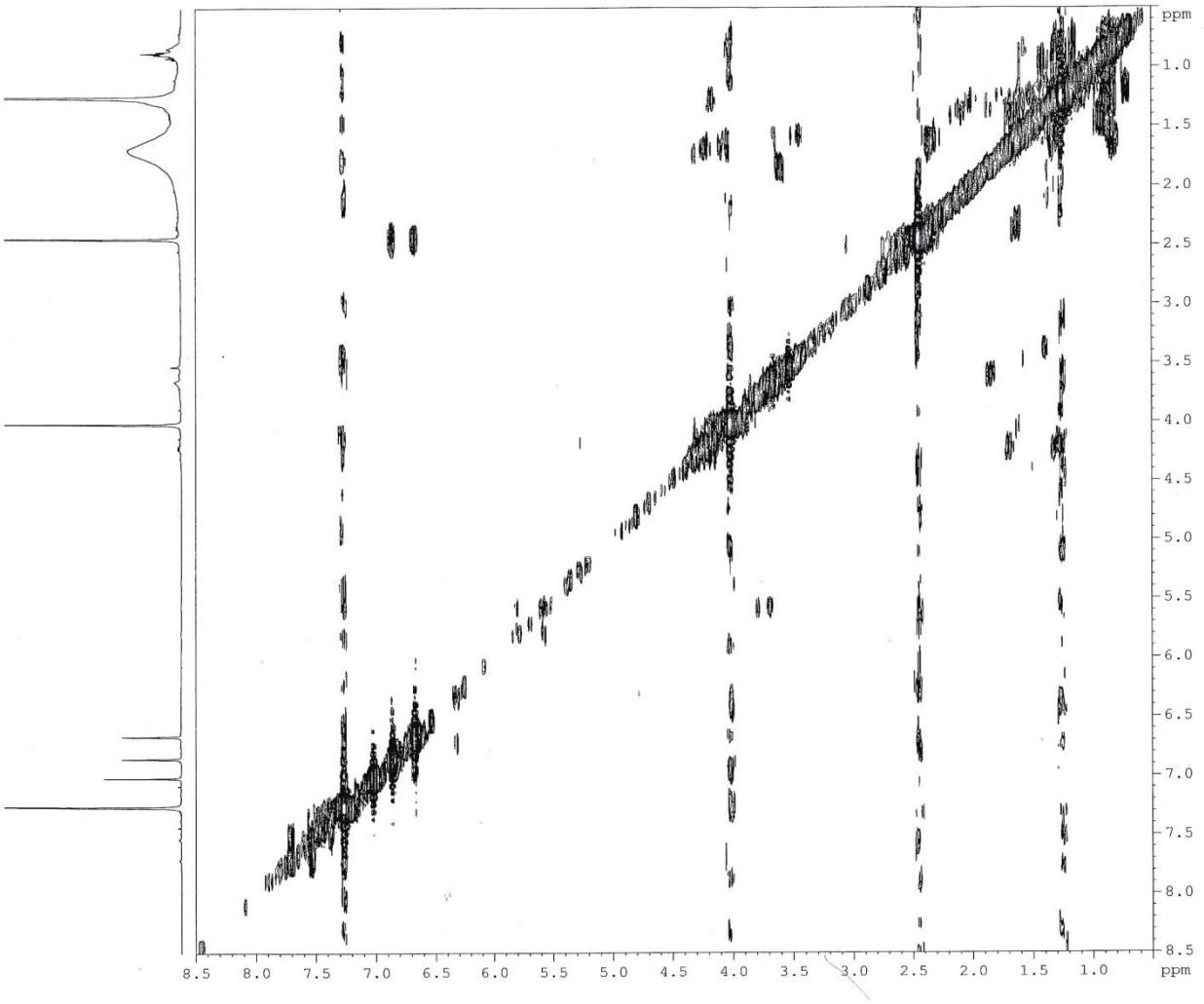

Figure. 5.3.12 COSY spectrum of alternethanoxin D (**87**), isolated from *A. sonchi* solid culture.

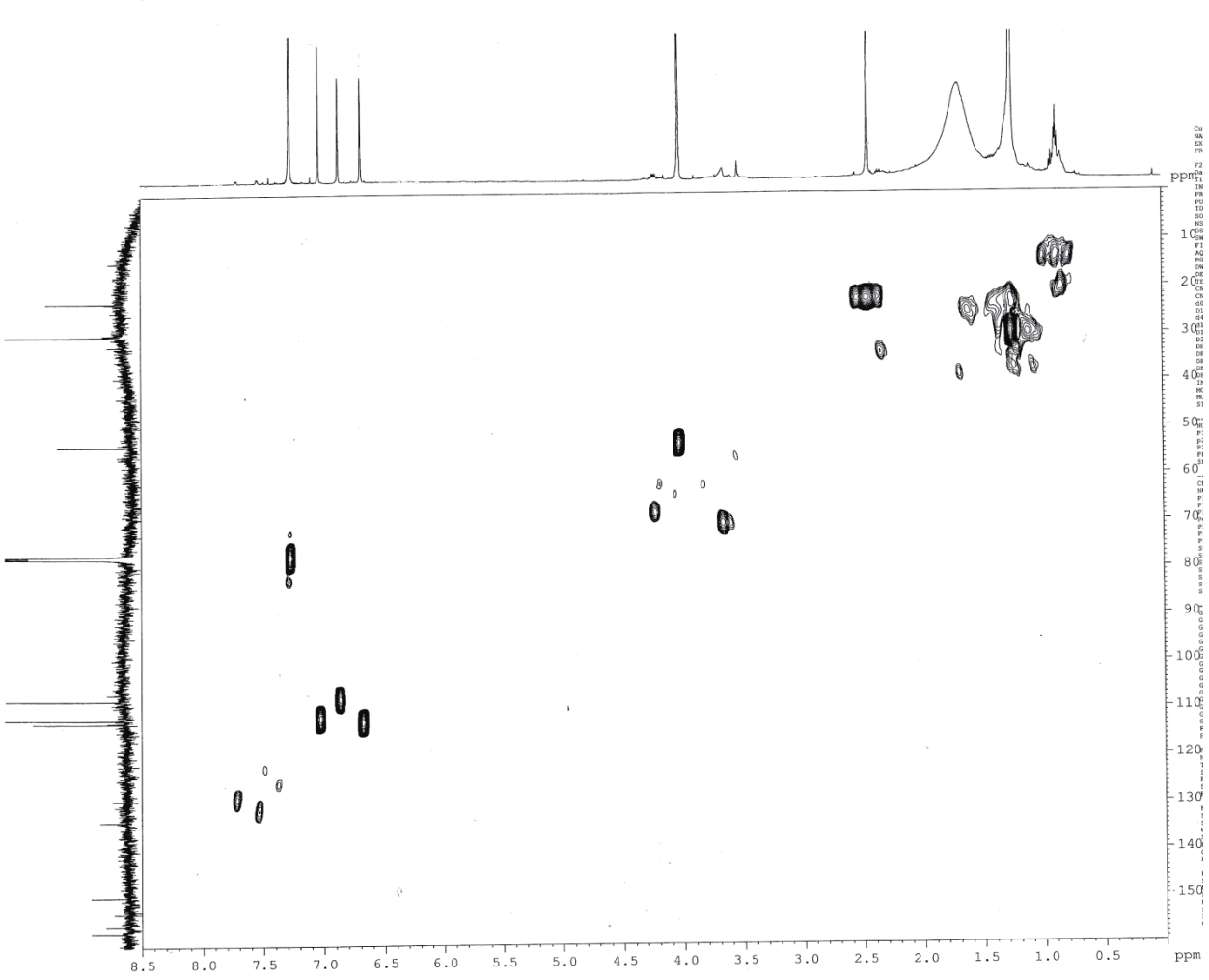

Figure. 5.3.13 HSQC spectrum of alternethanoxin D (**87**), isolated from *A. sonchi* solid culture.

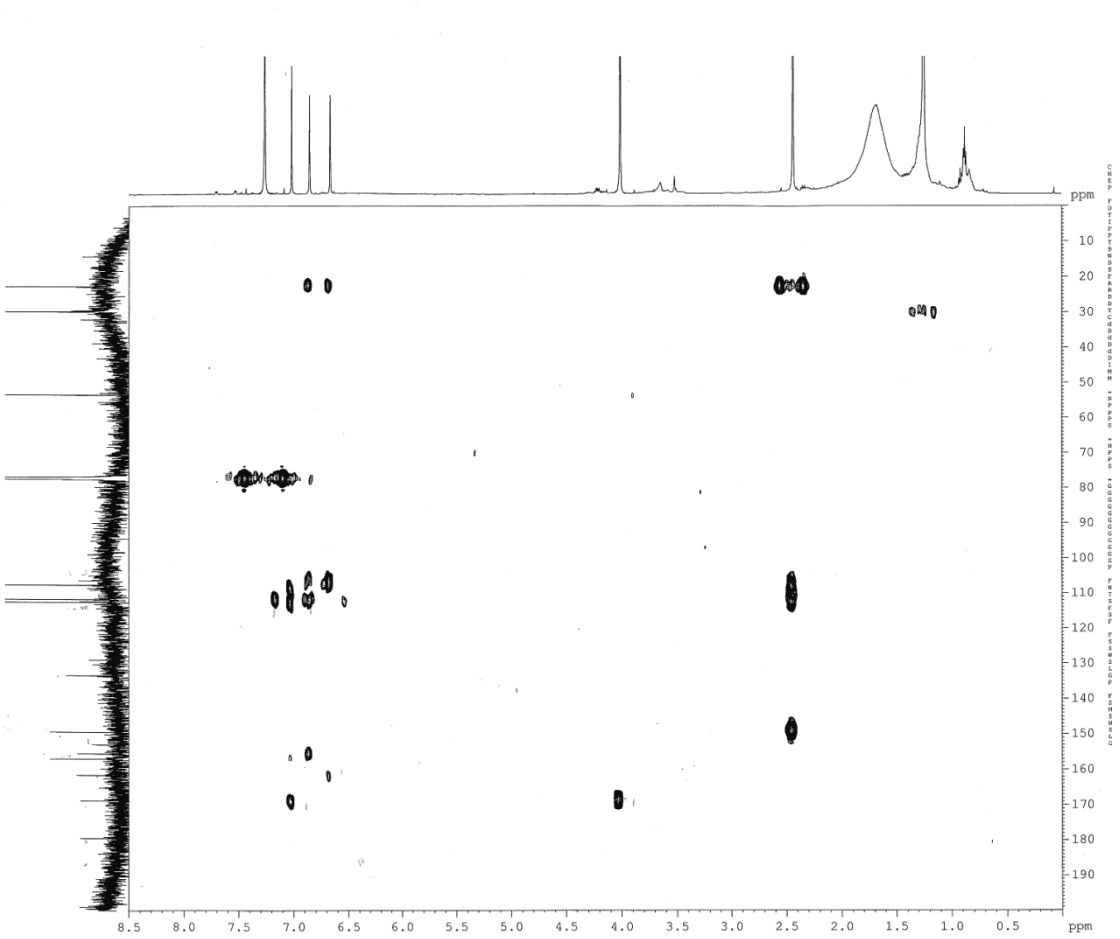

Figure. 5.3.14 HMBC spectrum of alternethanoxin D (**87**), isolated from *A. sonchi* solid culture.

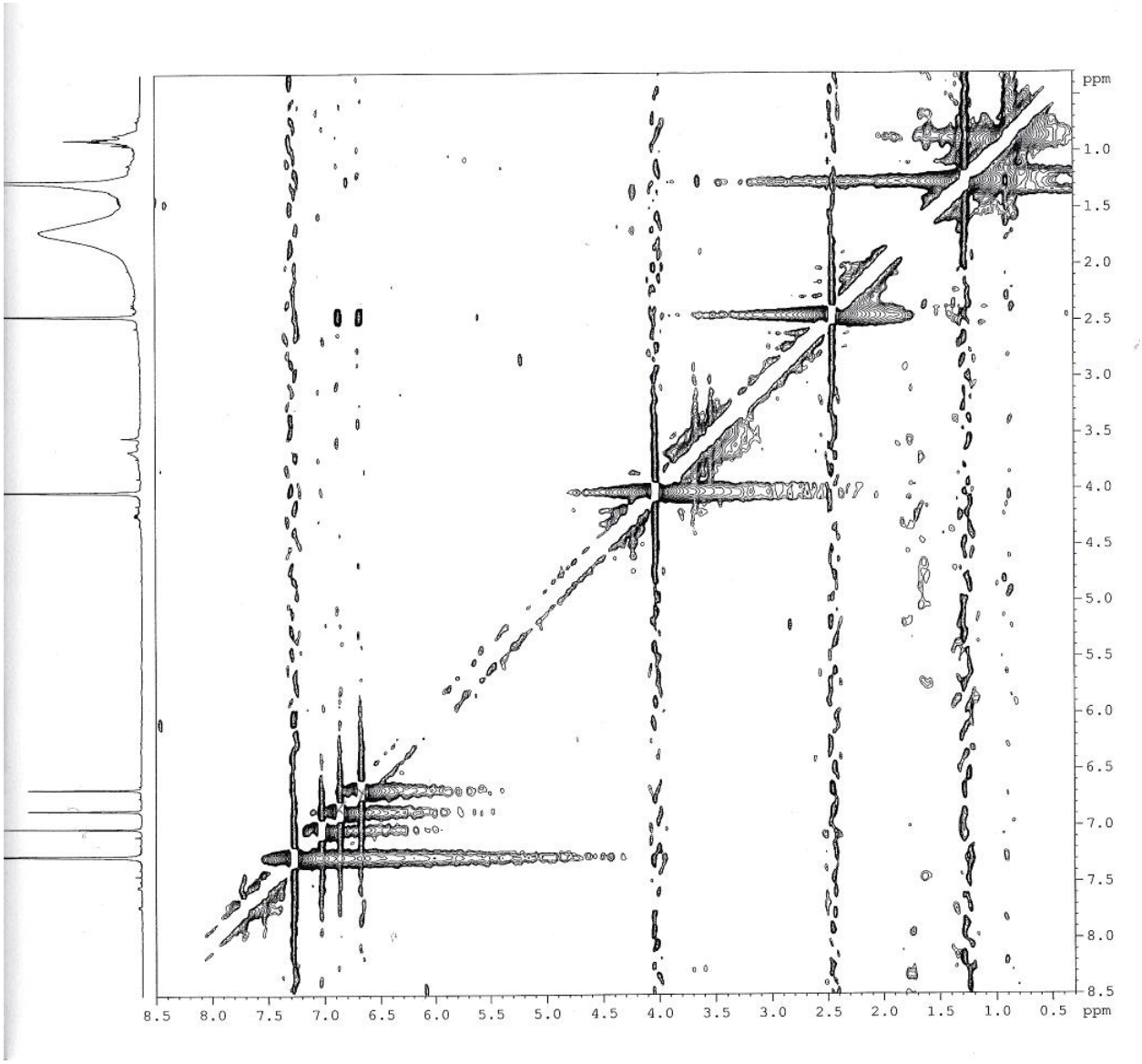

Figure. 5.3.15 NOESY spectrum of alternethanoxin D (**87**), isolated from *A. sonchi* solid culture.

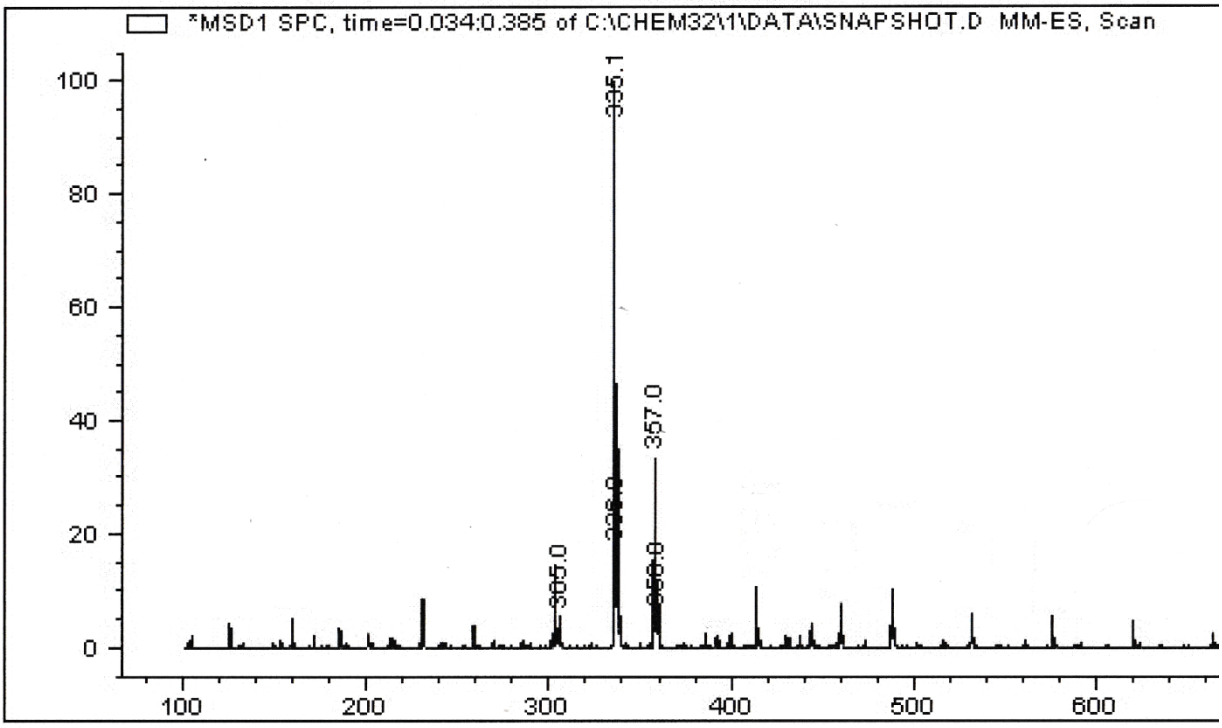

Figure. 5.3.16 ESI-MS spectrum of alternethanoxin D (**87**), isolated from *A. sonchi* solid culture.

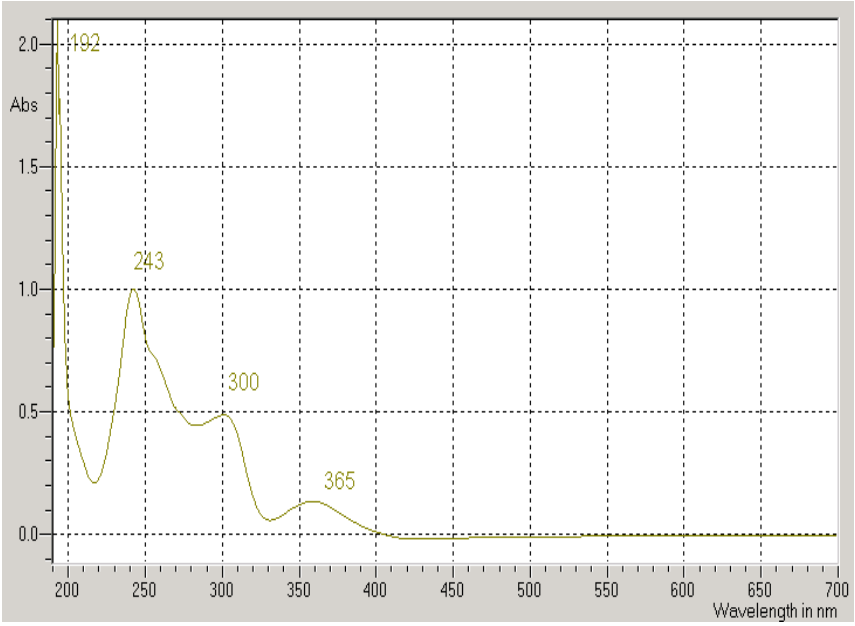

Figure. 5.3.17 UV spectrum of alternethanoxin D (**87**), isolated from *A. sonchi* solid culture.

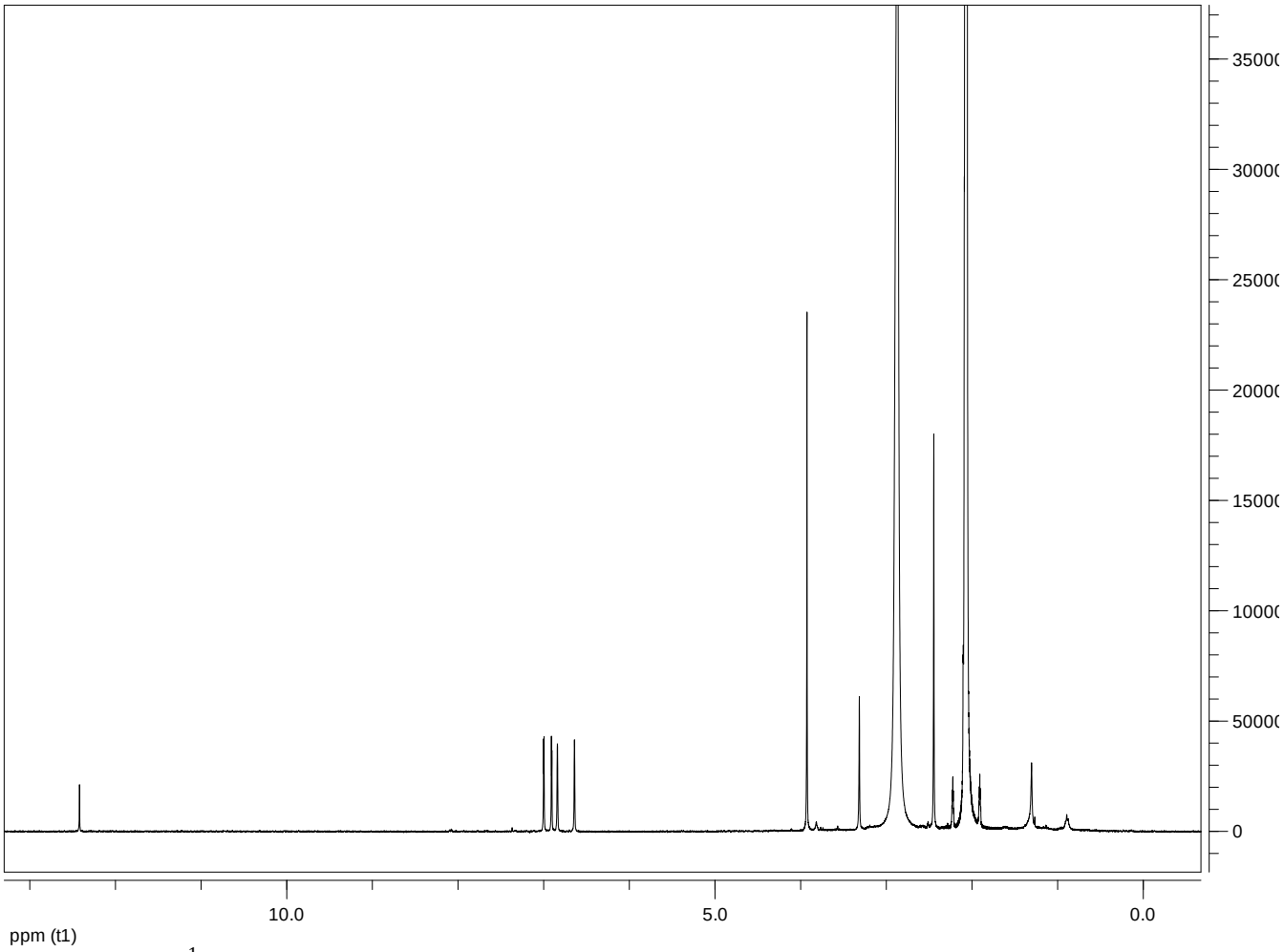

Figure. 5.3.18 ^{1}H-NMR spectrum of alternethanoxin E (**88**), isolated from *A. sonchi* solid culture.

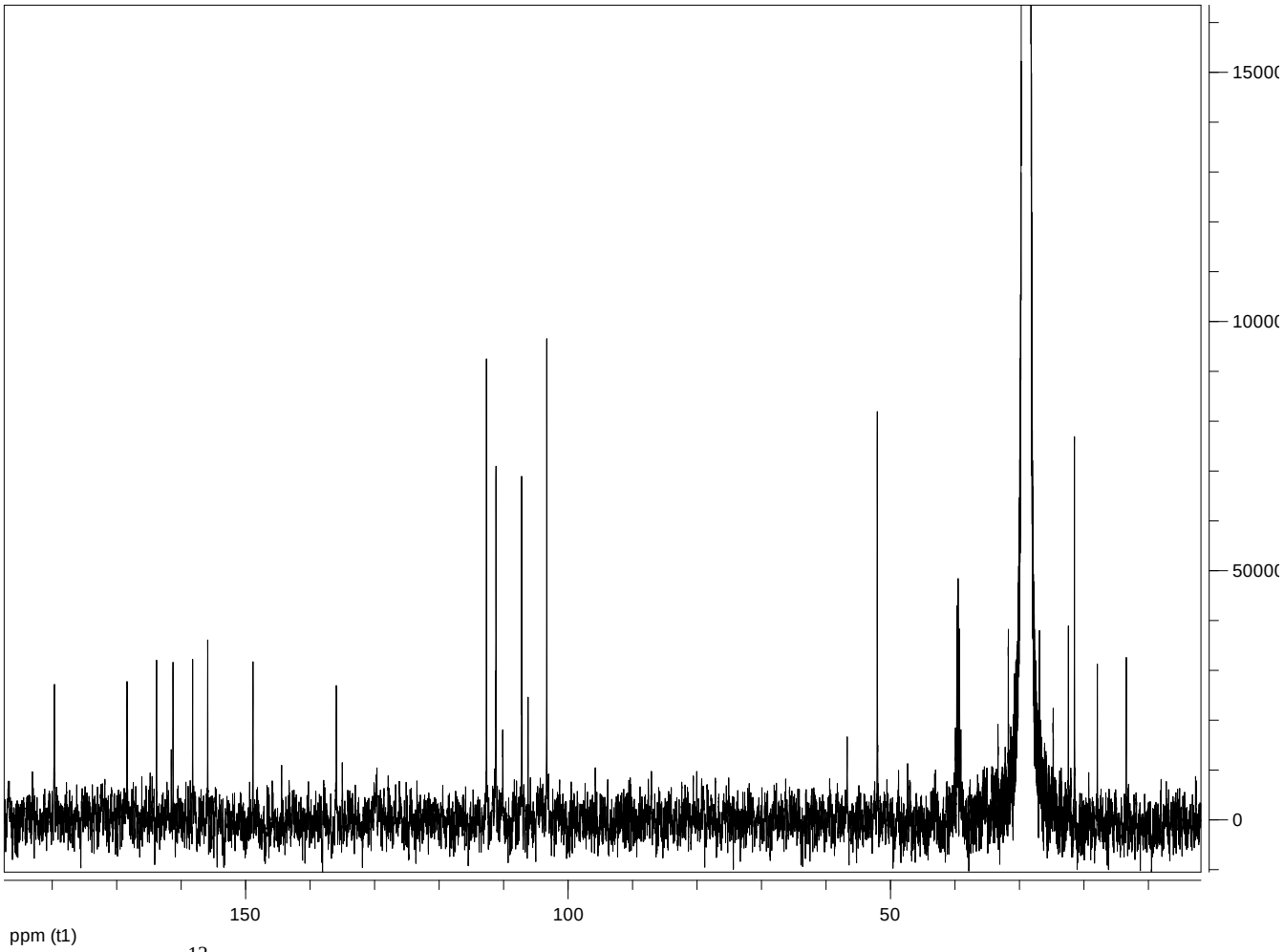

Figure. 5.3.19 ^{13}C-NMR spectrum of alternethanoxin E (**88**), isolated from *A. sonchi* solid culture.

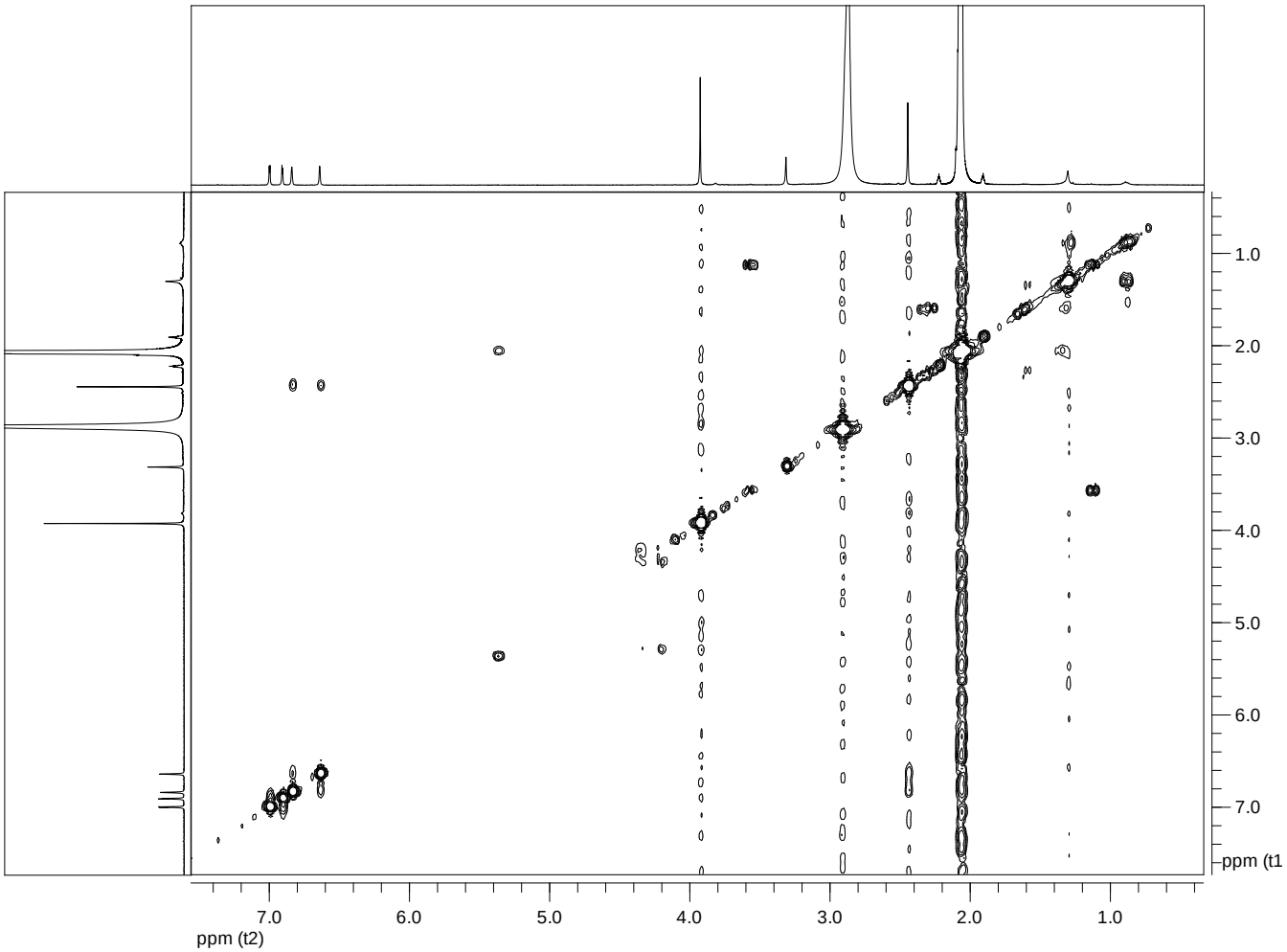

Figure. 5.3.20 COSY spectrum of alternethanoxin E (**88**), isolated from *A. sonchi* solid culture.

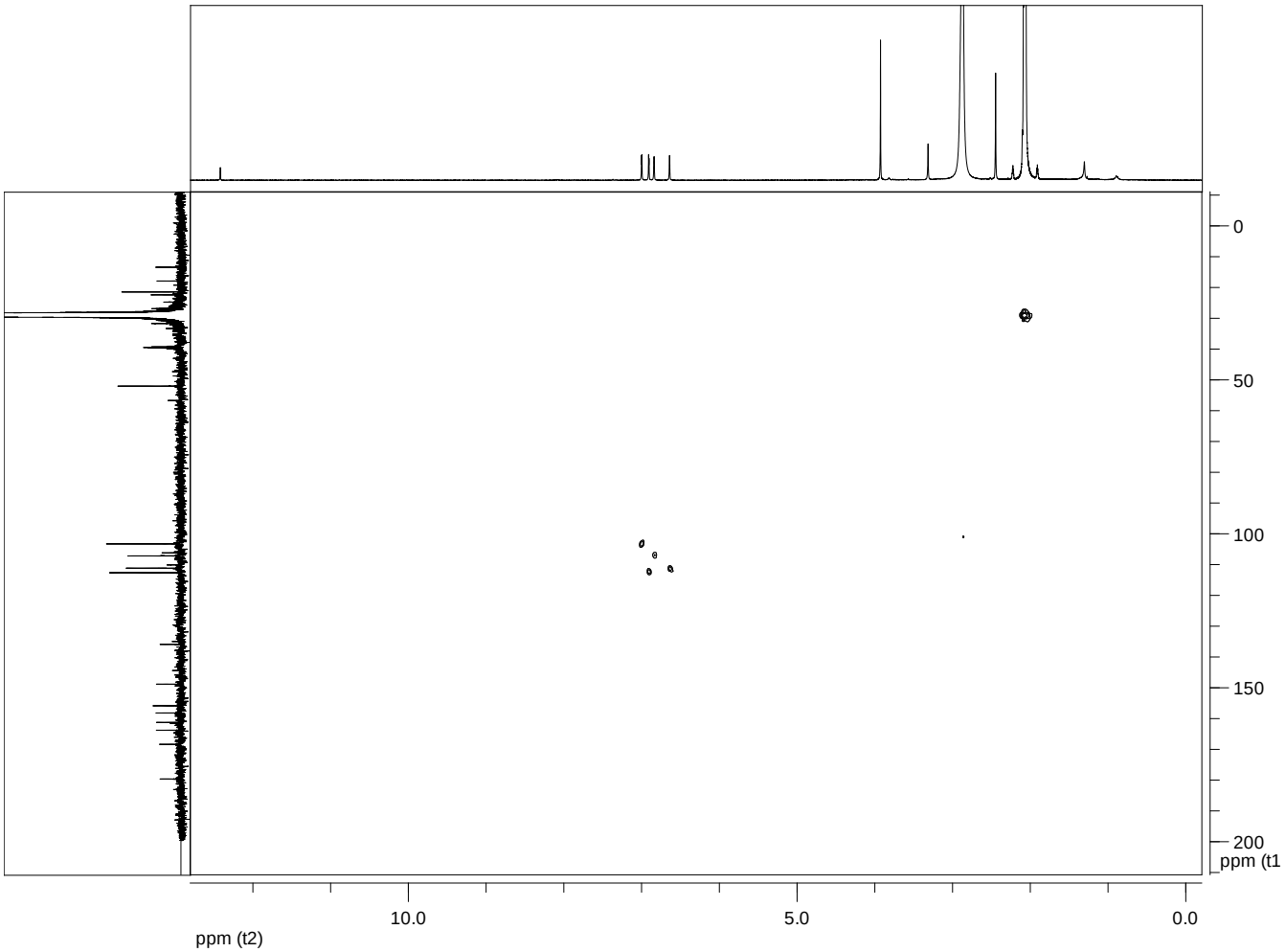

Figure. 5.3.21 HSQC spectrum of alternethanoxin E (**88**), isolated from *A. sonchi* solid culture.

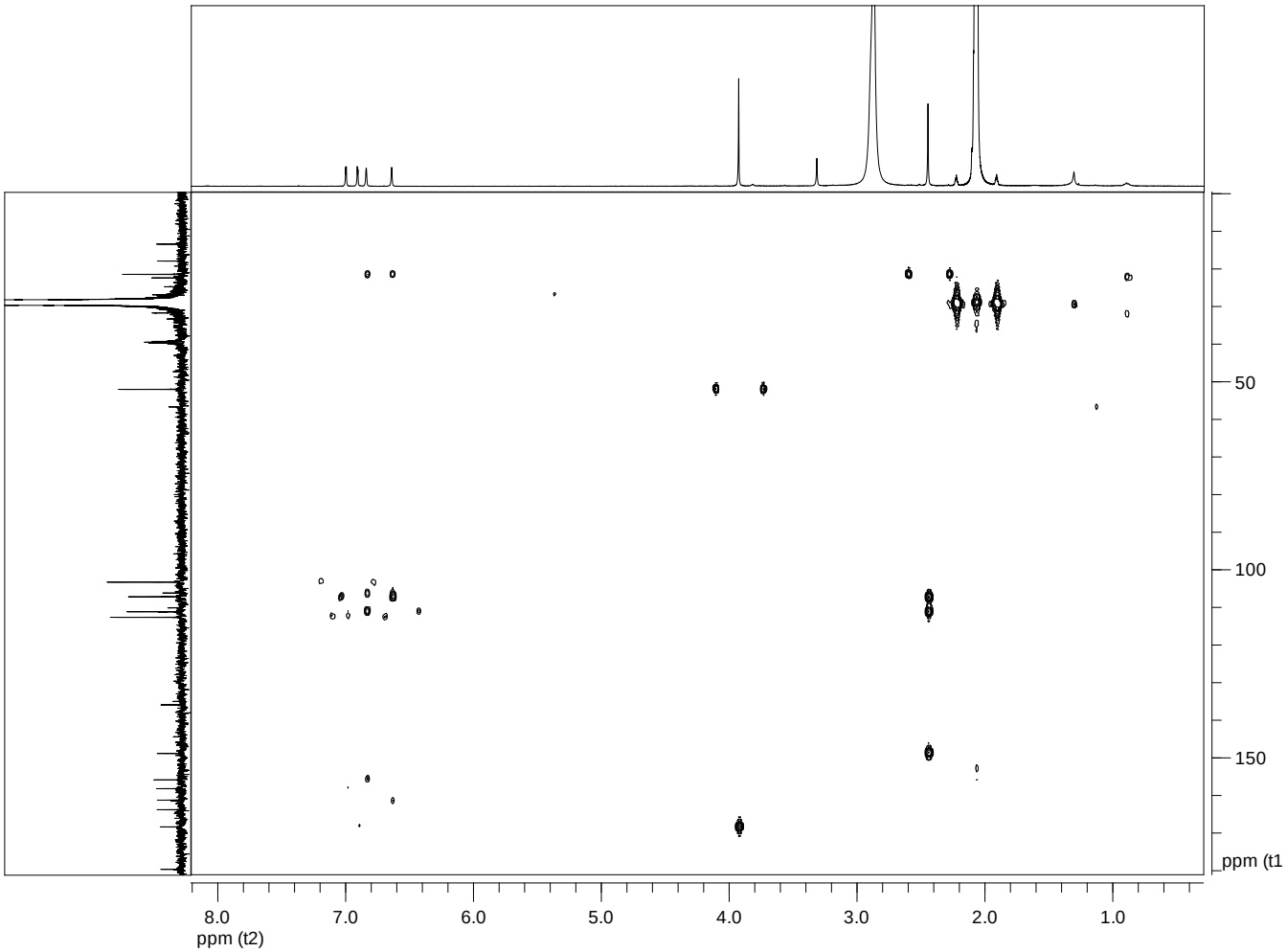

Figure. 5.3.22 HMBC spectrum of alternethanoxin E (**88**), isolated from *A. sonchi* solid culture.

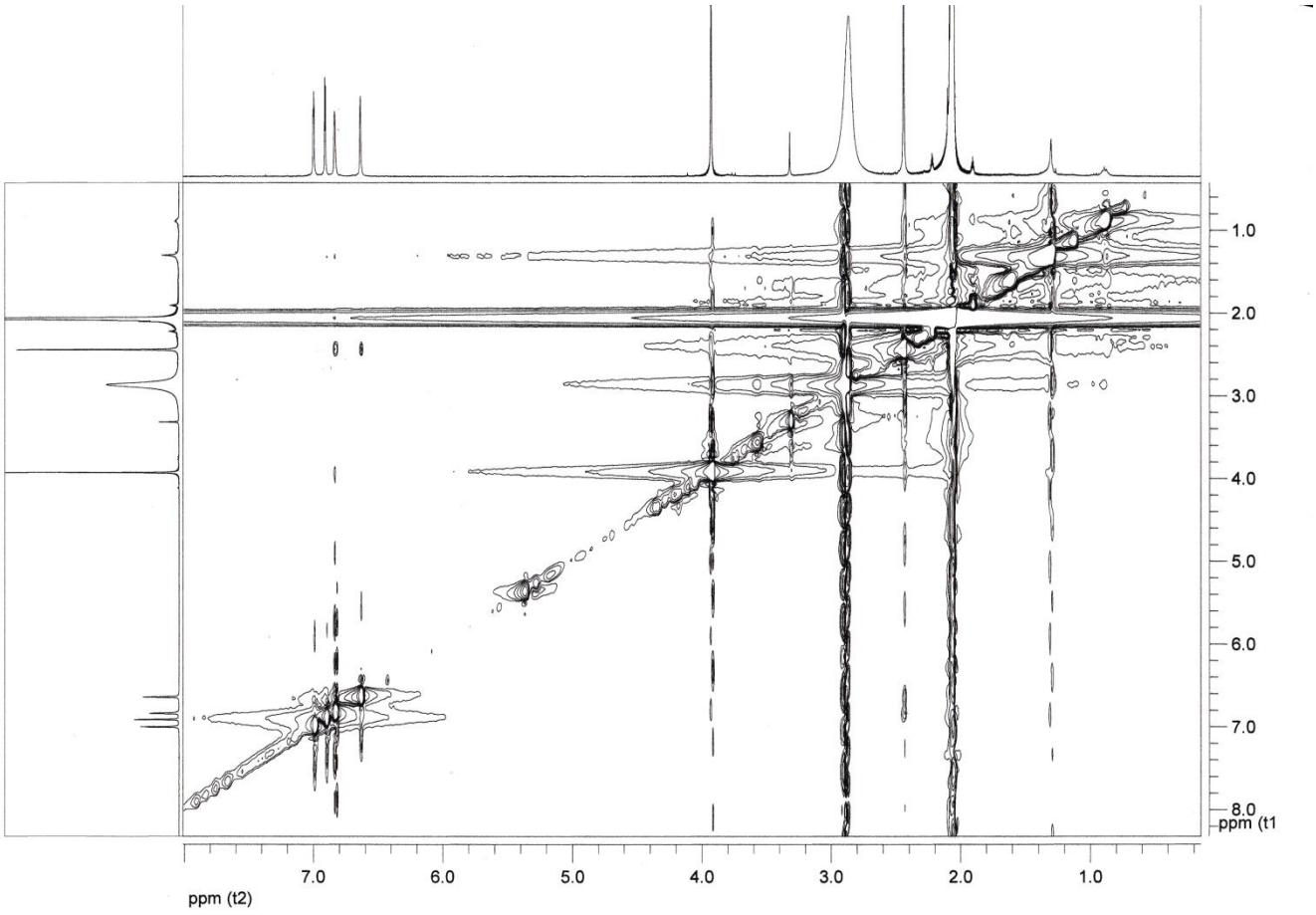

Figure. 5.3.23 NOESY spectrum of alternethanoxin E (**8**), isolated from *A. sonchi* solid culture.

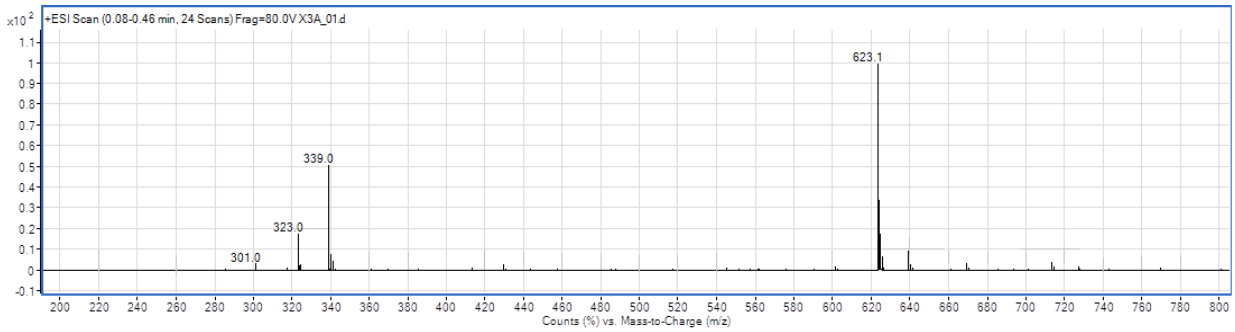

Figure. 5.3.24 ESI-MS spectrum of alternethanoxin E (**88**), isolated from *A. sonchi* solid culture.

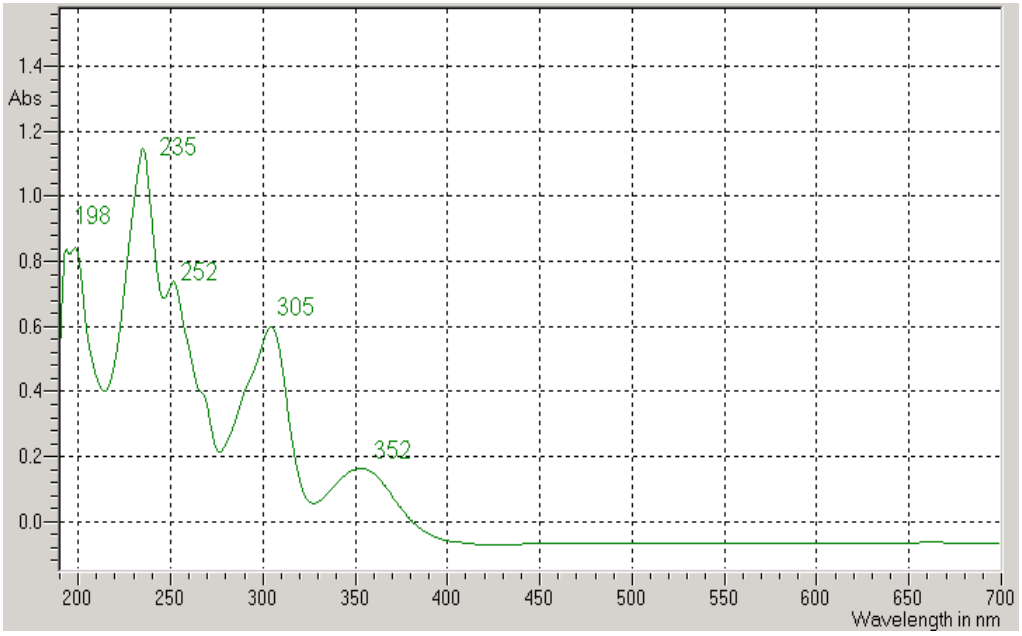

Figure. 5.3.25 UV spectrum of alternethanoxin E (**88**), isolated from *A. sonchi* solid culture.

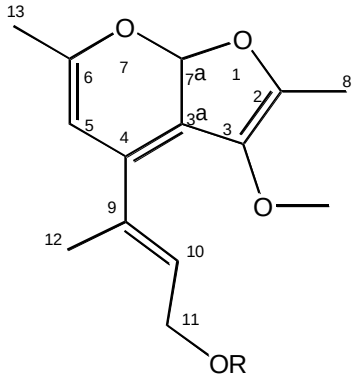

89 R=H
92 R=Ac

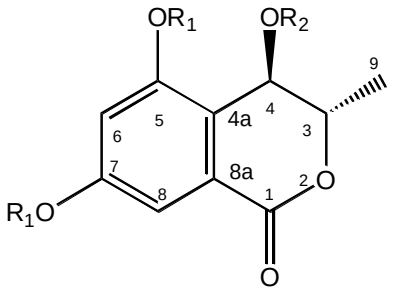

90 R_1= H, R_2= H
93 R_1= CH_3,R_2= H
94 R_1= CH_3, R_2= *S*-MPTA
95 R_1= CH_3, R_2= *R*-MPTA

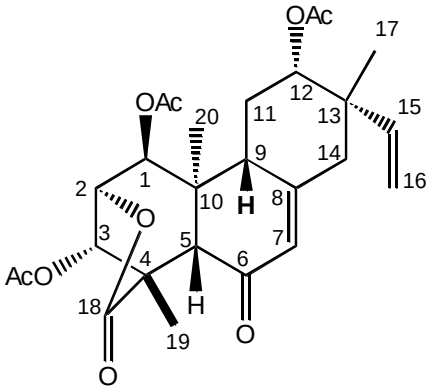

91

Figure. 5.4.1. Structures of: chenopodolan D and its 11-*O*-acetyl derivative (**89** and **92**); chenisocumarine and its 5,7-*O,O*'-dimethyl, 4-*O*-*S*-MTPA and 4-*O*-*R*-MTPA esters (**90** and **93**-**95**); chenopodolin B (**91**), isolated from *P. chenopodiicola* liquid culture.

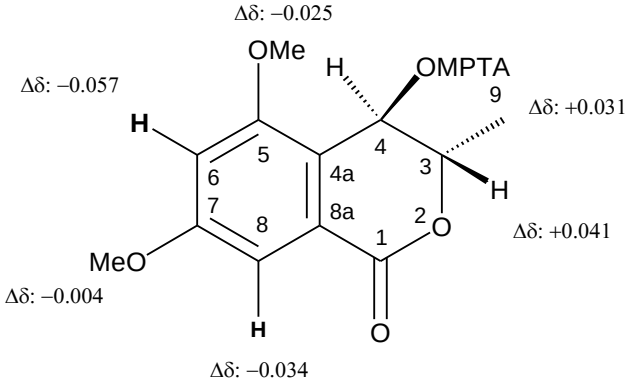

Figure. 5.4.2. Structures of 4-*O*-S- and 4-*O*-R-MTPA esters of 5,7-*O,O'*-dimethyl chenisocoumarin. (**94** and **95**, respectively), reporting the Δδ value obtained by comparison (**94**-**95**) of each proton system.

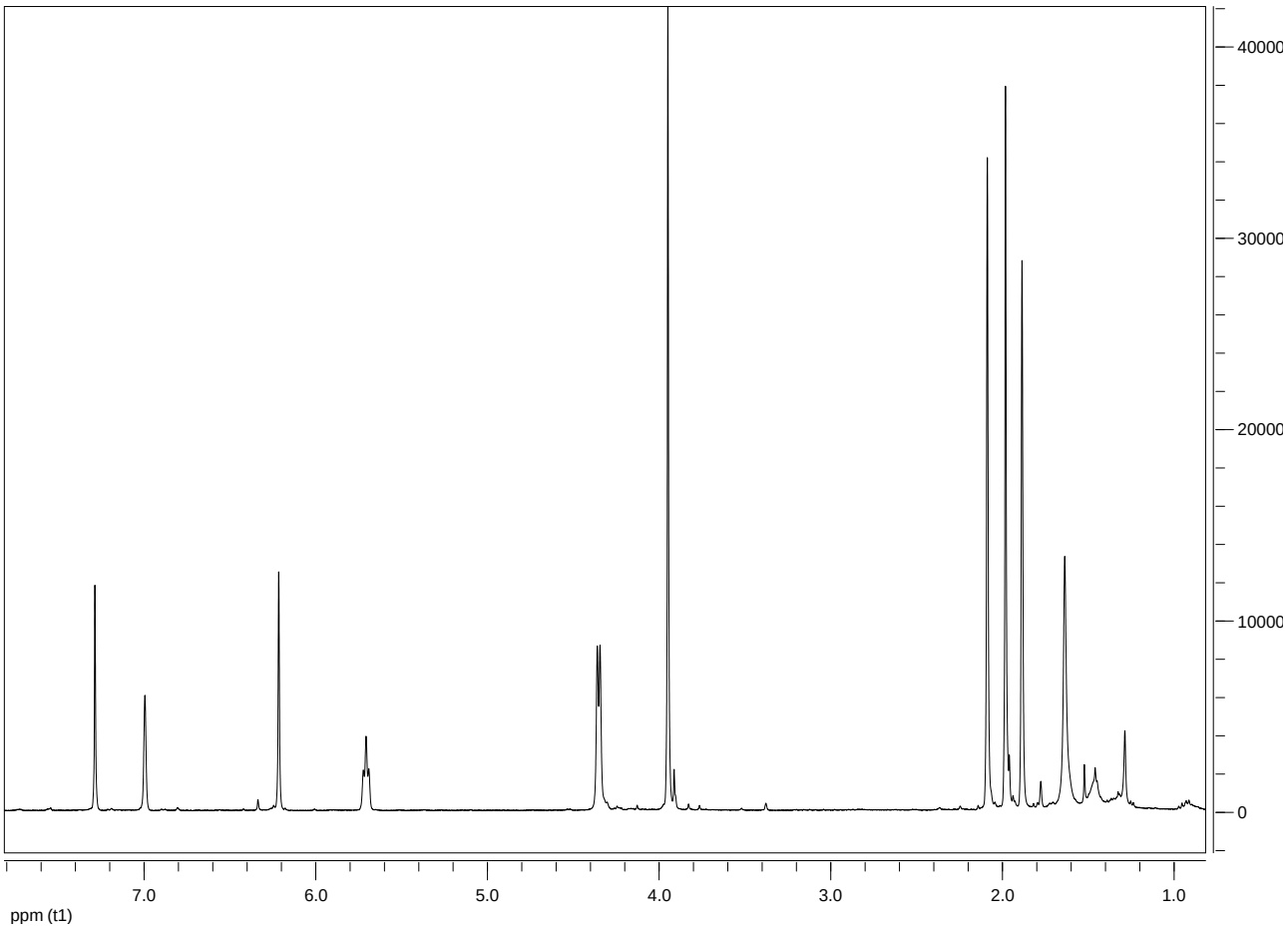

Figure. 5.4.3. ^{1}H NMR spectrum of chenopodolan D (**89**), isolated from *P. chenopodiicola* liquid culture.

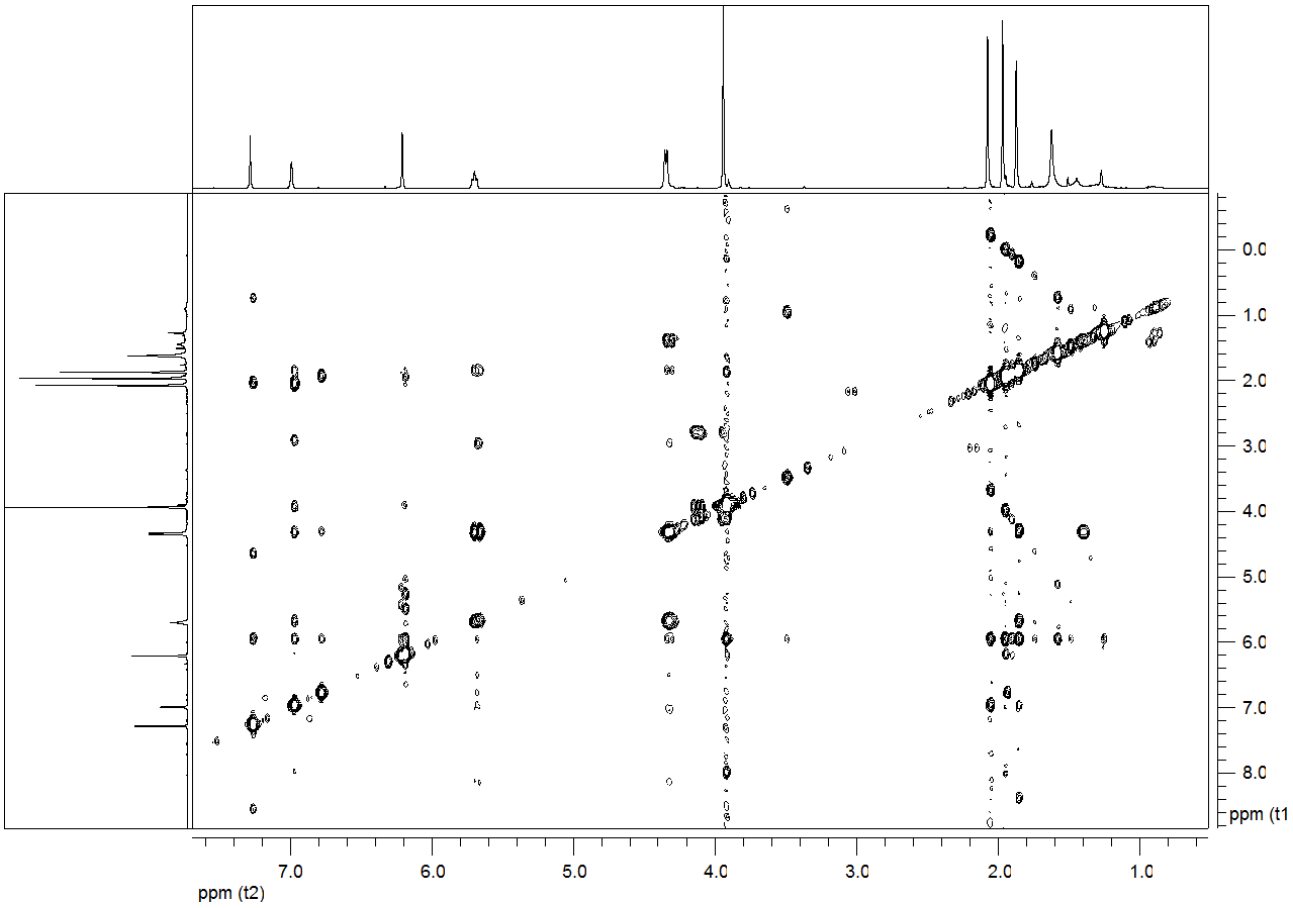

Figure. 5.4.4. COSY spectrum of chenopodolan D (**89**), isolated from *P. chenopodiicola* liquid culture.

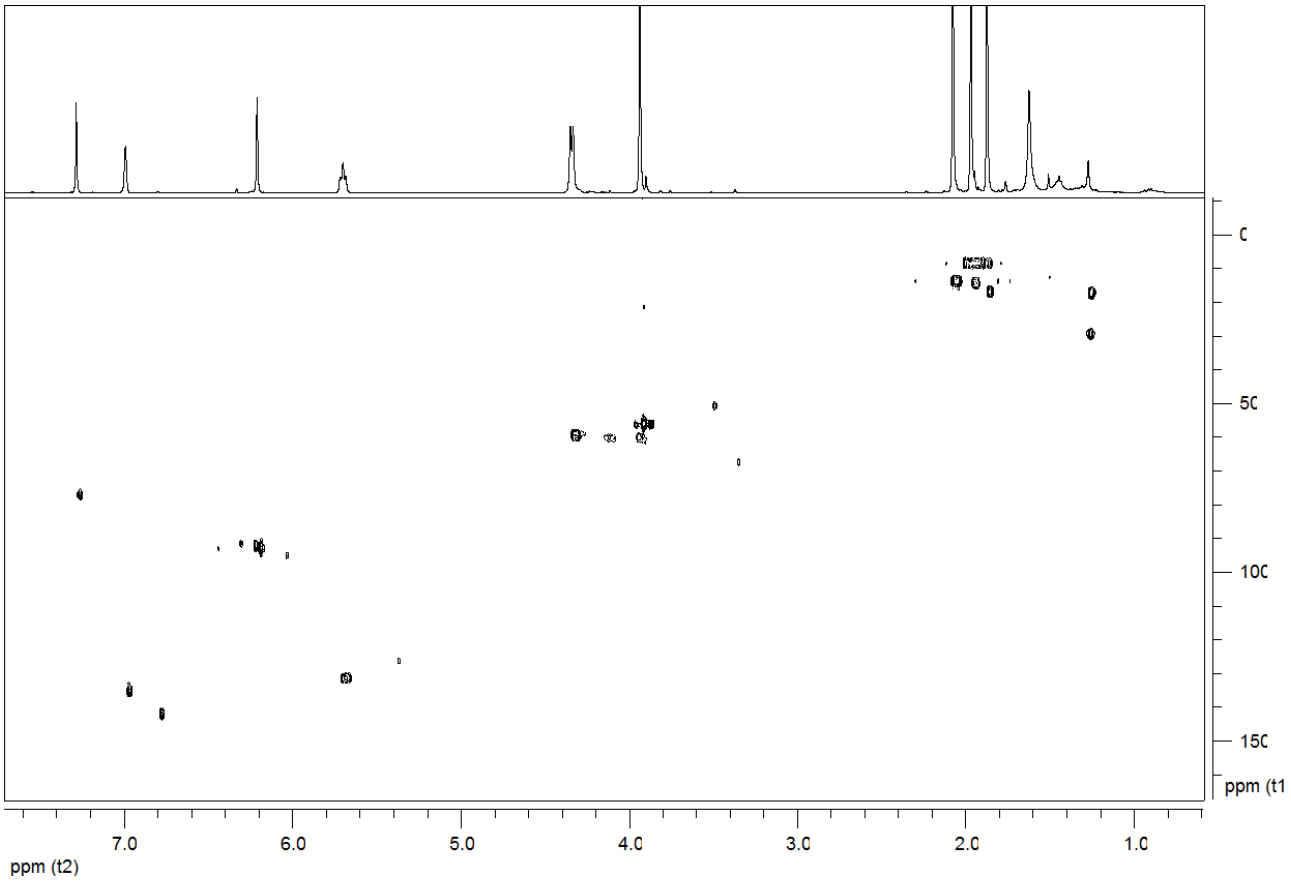

Figure. 5.4.5. HSQC spectrum of chenopodolan D (**89**), isolated from *P. chenopodiicola* liquid culture.

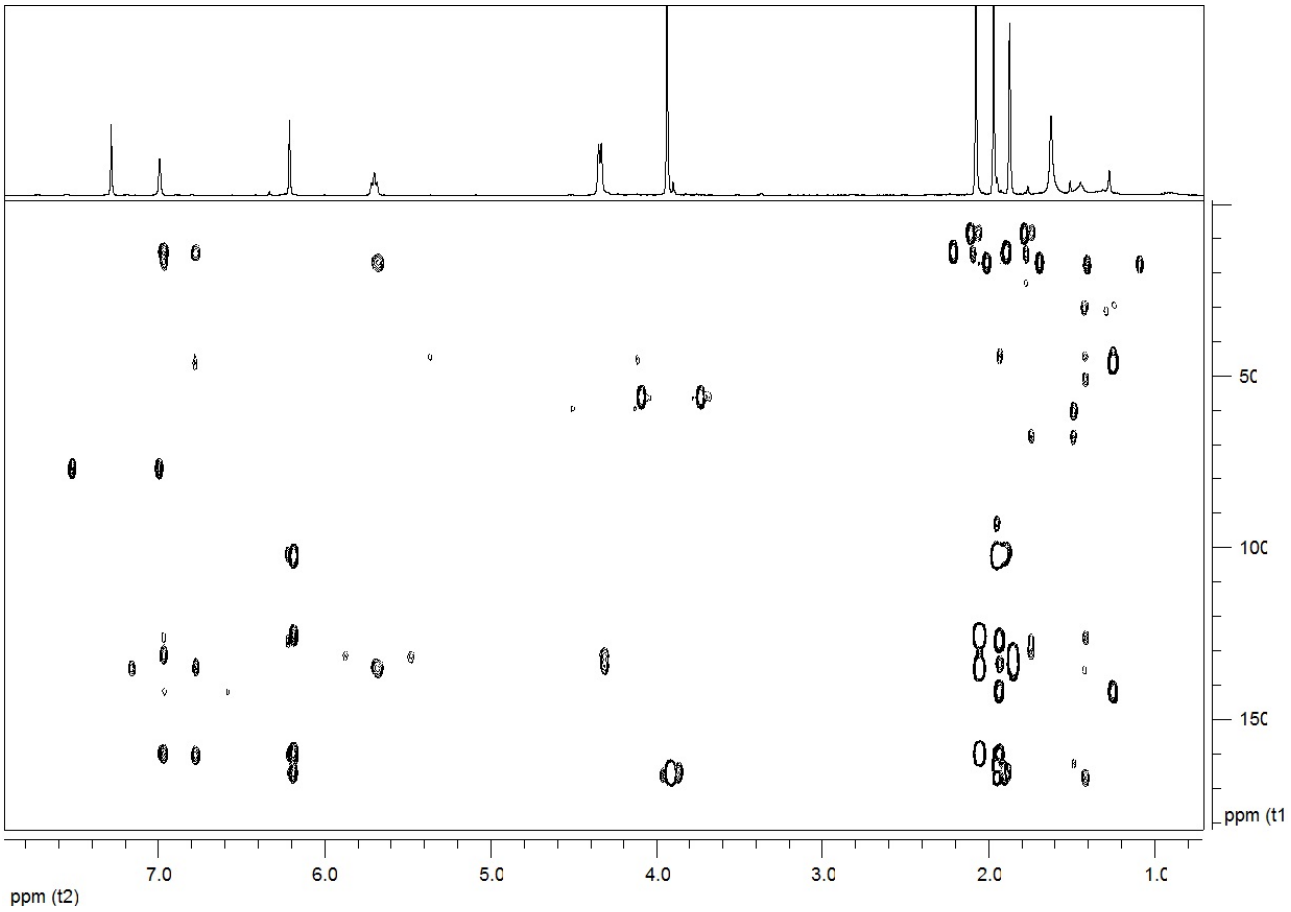

Figure. 5.4.6. HMBC spectrum of chenopodolan D (**89**), isolated from *P. chenopodiicola* liquid culture.

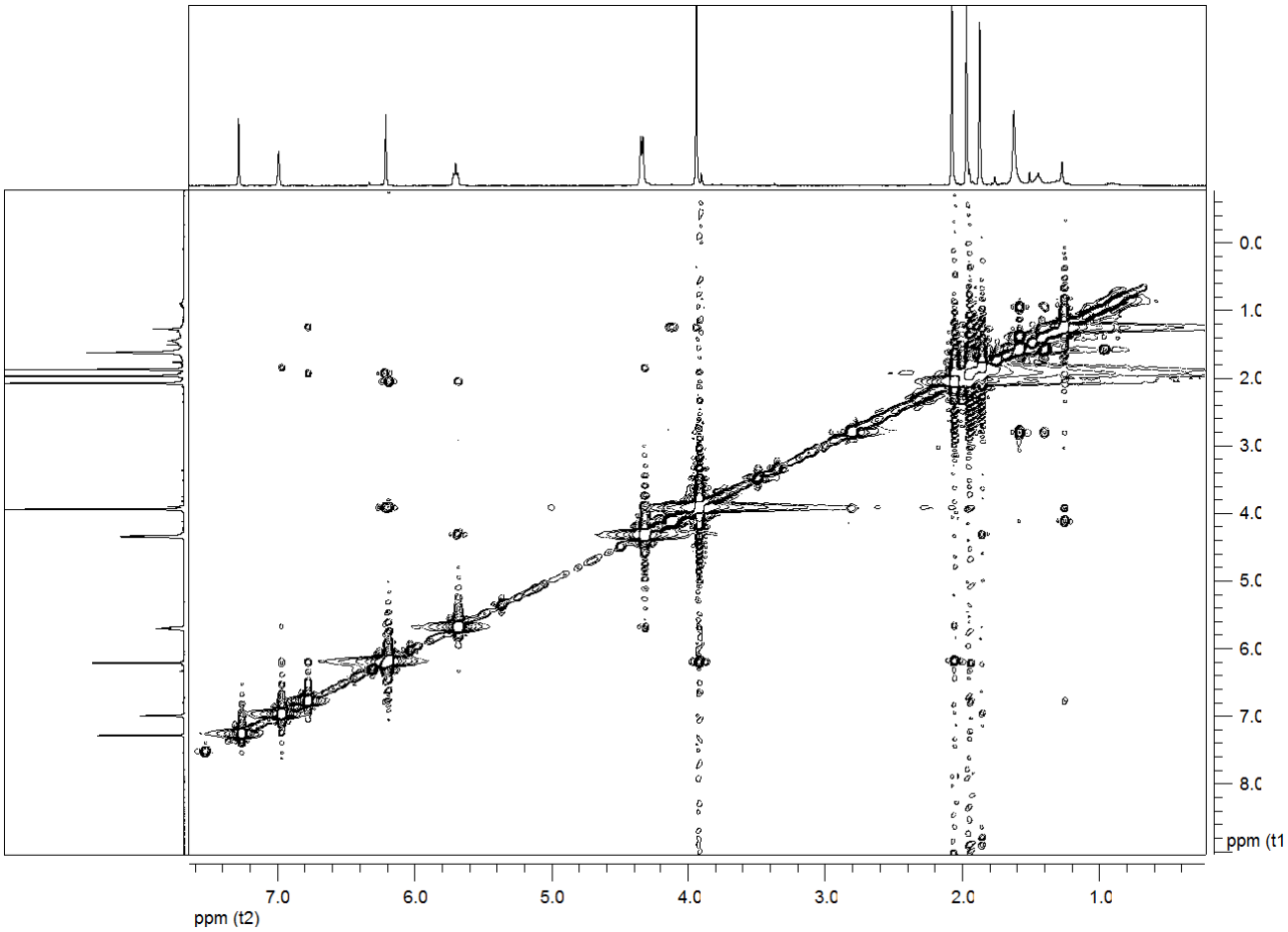

Figure. 5.4.7. NOESY spectrum of chenopodolan D (**89**), isolated from *P. chenopodiicola* liquid culture.

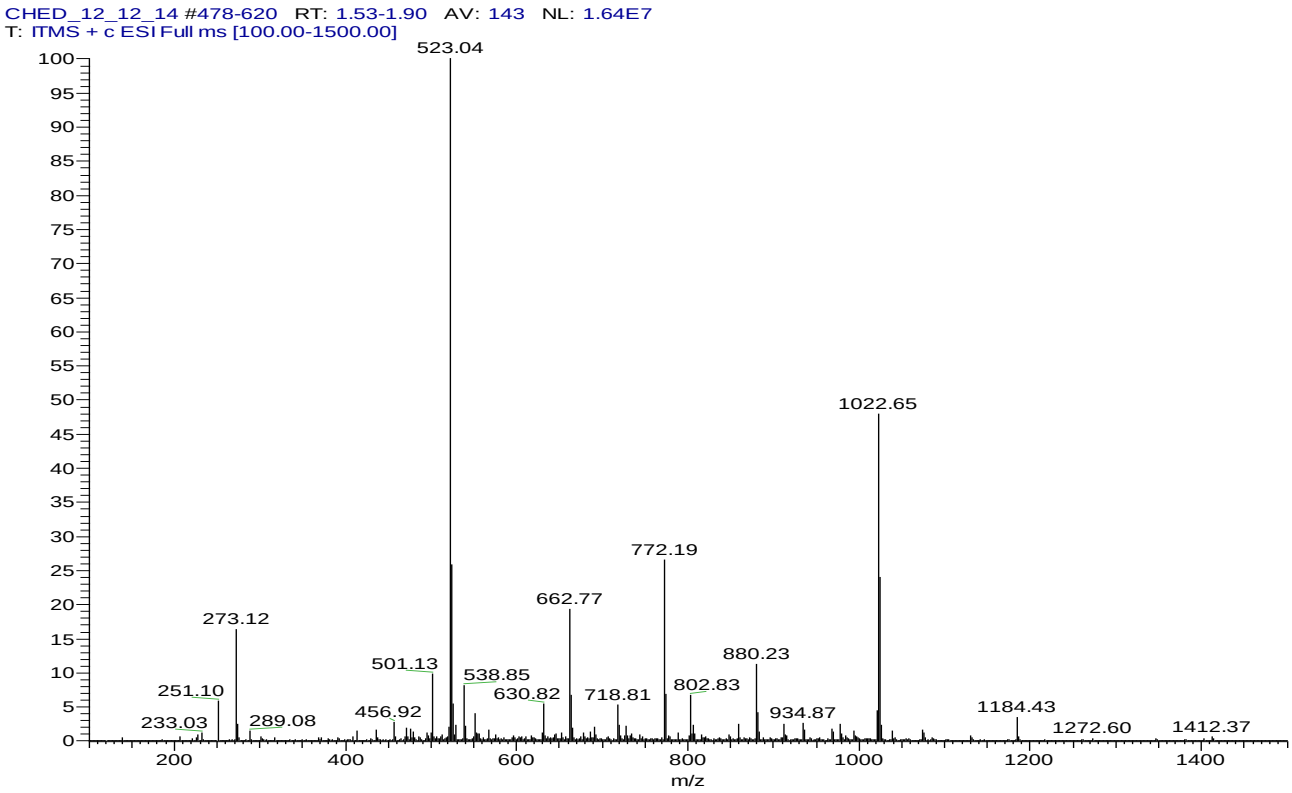

Figure. 5.4.8. ESI-MS spectrum of chenopodolan D (**89**), isolated from *P. chenopodiicola* liquid culture.

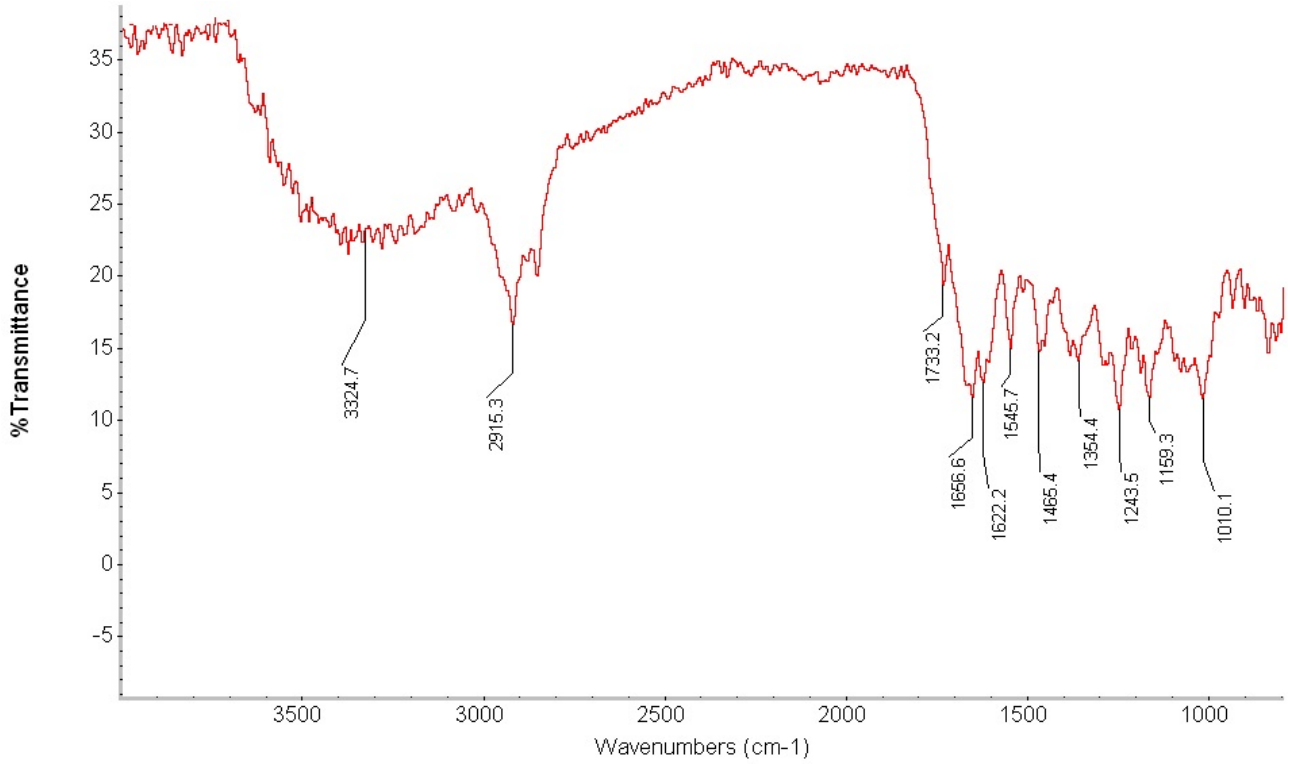

Figure. 5.4.9. IR spectrum of chenopodolan D (**89**), isolated from *P. chenopodiicola* liquid culture.

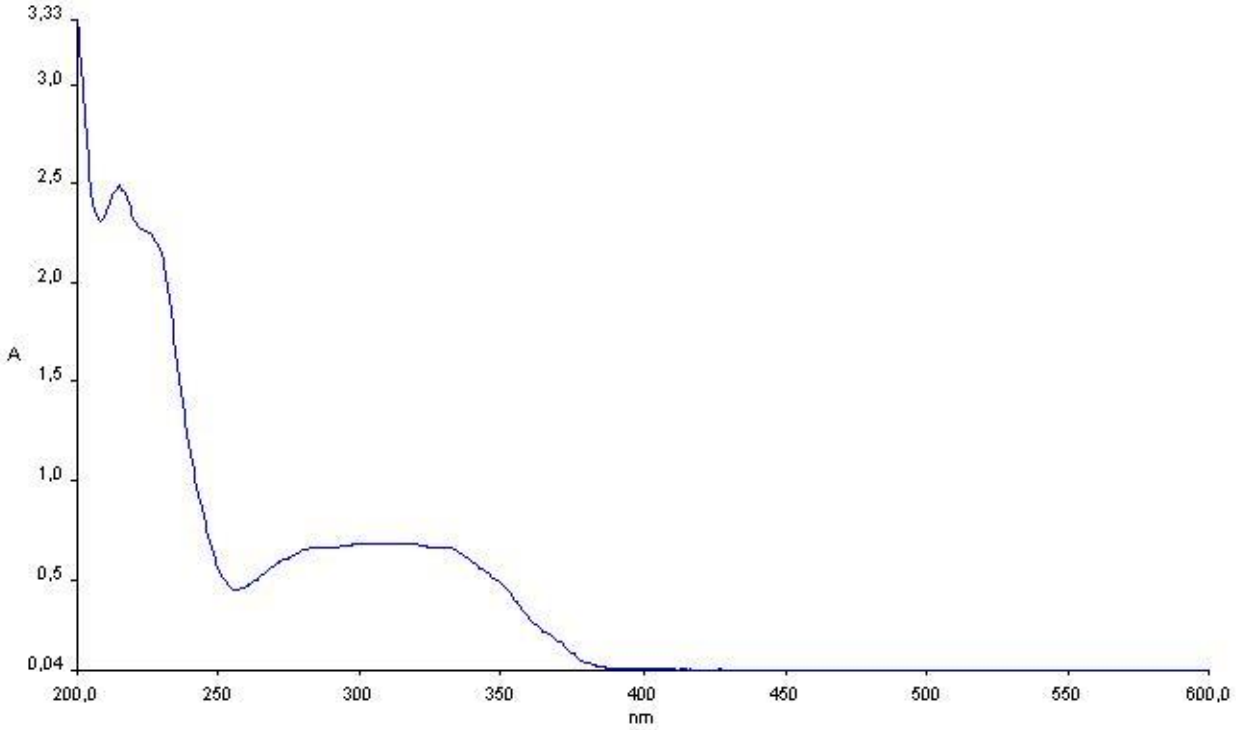

Figure. 5.4.10. UV spectrum of chenopodolan D (**89**), isolated from *P. chenopodiicola* liquid culture.

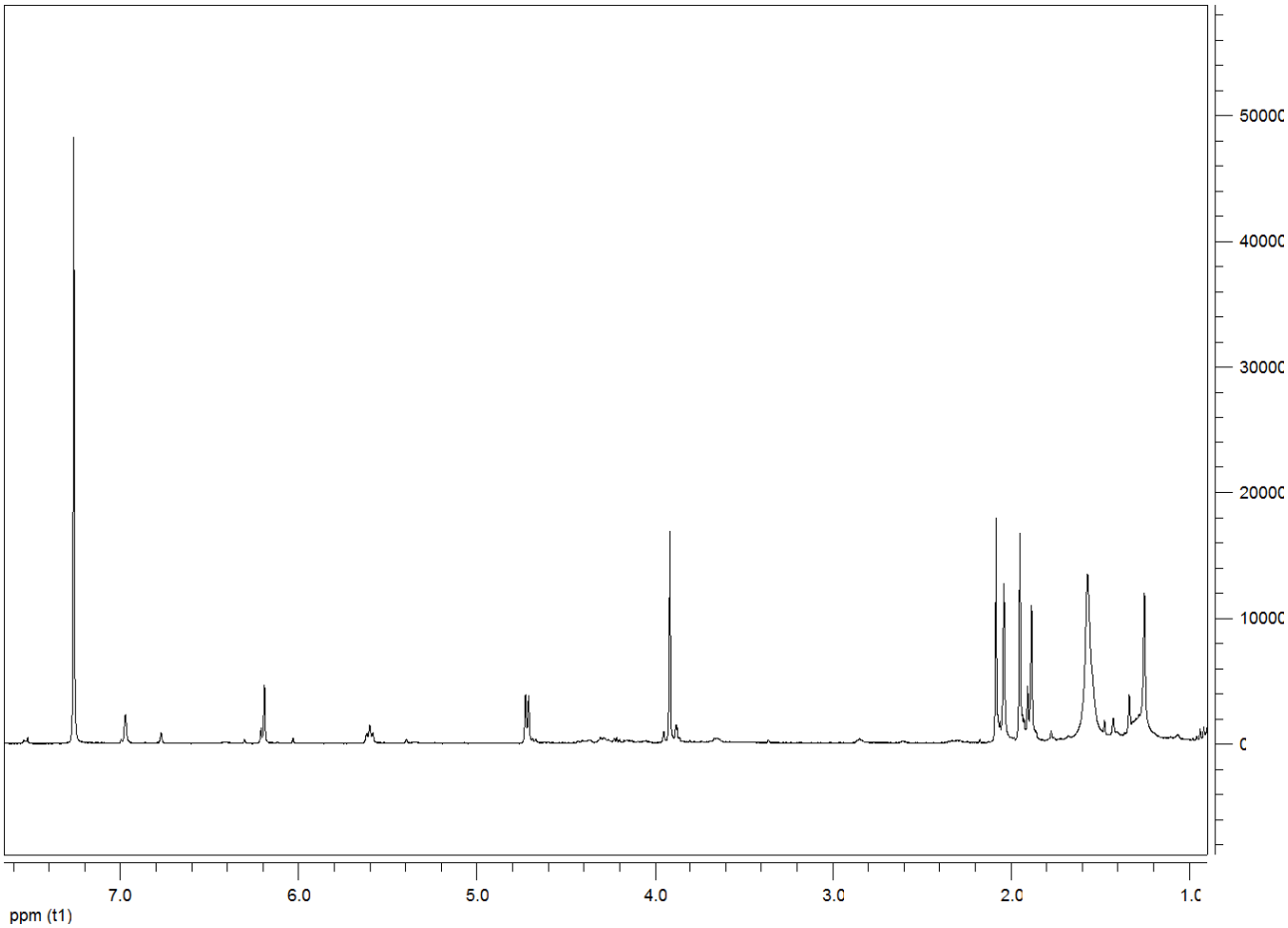

Figure. 5.4.11. ^{1}H NMR spectrum of 11-*O*-acetylderivative of chenopodolan D (**89**)

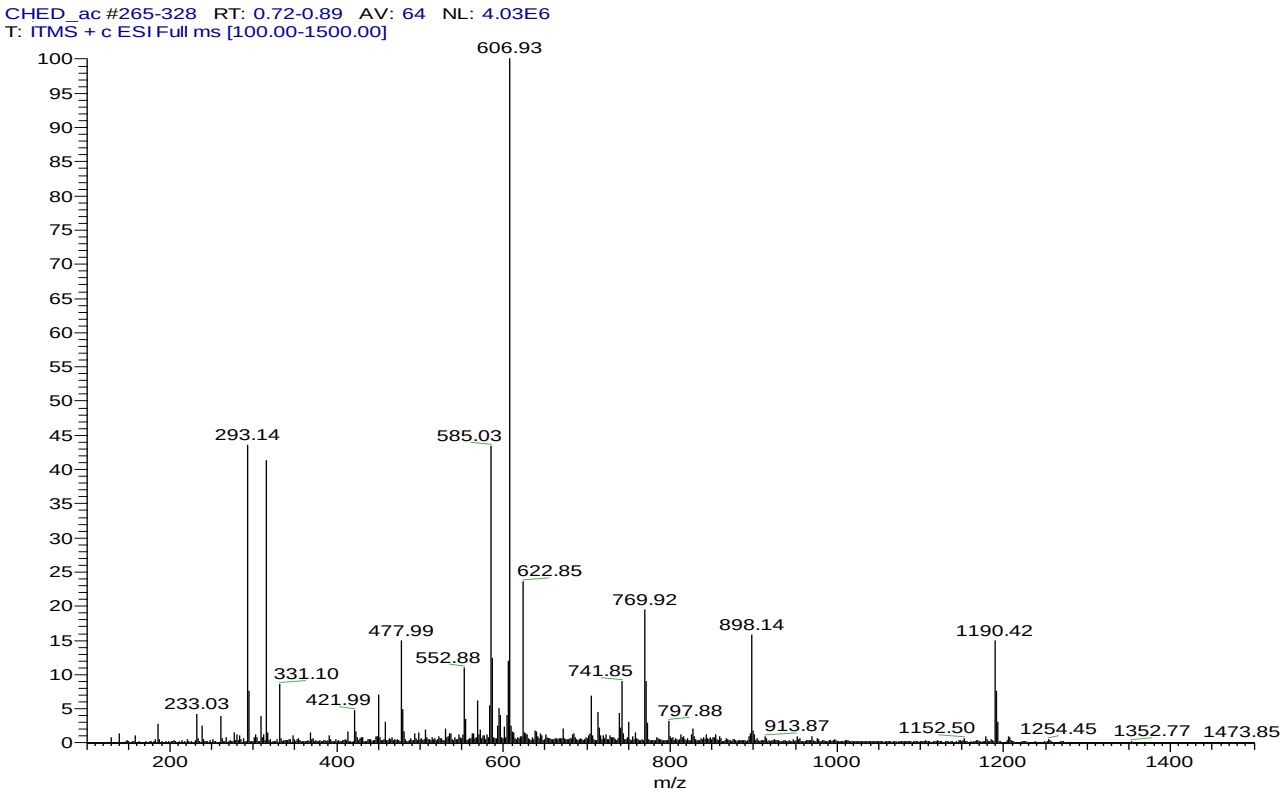

Figure. 5.4.12. ESI-MS spectrum 11-*O*-acetylderivative of chenopodolan D (**89**), isolated from *P. chenopodiicola* liquid culture.

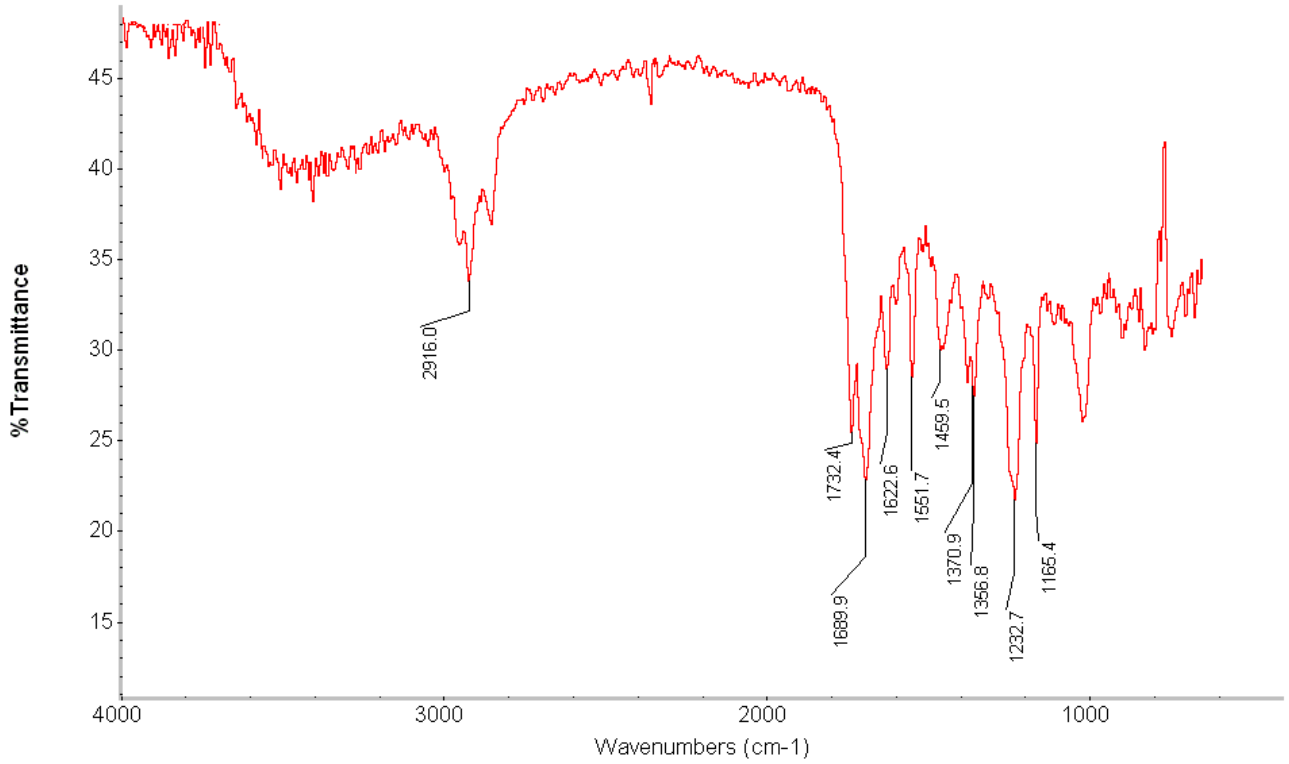

Figure. 5.4.13. IR spectrum 11-*O*-acetylderivative of chenopodolan D (**89**), isolated from *P. chenopodiicola* liquid culture.

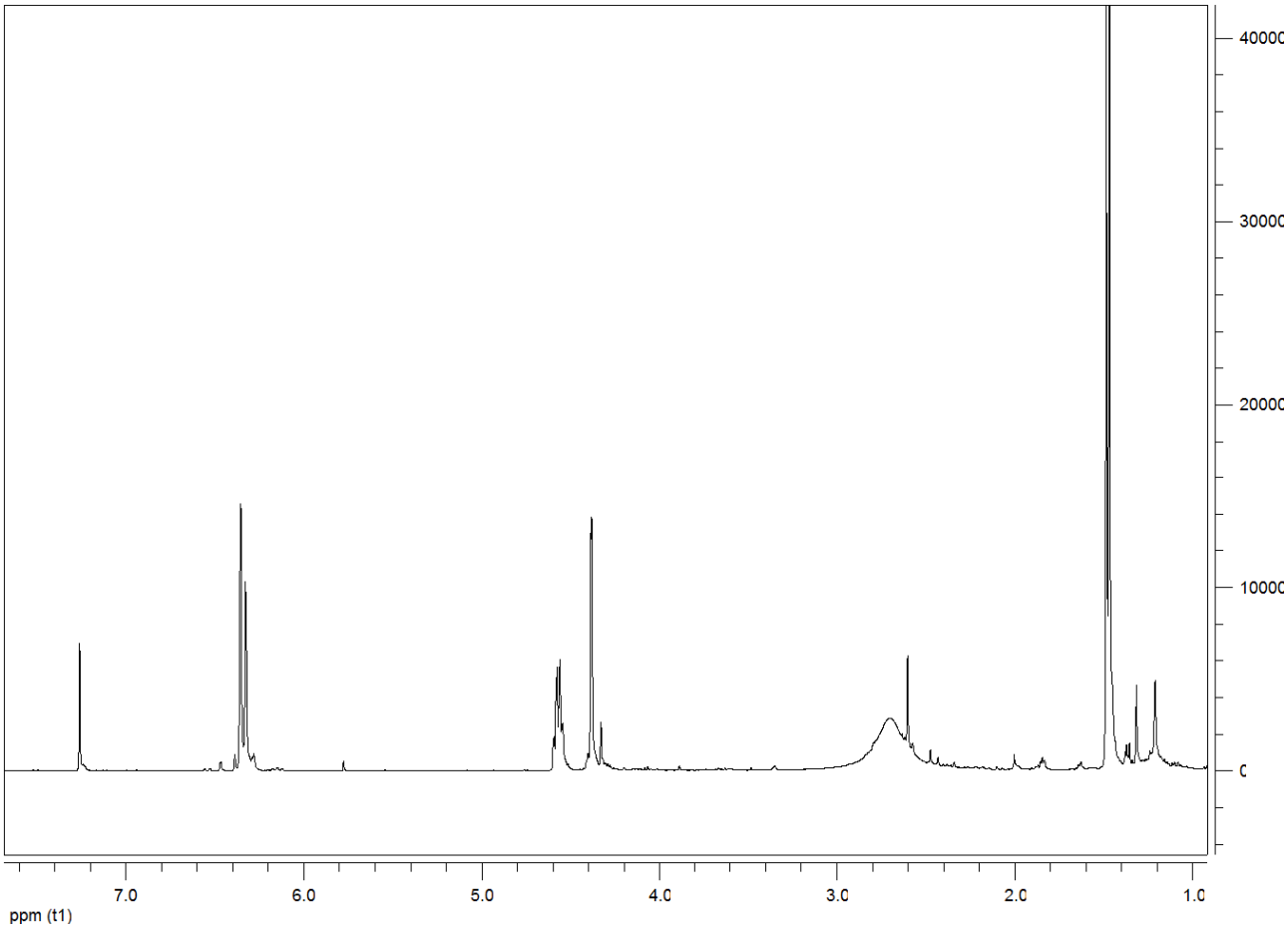

Figure. 5.4.14. ^{1}H NMR spectrum of chenisocumarine (**90**), isolated from *P. chenopodiicola* liquid culture.

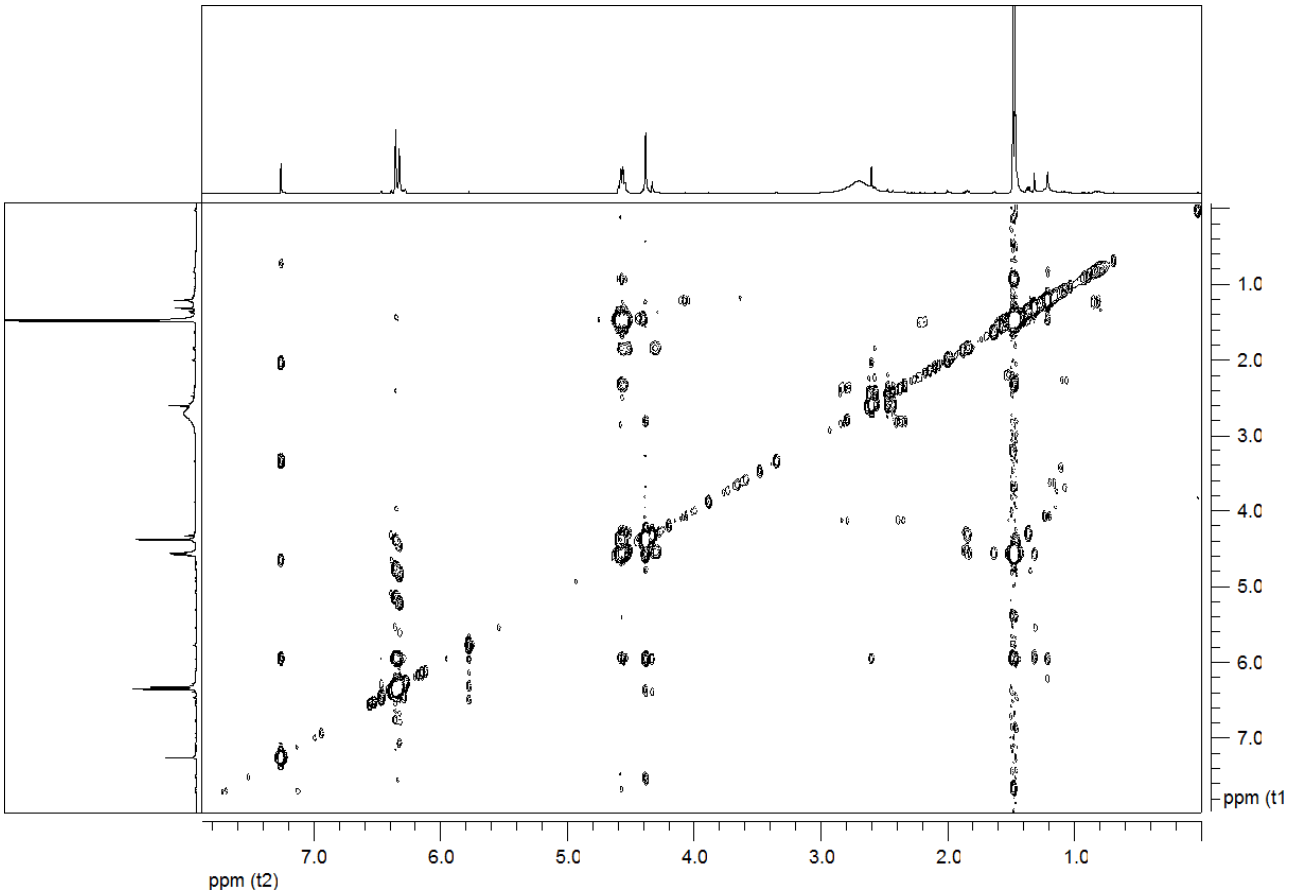

Figure. 5.4.15. COSY spectrum of chenisocumarine (**90**), isolated from *P. chenopodiicola* liquid culture.

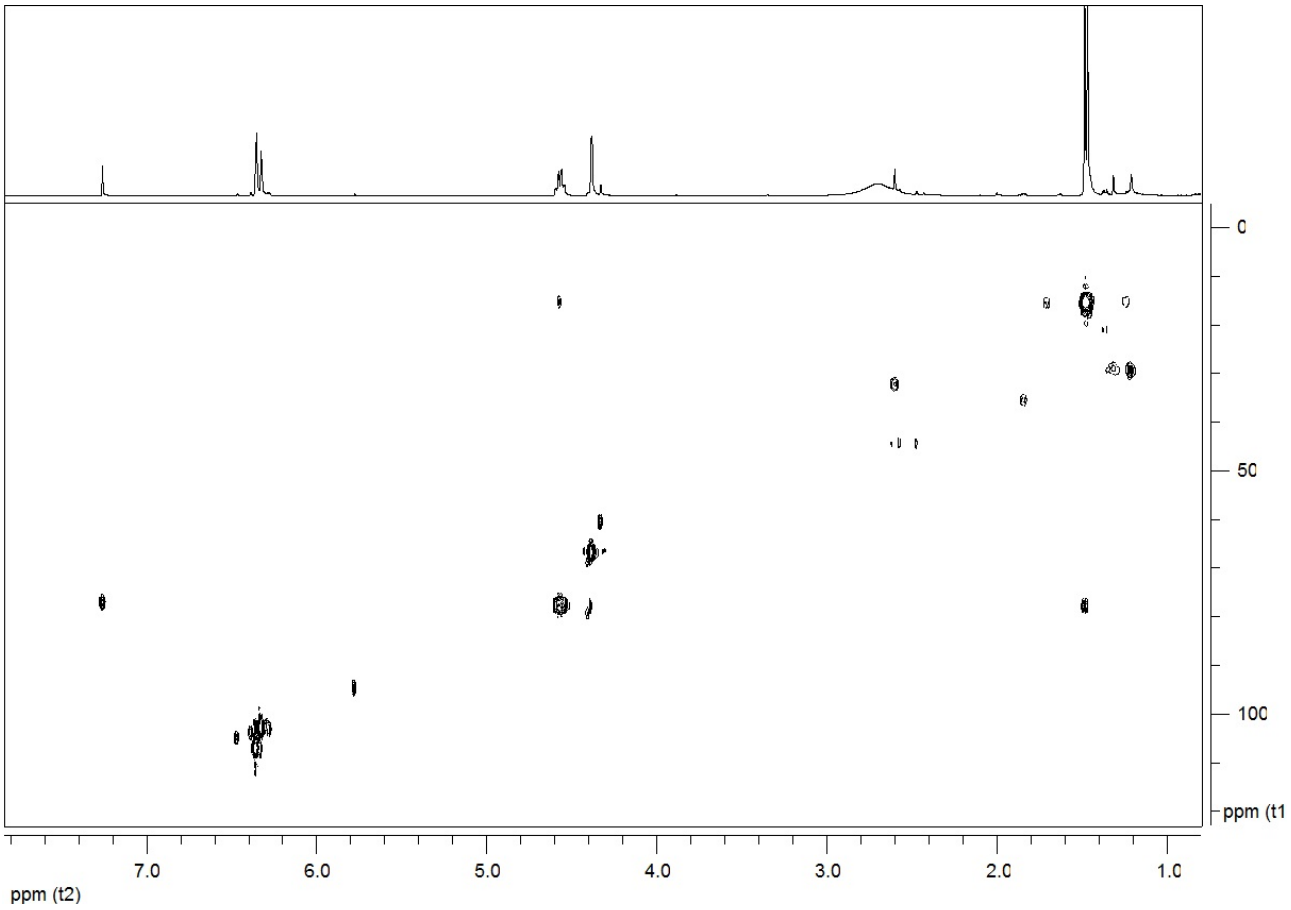

Figure. 5.4.16. HSQC spectrum of chenisocumarine (**90**), isolated from *P. chenopodiicola* liquid culture.

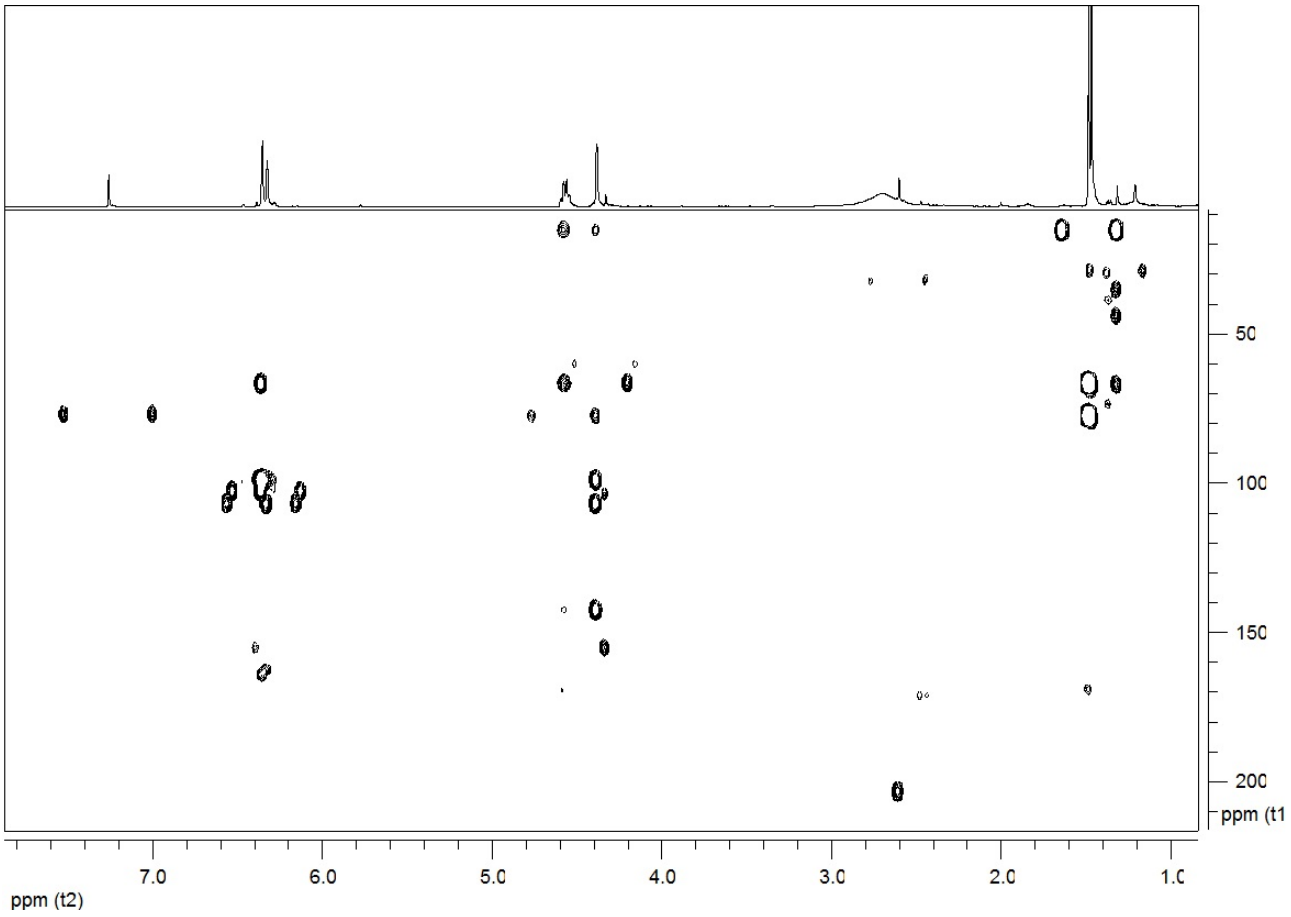

Figure. 5.4.17. HMBC spectrum of chenisocumarine (**90**), isolated from *P. chenopodiicola* liquid culture.

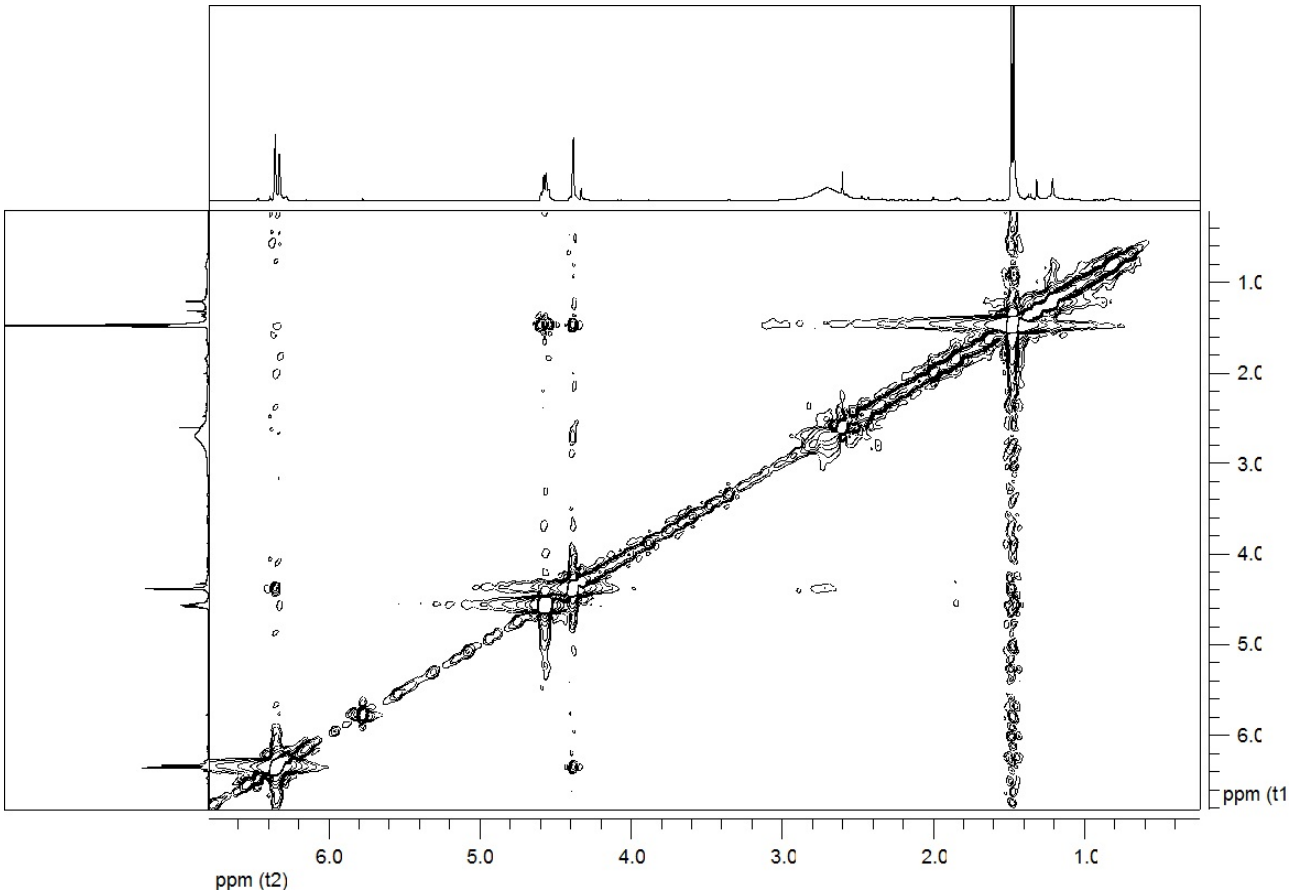

Figure. 5.4.18. NOESY spectrum of chenisocumarine (**90**), isolated from *P. chenopodiicola* liquid culture.

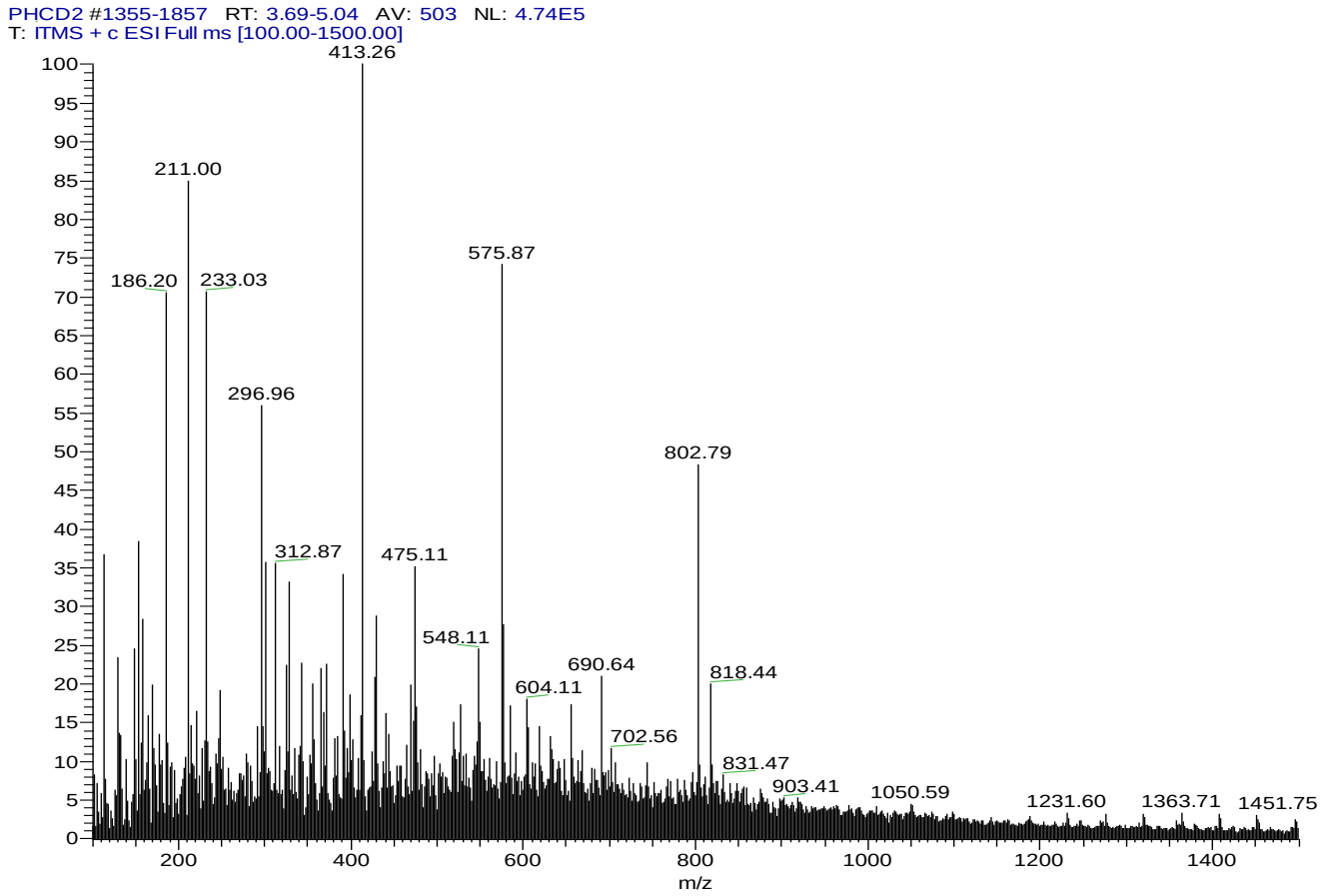

Figure. 5.4.19. ESI-MS spectrum of chenisocumarine (**90**) recorded in positive mode.

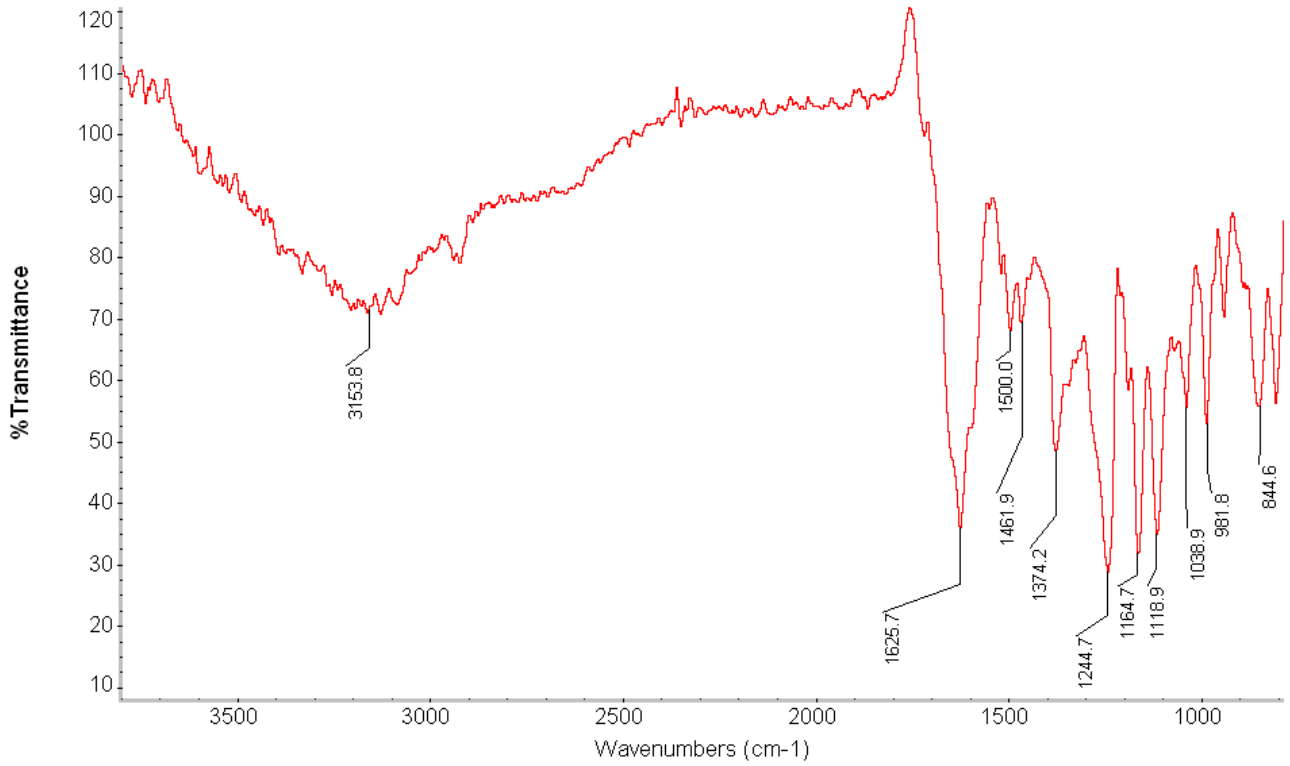

Figure. 5.4.20. IR spectrum of chenisocumarine (**90**).

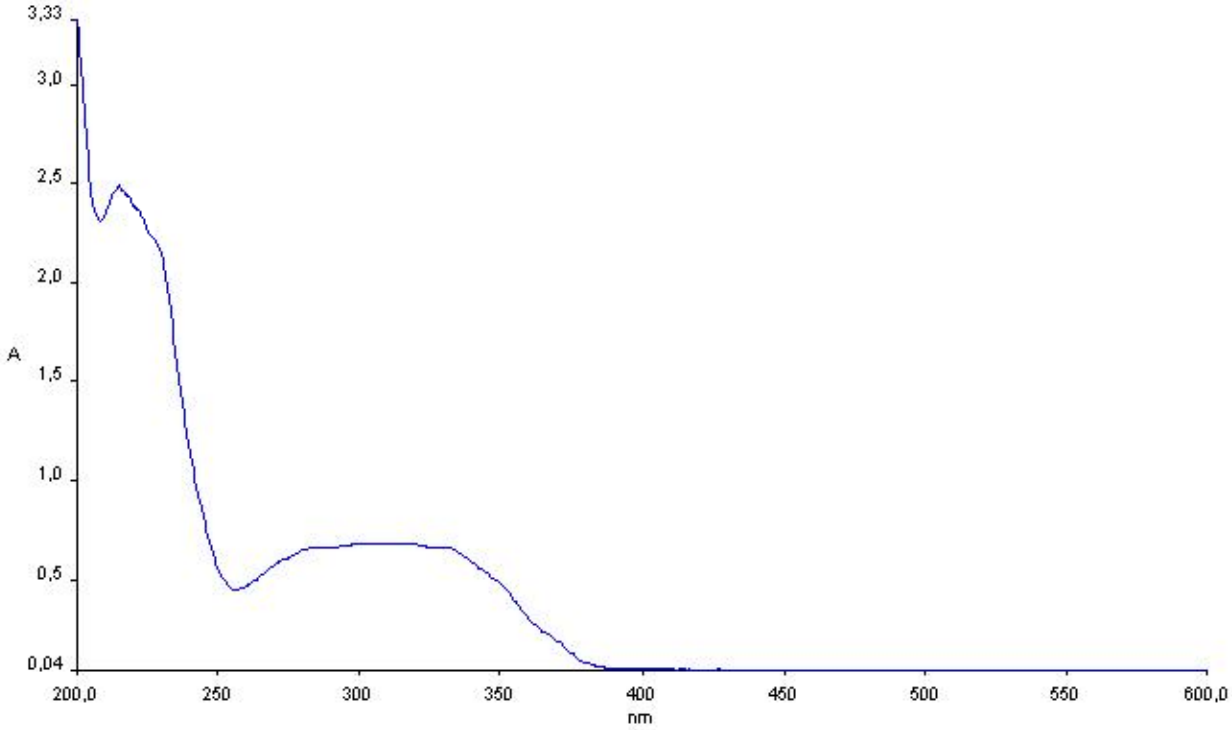

Figure. 5.4.21. UV spectrum of chenisocumarine (**90**).

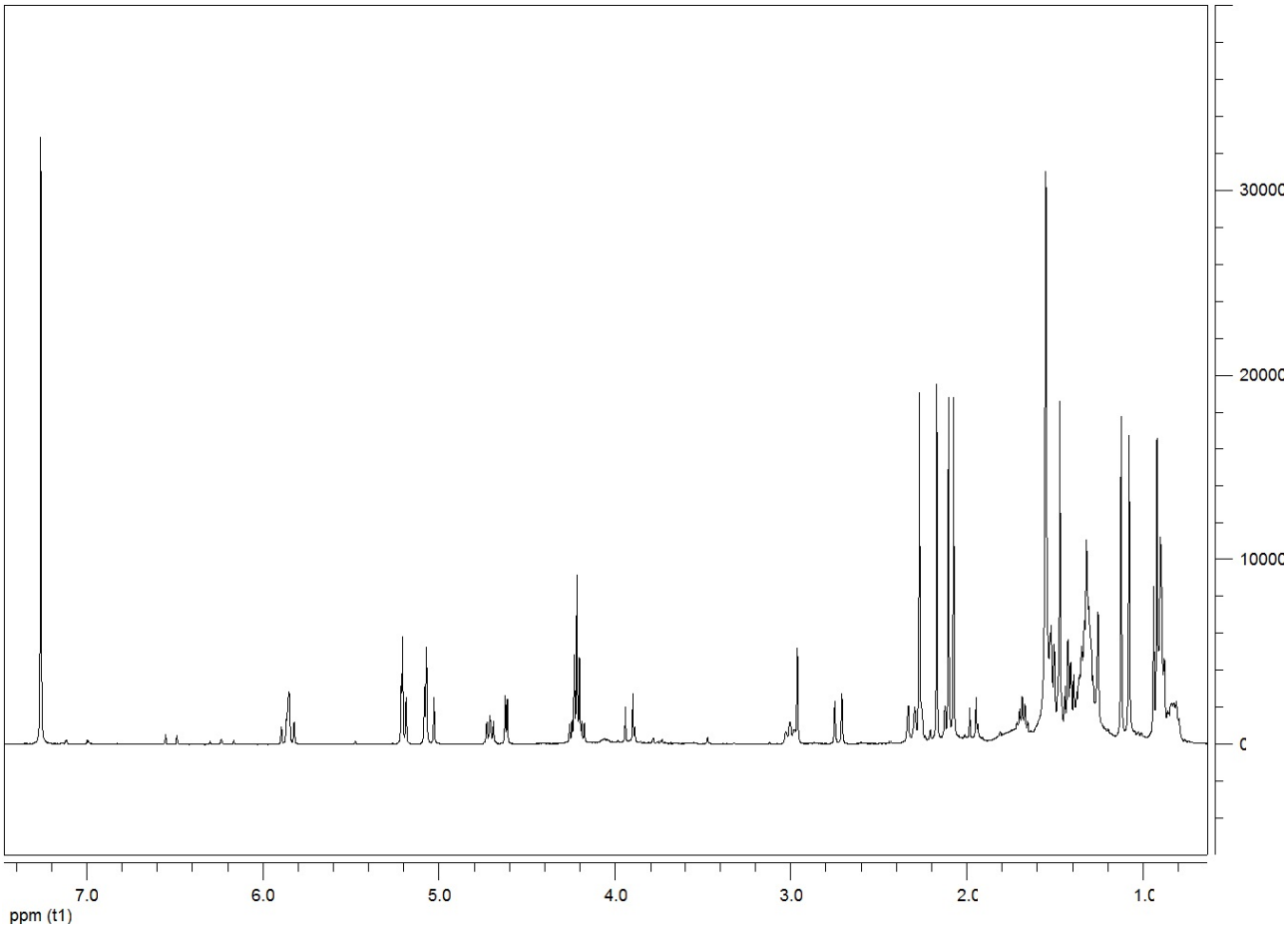

Figure. 5.4.22. ^{1}H NMR spectrum of chenopodolin B (**91**), isolated from *P. chenopodiicola* liquid culture.

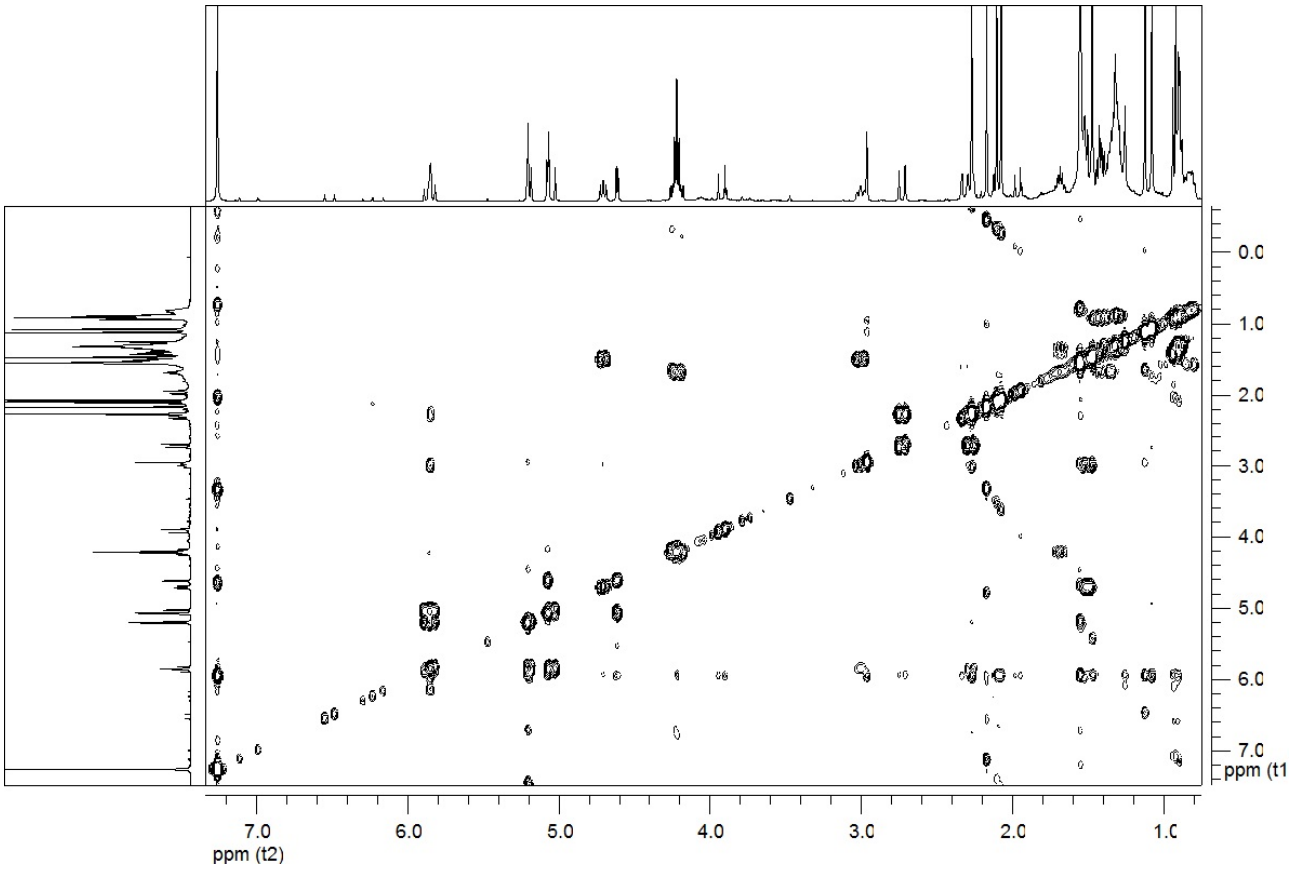

Figure. 5.4.23. COSY spectrum of chenopodolin B (**91**), isolated from *P. chenopodiicola* liquid culture.

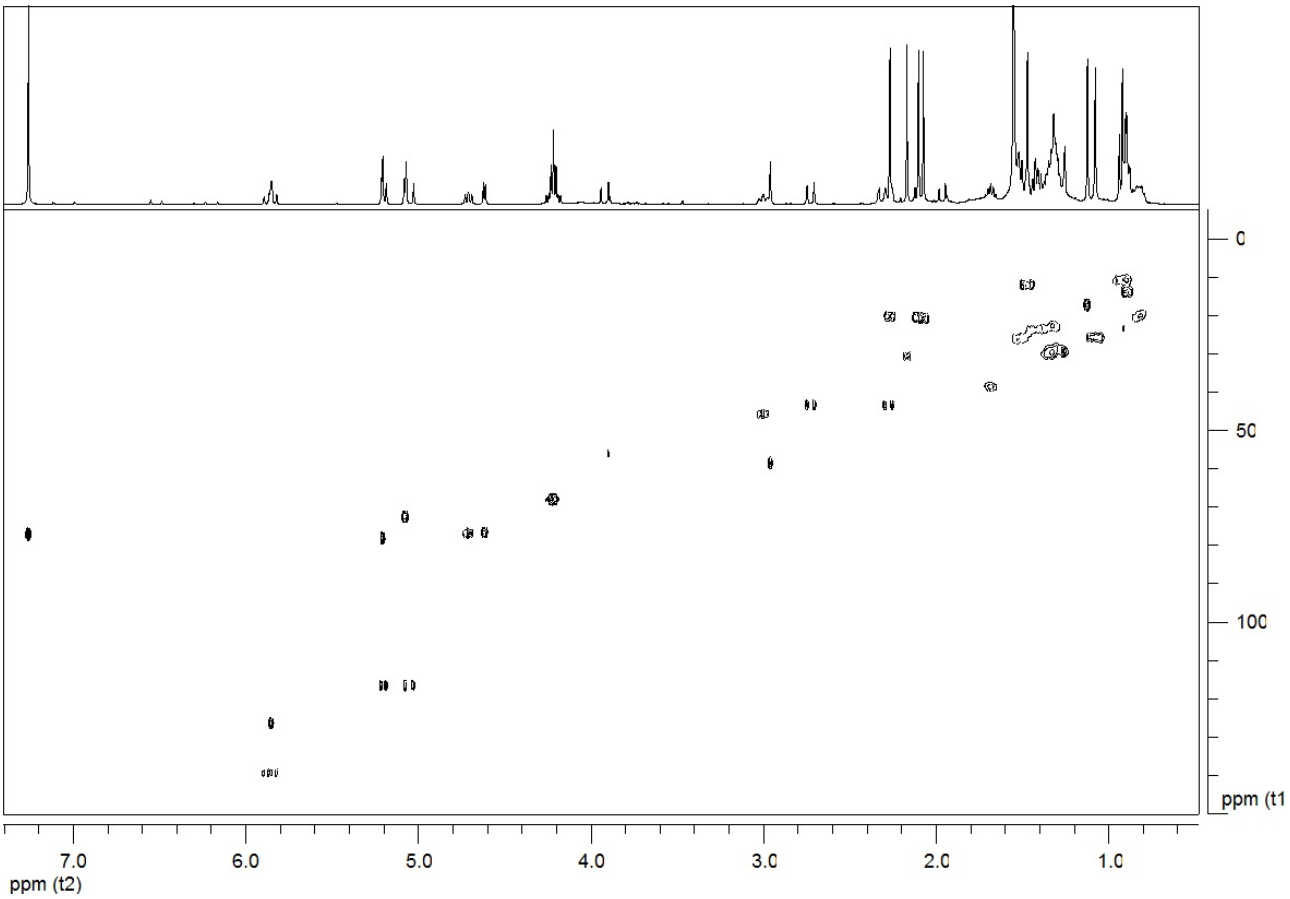

Figure. 5.4.24. HSQC spectrum of chenopodolin B (**91**), isolated from *P. chenopodiicola* liquid culture.

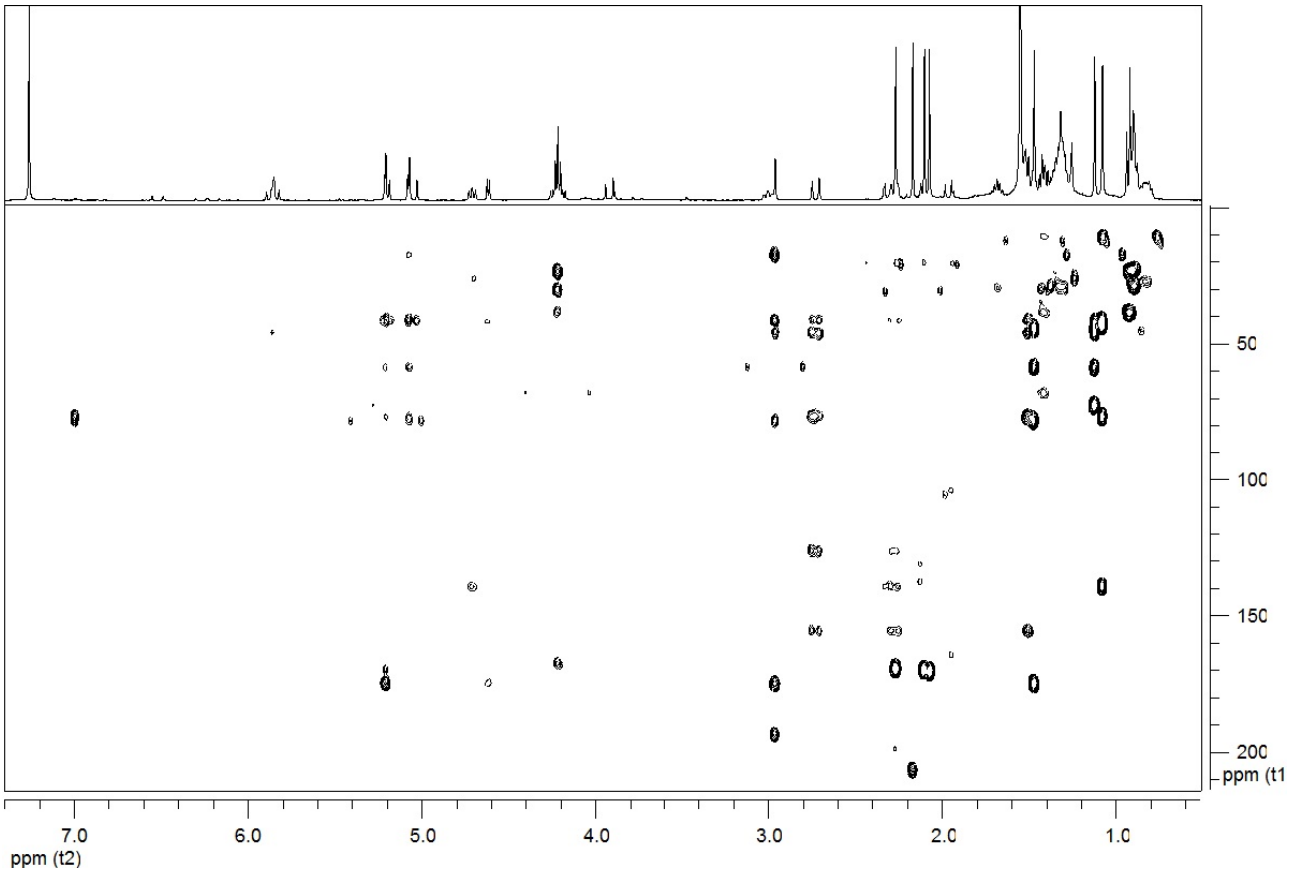

Figure. 5.4.25. HMBC spectrum of chenopodolin B (**91**), isolated from *P. chenopodiicola* liquid culture.

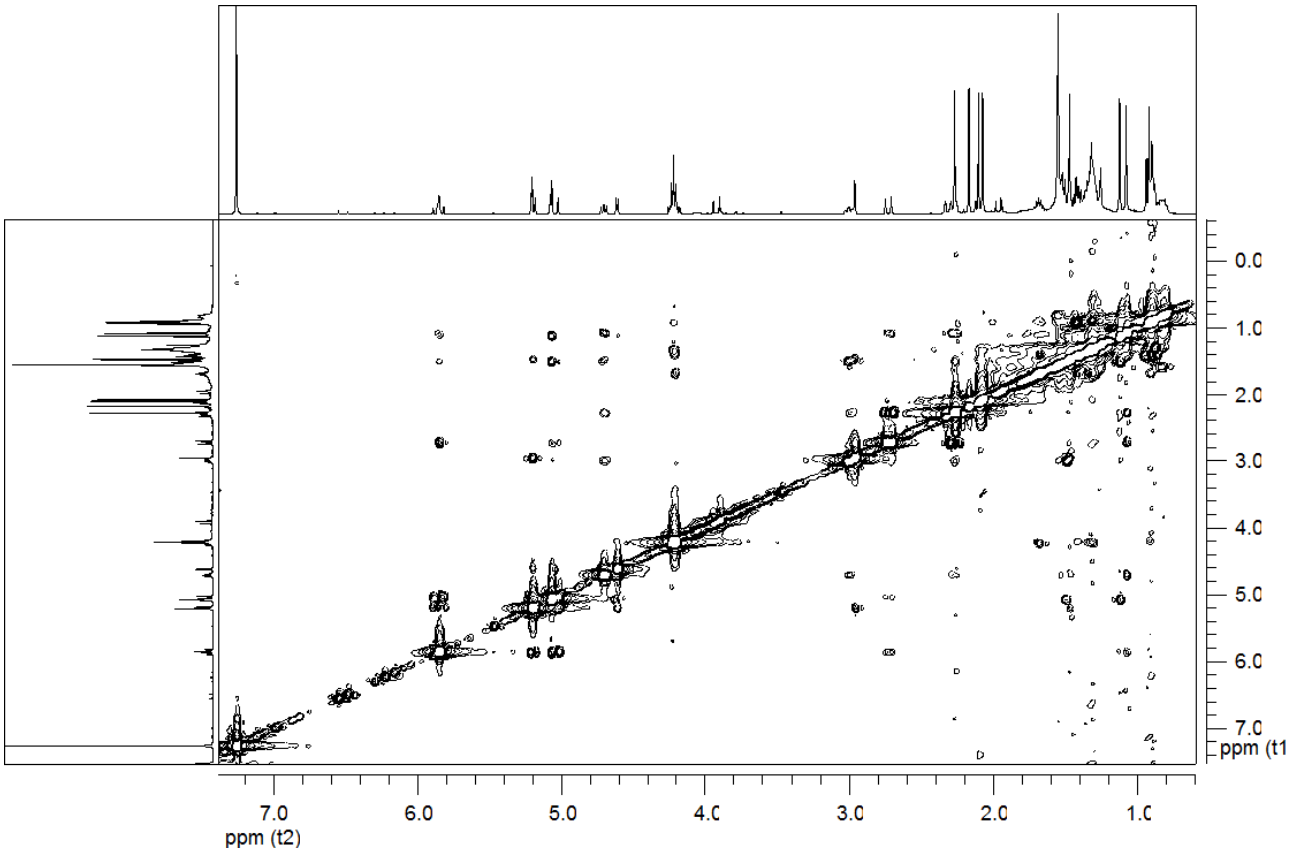

Figure. 5.4.26. NOESY spectrum of chenopodolin B (**91**), isolated from *P. chenopodiicola* liquid culture.

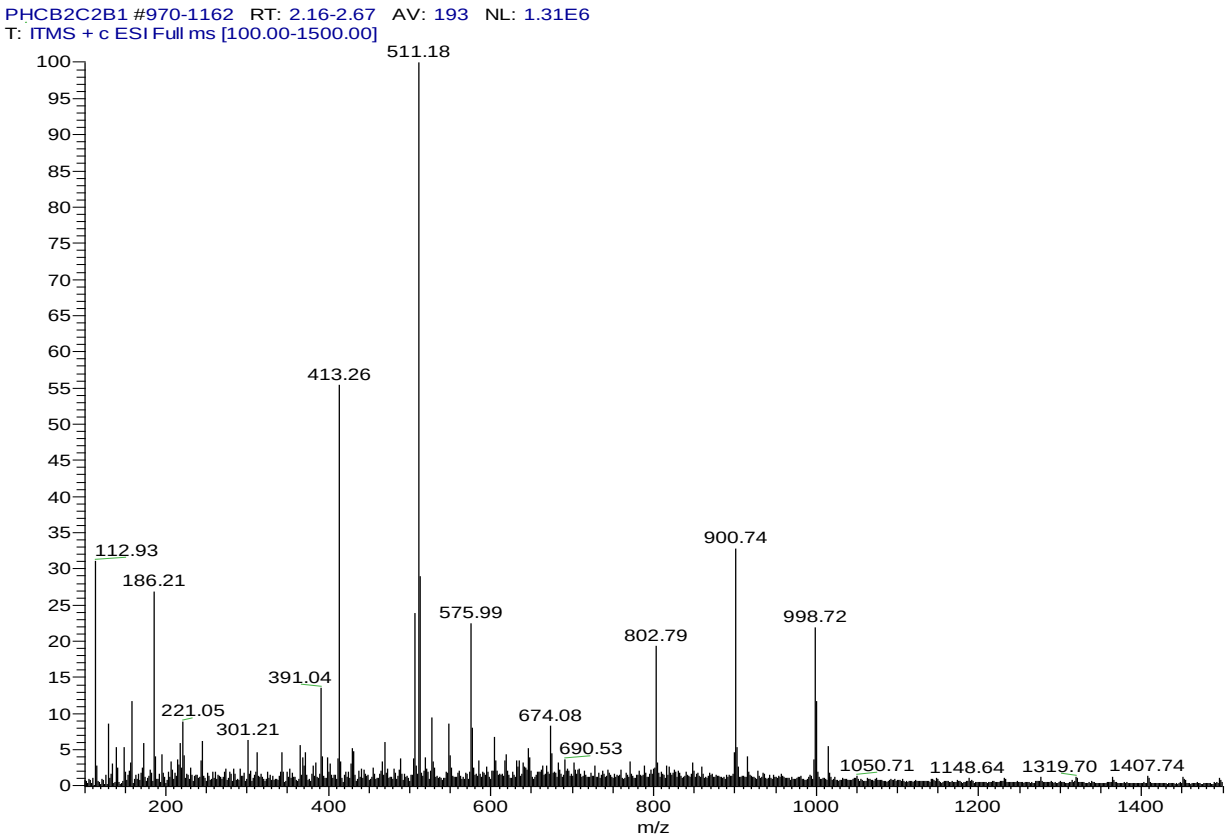

Figure. 5.4.27. ESI-MS spectrumof chenopodolin B (**91**) recorded in positive ion mode.

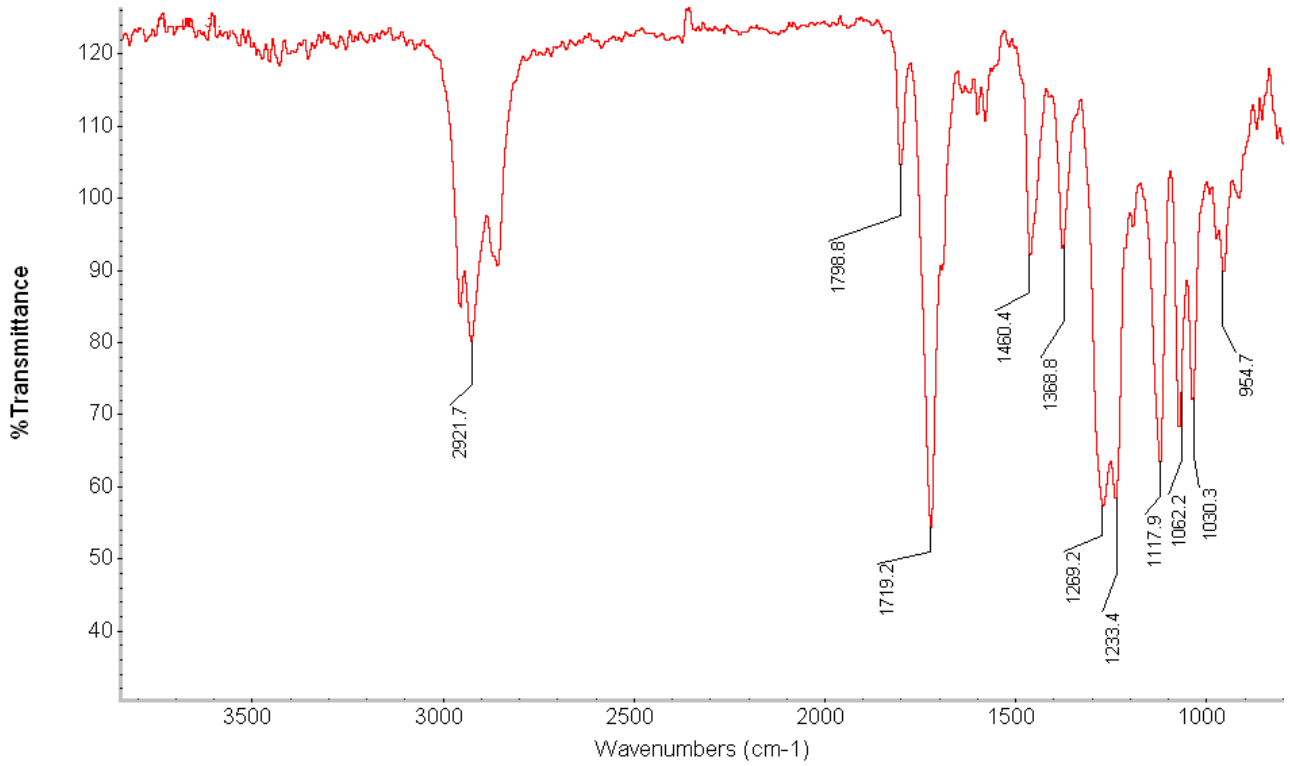

Figure. 5.4.28. IR spectrum of chenopodolin B (**91**).

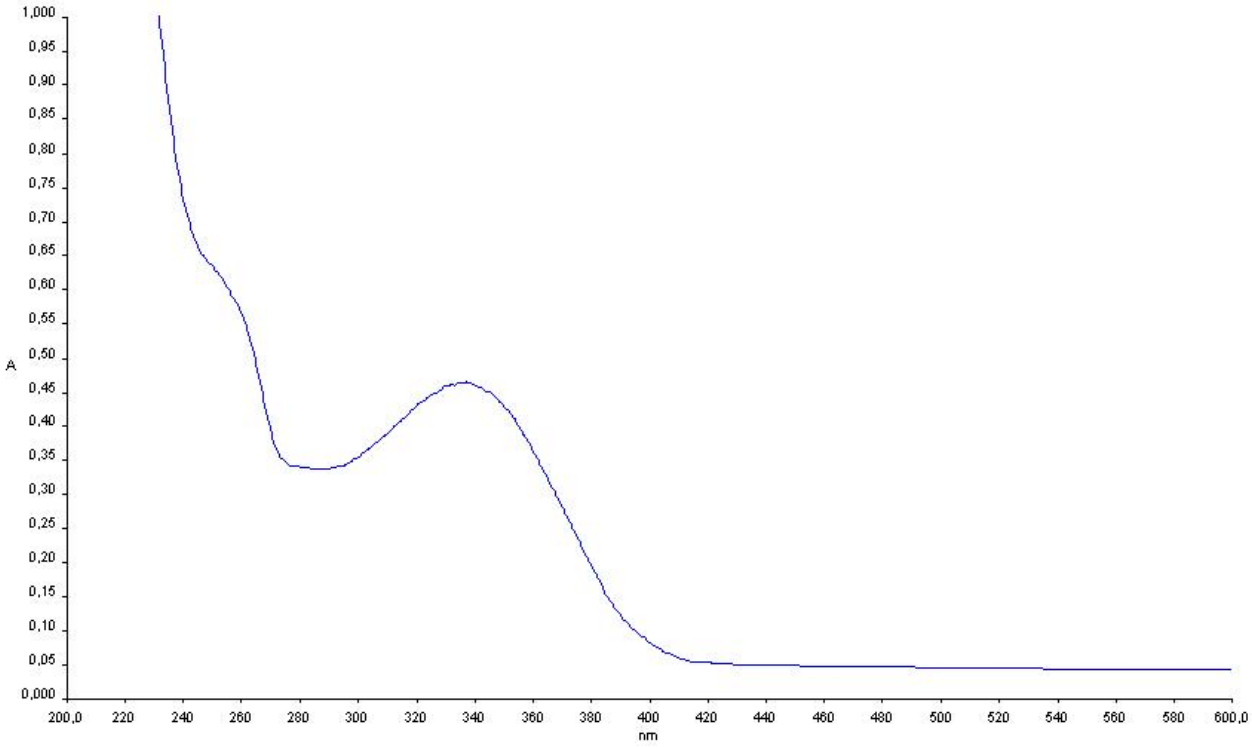

Figure. 5.4.29. UV spectrum of chenopodolin B (**91**).

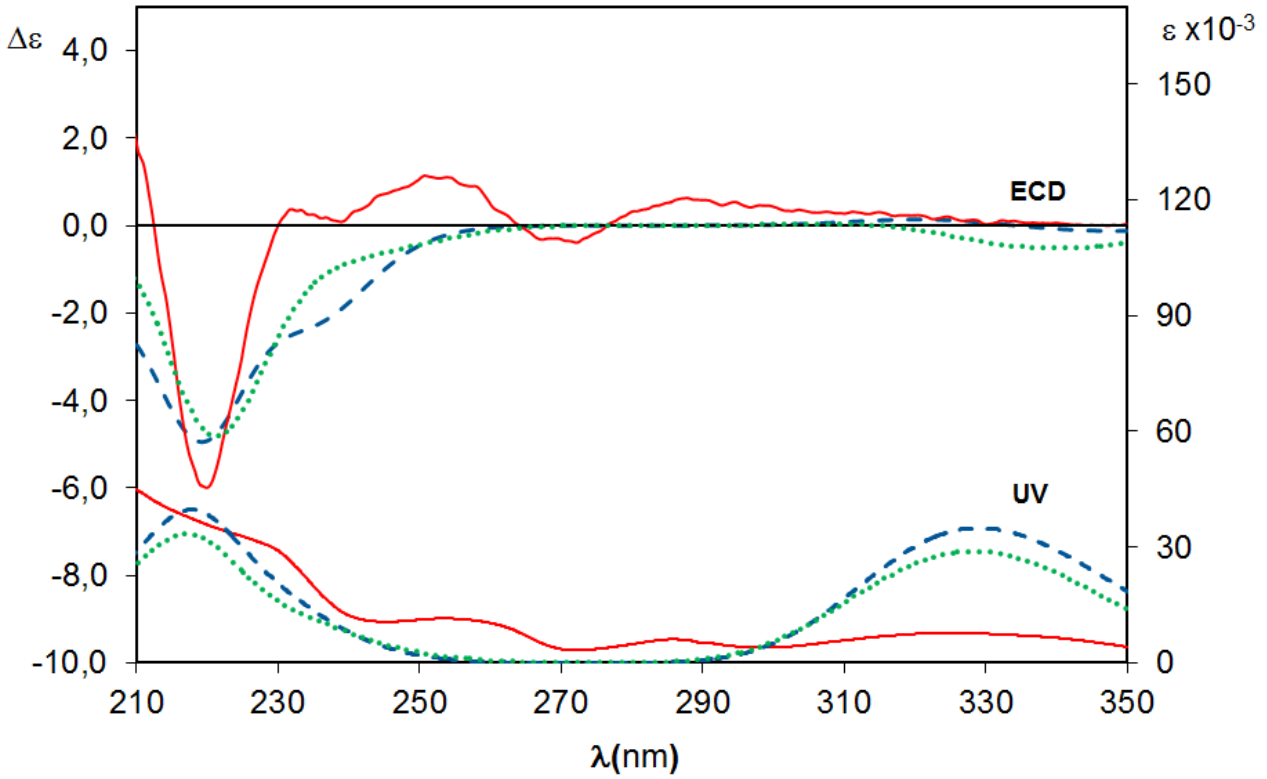

Fig. 5.4.30 Experimental UV and ECD spectra of (-)-**89** [solid red line, THF] and calculated UV and ECD spectra for (*R*)-**89** [TDDFT/CAM-B3LYP/aug-cc-pVDZ//DFT/B3LYP/TZVP/gas phase dotted green line; TDDFT/CAM-B3LYP/aug-cc-pVDZ//DFT/B3LYP/TZVP/IEFPCM(THF) dashed blue line; 0.2 eV bandwidth]. Calculated UV and ECD spectra are blue shifted of +20.0 nm and reduced 20 times.

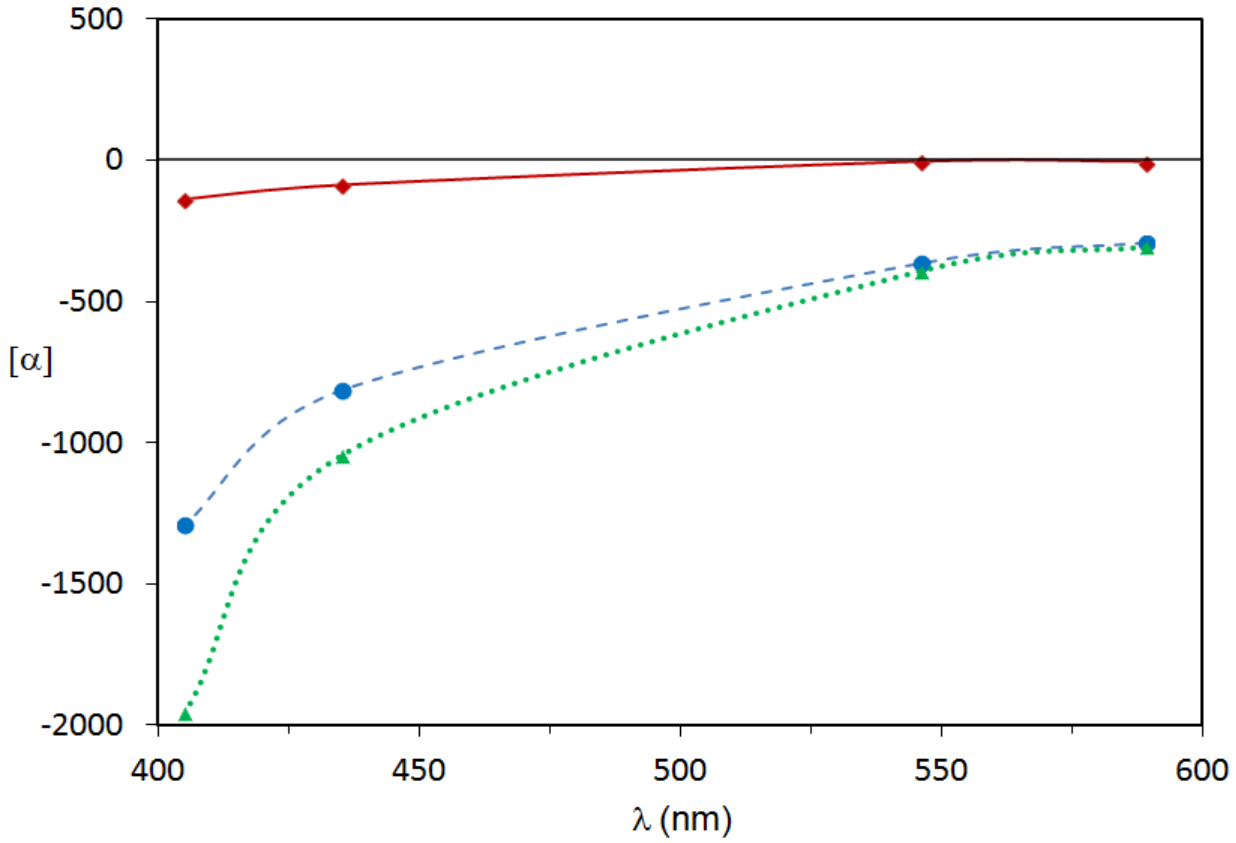

Fig. 5.4.31 Experimental ORD curve of (-)-**89** [solid red line (♦), $CHCl_3$] and calculated ORD for (*R*)-**89** [TDDFT/CAM-B3LYP/aug-cc-pVDZ//DFT/B3LYP/TZVP/gas phase, dotted green line (▲); TDDFT/CAM-B3LYP/aug-cc-pVDZ//DFT/B3LYP/TZVP/IEFPCM($CHCl_3$), dashed blue line (●)].

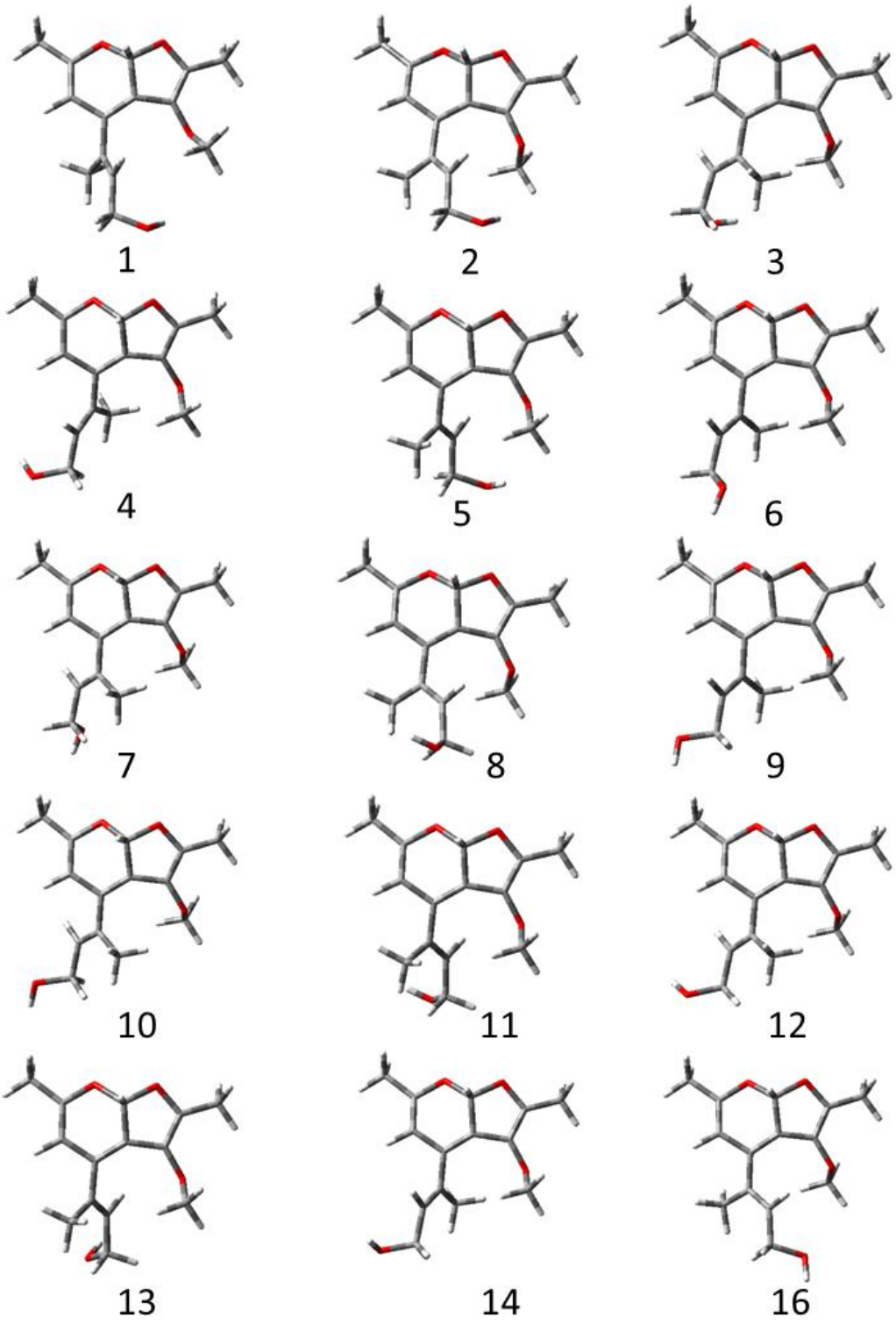

Figure 5.4.32. Computed [DFT/B3LYP/TZVP/IEF-PCM(THF)] most stable conformers of (*R*)-**89**.

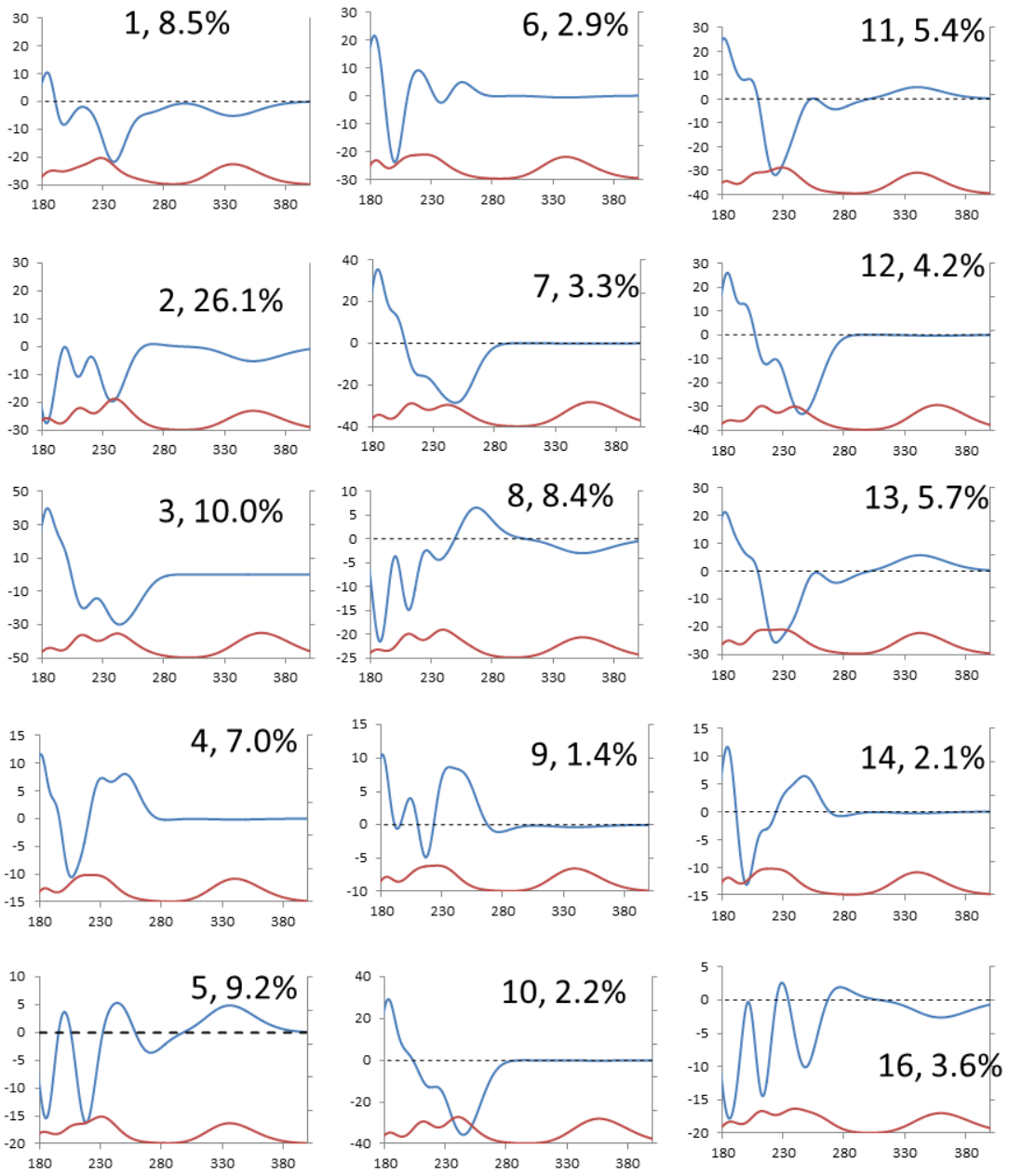

Figure 5.4.33 Computed single conformers ECD and UV spectra of (*R*)-**89** (TDDFT/CAM-B3LYP/aug-cc-pVDZ//DFT/B3LYP/TZVP/gas phase).

Table 5.1.1 ^{1}H and ^{13}C NMR Data of Gulypyrones A and B (**71** and **72**) [a,b]

	71			**72**		
position	δC[c]	δH (*J* in Hz)	HMBC	δC[c]	δH (*J* in Hz)	HMBC
2	164.3 *s*	-		166.2 *s*	-	Me-11
3	87.9 *d*	5.45 (1H) *s*		-	-	
4	170.9 *s*	-	H-3, OMe, Me-7	165.6 s	-	OMe, H-5
5	127.8 *s*	-	H-3, Me-7	91.1 *d*	6.2 (1H) *s*	Me-11
6	165.1 *s*	-	Me-7, Me-11	159.2 *s*	-	Me-7
7	9.2 *q*	1.92 (3H) *s*		11.4 *q*	1.94 (3H) *s*	
8	42.7 *d*	2.87 (1H) quin (7.0)	Me-10, Me-11	128.1 *s*	-	H-5, Me-7
9	69.8 *d*	4.05 (1H) *m*	H-8, Me-10, Me-11	132.1 *d*	6.69 (1H) *t* (5.5)	H_2-10, Me-11
10	21.3 *q*	1.27 (3H) *d* (6.2)	H-8, Me-11	56.7 *t*	4.41 (1H) *dd* (1.0, 5.5) 4.39 (1H) *dd* (1.0, 5.5)	
11	14.8 *q*	1.19 (3H) *d* (7.0)	H-8, Me-10	14.3 *q*	1.93 (3H) *s*	
OMe	56.1 *q*	3.82 (3H) *s*		55.3 *q*	3.91(3H) *s*	

[a]The chemical shifts are in δ values (ppm) from TMS.[b]2D ^{1}H, ^{1}H (COSY) ^{13}C, ^{1}H (HSQC) NMR experiments delineated the correlations of all the protons and the corresponding carbons.
[c]Multiplicities were assigned by DEPT spectrum.

Table 5.1.2. ^{1}H NMR Data of (*S*)- and (*R*)-MTPA Esters of Gulypyrones A (**78** and **79**) Recorded in $CDCl_3$[a]

	78	**79**
position	δH (*J* in Hz)	δH (*J* in Hz)
3	5.414 (1H) *s*	5.314 *s*
7	1.767 (3H) *s*	1.697 (3H) *s*
8	3.119 (1H) quint (7.4)	3.105 (1H) quint (7.0)
9	5.266 (1H) quint (6.2)	5.272 (1H) quint (6.2)
10	1.394 (3H) *d* (6.2)	1.441 (3H) *d* (7.0)
11	1.233 (3H) *d* (7.4)	1.187 (3H) *d* (6.2)
OMe	3.119 (3H) *s*	3.755 (3H) *s*
OMe	3.373 (3H) *s*	3.512 (5H) *s*
Ph	7.33–7.30 (5H) *m*	7.41–7.31 (5H) *m*

[a]The chemical shifts are in δ values (ppm) from TMS

Table 5.1.3. NMR Data of Phomentrioloxins B [a,b] and C [a] (**73** and **74**, respectively) Recorded in $CDCl_3$ at 400 MHz.

	73			**74**
position	δC[c]	δH (*J* in Hz)	HMBC	δH (*J* in Hz)
1	194.9 *s*	-	H-5, H-2	4.95 *dd* (11.0, 2.0)
2	73.7 *d*	4.57 (1H) *dd* (10, 2.0)	H-4, H-3	-
3	81.0 *d*	3.42 (1H) *dd* (10.0, 4.0)	H-5, H-4, H-3, H-2	3.61 *dd* (6.4,
4	63.9 *d*	4.65 (1H) *ddd* (6.0, 4.0, 1.9)	H-5	4.54 *ddd* (6.4, 6.0, 5.4)
5	146.4 *d*	7.14 (1H) *d* (6.0)	H-4	6.74 *dd* (6.0, 2.0)
6	124.4 *s*	-	H-4, H-5	-
1’	81.5 *s*	-	H-5	-
2’	95.7 *s*	-	H_2-8’	-
3’	130.6 *s*	-	H_2-8’, H_2-4’	-
4’	37.1 *t*	2.23 (2H) *m*	H_2-8’, H_2-5’	2.18 *m*
5’	26.7 *t*	2.23 (2H) *m*	H-6’, H_2-4’	2.18 *m*
6’	123.4 *d*	5.11 (1H) *m*	H_2-4’, H_2-5’	4.92 *m*
7’	123.1 *s*	-	Me-10’, Me-9’	-
8’	123.4 *t*	5.46 (1H) *d* (1.4)	H_2-4’, H_2-5’	4.87 *d* (1.2)
		5.35 (1H) *d* (1.4)		4.81 *d* (1.2)
9’[d]	25.6 *q*	1.68 (3H) *s*	H-6’, Me-10’	1.74 *s*
10’[d]	17.7 *q*	1.63 (3H) *s*	Me-9’	1.64 *s*
OMe	59.2 *q*	3.65 (3H) *s*	H-3	3.65 *s*
HO-1		-		2.83 *d* (11.0)
HO-2		3.44 (1H) *d* (2.0)		-
HO-4		2.86 (1H) *d* (1.9)		4.60 *d* (5.4)

[a]The chemical shifts are in δ values (ppm) from TMS. [b]2D ^{1}H, ^{1}H (COSY) ^{13}C, ^{1}H (HSQC) NMR experiments delineated the correlations of all the protons and the corresponding carbons. [c]Multiplicities were assigned by DEPT spectra. [d] These assignments could be reversed.

Table 5.2.1 NMR Data of Kongiidiazadione and Its 6-*O*-Acetyl Derivative (**84** and **85**, respectively) Recorded in $CDCl_3$ at 600 MHz. [a,b]

	84			**85**
Position	δH (*J* in Hz)	δ C[c]	HMBC	δ H (*J* in Hz)
1	-	192.0 *s*	H-C(4), H-C(5)	
2	-	191.1 *s*	H-C(5)	
3	-	147.9 *s*	H-C(4), H-C(5), H_2-C(6), OH	
4	6.68 (1H) *dt* (1.9, 1.5)	131.2 *d*	H_2-C(6), H-C(5)	6.54 (1H) *dt* (1.9, 1.6)
5	3.84 (1H) *m*	59.6 *d*	H-C(4), NH	3.84 (1H) *dd* (1.9, 3.7)
6	4.58 (1H) *br d* (17.4)	54.1 *t*	H-C(4), OH	4.98 (1H) *dd* (17.0, 1.6)
	4.07 (1H) *br d* (17.4)			4.83 (1H) *dd* (17.0, 1.6)
NH	3.84 (1H) *m*			3.88 (1H) *d* (3.7)
OH	1.88 (1H) *br s*			
$COCH_3$				2.13 (3H) *s*

[a]The chemical shifts are in δ values (ppm) from TMS. [b]2D ^{1}H, ^{1}H (COSY) ^{13}C, ^{1}H (HSQC) NMR experiments delineated the correlations of all the protons and the corresponding carbons.
[c]Multiplicities were assigned by DEPT spectra.

Table 5.2.2. Conformers Relative Free Energies (ΔG) and Population Percentages (pop%) of (5*R*)-**84** Calculated at Different Levels of Theory Both in Gas Phase and IEFPCM (MeOH) Implicit Solvation Model

	B3LYP/TZVP Gas phase		B3LYP/TZVP IEFPCM(MeOH)		M06-2X/TZVP IEFPCM(MeOH)	
Conformer	ΔG(Kcal/mol)	pop(%)	ΔG(Kcal/mol)	pop(%)	ΔG(Kcal/mol)	pop(%)
84a	0.00	37.9	0.00	25.4	0.00	22.3
84b	0.56	14.8	-0.04	27.3	0.095	19.0
84c	0.77	10.4	0.34	14.3	0.22	15.3
84d	0.53	15.5	0.89	5.6	0.80	5.7
84e	0.71	11.5	0.93	5.3	0.89	5.0
84f	1.27	4.5	0.72	7.6	0.28	13.7
841	1.63	2.4	1.12	3.9	0.64	7.5
84h	1.99	1.3	1.08	4.1	0.68	7.0
84i	1.83	1.7	1.57	1.8	1.28	2.6
84j	-	-	1.00	4.7	1.47	1.9

Table 5.2.3. Electronic Transitions Determining the ECD Spectrum of Compound (*R*)-**84** in the 180-600 nm Range.[a]

Compound	Transition number[b]	Wavelength (nm)	MOs	Rotational strength
(*R*)-**84**	1	505.0	40→41	+18.4
	2	278.7	39→41	+11.0
	3	245.8	38→41	-0.92
	4	205.3	37→41	-30.6

[a]Calculations at TDDFT/M062X/aug-cc-pVDZ//DFT/M062X/TZVP/IEFPCM(MeOH) level for the most abundant conformer **84a**.

Table 5.2.4. Conformers Relative Energies (ΔE_{el}) and Population Percentages (pop%) of (5*R*)-**84** Calculated at Different Levels of Theory Both in Gas Phase and IEFPCM (MeOH) Implicit Solvation Model.

	B3LYP/TZVP Gas phase		B3LYP/TZVP IEFPCM(MeOH)		M06-2X/TZVP IEFPCM(MeOH)	
Conformer	ΔE(Kcal/mol)	pop(%)	ΔE(Kcal/mol)	pop(%)	ΔE(Kcal/mol)	pop(%)
84a	0.00	27.1	0.00	19.0	0.00	14.3
84b	0.47	12.2	0.04	17.7	0.06	12.9
84c	0.67	8.6	0.11	15.9	0.08	12.5
84d	0.11	22.6	0.52	7.9	0.48	6.3
84e	0.30	16.3	0.58	7.1	0.51	6.1
84f	1.08	4.4	0.46	8.7	0.02	14.0
84g	1.23	3.4	0.48	8.4	0.04	13.3
84h	1.70	1.5	0.56	7.4	0.11	12.0
84i	1.17	3.8	0.95	3.8	0.46	6.6
84j	-	-	0.91	4.0	1.17	2.0

Table 5.3.1 ^{1}H and ^{13}C NMR Data of Alternethanoxins C-E (**86**-**88**)[a,b] Recorded in $CDCl_3$ at 600 MHz.

	86			**87**			**88**		
	δC[c]	δH (*J* in Hz)	HMBC	δC	δH (*J* in Hz)	HMBC	δC	δH (*J* in Hz)	HMBC
1	148.9 *s*			149.3 *s*		MeCO	155.9 *s*		H-3
2	126.2 *s*			128.9 *s*		H-3	106.2 *s*		H-3
3	110.1 *d* [d]	6.21 (1H) *s*[d]	MeCO	106.3 *d*	6.66 (1H) *s*	H-6, MeCO	107.2 *d*	6.84 (1H) *s*	MeCO
4	162.8 *s*[d]		H-3	153.0 *s*		H-3	148.9 *s*		MeCO
5	162.8 *s*[d]		H-3	161.4 *s*		H-6	158.2 *s*		H-6
6	110.1 *d*[d]	6.21 (1H) *s*[d]		111.6 *d*	6.93 (1H) *s*		111.2 *d*	6.64 (1H) *s*	
6a	136.3 *s*		H-8	155.3 *s*			161.2 *s*		H-6
7	166.2 *s*		H-9, H-8, OMe	168.6 *s*		H-9, MeO	103.3 *d*	6.99 (1H) *d* (2.2)	H-9
8	129.4 *d*	7.51 (1H) *d* (7.3)		112.4 *d*	7.06 (1H) *s*		168.4 *s*		OMe
9	122.1 *d*	7.45 (1H) *d* (7.3)		156.9 *s*			112.6 *d*	6.91 (1H) *d* (2.2)	
10	149.8 *s*		H-9, H-8	165.0 *s*			168.8 *s*		H-9
10a	127.7 *s*		H-9, H-8	133.2 *s*			135.9 *s*		
10b	110.0 *s*			112.7 *s*			110.1 *s*		
OMe	53.8 *q*	3.70 (3H) *s*		53.3 *q*	3.90 (3H) *s*		52.0 *q*	3.93 (3H) *s*	
<u>Me</u>CO	21.9 *q*	2.20 (3H) *s*	H-3	22.6 *q*	2.50 (3H) *s*	H-3	21.5 *q*	2.45 (3H) *s*	H-3
Me<u>CO</u>	199.2 *s*		H-3	179.8 *s*			179.6 *s*		
OH		12.19 *s*			12.10 *s*			12.14 *s*	

[a]The chemical shifts are in δ values (ppm) from TMS.
[b]2D ^{1}H, ^{1}H (COSY) ^{13}C, ^{1}H (HSQC) NMR experiments delineated the correlations of all the protons and the corresponding carbons.
[c]Multiplicities were assigned by DEPT spectrum. [d]Signals overlapped

Table 5.3.2 Biological Activity of Althernethanoxins A-E (**56-57**, **86-88**).

Compound	Phytotoxic activity[a]		Antimicrobial activity[b]	
	Sonchus arvensis	*Elytrigia repens*	*Bacillus subtilis*	*Candida tropicalis*
56	1.7±0.11	1.2±0.40	100	n.a.
57	0	0.5±0	>100	n.a.
86	2.4±0.23	1.1±0.29	10	25
87	0	0.5±0	10	25
88	0	0	n.a.	n.a.

[a]necrosis, mm ± std. deviation; [b] minimal inhibitory concentration, μg/disc; n.a. no activity

Table 5.4.1. ^{1}H and ^{13}C NMR Data of Chenopodolan D (**89**) and ^{1}H NMR Data of Its 11-*O*-Acetylderivative (**92**)[a,b] Recorded in $CDCl_3$ at 600 MHz.

Position	**89**			**92**
	δC[c]	δH (*J* in Hz)	HMBC	δH (*J* in Hz)
2	163.5 *s*		Me-8	
3	165.9 *s*		H-7a, OMe, Me-8	
3a	101.9 *s*		H-7a, Me-8	
4	126.2 *s*		H-7a, Me-13	
5	135.7 *d*	6.98 *s*	Me-13	6.96 *s*
6	160.1 *s*		H-5, H-7a, Me-13	
7a	93.7 *d*	6.18 *s*		6.19 *s*
8	14.4 *q*	1.95 (3H) *s*		1.93 (3H) *s*
9	135.9 *q*		H-10, H_2-11, Me-12	
10	131.7 *d*	5.68 *br t (* 6.6)[d]	H_2-11	
11	59.8 *t*	4.32 (2H) *br s*		4.73 *br s*
				4.71 *br s*
12	16.5 *q*	1.85 (3H) *s*[d]	H-10	1.88 (3H) *s*
13	13.7 *q*	2.05 (3H) *s*	H-5	2.04 (3H) *s*
OMe	56.1 *q*	3.92 *s*		3.92 (3H) *s*
MeCO				2.08 (3H) *s*

[a]The chemical shifts are in δ values (ppm) from TMS. [b]2D ^{1}H, ^{1}H (COSY) ^{13}C, ^{1}H (HSQC) NMR experiments delineated the correlations of all the protons and the corresponding carbons. [c]Multiplicities were assigned by DEPT spectrum. [d]Allylic coupling (< 1 Hz) was observed in the COSY spectrum between H-10 and Me-12

Table 5.4.2. Conformers Boltzmann Distribution of Chenopodolan D (**89**) $CDCl_3$ at 600 MHz.

	DFT/B3LYP/ TZVP (Gas Phase)		DFT/B3LYP/TZVP (IEFPCM=THF)		DFT/B3LYP/TZVP (IEFPCM=$CHCl_3$)	
Conformer	ΔG (Kcal/mol)	% Pop	ΔG (Kcal/mol)	% Pop	ΔG (Kcal/mol)	% Pop
89b	0.00	26.1	0.08	12.6	0.15	11.5
89c	0.57	10.0	0.39	7.5	0.30	8.9
89e	0.62	9.2	0.78	3.9	0.81	3.8
89a	0.66	8.5	0.39	7.5	0.27	9.4
89h	0.67	8.4	0.00	14.5	0.04	13.9
89d	0.80	7.0	0.51	6.2	0.49	6.5
89m	0.90	5.7	0.38	7.6	0.45	7.0
89k	0.93	5.4	0.04	13.6	0.00	14.8
89l	1.08	4.2	0.61	5.1	0.66	4.9
89o	1.17	3.6	-	-	-	-
89g	1.22	3.3	0.64	5.0	0.63	5.1
89f	1.30	2.9	1.00	2.7	0.98	2.8
89j	1.45	2.2	0.77	4.0	0.78	4.0
89n	1.50	2.1	0.75	4.1	0.68	4.7
89i	1.75	1.4	0.93	3.0	1.02	2.6
89p	-	-	0.98	2.7	-	-

Table 5.4.3. ^{1}H and ^{13}C NMR Data of Chenisocoumarin (**90**)[a,b] and Its 5,7-*O,O'*-Dimethyl Derivative (**93**) Recorded in $CDCl_3$ at 600 MHz.

Position	**90**			**93**
	δC^c	δH (*J* in Hz)	HMBC	δH (*J* in Hz)
1	169.0 *s*		H-8, H-3, Me-9	
3	67.2 *d*	4.57 *dq* (6.6, 1.8)	H-3, Me-9	4.54 *dq* (6.6, 1.3)
4	77.5 *d*	4.38 d (1.8)	Me-9	4.47 *d* (1.3)
4a	142.5 *s*		H-4, H-3	
5	155.3 *s*		H-6, H-4	
6	106.8 *d*	6.35 *d* (1.7)	H-8, H-4	6.54 *br s*
7	164.1 *s*		H-8	
8	99.2 *s*	6.33 *d* (1.7)	H-6, H-4	6.50 *br s*
8a	135.8 *s*			
9	15.8 *q*	1.48 (3H) *d* (6.6)	H-4, H-3,	1.50 (3H) *d* (6.6)
OMe				3.92 (3H) *s*
OMe				3.89 (3H) *s*

[a]The chemical shifts are in δ values (ppm) from TMS. [b]2D ^{1}H, ^{1}H (COSY) ^{13}C, ^{1}H (HSQC) NMR experiments delineated the correlations of all the protons and the corresponding carbons. [c]Multiplicities were assigned by DEPT spectrum.

Table 5.4.4. ^{1}H NMR data of 4-*O*- (*S*)- and 4-*O*- (*R*)-MTPA Esters of Chenisocumarine 5,7-*O,O'*-Dimetilderivative (**94** and **95**, Respectively) Recorded in $CDCl_3$ at 600 MHz.

	94	**95**
	δH (*J* in Hz)	δH (*J* in Hz)
3	4.702 *br q* (6.5)	4.661 *br q* (6.7)
4	5.945 *br s*	5.907 *br s*
6	6.637 *br s*	6.694 *br s*
8	6.544 *br s*	6.578 *br s*
9	1.448 (3H) *d* (6.5)	1.417 (3H) *d* (6.7)
OMe[a]	3.920 (3H) *s*	3.945 (3H) *s*
OMe[a]	3.870 (3H) *s*	3.874 (3H) *s*
OMe	3.430 (3H) *s*	3.371 (3H) *s*
Ph	7.381-7.312 *m*	7.414-7.307 *m*

[a]These assignments can be reversed

Table 5.4.5. ^{1}H and ^{13}C NMR Data of Chenopodolin B (**91**)[a,b] Recorded in $CDCl_3$ at 600 MHz.

Position	δ C[c]	δ H (*J* in Hz)	HMBC
1	72.4 *d*	5.07 (1H) *d* (4.9)	Me-20
2	76.9 *d*	4.62 (1H) *d* (4.9)	H-1, Me-19
3	78.1 *d*	5.21 (1H) *br s*	H-5, H-1
4	46.7 *s*		H-5, Me-19
5	58.7 *d*	2.96 (1H) *s*	H-1, H-3, Me-19
6	194.2 *s*		H-5
7	126.7 *d*	5.85 (1H) *s*	H_2-14
8	155.7 *s*		H_2-14, H_2-11, H-9
9	48. *d*	3.00 (1H) *m*	
10	42.1 s		H-5, H-2, Me-20
11	11.9 *t*	1.43 (2H) *m*	Me-20
12	76.8 *d*	4.71 (1H) *t*	H-14, H_2-11, Me-17
13	41.5 *s*		H_2-16, H_2-14, Me-17
14	43.3 *t*	2.73 (1H) d (16.0)	Me-17
		2.31 (1H) *d* (16.0)	
15	139.3 *d*	5.87 (1H) *dd* (17.8,11.2)	H-16B, H_2-14, H-12, Me-17
16	116.8 *t*	5.19 (1H) *d* (11.2)	Me-17
		5.03 (1H) *d* (17.8)	
17	25.5 *q*	1.08 (3H) *s*	H-12
18	175.4 *s*		H-5, H-3, Me-19
19	12.1 *q*	1.47 (3H) *s*	H-5
20	17.3 *q*	1.12 (3H) *s*	H-1, H-5
MeCO-12	170.6 *s*		H-12, MeCO-12
MeCO-3	174.8 *s*		H-5, H-1, H-2, Me-19
MeCO-1	169.4 *s*		H-1, MeCO-1
MeCO-1	20.1 *q*	2.27 (3H) *s*	
MeCO-3	20.7 *q*	2.10 (3H) *s*	
MeCO-12	20.7 *q*	2.07 (3H) *s*	

[a]The chemical shifts are in δ values (ppm) from TMS. [b]2D ^{1}H, ^{1}H (COSY) ^{13}C, ^{1}H (HSQC) NMR experiments delineated the correlations of all the protons and the corresponding carbons.
[c]Multiplicities were assigned by DEPT spectrum.